kovatti87_134_23

CLINICAL PERSPECTIVES OF RIGHT VENTRICULAR FUNCTION AS ASSESSED BY THREE-DIMENSIONAL ECHOCARDIOGRAPHY

Thesis

Doctor of the Hungarian Academy of Sciences

Dr. Attila Kovács

Semmelweis University

Budapest
2024

1. Table of Contents

2. Abbreviations

2D	two-dimensional
3D	three-dimensional
3DE	three-dimensional echocardiography
AC	arrhythmogenic cardiomyopathy
AEF	anteroposterior ejection fraction
AESV	end-systolic volume with anteroposterior motion enabled
AI	artificial intelligence
ANOVA	analysis of variance
ASD	atrial septal defect
AUROC	area under the receiver operating characteristic curve
BMI	body mass index
BSA	body surface area
CABG	coronary artery bypass grafting
CHD	congenital heart disease
CI	confidence interval
CMRI	cardiac magnetic resonance imaging
CO	cardiac output
CPB	cardiopulmonary bypass
CPET	cardiopulmonary exercise testing
CRT	cardiac resynchronization therapy
CVP	central venous pressure
DBP	diastolic blood pressure
DICOM	Digital Imaging and Communications in Medicine
DPG	diastolic pressure gradient
Ea	arterial elastance
ECG	electrocardiogram
EDV	end-diastolic volume
Eed	end-diastolic stiffness
Ees	end-systolic elastance
EF	ejection fraction
EROA	effective regurgitant orifice area
ESPVR	end-systolic pressure-volume relationship
ESV	end-systolic volume
FAC	fractional area change
FDA	Food and Drug Administration
FWLS	free-wall longitudinal strain
GAS	global area strain
GCS	global circumferential strain
GLS	global longitudinal strain
HFpEF	heart failure with preserved ejection fraction
HFrEF	heart failure with reduced ejection fraction
HR	heart rate or hazard ratio
HTX	heart transplantation
ICD	implantable cardioverter defibrillator
ICU	intensive care unit
IQR	interquartile range
ISHLT	International Society of Heart and Lung Transplantation

LA	left atrial
LEF	longitudinal ejection fraction
LESV	end-systolic volume with longitudinal motion enabled
LV	left ventricular
LVAD	left ventricular assist device
LVEF	left ventricular ejection fraction
MACE	Major Adverse Cardiovascular Events
MOOSE	Meta-analysis Of Observational Studies in Epidemiology
mPAP	mean pulmonary artery pressure
MR	mitral regurgitation
MVR	mitral valve replacement/repair
PA	pulmonary artery
PAC	pulmonary artery catheterization
pAMR	pathology antibody-mediated rejection
PASP	pulmonary artery systolic pressure
PAWP	pulmonary artery wedge pressure
PH	pulmonary hypertension
PISA	proximal isovelocity surface area
PREPARE-MVR	PRediction of Early PostoperAtive Right vEntricular Failure in Mitral Valve Replacement/Repair Patients
PV	pressure-volume
PVR	pulmonary vascular resistance
QUIPS	Quality In Prognosis Studies
RA	right atrial
REF	radial ejection fraction
RER	respiratory exchange ratio
RESV	end-systolic volume with radial motion enabled
ReVISION	Right VentrIcular Separate wall motIon quantificatiON
ROC	receiver operating characteristic
RV	right ventricular
RVD	right ventricular dysfunction
RVEF	right ventricular ejection fraction
RV-PA	right ventricular-pulmonary arterial
RVSLS	right ventricular septal longitudinal strain
RVSWi	right ventricular stroke work index
SAVR	surgical aortic valve replacement
SBP	systolic blood pressure
SD	standard deviation
SRV	systemic right ventricle
TAPSE	tricuspid annular plane systolic excursion
TAVR	transcatheter aortic valve replacement
TDI	tissue Doppler imaging
ToF	Tetralogy of Fallot
TR	tricuspid regurgitation
UCD	Unstructured Cell Data
VIF	variance inflation factor
VSD	ventricular septal defect
WASE	World Alliance Societies of Echocardiography

3. Introduction

Right ventricular (RV) morphology and function assessment in everyday clinical practice is integral to standard echocardiographic protocols. RV dysfunction is closely associated with symptom burden and excess mortality in patients with various cardiopulmonary conditions [1]. For example, in heart failure (HF) with reduced left ventricular (LV) ejection fraction (HFrEF), the prevalence of RV dysfunction is about 50%, while in HF with preserved EF (HFpEF) is about 33%, carrying a twofold increased risk for HF readmissions irrespective of LV function [2, 3]. Calculating just the prevalence of HF and pulmonary hypertension (PH), 400-800 million people may have RV dysfunction worldwide, the majority of them undetected [3]. Thus, diagnosing RV dysfunction, especially in the early stages of the disease, is of high clinical significance. Evidence suggests that standard HF therapy effectively improves RV function, which results in better clinical outcomes [2]. However, most echocardiographic parameters consist of simple two-dimensional (2D) measurements with limited ability to portray the RV's complex three-dimensional (3D) anatomy. These routinely assessed parameters (*e.g.*, tricuspid annular plane systolic excursion - TAPSE, fractional area change - FAC, and free-wall longitudinal strain - FWLS) can only partially assess the complex functional characteristics of the RV; therefore, they may fail to capture the full spectrum of RV dysfunction [4]. On the contrary, 3D echocardiography (3DE) enables direct volumetric measurements and provides more accurate quantification of ventricular performance. Additionally, 3D volumetric parameters have been extensively validated against cardiac magnetic resonance imaging (CMRI) and consistently show better correlation and less underestimation than 2D echocardiography-derived geometry measures [5]. However, even the most recent data about the prognostic value of RV function relies on simple, global functional parameters as no established tool was available for detailed analysis of global and segmental RV shape and mechanics.

After completing my PhD, I performed thousands of echos at intensive care units as a cardiology resident. By consulting the referring physicians and following up with the patients, I concluded that RV dysfunction emerged as a major determinator of patient outcomes in contemporary medicine, where numerous pharmacological and device therapies are available but only to treat the left ventricle. Still, the diagnostic arsenal of conventional echocardiography is inadequate, and a more comprehensive mechanical characterization is needed to capture subclinical RV dysfunction sensitively. During the following years spent with RV-related research at Semmelweis University, in collaboration with an artificial intelligence (AI) start-up company, we developed and validated a system for a deeper analysis of RV 3DE data. Beyond established markers of ventricular mechanics (longitudinal and circumferential strain), the software quantifies RV wall motion directions and their impact on global and segmental volume changes. Based on international collaborations and related literature data, this approach has further advantages with regard to RV function assessment, as also highlighted in a recent Scientific Statement of the American College of Cardiology [6]. Our RV solution has won several innovation awards, including the American Society of Echocardiography's Echovation Challenge, and has been recently cleared for clinical use by the United States Food and Drug Administration (FDA).

My current thesis is about the 3DE-derived assessment of RV dysfunction, and in particular, the development, technical, and clinical validation of our Right VentrIcular Separate wall motIon quantificatiON (ReVISION) software, aiming to show its added diagnostic and prognostic power in cardiopulmonary diseases.

4. Background

4.1. The importance of RV function – historical perspective

While the LV structure and function have received much attention, the RV shape and mechanics have usually been explored less in current science. The distinctions between the two ventricles and their structural differences had already been described in the Hippocratic era [7]. Scientists from ancient and medieval times attributed various roles to the right side of the heart. Galen believed that the blood of the RV mixes with the LV through the pores of the interventricular septum. Islamic anatomists were the first to find a direct connection between pulmonary circulation and the RV. These views only became accepted in the seventeenth century. Prominent medieval scientists, such as Vesalius and Harvey, accepted such concepts of the circulatory system, which are reminiscent of the ancient Greek views [7].

Clinical observations and animal experiments of the early twentieth century recognized the importance of ventricular interdependence, the phenomenon that the dysfunction and overload of one ventricle significantly affects its counterpart and, consequently, the global circulation [8, 9]. The theory that the RV is not an essential part of circulation began in the 1940s with the study of Starr and coworkers, who damaged the RV free wall in dogs by thermoablation and ligation of the right coronary artery [10]. The dogs experienced unaffected venous pressures, and they survived the procedure. Following these results, studies with similar designs reported preserved exercise capacity and maintained circulatory parameters [11, 12]. In parallel with these findings, Fontan and Baudet developed the cavopulmonary anastomosis procedure with promising results [13]. According to these data, the RV only acts as a conduit of the cardiovascular system, with little to no contribution to the circulation.

In the past few decades, novel diagnostic techniques and important epidemiology studies have brought RV function back into the scientific spotlight. RV myocardial infarction

was first described in the 1970s, and several studies later showed the strong prognostic role of RV involvement in myocardial infarction [14-16]. Since then, RV function has proven to be a prognostic factor in HFrEF [17], HFpEF [18], and PH [19]. RV function is also a cornerstone in managing novel clinical issues, such as mechanical circulatory support devices [20] or grown-up congenital heart disease patients [21].

Novel techniques in cardiovascular imaging have facilitated a deeper understanding of RV morphology and mechanics in physiological and pathological conditions, turning the "forgotten chamber" into an important diagnostic and therapeutic target for clinical and experimental research.

4.2. Anatomy and myofiber architecture of the RV

The RV is a more complex structure than the LV. When viewed from the front, it forms a triangular shape, while it is crescentic in cross-section. The interventricular septum bulges into the RV cavity during physiologic conditions, causing a concave surface. Traditionally, the RV is separated into three major parts (Figure 1): (1) the inlet, including the tricuspid valve, chordae tendineae, and papillary muscles; (2) the apical region, with a heavily trabeculated myocardium; and (3) the outlet or the RV outflow tract (infundibulum) [22]. The myocardium is a sophisticated 3D structure of myofibers that have a helical configuration with significant functional implications. These bundles deform the ventricle and produce ejection when they contract, and they assist diastole when they relax; the myofiber direction also helps to comprehend how the RV contracts in the 3D space.

On the epicardial surface, circumferentially oriented myofibers are present; these myofibers are components of the myofiber tracts that are shared with the LV, encompass the subpulmonary infundibulum, and advance more or less parallel with the atrioventricular groove

(Figure 1). At the apex, this layer spirals into the RV's deep (subendocardial) layer. However, this subendocardial fiber orientation is rather longitudinal. In physiologic conditions, the mid-layer containing circumferential fibers is absent [23]. However, congenital and acquired modifications of this myofiber architecture result in an altered motion pattern of the RV.

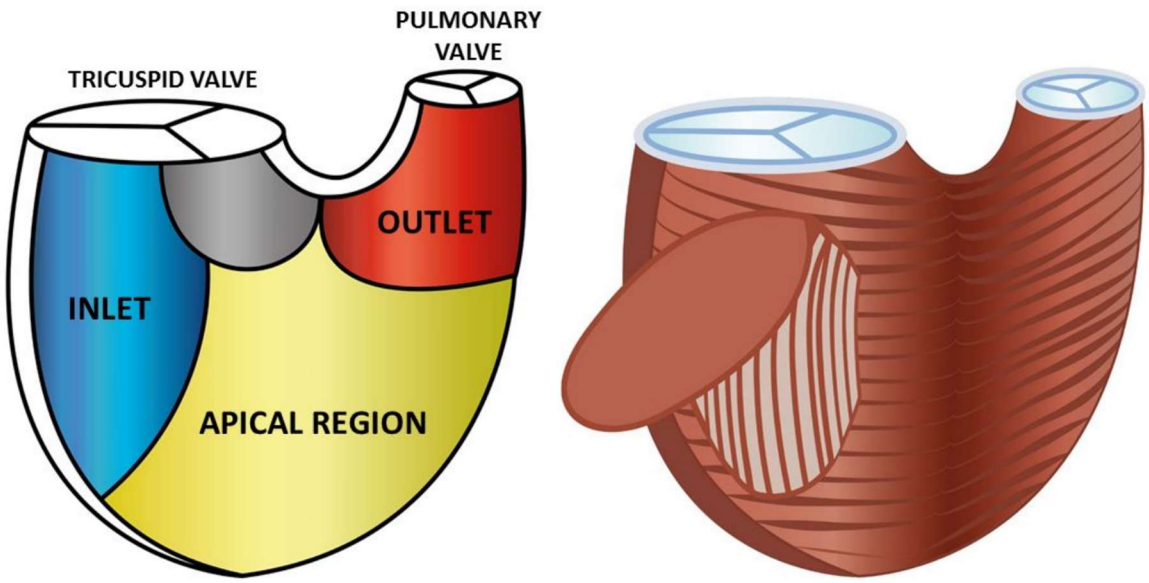

Figure 1. Schematic representation of the right ventricular regions (on the left) and myofiber orientation (on the right). On the epicardial surface, circumferentially oriented myofibers are present. The subendocardial fiber orientation is rather longitudinal (as shown inside the cavity).

4.3. Functional pattern of RV myocardial mechanics

The main determinants of RV function include the systemic venous return, the RV afterload, the pericardial compliance, and the RV contractility [3]. Energy expenditure is much lower in the RV than in the LV, attributable to compliant and low-resistance pulmonary circulation. This factor, along with lower pressures, a higher steady-state volume, and shorter isovolumic periods, results in a distinct pressure-volume (PV) loop compared to the LV (triangular in normal conditions). The systolic PV slope is shallower; therefore, smaller changes in pressure result in greater changes in volume, making the RV function highly sensitive to afterload. As RV adaptation to increased vascular load incorporates increased contractility, the

PV loop becomes more rectangular, and the end-systolic PV relationship shifts leftwards. RV failure develops when the RV becomes even more dilated while the PV relationship shifts right (decreasing contractility – uncoupling) [24]. The increased heart rate required to maintain cardiac output will increase wall stress and oxygen demand.

According to the law of Laplace, wall stress is inversely proportional to wall thickness but directly related to cavitary pressure and internal diameter. However, the complex shape of the RV will result in high intracavitary variation of wall stress. The more spherical parts of the RV (*i.e.*, the basal free wall) will be subject to higher wall stress, ultimately resulting in regional differences in remodeling and myocardial mechanics. Therefore, these segments' early loss of function in response to increased afterload is justified. Regional curvature analysis may estimate local wall stress in different pathological conditions [25]. Interventricular septal flattening is a well-established sign of RV overload, presenting mainly during systole due to pressure overload and during diastole due to volume overload. However, the 3D curvature evaluation of the free wall is also of research interest. During physiological conditions in end-diastole, the apical free wall bears higher convexity than the body of the free wall, whereas, in end-systole, the apex becomes even more convex; however, the body of the free wall flattens. Septal curvature is found to be unaltered throughout the cardiac cycle. No gender differences in regional RV curvature values were revealed. Aging, however, seems to result in a less compliant RV as changes in shape become less prominent [25].

From a mechanical perspective, the RV shows a unique, peristaltic-like contraction pattern: the activation starts from the inlet and ends at the infundibulum [26, 27]. During the isovolumic contraction, the subepicardial layer of the inflow tract acts as an early pressure generator and deforms the RV circumferentially. The circumferential contraction of the outflow tract is crucial for maintaining high tension during systole, while subvalvular contraction also aids unidirectional flow through the pulmonary valve. Subendocardial fibers are mainly

responsible for the longitudinal shortening during the ejection phase [28, 29]. The function of the interventricular septum also accounts for a significant part of global RV function, mainly through its longitudinal shortening. Notably, an inward motion of the septal myocardium into the RV cavity can also develop. Twist has no significant contribution to RV pump function [30].

Accordingly, three main mechanisms contribute to RV pump function (Figure 2): (1) shortening of the longitudinal axis with traction of the tricuspid annulus towards the apex; (2) inward (radial) movement of the RV free wall, which is often referred as the "bellows effect"; and (3) bulging of the interventricular septum into the RV during the LV contraction and stretching of the free wall insertion lines toward each other (causing shortening in the anteroposterior direction).

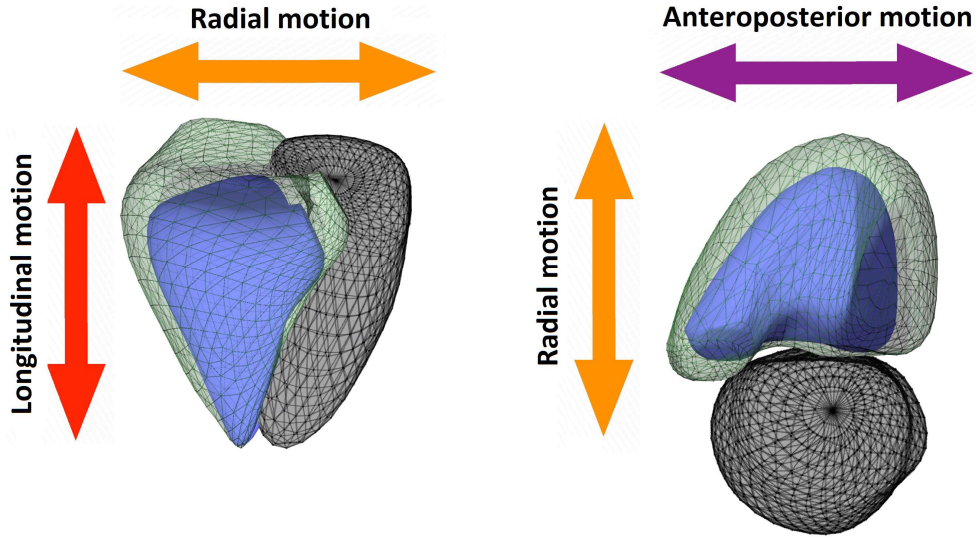

Figure 2. The three main mechanical components that contribute to the global RV pump function.

The relative contribution of the longitudinal, radial, and anteroposterior components of RV wall motion to global ejection was not well studied. Under normal conditions, longitudinal shortening was thought to be the main factor of RV pump function; however, recent studies suggest that longitudinal and radial motions are equally important [26]. Further, large studies

were needed to describe possible changes related to age and gender. Also, there are several diseases and clinical situations in which the normal ratio between the different mechanisms can vary, pointing at the (mal)adaptation of the chamber. The current thesis is mainly about these physiological and pathophysiological contraction patterns.

4.4. Echocardiography to characterize RV mechanics

It is difficult for 2D imaging methods to describe RV shape and function fully. This is true for echocardiography, the main method used to study the RV. It is recommended to use many planes from different echo windows to obtain images that match the various anatomical parts of the complex structure [31]. Still, RV function assessment is often based exclusively on tricuspid annular plane systolic excursion (TAPSE), which measures the displacement of the tricuspid annulus towards the apex on a single apical four-chamber view by M-mode echocardiography. Moreover, TAPSE refers only to the longitudinal shortening of the chamber. Instead of using 2D geometric assumptions (like for the LV) to estimate RV volumes, fractional area change (FAC) is calculated by tracing the areas of the RV cavity at end-diastole and end-systole on a four-chamber view. This technique is a 2D method that partly includes radial motion direction, but it only measures RV function in one slice of a very complicated 3D structure.

Speckle-tracking echocardiography is a useful method for a more quantitative, semi-automated analysis. This method uses the unique myocardial pattern on grey-scale images made of “speckles” with different brightness to calculate how much a particular segment shortens (negative strain) or lengthens (positive strain) [29]. Different directions of deformation (strains) are shown as percentages of the original length, while the values for each segment can be averaged to get a global measure of ventricular function. Systolic and diastolic strain and strain

rate parameters have been shown to be closely correlated with invasive, PV analysis-derived indices of myocardial contractility, active relaxation, and stiffness [32]. Global longitudinal strain (GLS) shows an established diagnostic and prognostic value regarding LV pathologies, and promising data have also been gathered for the RV [33]. Interestingly, it has been shown that myocardial mechanics are highly heritable, which highlights genetic and early developmental processes regarding the complex myofiber architecture [34]. However, the use of 2D speckle tracking for the RV is limited by the thin free wall and the intrinsic drawbacks of the 2D method. Even though the RV longitudinal strain has a proven extra predictive value compared to TAPSE, longitudinal strain still only includes one motion direction [1].

3DE was a major breakthrough in the development of cardiovascular ultrasound methods that improved upon the limitations of 2D evaluation. As the computational and transducer technologies progressed, the real-time 3D capture and display of cardiac structures from any perspective became possible. A crucial early step was the creation of fully sampled matrix-array transducers: these are transducers with around 3000 piezoelectric elements that work simultaneously. These elements are organized in horizontal and vertical lines to create a rectangular matrix. Their activation inside the matrix produces a scan line (axial or y direction, x or azimuthal direction, elevation or z direction) that helps obtain a volumetric data pyramid [35]. Three ways to get 3DE data are multiplane imaging, real-time, and ECG-gated multibeat acquisition. The multiplane imaging method gets several 2D views from different angles at a fast frame rate. The real-time method gets multiple pyramidal volumes per second in one heartbeat. In contrast, multibeat imaging gets images of better quality by getting some ECG-gated narrow volumes over several heartbeats that are combined to make a larger final pyramidal data set. The analysis of the 3D data after they are obtained allows the measurement of important parameters (volumes and EF) using software packages that are specific to or independent of the vendor and have been rigorously validated [5]. Current software options

provide automatic or semi-automatic detection of borders that may ask the user to mark some key anatomical landmarks or make manual adjustments if needed, thus offering a solution that collects high-quality data of the 3D shape and function of the heart without too much time pressure (Figure 3). In addition, novel postprocessing solutions have become available for a deeper analysis of shape and function. 3D speckle tracking, curvature analysis, and the ReVISION software, developed by our research group and described in this thesis in detail, are promising in terms of obtaining a deeper understanding of RV physiology and pathophysiology [26, 36].

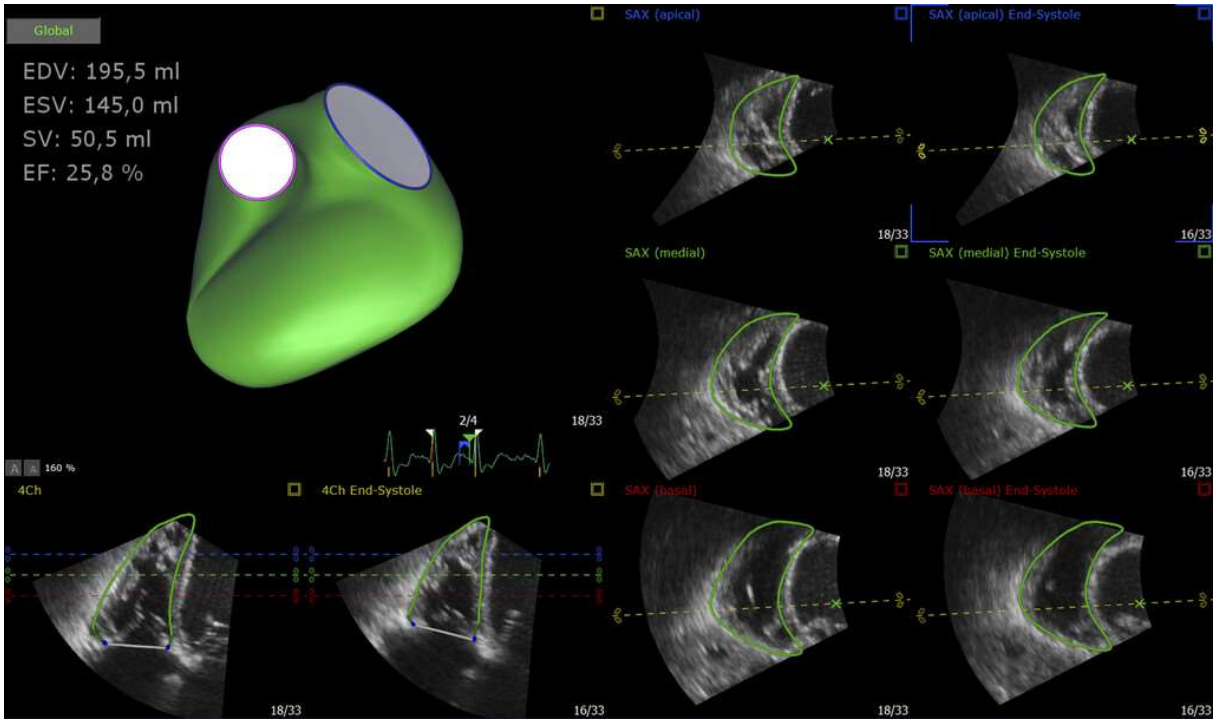

Figure 3. User interface of the most widely used 3D RV quantification software (TomTec 4D RV-Function). Using a semi-automated approach, initial contours can be corrected on multiple short and long-axis planes to reconstruct the 3D surface and calculate end-diastolic volume (EDV), end-systolic volume (ESV), stroke volume (SV), and ejection fraction (EF).

The gold standard for RV volume measurement is CMRI, which also enables myocardial tissue characterization. Nevertheless, novel techniques are also emerging in the field of CMRI. New advances in cardiac diffusion tensor imaging may allow the study of the myofiber structure [23]. Besides the precise assessment of RV ejection fraction, more

sophisticated parameters that describe regional and global contractile function are now accessible. In particular, feature tracking (similar to the speckle tracking method in echocardiography) does not need extra images to measure multidimensional strain. Also, it provides a quicker analysis time than previous techniques [23, 37]. The reproducibility of this approach, similar to that of volumetric measures, seems superior to that of echocardiography-derived strain values [38]). The further implementation of 3D feature tracking may hold additional value, especially regarding the RV. Notably, the ability to quantify 4D blood flow and hemodynamics in the RV has revealed forces in both the longitudinal and short-axis planes, resulting in a slingshot-like mechanism directing the blood flow toward the pulmonary valve under physiological conditions [39]. It also would be of great interest to correlate myocardial mechanics and subsequent flow dynamics in different overload conditions.

4.5. Effects of overload conditions on the RV - pressure overload

The primary role of the RV is to pump blood in the highly distensible, low-resistance pulmonary circulation. Less stroke work is required to accomplish this task, and by Laplace's law, the RV has a thinner and more compliant wall [3]. These cardiodynamic and structural characteristics are reflected in the response to conditions with pressure overload, such as PH or pulmonary valve stenosis. How the RV reacts to excessive pressure load depends on many factors, such as the disease's cause, severity, and duration. Another key factor is when the disease starts; conditions that begin earlier in life (such as congenital pulmonary stenosis) tend to be better tolerated than those that develop during adulthood.

In pulmonary arterial hypertension, RV afterload is increased due to pulmonary vascular remodeling. The challenge for the RV is to remain coupled to the increased afterload [40]. Ventriculoarterial coupling can be assessed with PV analysis of the RV as the ratio of end-

systolic elastance (ventricular contractility) [41] and arterial elastance (ventricular load) [42]. In the early stages of the disease, coupling is maintained by increasing the contractility of the RV. The major mechanisms include adaptive myocardial hypertrophy, which leads to increased wall thickness and reduced wall stress, and alterations of muscle properties, such as myocardial fiber orientation. The relative dominance of the circumferential fibers within the RV wall can be observed [43]. Consequently, a greater decline in radial contraction is often reported [44, 45], and radial motion seems to predict better RV pump function and pulmonary artery pressure than longitudinal shortening [46, 47]. Moreover, recent studies have demonstrated the prognostic value of the "bellows effect" in PH patients [47, 48]. Although the EF might be preserved and the coupling is maintained at rest, uncoupling will occur during exercise, suggesting the depletion of the RV contractile reserve [49]. Adaptations also include a notable deformation of the RV shape [36]. Beyond the aforementioned structural remodeling, changes can also be observed at the histological and molecular levels [50, 51].

With the advancement of the disease, the hypertrophic adaptation is exhausted [52], the stroke volume decreases, and the only mechanism to preserve stroke volume is RV dilation. The heart rate and arterial elastance increase to maintain cardiac output amid decreasing stroke volume. These processes lead to uncoupling, characterized by an increased end-systolic and arterial elastance ratio. The volumetric adaptation, which occurs via dilation at the cost of increased wall tension (stress) and increased pressure, has three major consequences: an increase in oxygen consumption combined with the deterioration of oxygen efficiency, an increase in RV stiffness, and alterations in ventricular interdependence. Because oxygen consumption is mainly determined by wall tension and pulmonary artery pressure [53, 54], it will increase if the RV dilates or the pressure rises. However, the oxygen supply is limited in pulmonary hypertension [55, 56]. Consequently, wall stress will be further augmented by the discrepancy between oxygen supply and consumption, and this change will induce diastolic

stiffening (described by the slope of the PV relation at end-diastole, also called end-diastolic elastance). With disease advancement, increased stiffness causes diastolic dysfunction [57] and is associated with a poor prognosis [58, 59].

RV-LV interactions should not be neglected in PH. There is a parallel interaction via the leftward bowing of the interventricular septum and an in-series interaction as the RV fails to supply an adequate LV preload [60]. The major cause of the septal shift is a prolonged duration of the RV contraction and interventricular mechanical asynchrony [61, 62]. The flattening of the interventricular septum can be observed during end-systole when the pressure in the still-contracting RV exceeds that in the already-relaxing LV. As a consequence, early diastolic LV filling is impeded [60]. Due to the septal shift, the pulmonary valve will close earlier, even though the RV is still contracting. This post-systolic isovolumetric contraction contributes to mechanical inefficiency because the energy of the contraction during this phase of the cardiac cycle is not used to pump blood in the pulmonary circulation. The isovolumetric relaxation is also prolonged, resulting in the delayed opening of the tricuspid valve. Thus, RV filling is shortened, which worsens the already-compromised RV output and, hence, the LV preload. The RV isovolumetric relaxation time correlates with systolic pulmonary artery pressure [63] and is an independent predictor of clinical outcomes [64]. Another interesting aspect of ventricular interdependence is functional linkage via common myofibers. In experimental pulmonary artery banding models, adding a mild aortic band increases the contractility of the pressure-stressed RV, and this change is probably attributable to the Anrep effect and the continuity of myofibers [65]. In addition, the function of the failing LV could be improved through pulmonary artery banding [66]. These studies suggest that better coordination of RV and LV contraction and temporal alignment of cardiac-cycle events can improve function, as also seen in bundle branch block activation delay.

RV structure and function undergo significant changes due to pressure overload, but RV remodeling can be largely reversed, and RV function can improve with proper treatment. Patients with PH showed markedly improved RV function and decreased RV wall thickness after lung transplantation, even with severe preoperative RV dysfunction [67-72]. The degree of improvement is variable and related to pulmonary artery pressure and the duration of disease prior to transplantation [73, 74]. Regaining radial contraction may serve as a sensitive marker of disease regression during follow-up in these patients. Because RV function is the most important determinant of morbidity and mortality in patients with pulmonary arterial hypertension [74], RV adaptation to pressure overload has been extensively studied. However, as we discover more, we also reveal more unknowns; therefore, we need more research to clarify how the RV changes (for better or worse) due to pressure overload.

4.6. Effects of overload conditions on the RV - volume overload

As previously discussed, the RV is characterized by a thinner and more compliant wall than its left counterpart. When RV preload increases, wall stress is maintained by dilation of the chamber, along with preserved end-systolic volumes in the early stages; these observations suggest increased contractile function through the Frank-Starling law, which effectively compensates for altered hemodynamic conditions. The significant elevation of RV preload may also be tolerable with maintained global function in acute and chronic settings, and these observations led to the conclusion that RV volume overload is a benign condition that lacks hemodynamically detrimental consequences. However, growing evidence from tricuspid and pulmonary regurgitation patients strongly emphasizes the negative effects of RV volume overload [75-78].

In the clinical setting, the main etiologic factors of RV volume overload are tricuspid regurgitation (TR), pulmonary valve regurgitation, and left-to-right shunts. The latter two entities are almost exclusively associated with congenital heart diseases; for such diseases, in addition to the presence of RV volume overload, other complex structural and functional aspects must be taken into consideration and will be discussed later. Approximately 80% of TR is functional, and the nature of the primary disease also significantly affects pathophysiology and presentation [77]. Most experimental TR models and clinical data are not focused on RV mechanics and/or mechanoenergetics. According to the available experimental data, acute, severe TR results in elevated RV end-diastolic volume and depressed RV performance, which also persists in the subacute phase [76]. A better understanding of RV function in TR would be of interest, considering that the independent prognostic significance of TR is well-known in a wide spectrum of cardiovascular disorders, and the current management of these patients is still a matter of debate [77].

4.7. Congenital heart diseases, arrhythmogenic cardiomyopathy

Congenital heart diseases (CHD) are different types of heart defects, in which RV features are also key factors of how the disease starts and worsens. The RV may face pressure and/or volume overload, depending on the kind of defect. In certain types of defects, the myofiber architecture also differs from the physiological architecture [79-81], and this effect may become more prominent based on the altered loading conditions of the RV [43, 82]. Beyond the myocardial structure, interstitial abnormalities also complicate CHD cases with unbalanced matrix deposition and secondary focal and diffuse fibrosis [83, 84]. Because of these complex factors, CHD patients present diverse RV geometry and mechanics forms.

Intracardiac shunts are the most common forms of CHD. In isolated forms, the shunt causes a volume overload for the RV; however, non-restrictive high-flow defects may also induce pulmonary vascular remodeling with elevated pulmonary pressures and resistance [85]. As discussed above, in a compensated state, increased preload results in the dilation of the RV, along with maintained/increased contractility [86]. In atrial septal defect (ASD) patients, global RV function measured by the RVEF is usually preserved or even supernormal. Speckle-tracking analysis and tissue Doppler imaging reveal higher GLS and systolic velocity in ASD patients than in controls, suggesting that the increased longitudinal shortening, especially in the apical segments, may be attributable to the increased systolic function [87]. This increase in apical longitudinal strain also correlates with the severity of the shunt [88]. Following transcatheter closure of the defect, the RV geometry and function rapidly change; the RV dimensions and global function significantly decrease in the first 24 hours following the procedure [89]. RV volumes remain unchanged during follow-up, while longitudinal function slightly increases [89, 90]. When a patient's shunt volume is high, and closure of the defect is not performed, severe volume overload induces PH with fixed near-systemic resistance of the pulmonary vascular bed (Eisenmenger's syndrome) [91]. Compared to idiopathic pulmonary arterial hypertension, CHD-associated PH is associated with more pronounced concentric RV hypertrophy [92-94]. Beyond morphological differences, RV mechanics are also markedly different in these patients; in contrast to the severely decreased RV radial shortening observed in pulmonary arterial hypertension patients, in Eisenmenger's syndrome, the transverse (radial) function of the RV is relatively preserved, predominantly in patients with posttricuspid shunts [94]. Moreover, the transverse strain of the RV is an independent predictor of mortality in this population [94].

In the case of ventricular septal defects (VSD), current evidence suggests that RV global function is rather impaired despite the volume overload that facilitates increased contractility

[95, 96]. Moreover, in contrast to LV function, RV systolic performance remains decreased after the closure of the VSD [96]. Since the most important aspect of VSDs is the structurally and functionally disrupted interventricular septum, these results emphasize the importance of the septal contribution to RV function [97].

In intracardiac shunts, the main driver of RV geometric and functional remodeling is the altered loading conditions of the ventricle, whereas in complex malformations of the heart, such as Tetralogy of Fallot (ToF), the RV myoarchitecture is primarily affected. As previously described, the RV free wall in healthy individuals consists of two layers. Conversely, in ToF patients, a prominent middle layer with circumferentially oriented myofibers is also found, similar to the LV architecture. These findings are also already present in fetal specimens [81]. Moreover, experimental studies have shown that the relative dominance of circumferentially oriented fibers may increase with RV dilation [43, 82]. Consequently, we may hypothesize a relative dominance of radial RV function. In the current era of ToF management, total surgical repair is performed in the first years of life; therefore, severe pulmonary stenosis and relevant ventricular septal defect are not expected in this population. However, pulmonary regurgitation as a consequence of the repair procedure is a common finding, resulting in a significant RV hemodynamic burden in many patients [75, 78]. This volume overload of the RV may be tolerated for the long term; however, current data support the finding that the restoration of valve function must be performed to preserve RV function [98]. Global RV function is impaired in the adult ToF population, and decreased longitudinal function can be seen with apical predominance [87, 99, 100]. Recent studies found increased free wall radial shortening, along with decreased longitudinal shortening, which partially compensates for impaired longitudinal motion [100]. Interestingly, a similar change in RV mechanics was observed in a porcine model of chronic pulmonary regurgitation, with decreased longitudinal motion and increased septal pumping [101], whereas in an acute regurgitation model, maintained RV longitudinal function

was seen [102]. Experimental and clinical data suggest that the restoration of pulmonary valve function may have a beneficial effect on RV longitudinal function [101, 103]. While outflow tract obstruction and consequent pressure overload of the RV are considered detrimental to RV function, residual obstruction in repaired ToF patients is associated with better circumferential strain values [104]. This phenomenon is also supported by experimental data, where the RV's combined pressure and volume overload demonstrate reduced dilation and increased contractility compared to isolated pulmonary regurgitation at the expense of marked diastolic dysfunction [105].

In a small but particularly interesting subset of CHD patients, the RV serves as the pump for systemic circulation (systemic right ventricle – SRV). This condition may be a result of palliative surgery, most commonly following the Fontan procedure in patients with hypoplastic left heart syndrome and after atrial switch (Mustard or Senning procedure) after the transposition of the great arteries, or it may be primary in patients with congenitally corrected transposition of the great arteries. Despite the radically different hemodynamic settings, SRV patients without significant intracardiac lesions are typically asymptomatic, and the global function of the SRV is preserved [106]. However, evidence suggests that single RV patients may have a mechanical disadvantage compared to single LV patients, with a progressive reduction in deformation parameters [107, 108]. In a cohort of patients with hypoplastic left heart syndrome and normal RV FAC, the preoperative RV longitudinal strain rate was associated with mortality and the need for heart transplantation [109]. Following cavopulmonary bypass surgery, measures of longitudinal SRV function, such as GLS, predict patient outcomes [110]; however, these measures may not correlate with global function, implying altered RV mechanics [111]. In a group of Senning-operated patients, the circumferential function of the SRV was significantly higher than the longitudinal function. Moreover, in another study, the transverse shortening was also strongly associated with exercise

performance [112, 113]. According to these results, SRV mechanics are characterized by dominantly circumferential shortening, unlike the normal RV, which resembles normal LV function.

Arrhythmogenic cardiomyopathy (AC) is an inherited cardiomyopathy that predominantly affects the RV; however, LV involvement is also common [114]. While the genetic background of AC is established, other factors, such as the volume load of the RV, may precipitate the disease and accelerate progression [115-118]. AC's most characteristic histological features are the fibro-fatty replacement of the myocardium and myocyte loss. These changes result in ventricular arrhythmias, which are the typical clinical manifestation of the disease; however, RV functional impairment and subsequent RV failure are also seen in more advanced stages [119]. Although in-depth analysis of RV morphology and mechanics reveals several markers of AC, clinical features still drive diagnosis, and we lack specific markers for subclinical disease. Whereas in overt stages, the dilation of the RV and globally reduced RV function are evident [120, 121], in early-phase AC, normal RV volumes and slightly reduced RV global function are expected, with maintained longitudinal shortening [122]. The regional assessment of RV longitudinal function suggests that the basal (subtricuspid) strain may be a marker of subclinical involvement [120, 123, 124], which appears to be different from the pattern seen in pulmonary arterial hypertension patients with maintained RV function [125]. These results are concordant with data from contrast-enhanced CMRI and electroanatomical voltage mapping studies [126], implying that the functional alterations of the RV parallel the histological progression of the disease.

4.8. The RV in (left) heart failure

HF, as a clinical scenario, is often perceived as solely left heart failure; however, the signs, symptoms, and prognosis of HF are heavily related to the RV. This statement is true for HFrEF and HFpEF [24]. The role of the interventricular septum cannot be overemphasized.

In HFrEF, right heart failure develops because of gradual increases in afterload due to PH and because of TR accompanied by volume overload. Elevated left-sided filling pressures reduce compliance, increase resistance, and induce chronic remodeling of the pulmonary vascular bed, thus increasing the RV afterload [3]. Due to the given pericardial space, the enlargement of one ventricle will affect its counterpart. Moreover, misalignment of interventricular interactions and normal cardiac cycle events can lead to mechanical dyssynchrony in overload conditions. Geometrically, this change often means that the septum bulging will be more prominent in the early stages, and the space for RV volume will drop. This effect may imply a heavier dependence on the longitudinal shortening of the free wall, as seen in other conditions in which a heavily distorted RV geometry is present [127]. RV failure develops when the RV begins to dilate and loses its longitudinal function. Numerous outcome studies have shown the predictive value of baseline longitudinal RV function, most recently by assessing RV longitudinal strain [128].

In HFpEF, it has been shown that more than 50% of total deaths are attributable to right heart failure [129]. A pulsatile overload burdens the pulmonary venous system in the presence of LV diastolic dysfunction and the loss of left atrial compliance. Typical comorbidities may even exaggerate pulmonary vasoconstriction, resulting in a disproportional increase in pulmonary pressures compared to the left side. When HFpEF patients have maintained LV EF, this does not mean that subclinical contractile dysfunction is not present. Because of the shared myofibers and interventricular septum, LV dysfunction will affect the RV. The deterioration of normal ventricular interdependence and the loss of the LV contribution *per se* reduce RV

function. The RV motion pattern incorporates a notable shortening in the anteroposterior direction, partly due to LV contraction (stretching the free wall over the septum) [26]. It is highly interesting how strongly this anteroposterior shortening is related to LV function and whether these effects worsen in parallel during the development of HF. A recent position paper from the European Society of Cardiology also emphasizes the importance of RV transverse (radial) motion as a potential screening parameter for pulmonary hypertension in patients with HFpEF [24]. Although the deterioration of radial shortening could be an early marker of the disease, the assessment of longitudinal function is still pivotal in determining global function and following up with these patients.

Changes in RV mechanical patterns in conduction abnormalities and during RV pacing also attract scientific interest. Pacing from the RV results in a contraction pattern similar to a left bundle branch block [130]. This effect again disintegrates ventricular interdependence and hampers the LV contribution to RV function. Regaining interventricular synchrony and improving RV function may be important factors in the established beneficial effects after upgrading to cardiac resynchronization therapy from RV pacing [131, 132]. A simple visual assessment of mechanical dyssynchrony by searching for apical rocking or septal flash of the septum may predict the success of resynchronization therapy, which could be similar to patients who present with intrinsic left bundle branch block [133].

The assessment of RV function by echocardiography is also key in the selection of candidate patients for ventricular assist device implantation [134]. The presence of RV dysfunction is unequivocally associated with worse outcomes. In a notable study, Carluccio et al. investigated and followed 200 patients with HFrEF but normal TAPSE [135]. RV free wall strain provided incremental prognostic value compared to the conventional measurement. Technically, this approach is justified because of deformation imaging measures of intrinsic contractile function (not just the displacement of the tricuspid annulus), which avoids errors

due to translational motion and imaging plane adjustment. Moreover, 3DE-derived RVEF was found to be superior to clinical risk factors and conventional echocardiographic measurements in predicting adverse outcomes in a patient population with various cardiac diseases [136]. These studies point to advanced techniques' incremental value, including diagnostic and prognostic benefits, in HF patients. However, the incorporation of non-longitudinal motion directions and geometrical analysis based on 3DE remains to be tested.

4.9. The RV in cardiac surgeries and heart transplantation

RV function is commonly found to be altered following cardiac surgeries, such as coronary artery bypass grafting (CABG), surgical valve repair, or heart transplantation [137-142]. The most prominent change is a decline in longitudinal shortening, even if the global RV function is preserved [143, 144]. This decline in long-axis RV function is persistent [145] and independent of the side of the surgical procedure [146]. Various hypotheses have been proposed to explain this postoperative loss in RV performance detected along the long axis.

One potential factor is cardiopulmonary bypass (CPB) during cardiac surgery. CPB triggers a systemic inflammatory response [147] through the contact activation of blood by the artificial surfaces of the extracorporeal circuit [148]. Proinflammatory cytokines are released; in addition to initiating inflammation, some cytokines, and also endothelin-1, cause vasoconstriction on the pulmonary arterioles; hence, RV afterload will increase [149, 150]. However, other studies have shown that RV function is similarly impaired regardless of CPB utilization [151, 152]. When comparing on-pump and off-pump CABG, Velissaris et al. reported that off-pump surgery triggers a considerable systemic stress hormone response that may be comparable to that of on-pump procedures [153].

Another theory emphasizes the role of pericardiotomy in the reduction of RV long-axis movement because the opening of the pericardial sac can hamper pericardial constraint and ventricular interdependence. Based on experimental simulations, an intact pericardium may reduce radial contractions of the ventricles, with a simultaneous increase in longitudinal function [154]. With a pericardial incision, this physiological function is impeded. Pericardiotomy significantly disturbs the myocardial blood flow in the RV [155] and has a detrimental effect on RV end-diastolic pressure [156]. Surgery without substantial opening of the pericardial sac, such as robotic-assisted minimally invasive CABG, minimally invasive surgical aortic valve replacement (SAVR), or mediastinal mass excision, does not cause a significant decline in the RV longitudinal function. In contrast, if the full opening of the pericardium is involved (CABG, SAVR, or left atrial myxoma excision), the RV longitudinal function is damaged immediately at the moment of pericardial incision [145, 157]. The deleterious effect of pericardiotomy could be demonstrated by comparing procedures that can be performed with or without the opening of the pericardial sac, such as transcatheter aortic valve replacement (TAVR) versus SAVR. All studies in patients undergoing SAVR consistently noted postoperative impairment of RV longitudinal function, whereas longitudinal function was preserved in TAVR patients [143, 158-160]. Notably, RV systolic function (EF and stroke volume) was maintained regardless of the technique used for aortic valve replacement, as radial RV contraction might compensate for the decline in longitudinal shortening [143]. In addition to the significant effect of the pericardial incision, its extent also influences postoperative RV function along the long-axis; a less prominent decline was reported following minimally invasive SAVR than after full sternotomy SAVR [161]. Moreover, RV longitudinal function was found to be preserved after minimally invasive surgical repair of the mitral valve, whereas traditional sternotomy resulted in its deterioration [162]. These findings suggest that minimally invasive approaches tend to have a less deleterious effect on longitudinal

RV function and that preservation of the pericardium might be beneficial. Once the pericardium is disrupted, the RV contraction pattern will be permanently altered, even if pericardial repair is performed [163].

Further factors include incomplete RV cardioplegic arrest (*e.g.*, caused by severe right coronary artery disease [164]), RV hypoperfusion during cardioplegia [165, 166], myocardial stunning due to cardioplegic arrest [167], geometrical changes of the RV chamber (in association with interventricular septal paradoxical motion) [144, 168-170], right atrial injury due to cannulation procedures [163], and postoperative pericardial adhesions.

The evaluation of RV function following orthotropic heart transplantation (HTX) deserves special attention because RV failure is still one of the major determinants of cardiac complications and mortality during the early postoperative period [171, 172]. The RV contraction pattern can also be altered in these patients [139, 173-175]. However, the magnitude of longitudinal functional decline tends to be greater, and the recovery appears to be much slower than observed after other cardiac surgeries [137, 140, 146, 176]. Additional factors may be involved beyond the previously discussed ones; hence, posttransplantation RV function is determined by a more complex interaction among the donor, the operation, and the recipient.

First, brain death and the consequent autonomic storm cause significant systolic and diastolic biventricular dysfunction, with a more prominent decline in RV function [177, 178]. Catecholamines might be one of the most important mediators of this process, as the cardioprotective effect of beta-blockers has also been demonstrated in experimental and clinical studies [179-181]. The preexisting pulmonary hypertension of the recipient and the transient pulmonary vasoconstriction induced by CPB might also be substantial factors [182] because increased afterload leads to dilation of the RV during the early postoperative period [183]. Nevertheless, pulmonary vascular resistance decreases after the procedure, and only slight elevations of pulmonary pressures are expected later, even in cases of severe preoperative

pulmonary hypertension [183-185]. Therefore, pulmonary pressure cannot be solely responsible for RV functional changes. Beyond the potential causes above, the loss of autonomic innervation of the RV myocardium may be another important factor [186]. There is growing evidence for the reinnervation of the transplanted heart by both sympathetic and parasympathetic fibers [187-189], which could hypothetically result in the recovery of RV longitudinal shortening over time. Different surgical techniques applied during heart transplantation can result in different geometries and functions of the right heart [190]. Finally, the potential deleterious effects of the applied immunosuppressive therapy should also be mentioned [191].

In conclusion, the decline in RV longitudinal function after cardiac surgery does not necessarily indicate a reduction in global RV systolic function. Therefore, longitudinal parameters are not accurate measures of RV function in these patients [173, 174, 192, 193], and reporting RV parameters that also incorporate radial function is highly recommended [194].

4.10. Athlete's right heart

Regular exercise training is associated with significant changes in cardiac dimensions and function, also called athlete's heart [195]. Depending on the hemodynamic demand of the given sports discipline, the characteristics of the cardiac adaptation may differ; endurance sports are associated with volume overload and consequent eccentric hypertrophy of the ventricles, whereas strength training results in concentric hypertrophy, predominantly in the LV [195]. Traditionally, it was believed that the RV is only exposed to volume overload due to increased cardiac output; however, recent data also suggest the presence of significant pressure overload [196-198]. The overall effects of these hemodynamic changes are still a matter of debate, considering the growing evidence for exercise-induced RV injury and AC [199]. However,

evidence suggests that a limited degree of pressure and volume overload may induce adaptive remodeling of the RV with increased contractility [200].

The morphological response of the RV to exercise is a continuous spectrum, from mild changes with low-moderate amounts of physical activity [201] to the most evident dilation in master elite athletes with decades of consistent high-intensity exercise [202]. Although very few prospective follow-up studies were performed in the field, current data suggest that the volumetric adaptation of the RV to exercise is more pronounced than that of the LV and that the eccentric type of hypertrophy is expected at all levels of training [203]. This chamber enlargement may affect the inflow tract more than the outflow region of the RV [204]. In parallel to the significant chamber enlargement, RV blood flow patterns are similar to healthy controls, confirming that pronounced morphological remodeling is not accompanied by hemodynamically unfavorable changes [205]. Physiological remodeling is further investigated by contrast-enhanced CMRI studies, which did not reveal any signs of RV fibrosis in healthy master athletes [206, 207]. Resting global RV function is often in the low-normal range [208], and in most studies, increased [202, 209, 210] or maintained longitudinal function [115] was measured, suggesting an RV functional shift with relatively higher longitudinal function and presumably decreased bellows motion. Following ultraendurance sports events, the RV dimensions increase and decreased EF and GLS can be seen. Moreover, these functional changes are evident even after 60 minutes of intensive exercise [211]. In an experimental endurance training model, moderate levels of chronic exercise were associated with RV dilation and increased free wall apical longitudinal strain, while intensive exercise induced a further increase in RV dimensions; however, RV longitudinal function and global performance deteriorated [117, 118]. In the context of mixed hemodynamic RV overload in exercise, these experimental and clinical results are consistent with pathological RV volume and pressure overload findings. As previously discussed, volume overload of the RV is associated with

relatively increased longitudinal function [212], whereas RV pressure overload primarily affects radial shortening, with prominently decreased bellows motion [44]. When the exercise load of the RV passes a certain level, RV damage develops [213]. This phenomenon may be accelerated when an AC-related genetic predisposition is present [115]. However, these alterations in RV mechanical patterns are also signs of a well-trained heart and, thus, may also serve as markers of a „good athlete's heart".

In summary, there is growing interest and evidence about the clinical significance of RV evaluation by 3DE, looking beyond RVEF and exploring mechanical changes on regional and segmental levels in various cardiopulmonary diseases. We designed our aims, software development efforts, and clinical studies accordingly.

5. Aims

5.1. Development and validation of a software tool to quantify RV contraction patterns

We aimed to develop a 3DE-based analysis pipeline with particular regard to the RV's motion decomposition, volumetric segmentation, and the calculation of longitudinal, circumferential, and area strains. We also sought to compare our echocardiography-based findings concerning the relative contribution of the three aforementioned motion components with those obtained by CMRI-based 3D reconstruction.

5.2. Establishing the normal RV contraction pattern

We aimed to quantify the relative contribution of longitudinal, radial, and anteroposterior motion components of global RV function and examine their determining factors in a large cohort of healthy adults from two centers using 3D echocardiography. Also, we aimed to describe these relative contributions in a cohort of healthy children and to look for changes as a function of age.

5.3. Exploring the changes of RV contraction pattern in different clinical scenarios

We aimed to characterize the changes in RV contraction patterns in different health and disease states: in athlete’s heart (including adolescent athletes), in pulmonary hypertension, and in patients after orthotopic heart transplantation.

5.4. Establishing the added prognostic value of 3D RV assessment

First, we aimed to show the added prognostic value of 3DE-derived RVEF over conventional echocardiographic parameters using our retrospective database of patients, then to perform a meta-analysis of studies to confirm this added value in predicting adverse cardiopulmonary outcomes. Second, we aimed to show the additive value of a more detailed assessment of RV contraction patterns in specific scenarios: in patients with severe primary mitral regurgitation undergoing open-heart surgery and in mixed populations of left-sided cardiac disease patients.

6. Methods

6.1. Development and validation of a software tool to quantify RV contraction patterns

6.1.1. The ReVISION analysis pipeline

The ReVISION analysis pipeline comprises four consecutive steps: (i) image acquisition and 3D RV model reconstruction, (ii) adjusting orientation, (iii) volumetric segmentation, and (iv) calculation of global and segmental metrics, including the quantification of the relative contribution of longitudinal, radial and anteroposterior motion components (Figure 4). Our software solution was implemented as a user-friendly and convenient online platform where the user can upload and analyze the reconstructed 3D models of the RV. The analytical components were written in C++, relying on the Eigen linear algebra library (version 3.3.7). The rest of the software stack uses ASP.NET in the backend and Typescript (version 3.9.5) in the front end.

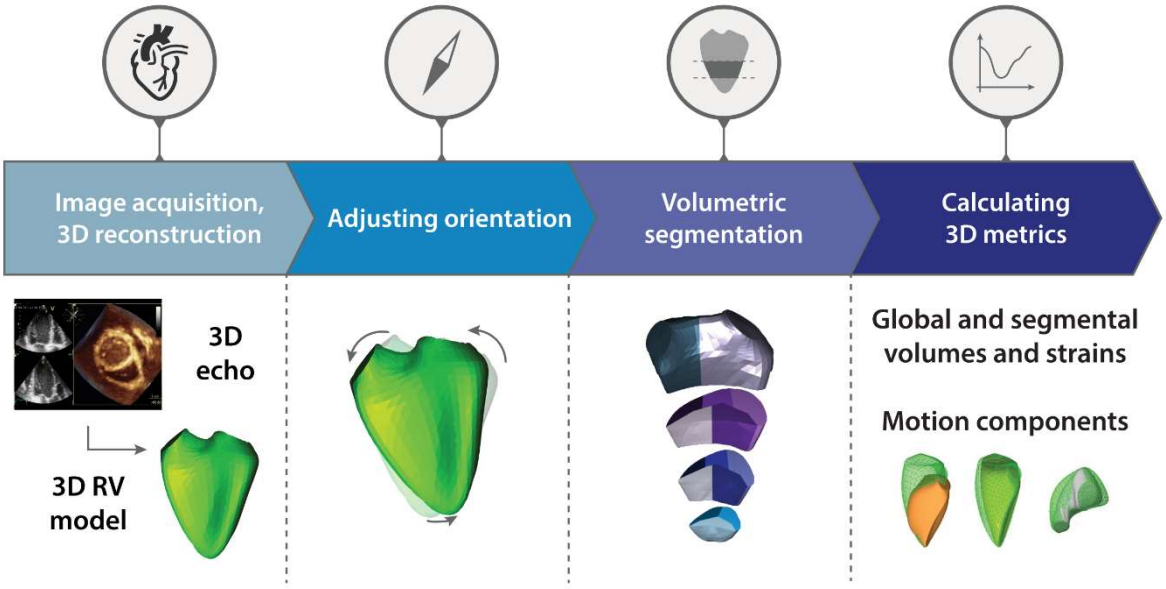

Figure 4. Schematic illustration of the ReVISION analysis pipeline. The pipeline comprises four consecutive steps: (i) image acquisition and 3D right ventricular model reconstruction, (ii) adjusting orientation, (iii) segmentation, and (iv) calculation of global and segmental 3D metrics. See text for further details.

6.1.2. Image acquisition and 3D RV model reconstruction

3DE datasets can be acquired with 3D-capable commercially available cardiac ultrasound systems. Then, these datasets are required to be processed using a dedicated software solution (4D RV-Function, TomTec Imaging, Unterschleissheim, Germany) to generate 3D models of the RV suitable for the ReVISION analysis. Following the image acquisition and 3D model reconstruction process, a series of UCD files and a header file can be exported for each subject from the dedicated software. Each UCD file contains a 3D polygon mesh representing a time instant (a frame) in the cardiac cycle. Each vertex in a mesh corresponds to a specific anatomical position, and this correspondence is consistent across time instants and patients. These files serve as the input for the next steps of the analysis.

6.1.3. Adjusting orientation

The exported files contain a series of $m_1, \dots, m_n$ meshes where $m_i = \{(x_1^i, y_1^i, z_1^i), \dots, (x_k^i, y_k^i, z_k^i)\}$ denotes a set of 3D coordinates. A local coordinate system is defined for each mesh series, where the basis vectors correspond to the longitudinal, radial, and anteroposterior directions (Figure 5). We denote these basis vectors as $B_l, B_r, B_a \in R^3$, respectively, and we use these basis vectors to transform each mesh (m_i) into $\hat{m}_i = \{B^{-1}v_k | v_k \in m_i\}$ where $B = [B_l, B_r, B_a]$.

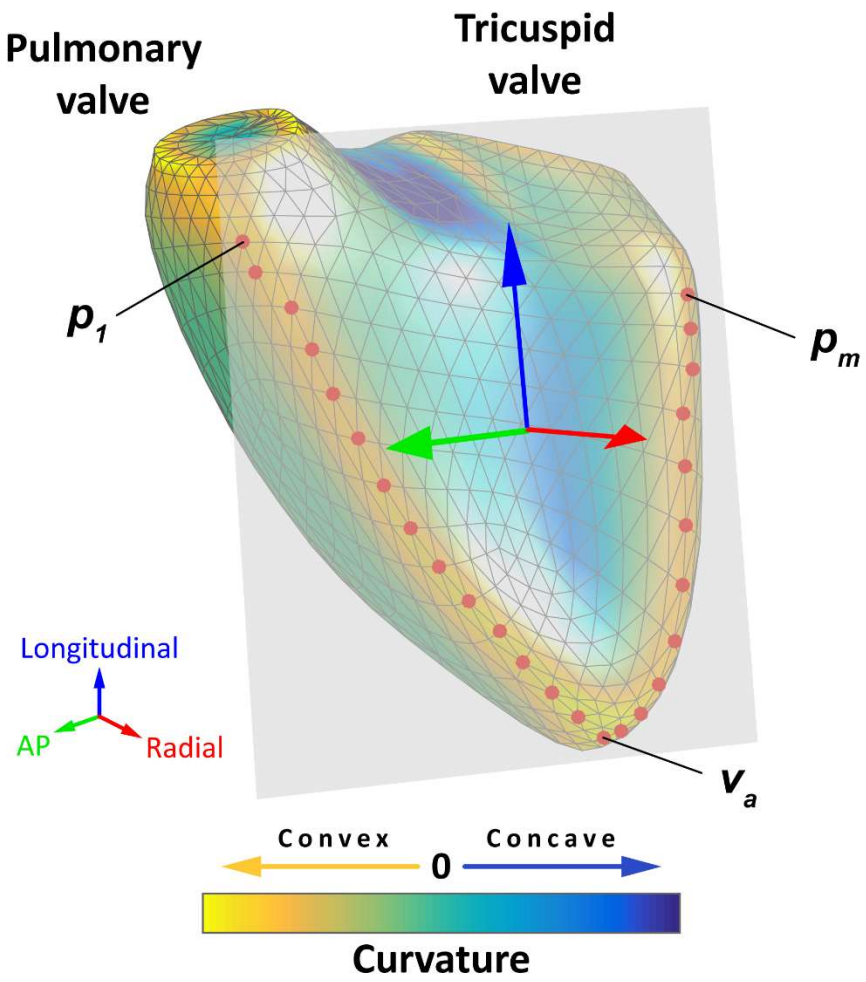

Figure 5. Schematic representation of the orientation adjustment. The 3D RV model is visualized from an anteroseptal point of view. The surface of the mesh is color-coded based on the local mean curvature: yellowish colors indicate the most convex surface, whereas the deepest blue colors correspond to the most concave surface. A local coordinate system is defined for each mesh series, where the basis vectors correspond to the longitudinal (blue arrow), radial (red arrow), and anteroposterior directions (green arrow). First, the points of the septum-free wall boundary (red dots) are selected automatically from predefined groups of vertices so that they have a maximal local mean curvature. Then, a plane is fitted to the selected points using orthogonal distance regression (grey plane), and the radial basis vector is defined as the normal vector of this plane. The longitudinal basis vector should point from the apex (v_a) towards the midpoint of the most basal vertex of the anterior and the most basal vertex of the posterior septum-free wall boundary ($v_e = \frac{p_1 + p_m}{2}$ where p_1 is the most basal vertex of the anterior and p_m is the most basal vertex of the posterior septum-free wall boundary). These two points are projected to the plane defined by the radial basis vector, and they are used to define the longitudinal basis vector. Finally, the anteroposterior basis vector can be determined using the other two basis vectors. See text for further details.

To define B, the following multi-step analysis is performed. First, the points of the septum–free wall boundary ($P = \{p_1, p_2, \ldots, p_m\}$) are selected automatically from predefined groups of vertices so that they have a maximal local mean curvature. Then, a plane is fitted to

the selected points using orthogonal distance regression [214], and B_r is defined as the normal vector of this plane. B_l should point from the apex (v_a – the vertex corresponding to the apex) towards the midpoint of the most basal vertex of the anterior and the most basal vertex of the posterior septum–free wall boundary ($v_e = \frac{p_1 + p_m}{2}$ where p_1 is the most basal vertex of the anterior and p_m is the most basal vertex of the posterior septum–free wall boundary). These two points are projected to the plane defined by B_r and denoted as $\hat{e}$ and $\hat{a}$, respectively. Then, the longitudinal basis vector is defined as $B_l = \frac{\hat{e} - \hat{a}}{\|\hat{e} - \hat{a}\|}$. Finally, we define the anteroposterior basis vector as $B_a = B_r \times B_l$. As the result of the orientation adjustment, the longitudinal direction will correspond to the vertical axis, and the radial and anteroposterior directions will be parallel to the horizontal plane.

6.1.4. Volumetric segmentation

Volumetric segmentation is performed on the end-diastolic mesh of each series to obtain 15 RV segments (Figure 6). First, the fraction of the mesh containing the inflow and outflow segments is separated by a horizontal slicing plane positioned at a predefined height along the longitudinal (*i.e.*, vertical) axis (d_1 – a vector defining the height of the slicing plane along the vertical axis). Then, the remainder of the mesh is trisected by two other horizontal planes at equidistant heights. The following parametric equation represents each horizontal slicing plane:

$$a^T n_i + d_i = 0$$

where the $n_1 = n_2 = n_3$ normal vectors of the slicing planes are vertical, and d_3 and d_2 are placed at equidistant heights between $d_1$and the most apical point of the RV (*i.e.*, the vertex with the minimal y-coordinate).

Next, the horizontal slices are divided further. The inflow segment is separated from the outflow segment by a vertical slicing plane along the midpoint of the central vertices of the tricuspid and pulmonary annuli. Using vertically aligned standard planes, the septal and free wall portions of the horizontal slices are divided into further segments. The vertical slicing planes split the slices into three free wall and two septal segments on the basal and mid levels, and into two free wall and one apical segments on the apical level aiming for equal volume distribution among the segments within the given slice. After the parcellation is completed, the newly generated (non-closed) sides of the segments are covered by smooth biharmonic surfaces. As the segmentation is performed on the end-diastolic mesh, the positions of the newly generated vertices are interpolated in all other frames using their barycentric coordinates.

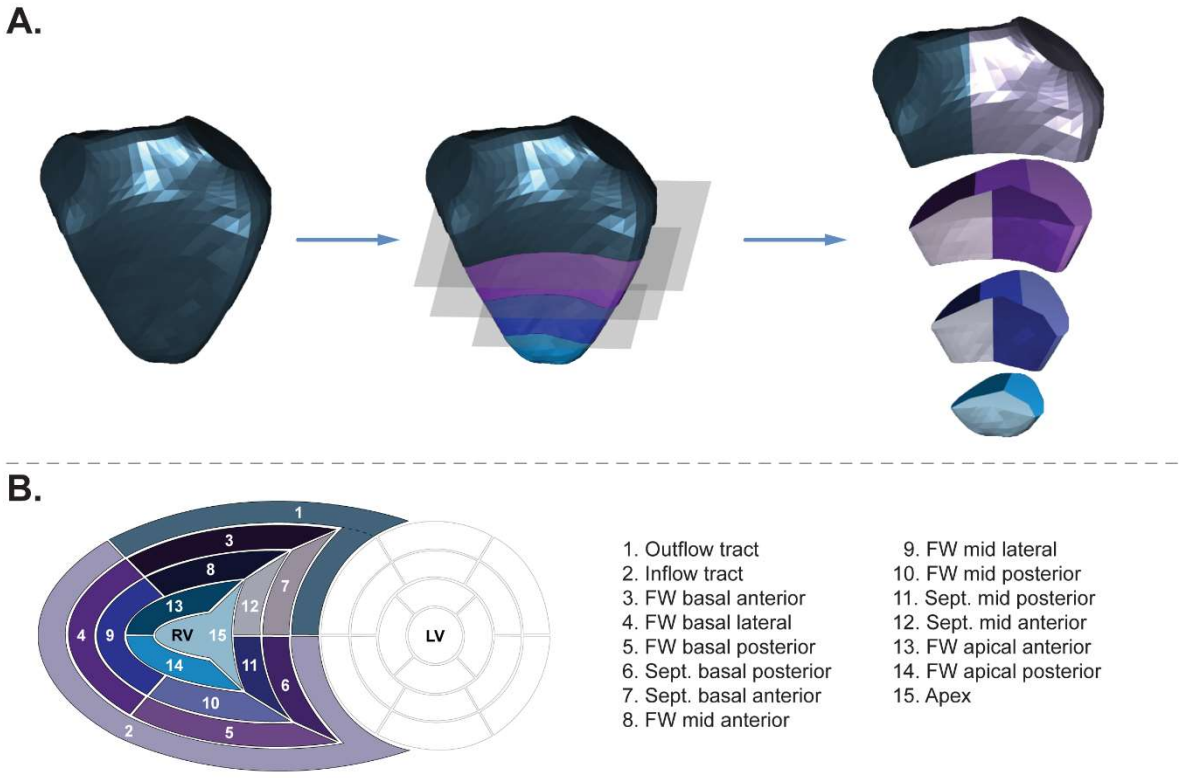

Figure 6. Volumetric segmentation of the right ventricle. Panel A: Segmentation is performed on the end-diastolic mesh of each series to obtain 15 segments. See text for further details. Panel B: The "Bull's eye" plot and the nomenclature of the 15 newly generated right ventricular segments. FW: free wall, Sept.: septum

6.1.5. Calculation of global and segmental metrics and quantifying the relative contribution of longitudinal, radial, and anteroposterior motion components

To calculate global longitudinal strain (GLS), forty-five longitudinally oriented contours (*i.e.*, longitudes) are generated by connecting the apex (v_a) and the predefined vertices of the RV base ($E = \left\{v_e^{(k)}\right\}_{k=1}^{n}$) through specific vertices of the middle section of the RV ($C = \left\{v_c^{(k)}\right\}_{k=1}^{n}$) with geodesic lines. This method ensures that the longitudes are distributed evenly on the surface of the mesh. The length of the j^{th} longitude (L_j^i) can be calculated as the sum of the $v_a - v_c^{(k)}$ and $v_c^{(k)} - v_e^{(k)}$ geodesic distances. The change in the length of each longitude can be monitored throughout the entire cardiac cycle, and GLS can be computed using the following formula:

$$GLS\ (\%) = 100 * \sum_{j=1}^{n} \left(\frac{L_j^{end-systole}}{L_j^{end-diastole}} - 1 \right)$$

For global circumferential strain (GCS) calculations, the inflow and outflow segments are omitted. Fifteen circumferential contours (*i.e.*, latitudes) are created by slicing the mesh with horizontal planes at equal distances along the longitudinal axis. After generating the set of circumferential contours ($\left\{C_j^{(i)}\right\}_{j=1\ldots n}$, where $C_j^{(i)} = (v_1, v_2, \ldots, v_l)$ is the list of vertices on a single contour), the length of the j^{th} circumferential contour is computed as:

$$C_j^i = \sum_{i=1}^{l-1} \|v_{i+1} - v_i\|$$

GCS is calculated using the contour lengths at end-diastole and end-systole:

$$GCS\ (\%) = 100 * \sum_{j=1}^{n} \left(\frac{C_j^{end-systole}}{C_j^{end-diastole}} - 1 \right)$$

Global area strain (GAS) quantifies the change in the endocardial surface area between end-diastolic and end-systolic frames. The surface area of the m_i triangle mesh can be assessed as:

$$A^i = \sum_{t \in T^i} \frac{\|(t_1 - t_3) \times (t_2 - t_3)\|}{2}$$

where $T^i = \{t_k \in R^3\}_{k=1\ldots}$ is the set of triangles of the $\hat{m}_i$ mesh.

Similar to previous calculations, GAS is defined as:

$$GAS\ (\%) = 100 * \left(\frac{A^{end-systole}}{A^{end-diastole}} - 1\right)$$

Motion decomposition is performed along the aforementioned directions (*i.e.*, longitudinal, radial, and anteroposterior) in a vertex-based manner (*e.g.*, for the longitudinal motion, we took into account only the movement of the vertices along the Y axis). That is for each $m_1, \ldots, m_n$ series of meshes where $m_i = \{(x_1^i, y_1^i, z_1^i), \ldots, (x_k^i, y_k^i, z_k^i)\}$

$$m_i^y := \{(x_1^i, y_j^i, z_1^i) | (x_j^i, y_j^i, z_j^i) \in m_i\}$$

The volume of each mesh (or segment) is calculated using the shoelace formula [215]. Let T be the set of triangles $\hat{m}_i$ mesh. For each $t = \{(x_1, y_1, z_1), (x_2, y_2, z_2), (x_3, y_3, z_3)\} \in T$ the volume of tetrahedron bounded by the vertices of t and the origin:

$$V_t := \frac{1}{6}(-x_3 y_2 z_1 + x_2 y_3 z_1 + x_3 y_1 z_2 - x_1 y_3 z_2 - x_2 y_1 z_3 + x_1 y_2 z_3)$$

Note that V_t is signed, meaning that its value may be negative if the normal vector of the triangle points towards the origin. According to the signed tetrahedron method, the volume of $\hat{m}_i$ mesh is the sum of the signed $V_t$volumes:

$$V = \sum_{t \in T} V_t$$

Using ReVISION, volume changes due to the RV wall motion along the three directions can be separately quantified, and the corresponding EF value can be calculated (*i.e.*, radial ejection fraction - REF). The relative contribution of the RV wall motion along the three different directions to global RVEF can be expressed by the ratio of the given direction's EF to global EF (*i.e.*, REF/RVEF).

Beyond the global parameters, we can calculate regional metrics (*i.e.*, septal and free wall longitudinal or area strains; basal-, mid-, and apical-level circumferential or area strains) and also segmental metrics for each of the 15 segments (segmental strains and volumes).

6.1.6. Reproducibility of global and segmental RV metrics

Although the second, third, and fourth steps of the ReVISION pipeline (*i.e.*, the orientation adjustment, the motion decomposition, the volumetric segmentation, and the calculation of metrics) are fully automated, and they do not introduce any additional observer-related variability, we sought to analyze how the differences in 3D contouring and 3D model reconstruction (using the dedicated TomTec software solution) affect the results of our analysis.

6.1.6.1. Study population

To assess the reproducibility of global and segmental RV metrics, ten healthy, sedentary control subjects (5 males, 21±2 years), ten elite water polo athletes (5 males, 21±5 years, 22±4 hours of training per week), and ten end-stage HF patients with reduced LVEF (7 males, 57±14 years) were retrospectively identified in our database. Thus, subjects represented a wide range of cardiac volumes and functions. The study protocol conforms with the principles outlined in

the Declaration of Helsinki and the local regulatory and data protection standards [216]. All subjects in our database were enrolled as part of prospective studies (each approved by the Regional and Institutional Committee of Science and Research Ethics, approval No. 13687-0/2011-EKU and 034309-006/2014/OTIG) and provided written informed consent prior to enrollment to the archiving and analysis of their datasets and the publication of subsequent results.

6.1.6.2. 3D echocardiography

Echocardiographic examinations were performed with a commercially available ultrasound system (GE Vivid E95, 4Vc-D probe, Horten, Norway) in all cases. Beyond the conventional echocardiographic protocol, ECG-gated full-volume 3D datasets reconstructed from four cardiac cycles and optimized for the RV were obtained from an apical view, targeting a minimum volume rate of 25 volumes/second. Datasets were processed using a commercially available dedicated software solution (4D RV-Function 2, TomTec Imaging, Unterschleissheim, Germany), and RV EDV, ESV, EF, 2D free wall, and septal longitudinal strain were measured. The 3D models of the RV were exported frame by frame throughout the cardiac cycle for further analysis with the ReVISION method.

6.1.6.3. Analyzing intra- and interobserver reproducibility

To assess the intraobserver reproducibility of the parameters, the operator, who performed the first measurements, repeated the 3D reconstruction (using TomTec 4D RV-Function 2) and analysis of the RV models blinded to previous results. Then, a second experienced operator also performed the 3D reconstruction (with TomTec 4D RV-Function 2)

and the ReVISION analysis of the same subjects in a blinded fashion in order to determine interobserver reproducibility.

6.1.6.4. Comparison of ReVISION- and TomTec-derived RV longitudinal strains

Using the first series of measurements taken by the original operator, the correlations were assessed between RV longitudinal strain values computed with the ReVISION method (3D global, free wall, and septal longitudinal strain) and the TomTec 4D RV-Function 2 (2D free wall, and septal longitudinal strain). In the calculation of RV longitudinal strains, an important technical difference should be noted between the two software solutions: the TomTec 4D RV-Function 2 assesses 2D free wall and septal longitudinal strains using 2D standard apical four-chamber views derived from the 3D datasets, whereas the ReVISION method calculates 3D global, free wall, and septal longitudinal strains using the reconstructed 3D meshes of the RV, as described above.

6.1.6.5. Statistical analysis

The intra- and interobserver variability and reliability were evaluated using the intraclass correlation coefficient and the coefficient of variation, respectively. The correlations between the ReVISION- and TomTec-derived longitudinal strain measurements were quantified using Pearson correlation coefficients. A p value <0.05 was considered significant. All statistical analyses were performed in R (version 3.6.2, R Foundation for Statistical Computing, Vienna, Austria).

6.1.7. Comparison of 3DE- and CMRI-derived metrics

6.1.7.1. Study population

Six healthy, sedentary control subjects (3 males, 21±2 years) without any known cardiovascular disease or risk factors, along with six healthy elite athletes of various sports disciplines (4 males, 23±8 years, 15±6 hours of training per week) and six HF patients with reduced LVEF in a stable clinical and hemodynamic condition (5 males, 73±7 years) were retrospectively identified in our database to match our predefined criterion of having a 3DE and a CMRI examination within 30 days. This population was used to investigate the agreement between the 3DE- and CMRI-based 3D RV models concerning the relative contribution of longitudinal, radial, and anteroposterior motion components. All analyses and measurements were performed blinded to the results assessed with the other imaging modality. The study protocol conforms with the principles outlined in the Declaration of Helsinki and the local regulatory and data protection standards [216]. All subjects in our database were enrolled as part of prospective studies (each approved by the Regional and Institutional Committee of Science and Research Ethics, approval No. 13687-0/2011-EKU and 034309-006/2014/OTIG) and provided written informed consent prior to enrollment to the archiving and analysis of their datasets and the publication of subsequent results.

6.1.7.2. 3D echocardiography

Echocardiographic examinations, 3D model reconstruction, and analyses were performed in the same way as explained in the previous section.

6.1.7.3. CMRI protocol

CMRI examinations were conducted using a 1.5 Tesla MRI scanner (Achieva, Philips Medical Systems, Eindhoven, The Netherlands) with a 5-channel cardiac coil. Retrospectively-gated, balanced steady-state free precession cine images were acquired in conventional long- and short-axis views covering the LV and RV. Short-axis cine images were obtained with 8-millimeter slice thickness (no inter-slice gaps), in-plane resolution of 1.5 millimeters x 1.5 millimeters, and temporal resolution of 25 phases per cardiac cycle.

6.1.7.4. Reconstruction of 3D RV meshes from CMR images

After the end-diastolic and end-systolic cardiac phases were identified, the epi- and endocardial layers were manually traced in cine short-axis images, and RV EDV, ESV, and EF were assessed with a dedicated post-processing software solution (Medis Qmass 7.6, Medis, Leiden, The Netherlands). The endocardial contours of the RV were exported to separate files as a series of 2D point coordinates. These files were supplied into a 3D mesh reconstruction pipeline that comprises four consecutive steps: (i) pre-processing of contour data, (ii) creating 3D point clouds from contour data, (iii) re-indexing of the vertices in the 3D point clouds, and (iv) fitting closed surfaces to the 3D point clouds.

In the pre-processing step, a cubic B-spline (containing exactly 200 points) was fitted to the 2D contour points of each slice. To create a 3D object from the 2D contours, point coordinates were converted to millimeters, and the z coordinates were also generated based on the position of the slice along the vertical axis of the RV. The slices were ordered; therefore, the first slice was always the closest to the apex ($z = 0$), and each slice is located 8 millimeters above the previous one. By convention, the center of each point cloud (*i.e.*, set of contour points) was shifted to the origin.

As the next step, the 3D points (*i.e.*, vertices) in the point clouds were re-indexed. With appropriate re-indexing, a vertex with a given index was located approximately at the same anatomical position in the end-diastolic and end-systolic phases, which was essential to perform the motion decomposition. First, the middle slice of the end-systolic point cloud was re-indexed in a way that the mean squared error between the corresponding vertices of the end-diastolic and end-systolic slices became minimal:

$$I^* = \arg\min_I \sum_k \left\| \vec{R}_k - \vec{S}_{I\,(k)} \right\|_2^2$$

where R is the reference slice (*i.e.*, the middle slice of the end-diastolic point cloud), S is the slice that is being re-indexed (*i.e.*, the middle slice of the end-systolic point cloud), and I is the function for re-indexing that returns the corresponding index of the contour point in S for the k^{th} point of R. Then, the same method was applied to re-assign the indices of the remaining slices within each point cloud using the previously re-indexed middle slice as a reference.

Preceding the surface fitting, duplicates of the most basal and apical slices were placed 4 millimeters above and below the original ones. Then, a closed triangle mesh was fitted to the vertices using the surface interpolation algorithm as implemented in the *geomdl* Python library (version 5.2.10) [217]. As a result, the slices were covered by a triangle mesh; however, the top and bottom remained open. To close the top and bottom of the mesh, constrained Delaunay triangulation was performed, ensuring that the triangulation is successful even if the shape of the given object is not convex [218]. Finally, the volume of each mesh was calculated using the shoelace formula.

The entire 3D mesh reconstruction pipeline was implemented in Python (version 3.8.2, Python Software Foundation, Wilmington, Delaware, USA).

To validate the reconstruction process, the RV EDV, ESV, and EF derived from the reconstructed meshes were compared to those computed using the dedicated post-processing software. An excellent agreement was observed in all three metrics [219].

6.1.7.5. Comparison of 3DE- and CMRI-derived metrics

To enable the comparison of 3DE- and CMRI-derived metrics within the same patient, we had to ensure that the meshes are aligned in the same orientation. To that end, 3DE- and CMRI-derived end-diastolic meshes were visualized, and their orientation was adjusted manually by an experienced operator to match the orientation of the 3DE-derived mesh. Then, the rotation matrix was extracted and was applied to the end-systolic CMRI mesh of the same patient as well. After adjusting the orientation of the CMRI-derived meshes, their motion was decomposed as described previously [26].

The correlations between 3DE-derived measurements and the corresponding CMRI-derived values were quantified using Pearson correlation coefficients, and Bland-Altman analyses were performed to assess the bias and limits of agreement. Paired Wilcoxon signed-rank test vs null values was applied to test the significance of the biases. A p value <0.05 was considered significant. All statistical analyses were performed in R (version 3.6.2, R Foundation for Statistical Computing, Vienna, Austria).

6.2. Establishing the normal RV contraction pattern

6.2.1. Normal RV contraction pattern in adults

6.2.1.1. Study population

Healthy volunteers of a wide age range were included from two centers (Semmelweis University, Budapest, Hungary, and University of Occupational and Environmental Health, School of Medicine, Kitakyushu, Japan). Subjects were recruited from a community screening program, medical students, hospital employees, their relatives, and patients referred for cardiology examination without known or subsequently established cardiovascular disease. The study protocol was approved by both centers' institutional ethical review board (approval number: Semmelweis University: 169/2018, University of Occupational and Environmental Health: UOEHCRB18-015), and all participants gave their written informed consent to the study. To adequately assess the effect of ethnicity, age, and gender, both participating centers aimed to enroll at least 150 patients with equal gender distribution across predefined age groups (30 males and 30 females per group). A total of 486 (Hungary: 223, Japan: 263) subjects were screened to achieve the aimed subject number. Thirty-three patients were excluded due to the presence of an exclusion criterion, and 3D RV analysis was not feasible in 15% (n=68) of the cases. The final study population with balanced age, gender, and ethnic distribution was selected from this pool (n=385). A routine physical examination, including anthropometric measurements, was performed in each subject, followed by blood pressure measurement and a 12-lead ECG examination. Body surface area (BSA) was calculated using the Mosteller formula [220]. Inclusion criteria were: age >20 years, no history and/or symptoms of any cardiovascular or pulmonary disease, and absence of cardiovascular risk factors, such as arterial hypertension, diabetes, smoking, and dyslipidemia. Exclusion criteria were: body mass index (BMI) ≥30 kg/m^2, any abnormality on ECG, moderate or severe valvular heart disease or wall motion abnormality and/or LVEF <50% found during echocardiography, poor echocardiographic

windows and factors which may affect cardiac morphology and function, such as pregnancy or regular high-intensity sports activity (>3 hours/week).

6.2.1.2. 2D and 3D echocardiography

Echocardiographic acquisitions were performed on Philips EPIQ 7 (equipped with X5-1 transducer) and GE Vivid E95 (equipped with 4V-D or 4Vc-D transducers) ultrasound systems. Standard acquisition protocol consisting of loops from parasternal, apical, and subxiphoid views was used according to current guidelines [221]. LV internal diameters, wall thicknesses, relative wall thickness, and mass; left atrial (LA) 2D end-systolic volume; mitral inflow velocities such as early (E) and late diastolic (A) peak velocities, their ratio, and E wave deceleration time; systolic (s′), early diastolic (e′), and atrial (a′) velocities of the mitral lateral and septal annulus; and average E/e′ were measured accordingly. RV basal diameter was measured as the maximal transverse dimension in the basal one-third of the RV inflow from the RV-focused apical 4-chamber view on the end-diastolic frame. RV areas and FAC were measured by manual tracing of the RV endocardial border in end-diastole and end-systole. M-mode-derived TAPSE was calculated as the peak longitudinal excursion of the tricuspid annulus. Right atrial volume was estimated using the Simpson method. Systolic (s'), early (e'), and late diastolic (a') velocities at the tricuspid free wall annulus were measured using pulsed wave tissue Doppler imaging (TDI). Peak pulmonary arterial systolic pressure (PASP) was calculated from the tricuspid regurgitant jet signal velocity and right atrial pressure, which was estimated by the inferior vena cava diameter and collapsibility. Reliable measurement of PASP was achievable only in 195 cases; however, the distribution was consistent across age categories and genders (p for trend=0.85).

Beyond the routine echocardiographic protocol, ECG-gated full-volume 3D datasets reconstructed from 4 or 6 cardiac cycles optimized for the right- or left ventricle were obtained for off-line analysis. Image quality was verified at the bedside to avoid “stitching” and “drop-out” artifacts of the 3D data. Further measurements were performed on a separate workstation using dedicated software (4D RV-Function 2 and 4D LV-Analysis 3, TomTec Imaging). The algorithm detects the endocardial surface of the RV and LV, and following manual correction, it traces its motion throughout the cardiac cycle. We determined end-diastolic (EDVi), end-systolic (ESVi), and stroke volume indices (SVi) normalized to BSA, and to characterize global RV and LV functions, EF was also assessed. We measured LV mass index (Mi) normalized to BSA by tracing the end-diastolic epicardial contour. Moreover, LVGLS, LVGCS, 2D RV free wall (FWLS), and septal longitudinal strain were also calculated.

6.2.1.3. Analysis of RV contraction pattern

The 3D RV deformation analysis was previously described in detail. By the decomposition of the model's motion along the three anatomically relevant orthogonal axes, we can measure the volume change of the RV attributable to the according direction separately. Therefore, we were able to measure so-called longitudinal (LEF/RVEF), radial (REF/RVEF), and anteroposterior (AEF/RVEF) EF indexed to the global RVEF. These measures quantify the relative contribution of the given direction to global RV performance. Note that the absolute volume change of the chamber is generated by the aggregated contribution of the three motion components. This composition is not additive, and consequentially, the sum of the decomposed volume changes is not equal to the global volume change – in other words, the relative contribution of the motion components does not add up to 100%. This is attributable to the fact that the decomposition of the RV motion is performed on the end-diastolic frame. By permitting the motion in only one axis and omitting motion in the other axes of the RV, the contribution

of a given motion direction to the global RV volume loss will be mathematically overestimated. We computed 3D RV GLS and GCS as previously described to assess longitudinal and circumferential myocardial deformation.

6.2.1.4. Statistical analysis

Data are presented as mean ± standard deviation (SD). The normal distribution of our variables was confirmed by a Shapiro-Wilk test. Unpaired Student's t tests were used to compare groups, and Pearson tests were performed for correlation analysis. In the case of 3D RV parameters, two-way ANOVA was used with two factors (age and gender), and their interactions were assessed to compare age groups. Repeated measures ANOVA was used to compare the relative contributions in the pooled population and across age categories as well. Multiple linear regression analysis was applied to find independent predictors that determine RV motion components. To avoid multicollinearity issues, tolerance was set as >0.5. p values <0.05 were considered statistically significant.

6.2.2. Normal RV contraction pattern in children

6.2.2.1. Study population

Healthy children aged <18 years were included from two centers: Boston Children's Hospital, Boston, MA, USA; and the Heart and Vascular Center of Semmelweis University, Budapest, Hungary. Subjects at the Boston site were identified retrospectively from an existing database of 3DE images with accompanying clinical and demographic information. Patients in this database had presented to the outpatient clinic between 2014 and 2020 for evaluation of a common cardiac condition (most frequently murmur, chest pain, syncope, or family history of

cardiac condition), and were judged to have a structurally and functionally normal heart, and were discharged from further follow-up. Exclusion criteria included structural abnormalities other than patent foramen ovale or trivial branch pulmonary stenosis (maximum instantaneous gradient < 15 mmHg within the first two years of life); arrhythmia (other than rare atrial or ventricular premature beats) including sinus bradycardia or tachycardia (heart rate z-score < -2 or > +2 for age), acquired heart disease (cardiomyopathy, chemotherapy exposure, and Kawasaki disease), or co-morbidities with a potential impact on ventricular size and function (*i.e.*, hypertension, renal failure, anemia, history of prematurity, chronic lung disease, pulmonary hypertension, obstructive sleep apnea, and connective tissue disorder).

Healthy volunteers at the Semmelweis site were recruited from local schools; no individuals were identified subsequently with significant cardiac abnormalities revealed by echocardiography, ECG, blood pressure measurement, or review of medical history**.** Study protocols were approved by both centers' institutional review boards. Given the retrospective nature of recruitment at Boston Children's Hospital, informed consent was waived at that site. At Semmelweis University, the families of all participants provided written informed consent to participate in the study.

Blood pressure, height, and weight were recorded for all subjects.

6.2.2.2. 2D and 3D echocardiography

Echocardiographic acquisitions were performed using the Philips (iE33 and EPIQ, Philips, Cambridge, MA) and GE (E95, GE Healthcare, Horten, Norway) ultrasound systems, in accordance with the American Society of Echocardiography standards for performing a pediatric echocardiogram [222]. Parameters recorded from the 2D echo images included TAPSE, RV length, FAC, and qualitative assessment of the degree of TR. LV volumes were

calculated from the 5/6 x area x length formula and presented in raw fashion, as well as being indexed to BSA.

In addition to the standard 2D echocardiographic protocol, ECG-gated full-volume 3D data sets reconstructed from four or six cardiac cycles optimized for RV views were obtained for offline analysis. At the Semmelweis site, images were obtained from the apical window using the 4Vc-D transducer (GE Healthcare, Horten, Norway). At the Boston site, images were obtained from the apical or subcostal window using the X5 probe (Philips, Cambridge, MA) in a patient-specific fashion (*i.e.*, the window providing better image quality was used). Image quality was verified at the bedside to minimize stitching and dropout artifacts of the 3D data; breath-holding maneuvers were used as appropriate for the developmental age of the child.

3D datasets were analyzed off-line using dedicated software (4D RV-Function; TomTec Imaging, Unterschleissheim, Germany).

6.2.2.3. Analysis of RV contraction pattern

The 3D RV deformation analysis used has been previously described in detail.

6.2.2.4. Statistical analysis

Continuous data were presented as mean ± SD or median and interquartile range. Categorical data were presented as counts and percentages (% of the total population). Outcomes were summarized according to age groups representing different categories of patient body size: *Infants*: <1 year, *Toddlers* >1 - 5 years, *School-Aged*: >5 - 10 years, *(Pre)Teens* >10 - 18 years. One-way ANOVA or the Kruskal Wallis H test was performed to compare the distribution of parameters by age group as appropriate. Wilcoxon signed-rank test was used to assess for differences in the contribution of LEF, REF, and AEF within each pre-specified age group, with Bonferroni correction applied (*i.e.,* level of statistical significance set at $p<0.017$).

In order to assess the impact of patient sex on the EF parameters, a general linear model was used to compare EF means by sex with adjustment for age to produce least-squares means.

Data analyses were performed with SAS software (version 9.4, SAS Institute Inc., Cary, North Carolina) and R 4.1.2 (The R Foundation for Statistical Computing, Vienna, Austria). p values <0.05 were used to indicate statistical significance.

6.3. Exploring the changes of RV contraction pattern in different clinical scenarios

6.3.1. RV contraction pattern in elite athletes

6.3.1.1. Study population

Healthy, young top-level water polo athletes (n=60, 30 women and 30 men), all members of the national teams in the corresponding age group, were enrolled as a part of our Center's complex sports cardiology screening program (Medical Research Council ETT-TUKEB no. 13687–0/2011-EKU). Study participants gave prior written informed consent to the examinations. All of the measurements were performed during the in-season competition phase and at least 24 hours after the last athletic training. Detailed medical history and training regime were obtained along with a standard physical examination and 12-lead ECG. Echocardiography and then cardiopulmonary exercise testing (CPET) were performed. Subjects with uncommon echocardiographic and/or ECG changes, suboptimal echocardiographic image quality, or athletes who suspended regular training in the last six months were excluded. Twenty female and twenty male age-matched healthy, sedentary volunteers (no previous participation in intensive training, <3 h of exercise/week) served as the control group.

6.3.1.2. 2D and 3D echocardiography, and analysis of RV contraction pattern

Echocardiographic examinations were performed on a commercially available ultrasound system (Philips EPIQ 7G, X5-1 transducer, Best, The Netherlands) as previously described. Beyond conventional echocardiographic examination, ECG-gated full-volume 3D data sets reconstructed from four or six cardiac cycles optimized for the LV or RV were obtained for further analysis on a separate workstation. To characterize global LV function, EF and deformation parameters, such as GLS and GCS, were also assessed. The 3D model of the

RV was exported frame by frame throughout the cardiac cycle for further analysis using ReVISION.

6.3.1.3. Cardiopulmonary exercise testing

Cardiopulmonary exercise testing for peak oxygen uptake (VO_2 and VO_2/kg) quantification was performed on a treadmill on institutional, sport-specific, incremental protocols (starting with a 1-min sitting resting phase, followed by 1–2 min flat walk of 6 km/h as a warm-up, then by continuous 8–10 km/h uphill running with an increasing slope of 1.0–1.5% every minute until exhaustion) [223]. The volume and composition of the expired gases were analyzed breath by breath using an automated cardiopulmonary exercise system (Respiratory Ergostik, Geratherm, Bad Kissingen, Germany). Participants were encouraged to achieve maximal effort. The maximal intensity was considered to be achieved if the athlete reported maximal subjective exhaustion and either the respiratory exchange ratio (RER) was over 1.1 and/or flattening could be seen in the oxygen uptake and the heart rate curves.

6.3.1.4. Statistical analysis

Statistical analysis was performed using dedicated software (Statsoft Statistica, v12, Tulsa, OK). Data are presented as mean ± SD. A Shapiro-Wilk test was used to test normal distribution. Two-way ANOVA with two factors (sex and sport activity) and their interactions (sex × sport) was used to compare groups, and in the case of a significant interaction, Tukey's post hoc analysis was performed to compare the four study groups. A Pearson or Spearman test was applied for correlation analysis as appropriate. p values of <0.05 were considered significant.

6.3.2. RV contraction pattern in adolescent athletes

6.3.2.1. Study population

Healthy, competitive, adolescent athletes were identified (n=215) from our center's complex sports cardiology screening program to be included in a retrospective, cross-sectional study. We defined adolescents as those over the age of 10 and under the age of 18. As an inclusion criterion, all athletes should have 3D transthoracic echocardiographic images available. A detailed medical history and training regime were obtained along with a standard physical examination and a 12-lead ECG. 2D and 3D echocardiography and then CPET were performed on all athletes on the same day (time difference range between investigations: 0 to 3 hours). An age- and sex-matched healthy, sedentary population (n=38) (no previous participation in intensive training, <3 h of exercise/week) served as the control group. These individuals also underwent the aforementioned screening protocol except for CPET. This control group was recruited from local schools on a voluntary basis; no individuals were identified subsequently with significant cardiac abnormalities revealed by echocardiography, ECG, blood pressure measurement, or review of medical history. All participants and/or their legal family representatives provided written, informed consent to the study procedures. This study is in accordance with the Declaration of Helsinki and approved by the local ethics committee.

6.3.2.2. 2D and 3D echocardiography, and analysis of RV contraction pattern

Transthoracic echocardiographic examinations and analysis by ReVISION were performed as previously described.

6.3.2.3. Cardiopulmonary exercise testing

CPET was performed as previously described.

6.3.2.4. Statistical analysis

Using our previous study of a similar methodology with smaller but more balanced sample sizes (60 athletes vs 40 controls) [224], we determined the effect sizes (Cohen's d) of representative parameters that describe left- and right ventricular morphology and function (LV EDVi, LVEF, RVEDVi, RVEF, LEF/RVEF). After calculating Cohen's d, all of these parameters were considered to have a relatively large/medium effect size (Cohen's d values respectively: 2.616, 1.527, 2.418, 1.193, 1.175). Using these calculated effect sizes, we performed a power analysis on the retrospectively identified participants from our database. In all cases, the statistical power exceeded 0.80, reassuring that the outlined sample size that we proposed for our current study was appropriate despite its unbalanced nature. Statistical analysis was performed using dedicated software (StatSoft Statistica, v12, Tulsa, OK, USA). Continuous variables are presented as mean ± SD, whereas categorical variables are reported as frequencies and percentages. After verifying the normal distribution of each variable using the Kolmogorov-Smirnov test, groups were compared with the unpaired Student's t test or Mann–Whitney U test for continuous variables and the $\chi 2$ or Fisher's exact test for categorical variables, as appropriate. The Pearson or Spearman test was computed to assess the correlation between continuous variables. A p value of <0.05 was considered statistically significant.

6.3.3. Comprehensive mechanical characterization of the athlete's heart

6.3.3.1. Study population

Healthy, competitive, elite athletes were retrospectively identified (n=425) from our centre's complex sports cardiology screening program; the majority of them (n=304) are members of the national teams in the corresponding age group. As an inclusion criterion, all athletes should have 3D transthoracic echocardiographic images available. A detailed medical history and training regime were obtained along with a standard physical examination and a 12-lead ECG. 2D and 3D echocardiography and then CPET were performed on all athletes on the same day. We have excluded three athletes due to suboptimal 3D image quality for the analysis of the right ventricle. An age- and sex-matched healthy, sedentary population (no previous participation in intensive training, <3 h of exercise/week) served as the control group. These individuals also underwent the aforementioned screening protocol, including CPET. All participants provided written, informed consent to the study procedures. This study is in accordance with the Declaration of Helsinki and approved by the Medical Research Council (ETT-TUKEB No. 13687-0/2011-EKU).

6.3.3.2. 2D and 3D echocardiography, and analysis of RV contraction pattern

Transthoracic echocardiographic examinations were performed as described above to calculate biventricular volumes, EFs, GLS, and GCS.

6.3.3.3. Cardiopulmonary exercise testing

CPET was performed as described above.

6.3.3.4. Statistical analysis

Statistical analysis was performed using dedicated software (StatSoft Statistica, v12, Tulsa, OK, USA). Continuous variables are presented as mean ± SD, whereas categorical variables are reported as frequencies and percentages. After verifying the normal distribution of each variable using the Shapiro–Wilk test, groups were compared with the unpaired Student's t test or Mann–Whitney U test for continuous variables and the χ^2 or Fisher's exact test for categorical variables, as appropriate. Multiple-group comparisons were performed using one-way analysis of variance (ANOVA, with Fisher's post hoc test) or Kruskal–Wallis test (with Dunn's post hoc test) and two-way analysis of variance (ANOVA, with Fisher's post hoc test) with the factors 'Sex' and 'Exercise' and also with the factors 'Age' and 'Sex'. We also calculated the p value for sex-exercise interaction (P_{Inter}), as well as the p value for age-sex interaction (P_{Inter}). The Pearson or Spearman test was computed to assess the correlation between continuous variables. Concerning LV GLS, LV GCS, RV GLS, and RV GCS, individual values of athletes were normalized to the mean value of the control group to calculate their relative changes. Univariable and multivariable linear regression analysis (using ordinary least squares) were applied to determine the predictors of VO_2/kg in the entire study cohort. The standard errors of the regression coefficients were calculated from 10000 bootstrap resamples. A p value of <0.05 was considered statistically significant.

6.3.4. RV contraction pattern in pulmonary hypertension

6.3.4.1. Study population

This study is a post hoc and exploratory analysis of data from the prospectively recruiting EXERTION study (ClinicalTrials.gov Identifier: NCT04663217). The EXERTION study was in accordance with the principles of the Declaration of Helsinki and was approved

by the local Ethics Committee of the Faculty of Medicine at the University of Giessen (Az: 117/16). All patients gave written informed consent. The inclusion and exclusion criteria for the EXERTION study are outlined elsewhere but briefly discussed here. For the current analysis, patients with atrial fibrillation were excluded because of impaired comparability of cardiac cycles due to altering cycle length. The patients either received initial invasive diagnostic evaluation for suspected PH or were enrolled in the course of a known PH diagnosis. PH was diagnosed in accordance with current guidelines [225]. The diagnoses were made by a multidisciplinary board comprising pneumologists and radiologists. If PH was excluded at the initial invasive diagnostic evaluation, the patient was classed as a control. All patients underwent echocardiography, including 3D and strain echocardiography, as well as right heart catheterization with a fluid-filled balloon-tipped thermodilution catheter and a conductance catheter to measure RV pressures and volumes (Figure 7A, B). The interval between echocardiography and right heart catheterization was mainly one day (four patients received echocardiography within three days of right heart catheterization, and two patients within five days). In each case, no adjustment of relevant medication, especially PH-specific medication and diuretics, was performed during the interval between echocardiography and right heart catheterization.

6.3.4.2. 2D and 3D echocardiography, and analysis of RV contraction pattern

Echocardiography and ReVISION analyses were performed as described previously.

6.3.4.3. Right heart catheterization

All participants underwent a standard right heart catheterization in conformance with updated guidelines [225] to measure mean pulmonary artery (PA) pressure (mPAP), central

venous pressure, RV pressure, and PA wedge pressure (PAWP). Cardiac output (CO) was measured by the (in-)direct Fick method in all patients (35 patients [66%] with the direct Fick method). Cardiac index was defined as the ratio of CO and calculated BSA. Pulmonary vascular resistance (PVR) was calculated as PVR = (mPAP – PAWP) / CO. Concerning RV conductance catheterization, a 4F conductance catheter (CA-No. 41063, CD Leycom, Zoetermeer, the Netherlands, see Figure 7A) was inserted into the internal jugular vein via an 8F introducer sheath. The catheter was positioned within the RV with the catheter tip reaching apically under echocardiographic guidance and supervision of PV loops, which were simultaneously obtained by the intracardiac analyzer (Inca, CD Leycom). PV loops were displayed on-screen in real-time for consecutive cardiac cycles and were calibrated to resting volumetry derived from 3DE. The multi-beat method was applied to determine end-systolic elastance (Ees) and arterial elastance (Ea). Sequential resting PV loops were initially recorded. The Valsalva maneuver was then executed for preload reduction, resulting in a stepwise leftward shift of end-systolic PV points of consecutive loops, which were concatenated by a regression line representing the end-systolic PV relationship (ESPVR). The intersection of the ESPVR and the x-axis determined V0 (Figure 7C), which theoretically represents the unstressed RV volume. A line was constructed connecting V0 and the end-systolic PV coordinate of a resting PV loop, and Ees was determined as the slope of that line. Ea was determined as the ratio of RV end-systolic pressure to stroke volume (Figure 7C). PV loops were recorded successively and were checked for suitability. Three to five applicable PV loops were included for each patient, and mean values were calculated for both Ees and Ea. End-diastolic elastance (Eed) was calculated as the end-diastolic PV relationship ($dP/dV = \alpha * \beta * e^{(\beta * EDV)}$; see Figure 7C) averaged on three PV loops.

The study population was divided into three groups according to RV-PA coupling. Severe RV-PA uncoupling was defined as Ees/Ea < 0.8. Near-normal and intermediate RV-PA

uncoupling were defined based on the median Ees/Ea value in the remaining patients: Ees/Ea below the median value was classed as intermediate uncoupling, and Ees/Ea equal to or greater than the median value was classed as no or mild uncoupling.

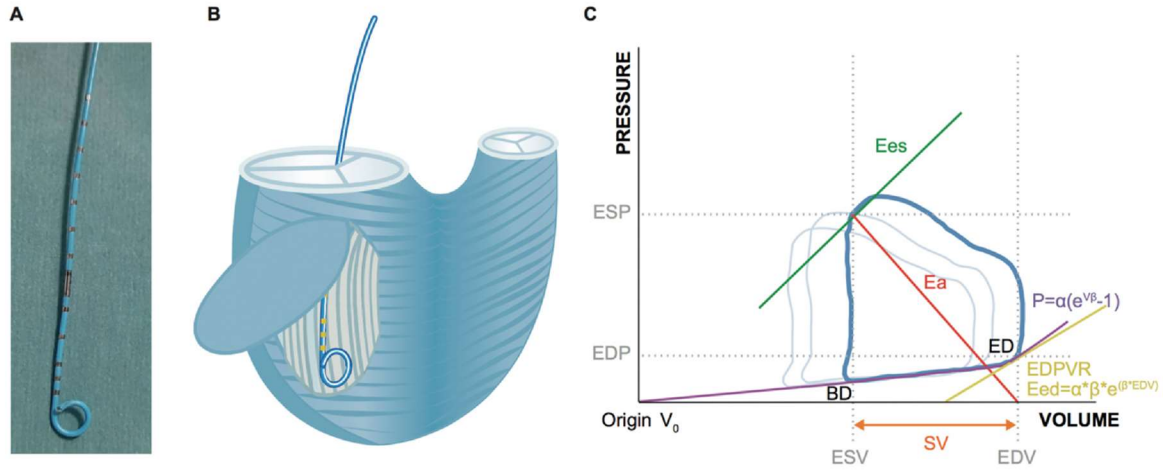

Figure 7. Conductance catheterization of the right ventricle. (A) A conductance catheter. The electrodes generate a segmented electric field within the RV lumen. Conductivity alters with RV volume alteration, and volume can be derived in real time. Pressure is measured simultaneously, allowing the generation of PV loops. (B) Model of the RV myocardium with a correctly positioned conductance catheter (apical pigtail and all electrodes within the right ventricle). Subendocardial myofibers are longitudinally orientated, whereas subepicardial myofibers run radially. (C) PV loop schematic showing derived parameters. α: curve fit parameter, β: end-diastolic stiffness, BD: beginning of diastole, Ea: arterial elastance, ED: end of diastole, EDP: end-diastolic pressure, EDPVR: end-diastolic PV relationship, EDV: end-diastolic volume, Eed: end-diastolic elastance, Ees: end-systolic elastance, ESP: end-systolic pressure, ESV: end-systolic volume, P: pressure, RV: right ventricular, SV: stroke volume, V: volume, V0: pressure-released volume

6.3.4.4. Hemodynamic risk stratification

Risk assessment was performed per the current European Society of Cardiology/European Respiratory Society (ESC/ERS) guidelines [225]. A truncated version of the ESC/ERS risk stratification scheme, including cardiac index, indexed SV (SVi), central venous pressure, and mixed venous oxygen saturation, was applied. Each hemodynamic variable was graded in a 3-strata model where 1 = ‘Low risk’, 2 = ‘Intermediate risk’, and 3 = ‘High risk’. Dividing the sum of all grades by the number of available variables for each patient

rendered a mean grade. The mean grade was rounded off to the nearest integer, which was used to define the patient's hemodynamic risk group.

6.3.4.5. Statistical analysis

The Shapiro-Wilk test for normality was applied to each parameter included. Normally distributed data are presented as mean ± SD. Non-normally distributed data are presented as median [interquartile range]. To assess differences between groups, we used Chi-square tests for categorical data, t tests for normally distributed continuous data, and Wilcoxon rank tests for continuous data with a non-normal distribution. Receiver operating characteristic analyses were performed to assess the discriminatory power of parameters for the detection of patients at high risk. Each analysis was performed in R version 4.0 (The R Foundation for Statistical Computing, Vienna, Austria); $p<0.05$ indicated statistical significance.

6.3.5. RV contraction pattern after heart transplantation

6.3.5.1. Study population

From December 2014 to January 2017, we retrospectively collected those echocardiograms of HTX recipients, followed by our Center, where transthoracic 3D datasets were acquired and suitable for further analysis (n=66). Those patients who were already discharged from the intensive care unit after HTX or arrived to regular follow-up visits were included. Exclusion criteria were (i) hemodynamic instability and/or need for inotropic agents; (ii) previous rejection ≥ ISHLT grade 2R or ≥ pAMR2; (iii) postoperative need for ventricular assist device; (iv) severe TR or any severe valvular disease; (v) non-sinus rhythm on ECG; (vi) diagnosis of chronic allograft vasculopathy; (vii) suboptimal 3DE image quality (inadequate

visualization of the entire RV endocardial surface inclusive of RV outflow tract - also confirmed on short-axis planes—and/or the presence of stitching artifacts). Finally, 51 patients were included in the current analysis. An age- and gender-matched control population (n=30) was selected with a normal echocardiographic report without any known cardiovascular or other diseases and free from any medication using our existing database of healthy volunteers. To create a relevant database, each patient's medical history, preoperative, intraoperative, and follow-up data were collected using the in-hospital electronic medical records. In both groups, anthropometric, blood pressure, and heart rate values were determined at the time-point of the analyzed echocardiogram.

6.3.5.2. 2D and 3D echocardiography, and analysis of RV contraction pattern

Echocardiography and ReVISION analyses were performed as described previously.

6.3.5.3. Statistical analysis

Data are presented as mean ± SD or median (interquartile range). Shapiro-Wilk test was used to test normal distribution. Based on that, unpaired Student's t test or Mann-Whitney U test was used to compare groups. A chi-square test was applied to compare categorical variables. A one-way ANOVA was used to compare the three wall motion components' relative contribution, followed by Tukey's post hoc test. Pearson's or Spearman's test was performed for correlation analysis as appropriate. p values <0.05 were considered significant.

6.4. Establishing the added prognostic value of 3D RV assessment

6.4.1. Added prognostic value of 3D echocardiography over conventional RV functional measures

6.4.1.1. Study population

Clinically, hemodynamically stable patients who underwent clinically indicated transthoracic echocardiography at the Semmelweis University Heart and Vascular Center between May 2015 and May 2019 were retrospectively identified. Inclusion criteria were: (1) 18 years of age or older; (2) established left-sided cardiac disease with previous or planned cardiac intervention or surgery with any value of LV and RVEF; (3) 3D images obtained suitable for 3D LV and RV quantification; (4) availability of 2-year follow-up data. Exclusion criteria were: (1) primary RV diseases (primary pulmonary hypertension, arrhythmogenic cardiomyopathy, congenital heart diseases affecting the right heart); (2) acute cardiovascular conditions (acute coronary syndrome, myocarditis, pulmonary embolism, etc.); (3) inadequate echocardiographic image quality. Clinical characteristics, such as demographics, medical history, physical status and vitals, and laboratory parameters, were extracted retrospectively from electronic medical records. Our retrospective study is in accordance with the Declaration of Helsinki and was approved by the Regional and Institutional Committee of Science and Research Ethics.

6.4.1.2. 2D and 3D echocardiography

Echocardiography analyses were performed as described above.

6.4.1.3. Study outcomes

Follow-up data [status (dead or alive), date of death] was obtained from Hungary's National Health Insurance Database. The primary endpoint of our study was all-cause mortality at two years.

6.4.1.4. Statistical analysis

Continuous variables are expressed as mean ± SD, whereas categorical variables were reported as frequencies and percentages. After the verification of the normal distribution of variables using the Shapiro-Wilk test, the clinical and echocardiographic characteristics were compared with unpaired Student's t test or Mann-Whitney U test for continuous variables, and Chi-squared or Fisher's exact test for categorical variables, as appropriate. Cox proportional hazard models were used to compute hazard ratios (HR) with 95% confidence intervals (95% CI). Receiver-operator characteristic (ROC) curves were generated to assess the discriminatory power of RV systolic functional parameters with regard to the endpoint. Youden's index was used to identify each parameter's optimal cut-off points; these values were then used to dichotomize the study population. Outcomes of the dichotomized groups were visualized on Kaplan-Meier curves and compared by log-rank test. A p value <0.05 was considered statistically significant. Analysis was performed in R (version 3.6.2, R Foundation for Statistical Computing, Vienna, Austria).

6.4.2. Added prognostic value of 3D echocardiography over conventional RV functional measures – meta-analysis

6.4.2.1. Data sources and study selection

Our meta-analysis was conducted according to the Meta-analysis Of Observational Studies in Epidemiology (MOOSE) Guidelines [226]. The study protocol was preregistered on PROSPERO (registration number CRD42018110771). Two collaborators independently assessed articles from PubMed and EMBASE from inception until 11 March 2022 using a predefined search strategy with the following inclusion criteria: (1) English language studies published in peer-reviewed scientific journals; (2) studies reporting original investigations on human subjects; (3) adult age (>18 years) of all included participants; (4) studies with more than 20 subjects; (5) studies with 3DE performed and RVEF measured; (6) studies with all-cause mortality and/or adverse cardiopulmonary outcomes reported as hazard ratios (HRs, and 95% confidence intervals, CI) per unit change in 3DE-derived RVEF; and (7) at the same time, on the same cohort, reported at least one of the following RV functional parameters: TAPSE, FAC or FWLS. A manual reference check of eligible full-text articles was performed to identify studies missed by our systematic search. Disagreement was resolved by consensus. When separate publications from the same research group on seemingly overlapping cohorts were identified, the study involving the higher number of subjects was included in our final analysis.

6.4.2.2. Data extraction and quality assessment

Data were extracted on study design, baseline characteristics of the cohorts, echocardiographic parameters, feasibility and interobserver reproducibility of RVEF, and the predefined outcomes for all included studies by two collaborators. Study quality was ascertained using the Quality In Prognosis Studies (QUIPS) tool in consensus [227].

6.4.2.3. Data synthesis and analysis

HRs and respective 95% CIs reporting the association between the unit change of the prespecified echocardiography-derived RV functional parameters (RVEF and TAPSE, or FAC, or FWLS) and clinical outcomes were extracted from eligible publications. We limited our inclusion to studies that allocated HRs for RVEF and TAPSE, or FAC, or FWLS to the same endpoint within each study, as per the inclusion criteria. The majority of studies reported HRs and 95% CIs relative to 1 unit increase in 3D RVEF (1% increase), TAPSE (1mm increase), FAC (1% increase), and FWLS (1% increase in absolute value). Others reported these effect sizes per SD change [228]. To facilitate comparison of RVEF with TAPSE, FAC, and FWLS, all HRs and 95% CIs were rescaled by the within-study SD of the respective echocardiographic parameter to present a standardized change in the absolute value of each parameter (RVEF and TAPSE, or FAC, or FWLS) as previously described [33]. Each SD reduction in the given echocardiographic parameter represents an increase in hazard, resulting in direct comparability of the predictive value of these parameters. Then, the difference in logHRs (log of the ratio of HRs) of RVEF versus TAPSE, FAC, or FWLS, respectively, were calculated within each study, and these estimates were pooled using a random-effects model (DerSimonian-Laird). This derived the pooled estimate and 95% CI, which was then transformed to be on the HR scale to quantify the association of RVEF with adverse clinical outcomes relative to the other metrics. A ratio of >1.00 denotes that 1 SD reduction in RVEF is related to a greater hazard increment relative to 1 SD reduction in the other metric. Therefore, these pooled estimates represent the overall difference in association of 1 SD reduction in RVEF versus 1 SD reduction in TAPSE, FAC, or FWLS, respectively. Forest plots were generated to visualize these differences. Statistical heterogeneity (referred to as heterogeneity) was assessed using the Cochran Q homogeneity test, and Higgins and Thompson I^2 [229]. The I^2 heterogeneity was categorized as follows: 0-50% low, 50-75% moderate, >75% high. As a post hoc analysis using mixed-

effects meta-regression, we explored whether follow-up duration, differences in baseline disease of cohorts (primary diagnosis of pulmonary hypertension vs other cardiopulmonary conditions), or the type of endpoints (mortality only vs composite) explained heterogeneity of the pooled estimates, yielding pseudo-R^2 values (which refers to the percentage of heterogeneity explained by the given variable). Additionally, we performed a subgroup analysis to compare the pooled estimates of studies reporting on cohorts with a primary diagnosis of PH versus those that included patients with other cardiopulmonary conditions.

All statistical analyses were performed in Stata 17.0 (StataCorp LLC, College Station, TX, USA). A two-tailed $p<0.05$ was considered statistically significant.

6.4.2.4. Sensitivity analyses

Funnel plots were constructed to visually inspect the small-study effect (corresponding to publication bias) according to each echocardiographic parameter and related clinical outcomes. The nonparametric Begg's rank correlation test was used to quantify the association between the effect sizes and measures of precision (standard errors). Nonparametric trim-and-fill analysis, as per Duval and Tweedie, was performed to correct for the small-study effect using the R0 estimator [230]. We used the DerSimonian Laird random-effects method for both the iteration and pooling steps during the trim-and-fill analyses.

6.4.3. Perioperative changes and prognostic value of RV contraction pattern in patients with severe mitral regurgitation

6.4.3.1. Study population

Between October 2016 and November 2018, we prospectively screened 154 patients with severe primary mitral valve regurgitation (MR) who were referred to open-heart mitral valve replacement or repair (MVR) at the Heart and Vascular Center of Semmelweis University. Patients with LV or RV dysfunction (3DE LVEF < 50% or RVEF < 45% at enrolment, respectively), history of cardiac surgery, pulmonary embolism, primary pulmonary hypertension, infective endocarditis, primary cardiomyopathies, moderate-to-severe aortic valve disease, moderate-to-severe mitral stenosis, severe TR, severe chronic obstructive pulmonary disease, congenital heart disease, malignancy, irregular heart rhythm inhibiting 3D reconstruction, or inadequate echocardiographic image quality (2D or 3D) were excluded. In total, 72 patients were enrolled. In the present study, we focused on the analysis of those 42 patients who underwent perioperative pulmonary artery catheterization (PAC) as well. Thirty age-matched and gender-matched healthy volunteers (no history and/or symptoms of any cardiovascular or pulmonary disease, and absence of cardiovascular risk factors, such as arterial hypertension, diabetes, smoking, and dyslipidaemia) served as the control group. The protocol of the PREPARE-MVR study (Figure 8, ClinicalTrials.gov Identifier: NCT03438825) conforms with the principles outlined in the Declaration of Helsinki, and it was approved by the Regional and Institutional Committee of Science and Research Ethics (approval No. 2016/175). All study participants provided written informed consent.

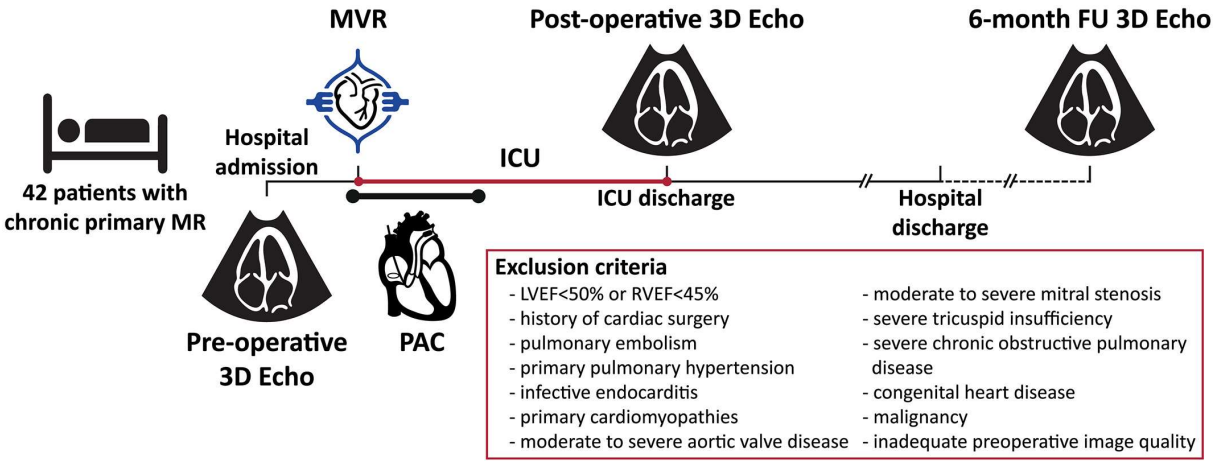

Figure 8. Outline of the PREPARE-MVR study protocol. FU: follow-up, ICU: intensive care unit, LVEF: left ventricular ejection fraction, MR: mitral regurgitation, MVR: mitral valve replacement/repair, PAC: pulmonary artery catheterization, RVEF: right ventricular ejection fraction

6.4.3.2. 2D and 3D echocardiography, and analysis of RV contraction pattern

Echocardiographic examinations were performed on a commercially available ultrasound system (GE Vivid E95, 4Vc-D probe, Horten, Norway). All patients underwent comprehensive 2D and 3D echocardiographic evaluation pre-operatively (1 day prior to surgery) and at intensive care unit (ICU) discharge. A follow-up echocardiogram (2D and 3D) was also acquired six months after surgery. Owing to inadequate post-operative image quality or new-onset atrial fibrillation, seven patients were excluded from further follow-up by 3DE. The volume of MR and the effective regurgitant orifice area (EROA) were measured using the proximal isovelocity surface area (PISA) method. Severe MR was defined by an EROA > 40 mm^2 and regurgitant volume > 60 ml [231]. The left atrial ESVi (LAESVi) was calculated by 4D LALV function (TomTec Imaging, Unterschleissheim, Germany). All other echocardiographic and ReVISION analyses were performed as described above.

6.4.3.3. Pulmonary artery catheterization

All patients underwent PAC pre-operatively, and the hemodynamic monitoring was extended for the first 24 hours postoperatively. Seven standard time points of measurements (2, 4, 6, 8, 12, 16, and 24 hours after surgery) were averaged to calculate mean postoperative values. Central venous pressure (CVP), systolic, diastolic, and mean pulmonary artery pressure (mPAP), PAWP, PVR, RVSVi, and CO were monitored. Diastolic pressure gradient (DPG) was computed as the difference between diastolic PAP and PAWP. To quantify RV function invasively, the RV stroke work index (RVSWi) was calculated as (mPAP − CVP) * RVSVi. Postoperative RVD was defined as RVSWi < 300 mmHg·ml/m^2 [3].

6.4.3.4. Statistical analysis

Continuous values are expressed as median [inter-quartile range]. Normal distribution was tested using the Shapiro–Wilk test. Group comparisons (controls vs patients) were performed using Student's t test or Mann–Whitney U test, as appropriate. Linear regression models were created to assess the association between continuous variables. To compare echocardiographic parameters from the three predefined time points, one-way repeated measures ANOVA with Tukey's post hoc test or Friedman test with Nemenyi post hoc test was performed depending on normality. Logistic regression models were built to predict postoperative RVD from parameters assessed preoperatively. All linear and logistic regression models were adjusted for age, gender, type of surgery, and tricuspid valve repair. A p value of < 0.05 was considered significant in all tests. All statistical analyses were performed in R (version 3.4.1, R Foundation for Statistical Computing, Vienna, Austria).

6.4.4. Added prognostic value of circumferential RV mechanics in left-sided cardiac diseases

6.4.4.1. Study population

Clinically and hemodynamically stable patients with an established diagnosis of left-sided cardiac disease were identified from the previously published RVENet dataset [https://rvenet.github.io/dataset/], which comprises individuals who underwent clinically indicated 2D and 3D transthoracic echocardiography at our Center between November 2013 and March 2021. Exclusion criteria were 1) suspicion or presence of any primary right-sided cardiac disease at the first report or during the review process of the previously acquired datasets and 2) suboptimal LV and RV 3D dataset image quality for the respective 3D analysis. Demographic and clinical data (age, body surface area, body mass index, systolic and diastolic blood pressure, heart rate, cardiovascular risk factors, comorbidities, medical history, and laboratory parameters) were retrieved from the electronic clinical records. Obtaining written informed consent was waived due to the retrospective nature of the analysis. Our study protocol follows the Declaration of Helsinki, which was approved by the Semmelweis University Regional and Institutional Committee of Science and Research Ethics (approval No. 190/2020).

6.4.4.2. 2D and 3D echocardiography, and analysis of RV contraction pattern

Transthoracic echocardiographic examinations were performed as previously described to quantify biventricular volumes, EFs, GLS, and GCS.

6.4.4.3. Study outcomes

The patients were followed up for a maximum of 6 years. Follow-up data (status [dead or alive], date of death) was obtained from Hungary's National Health Insurance Database. The primary endpoint of our study was all-cause mortality.

6.4.4.4. Statistical analysis

Statistical analysis was performed using SPSS (v22, IBM, Armonk, NY, USA) and R (version 3.6.2, R Foundation for Statistical Computing, Vienna, Austria). Continuous variables are expressed as mean ± SD, whereas categorical variables were reported as frequencies and percentages. After verifying the normal distribution of variables using the Shapiro-Wilk test, the clinical and echocardiographic characteristics were compared with unpaired Student's t test or Mann-Whitney U test for continuous variables, and Chi-squared or Fisher's exact test for categorical variables, as appropriate. Multiple group comparisons (>2) were performed using ANOVA (with Tukey post hoc test) or Kruskal-Wallis test (with Dunn post hoc test) and $\chi 2$ or Fisher exact test, as appropriate. Using univariable Cox regression, we identified factors associated with all-cause mortality. Targeting a maximum of 1 covariate per 10 events, we built several sequential multivariable Cox proportional hazards models. First, we constructed a baseline model that included only clinical and laboratory parameters, and then, in two consecutive steps, we added different LV and RV functional parameters to the model. As the final step, the constructed multivariable models were compared based on the Akaike Information Criterion (AIC) to determine which one is the best fit for our data. Collinearity was tested using the variance inflation factor (excessive if variance inflation factor >3). The survival of the subgroups was visualized via Kaplan-Meier curves, and the results were compared using log-rank tests. Cox proportional hazard models were used to compute HRs with 95% CIs

between the groups. ROC curves were constructed to investigate the discriminative power of 2D and 3D echocardiographic parameters with regard to the primary endpoint. Metrics with more than 10% missing values were not included in these analyses. A p value of <0.05 was considered statistically significant.

6.4.5. Changes and prognostic value of RV contraction pattern in different degrees of LV systolic dysfunction

6.4.5.1. Study population

Consecutive patients with sinus rhythm and left-sided heart disease who underwent clinically indicated transthoracic echocardiography between October 2010 and December 2012 at the University of Padua (Italy) were enrolled in a single-center prospective observational study. The following inclusion criteria were used: 18 years of age or older; left-sided structural heart disease with any value of LVEF; recordings of both LV and RV 3DE full-volume data sets; sufficient image quality and volume rate to measure LV and RV volumes; availability of follow-up data. Exclusion criteria were: primary RV disease (*e.g.*, arrhythmogenic RV cardiomyopathy); primary tricuspid or pulmonary valve disease; severe TR (even if functional or pacemaker-related); congenital heart diseases affecting the right heart; type I, III, IV or V PH; pericardial diseases; acute myocarditis. Demographic and clinical data (age, weight, height, BSA, BMI, cardiovascular risk factors, and comorbidities) were retrieved from the electronic clinical records of the hospital database. The study was approved by the local Ethics Committee and carried out according to the principles of the Declaration of Helsinki. Participants provided their written informed consent.

6.4.5.2. 2D and 3D echocardiography, and analysis of RV contraction pattern

Patients underwent complete echocardiographic examination at baseline, including both conventional and 3DE data acquisition using the Vivid E9 system (GE Vingmed Ultrasound, Horten, Norway) equipped with M5S and 4V-D probes. Echocardiographic and ReVISION analyses are described above.

LVEF was classified as normal (≥50%), mildly reduced (50%>EF≥40%), moderately reduced (40%>EF≥30%), or severely reduced (<30%). RVEF was classified as normal (>45%) or reduced (≤45%).

6.4.5.3. Study outcomes

The primary endpoint of our study was the composite of the first HF hospitalization (defined as hospital admission due to worsening signs and symptoms of HF, requiring intravenous treatment aimed predominantly at managing fluid overload and hemodynamic compromise) or cardiac death (defined as death resulting from an acute myocardial infarction, heart failure, cardiovascular procedures, and sudden cardiac death), whichever occurred first. Follow-up data were collected by an investigator who was not involved in the echocardiographic measurements through the analysis of clinical records and telephone contacts to patients, physicians, or the next of kin when the patient was not available. The last follow-up update was performed on 10 July 2019, and 13 patients (4.5%) were lost to follow-up.

6.4.5.4. Statistical analysis

Continuous variables were expressed as mean ± SD or median [interquartile range], whereas categorical variables were reported as frequencies and percentages. After verifying the normal distribution of each variable using the Shapiro-Wilk test, the clinical and echocardiographic characteristics of patient subsets were compared with unpaired Student's t test or Mann-Whitney U test for continuous variables, and Chi-squared or Fisher's exact test for categorical variables, as appropriate. Multiple group comparisons (>2 groups) were performed using ANOVA (with Tukey's post hoc test) or Kruskal-Wallis test (with Dunn's post hoc test) and Chi-squared or Fisher's exact test, as appropriate. Spearman's rank correlation coefficients were computed to assess the correlation between continuous variables. Cox proportional hazard models were used to compute HRs with 95% CI. Including significant variables identified in the univariable Cox regression analysis, multivariable Cox regression models were built to identify independent predictors of outcomes. The collinearity of variables was tested at each multivariable model using the variance inflation factor (excessive if VIF>3). HR values of LEF/RVEF, REF/RVEF, and AEF/RVEF refer to the effect of 0.01 unit change. Variables with >10% missing values were not included in multivariable analyses. ROC curves were generated to assess the discriminatory power of RV systolic functional parameters with regard to the composite endpoint. Youden’s index was used to identify the optimal cut-off points of each parameter, and these values were used to dichotomize the study population. Outcomes of the dichotomized groups were visualized on Kaplan-Meier curves and compared by log-rank test.

A p value of <0.05 was considered statistically significant. Statistical analysis was performed in R (version 3.6.2, R Foundation for Statistical Computing, Vienna, Austria).

7. Results

7.1. Development and validation of a software tool to quantify RV contraction patterns

7.1.1. Reproducibility of global and segmental RV metrics

The results of the intra- and interobserver variability and reliability analyses are summarized in Tables 1 and 2. Reproducibility of global EDV, ESV, and decomposed ESVs was high, which is consistent with our previous reports using the earlier versions of the ReVISION software. Regarding the 15 segments, a smooth base-to-apex gradient could be observed (Table 2, Figures 9 and 10), with the inflow tract and basal segments having the lowest variability and the highest reliability and free wall apical segments exhibiting the highest variability and the lowest reliability. As the orientation adjustment, the motion decomposition, the volumetric segmentation, and the calculation of metrics are fully automated; it should be emphasized that the observed intra- and interobserver variability is related exclusively to the 3D RV model reconstruction that is performed using TomTec 4D RV-Function 2.

Table 1. 3DE parameters measured by the two operators in the reproducibility analysis.

	Operator 1		**Operator 2**
	1st measurements	2nd measurements	
3D RVEDV, ml	167.5 ± 63.1	174.2 ± 66.3	183.2 ± 64.3
3D RVESV, ml	95.4 ± 55.7	98.4 ± 60.6	99.8 ± 56.2
LESV, ml	134.2 ± 58.6	140.8 ± 63.5	144.9 ± 60.5
RESV, ml	131.2 ± 55.2	135.3 ± 59.5	143.4 ± 58.4
AESV, ml	130.9 ± 62.8	135.9 ± 66.7	141.0 ± 62.9
3D RVGLS, %	-17.6 ± 7.1	-18.5 ± 7.9	-18.4 ± 7.5
3D RVGCS, %	-19.5 ± 9	-20.7 ± 9.4	-19.4 ± 7.5
3D RVGAS, %	-31.6 ± 12.2	-32.8 ± 13.2	-33.2 ± 12.1
Outflow tract EDV, ml	47.9 ± 19.0	51.5 ± 21.0	55.9 ± 20.4
Outflow tract ESV, ml	29.5 ± 15.9	31.6 ± 18.3	31.8 ± 17.1
Inflow tract EDV, ml	33.9 ± 12.5	35.2 ± 13.7	34.4 ± 12.8
Inflow tract ESV, ml	22.8 ± 11.2	24.5 ± 13.3	22.9 ± 12.8
FW basal anterior EDV, ml	14.3 ± 7.4	14.5 ± 6.5	16.0 ± 6.3
FW basal anterior ESV, ml	7.1 ± 5.6	6.8 ± 5.3	7.3 ± 4.7
FW basal lateral EDV, ml	11.7 ± 5.0	11.7 ± 4.5	12.3 ± 4.4
FW basal lateral ESV, ml	5.3 ± 4.0	5.2 ± 3.9	5.5 ± 3.6
FW basal posterior EDV, ml	8.5 ± 3.9	8.5 ± 4.0	8.4 ± 3.5

FW basal posterior ESV, ml	4.5 ± 3.2	4.5 ± 3.4	4.6 ± 3.2
Sept. basal posterior EDV, ml	8.3 ± 3.4	8.5 ± 3.2	9.2 ± 3.3
Sept. basal posterior ESV, ml	4.4 ± 3.0	4.2 ± 2.9	4.5 ± 2.7
Sept. basal anterior EDV, ml	6.5 ± 2.8	6.6 ± 2.7	6.7 ± 2.6
Sept. basal anterior ESV, ml	3.6 ± 2.4	3.6 ± 2.4	3.7 ± 2.3
FW mid anterior EDV, ml	8.5 ± 4.5	8.8 ± 4.2	9.8 ± 4.3
FW mid anterior ESV, ml	4.1 ± 3.4	3.8 ± 3.2	4.3 ± 2.9
FW mid lateral EDV, ml	7.3 ± 3.1	7.4 ± 3.0	7.9 ± 3.2
FW mid lateral ESV, ml	3.2 ± 2.3	3.1 ± 2.3	3.4 ± 2.2
FW mid posterior EDV, ml	3.8 ± 1.7	3.8 ± 1.7	3.8 ± 1.8
FW mid posterior ESV, ml	1.9 ± 1.3	1.9 ± 1.4	1.9 ± 1.4
Sept. mid posterior EDV, ml	5.2 ± 2.2	5.4 ± 2.3	5.8 ± 2.5
Sept. mid posterior ESV, ml	2.7 ± 1.9	2.7 ± 1.9	2.9 ± 1.8
Sept. mid anterior EDV, ml	3.5 ± 1.4	3.6 ± 1.4	3.7 ± 1.5
Sept. mid anterior ESV, ml	1.9 ± 1.3	1.9 ± 1.2	2.0 ± 1.2
FW apical anterior EDV, ml	2.1 ± 1.3	2.2 ± 1.3	2.5 ± 1.4
FW apical anterior ESV, ml	1.1 ± 1.0	1.1 ± 1.1	1.2 ± 1.0
FW apical posterior EDV, ml	1.1 ± 0.6	1.1 ± 0.5	1.2 ± 0.7
FW apical posterior ESV, ml	0.5 ± 0.4	0.5 ± 0.4	0.6 ± 0.4
Apex EDV, ml	5.1 ± 2.5	5.2 ± 2.3	5.5 ± 2.8
Apex ESV, ml	3.0 ± 2.1	2.9 ± 2.1	3.2 ± 2.2

AESV: anteroposterior end-systolic volume, EDV: end-diastolic volume, ESV: end-systolic volume, FW: free wall, GAS: global area strain, GCS: global circumferential strain, GLS: global longitudinal strain, LESV: longitudinal end-systolic volume, RESV: radial end-systolic volume, RV: right ventricular, Sept.: septum

Table 2. Intra- and interobserver variability and reliability of global and segmental right ventricular metrics.

	Intraobserver reproducibility		**Interobserver reproducibility**	
	ICC (95% CI)	CV	ICC (95% CI)	CV
3D RVEDV	0.945 (0.898 - 0.970)	5.840 %	0.902 (0.758 – 0.953)	9.298 %
3D RVESV	0.955 (0.918 – 0.975)	6.529 %	0.947 (0.904 – 0.971)	9.131 %
LESV	0.943 (0.895 – 0.969)	6.525 %	0.920 (0.836 – 0.959)	9.471 %
RESV	0.938 (0.889 – 0.966)	6.514 %	0.895 (0.785 – 0.946)	10.333 %
AESV	0.952 (0.912 – 0.974)	6.761 %	0.932 (0.862 – 0.965)	10.322 %
3D RVGLS	0.937 (0.881 – 0.966)	9.296 %	0.911 (0.841 – 0.951)	12.240 %
3D RVGCS	0.944 (0.892 – 0.971)	11.588 %	0.845 (0.731 – 0.913)	18.011 %
3D RVGAS	0.972 (0.946 – 0.985)	5.995 %	0.951 (0.902 – 0.975)	8.271 %
Outflow tract EDV	0.818 (0.686 – 0.898)	10.448 %	0.674 (0.422 – 0.819)	17.711 %
Outflow tract ESV	0.854 (0.745 – 0.918)	11.670 %	0.787 (0.639 – 0.879)	16.414 %
Inflow tract EDV	0.895 (0.815 – 0.942)	5.889 %	0.883 (0.793 – 0.935)	9.119 %
Inflow tract ESV	0.919 (0.855 – 0.956)	7.357 %	0.914 (0.843 – 0.953)	9.414 %
FW basal anterior EDV	0.878 (0.786 – 0.932)	9.999 %	0.803 (0.645 – 0.892)	16.974 %
FW basal anterior ESV	0.907 (0.834 – 0.949)	13.648 %	0.864 (0.763 – 0.924)	19.973 %
FW basal lateral EDV	0.919 (0.856 – 0.956)	8.499 %	0.856 (0.749 – 0.920)	12.475 %
FW basal lateral ESV	0.938 (0.888 – 0.966)	12.626 %	0.904 (0.829 – 0.947)	16.693 %
FW basal posterior EDV	0.937 (0.887 – 0.966)	8.528 %	0.892 (0.810 – 0.940)	13.269 %
FW basal posterior ESV	0.940 (0.892 – 0.967)	10.607 %	0.918 (0.853 – 0.955)	14.988 %
Sept. basal posterior EDV	0.888 (0.802 – 0.938)	9.302 %	0.806 (0.650 – 0.893)	13.187 %

Sept. basal posterior ESV	0.926 (0.868 – 0.960)	12.383 %	0.868 (0.769 – 0.927)	16.650 %
Sept. basal anterior EDV	0.938 (0.890 – 0.966)	8.321 %	0.876 (0.782 – 0.931)	13.294 %
Sept. basal anterior ESV	0.953 (0.914 – 0.974)	10.262 %	0.904 (0.829 – 0.947)	16.537 %
FW mid anterior EDV	0.881 (0.790 – 0.934)	13.051 %	0.833 (0.659 – 0.914)	16.636 %
FW mid anterior ESV	0.929 (0.872 – 0.961)	15.034 %	0.876 (0.782 – 0.931)	19.886 %
FW mid lateral EDV	0.887 (0.800 – 0.937)	11.484 %	0.877 (0.773 – 0.933)	11.708 %
FW mid lateral ESV	0.935 (0.884 – 0.965)	15.028 %	0.911 (0.842 – 0.951)	17.802 %
FW mid posterior EDV	0.840 (0.723 – 0.910)	13.812 %	0.790 (0.644 – 0.881)	16.231 %
FW mid posterior ESV	0.897 (0.817 – 0.943)	16.277 %	0.881 (0.790 – 0.933)	18.573 %
Sept. mid posterior EDV	0.893 (0.810 – 0.930)	11.051 %	0.886 (0.724 – 0.945)	11.087 %
Sept. mid posterior ESV	0.924 (0.864 – 0.958)	13.877 %	0.906 (0.832 – 0.948)	14.244 %
Sept. mid anterior EDV	0.859 (0.754 – 0.921)	12.028 %	0.820 (0.691 – 0.890)	14.455 %
Sept. mid anterior ESV	0.865 (0.764 – 0.925)	14.670 %	0.859 (0.754 – 0.921)	17.253 %
FW apical anterior EDV	0.764 (0.604 – 0.866)	19.717 %	0.764 (0.573 – 0.871)	20.048 %
FW apical anterior ESV	0.872 (0.769 – 0.930)	18.407 %	0.867 (0.768 – 0.927)	23.412 %
FW apical posterior EDV	0.664 (0.456 – 0.803)	22.065 %	0.608 (0.381 – 0.767)	25.802 %
FW apical posterior ESV	0.772 (0.615 – 0.870)	19.669 %	0.771 (0.601 – 0.872)	24.043 %
Apex EDV	0.883 (0.789 – 0.936)	11.067 %	0.868 (0.769 – 0.927)	12.545 %
Apex ESV	0.936 (0.885 – 0.965)	12.204 %	0.841 (0.725 – 0.911)	16.263 %

CI: confidence interval, CV: coefficient of variation, ICC: intraclass correlation coefficient
Other abbreviations as in Table 1.

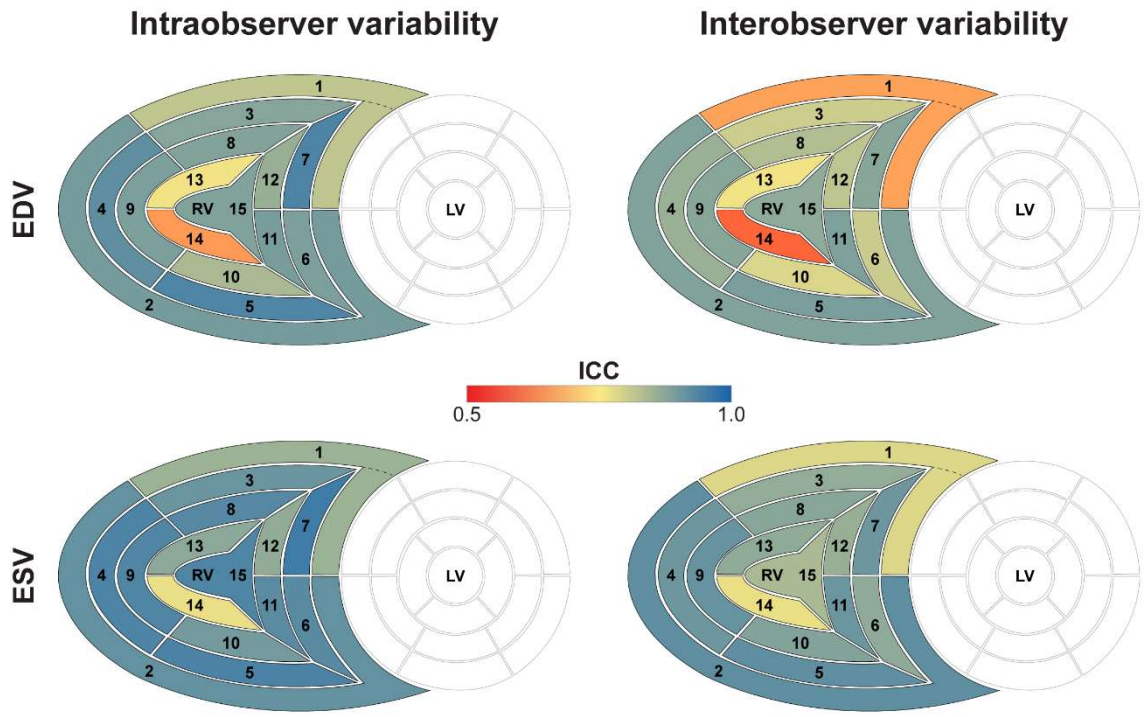

Figure 9. Intra- and interobserver variability of RV segmental end-diastolic and end-systolic volumes. The 15 segments are color-coded based on the value of the intraclass correlation coefficient (ICC): reddish colors indicate a lower, whereas blueish colors correspond to a higher value of intraclass correlation coefficient in the given segment. Segment numbers as defined in Figure 6.

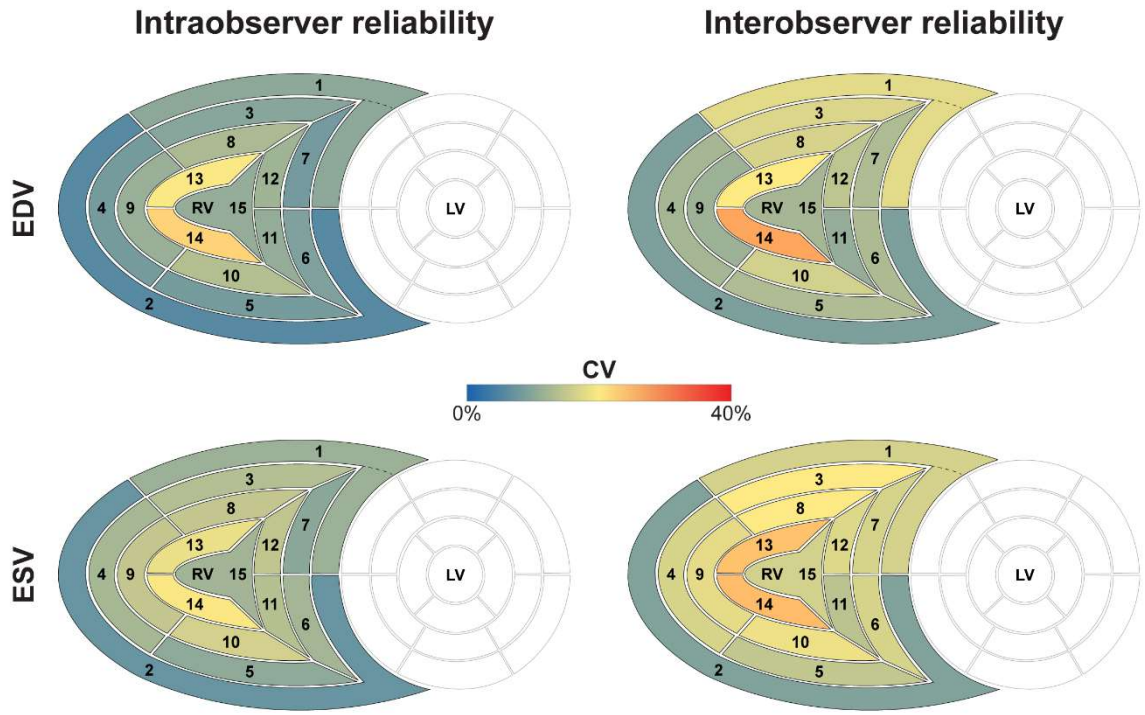

Figure 10. Intra- and interobserver reliability of right ventricular segmental end-diastolic and end-systolic volumes. The 15 segments are color-coded based on the value of the coefficient of variation (CV): reddish colors indicate a higher, whereas blueish colors correspond to a lower value of coefficient of variation. Segment numbers as defined in Figure 6.

Three-dimensional GLS correlated robustly with both 2D free wall and septal longitudinal strains (r=0.907 and r=0.891, both p<0.001, Table 3). When we analyzed free wall and septal longitudinal strains separately with our software solution, both 3D free wall and septal longitudinal strains showed strong correlations with the corresponding TomTec-derived values (r=0.920 and r=0.919, both p<0.001, Table 3).

Table 3. Correlations between the ReVISION- and TomTec-derived RV strains (n=30).

		TomTec	
		2D free wall longitudinal strain	2D septal longitudinal strain
ReVISION	3D GLS	r=0.907 p<0.001	r=0.891 p<0.001
	3D free wall longitudinal strain	r=0.920 p<0.001	
	3D septal longitudinal strain		r=0.919 p<0.001

7.1.2. Comparison of 3DE- and CMRI-derived metrics

The mean values of the measurements performed with the two imaging modalities are presented in Table 4. 3DE- and CMRI-derived volumes correlated robustly, and a systematic underestimation by 3DE could be seen (Figure 11, Table 5), which is in line with previous studies [5, 136]. RV EF demonstrated a good correlation, and only a negligible bias could be observed between its values derived from the two imaging modalities (Table 5). The comparison of 3DE- and CMRI-derived ESVs after motion decomposition along the three aforementioned directions is illustrated in Figure 12. Strong correlations could be reported (Pearson correlation coefficients >0.9 of the three motion components), and similar to global RV volumes, a consistent underestimation of volumes by 3DE could also be detected in the values of the decomposed volumes (Table 5). Not surprisingly, the values of the decomposed EFs showed slightly weaker but highly significant correlations between the two modalities, and in addition, bias was found to be non-significant in all of them (Figure 13, Table 5).

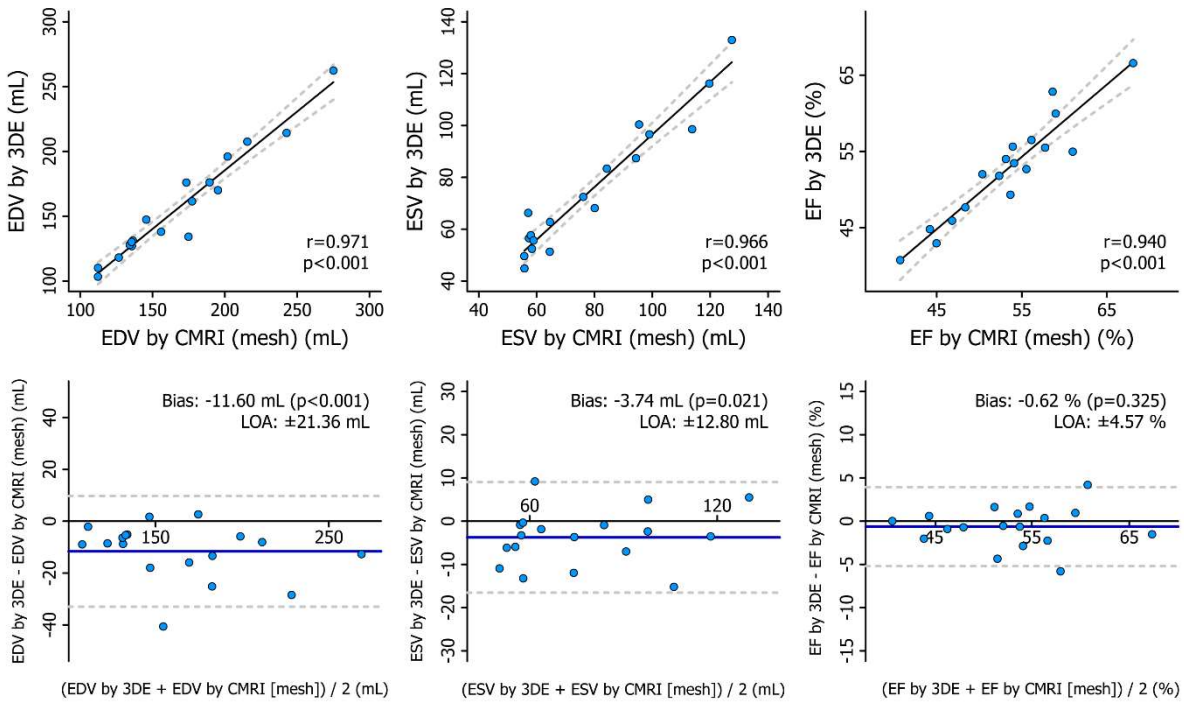

Figure 11. Correlation and agreement between 3DE- and CMRI-derived measurements of RV end-diastolic volume, end-systolic volume, and ejection fraction depicted by correlation and Bland-Altman plots.

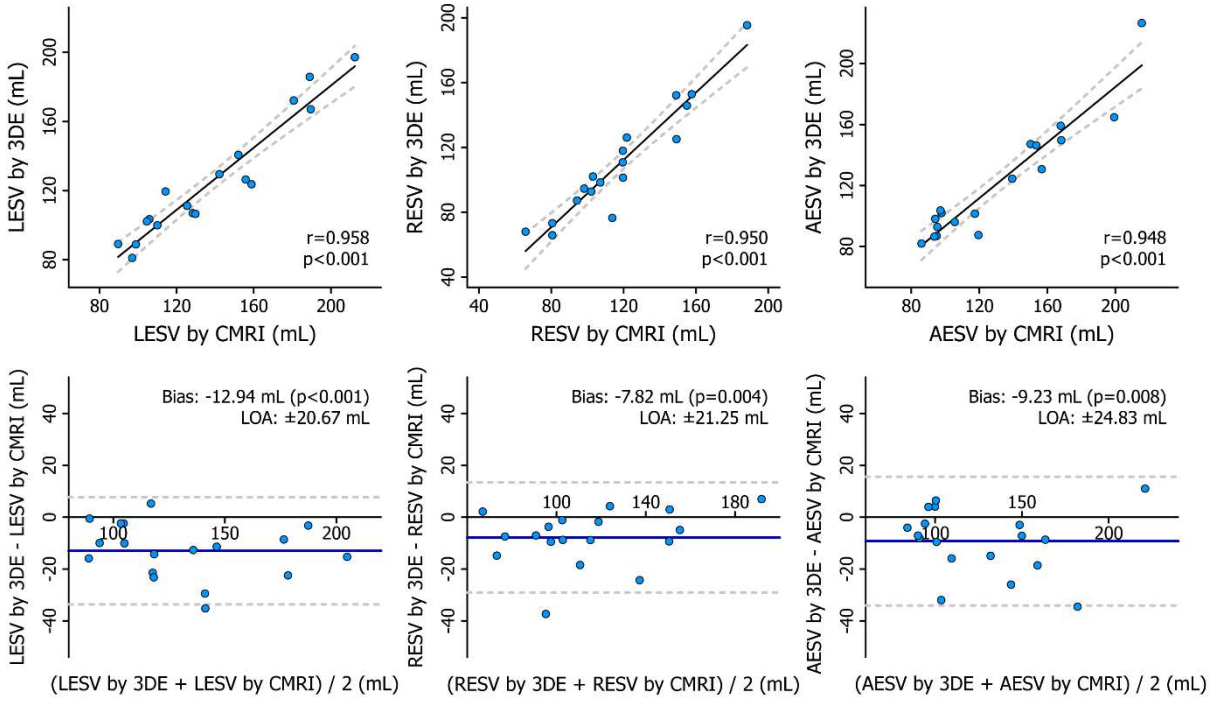

Figure 12. Correlation and agreement between 3DE- and CMRI-derived measurements of RV decomposed end-systolic volumes depicted by correlation and Bland-Altman plots. AESV: anteroposterior end-systolic volume, LESV: longitudinal end-systolic volume, RESV: radial end-systolic volume

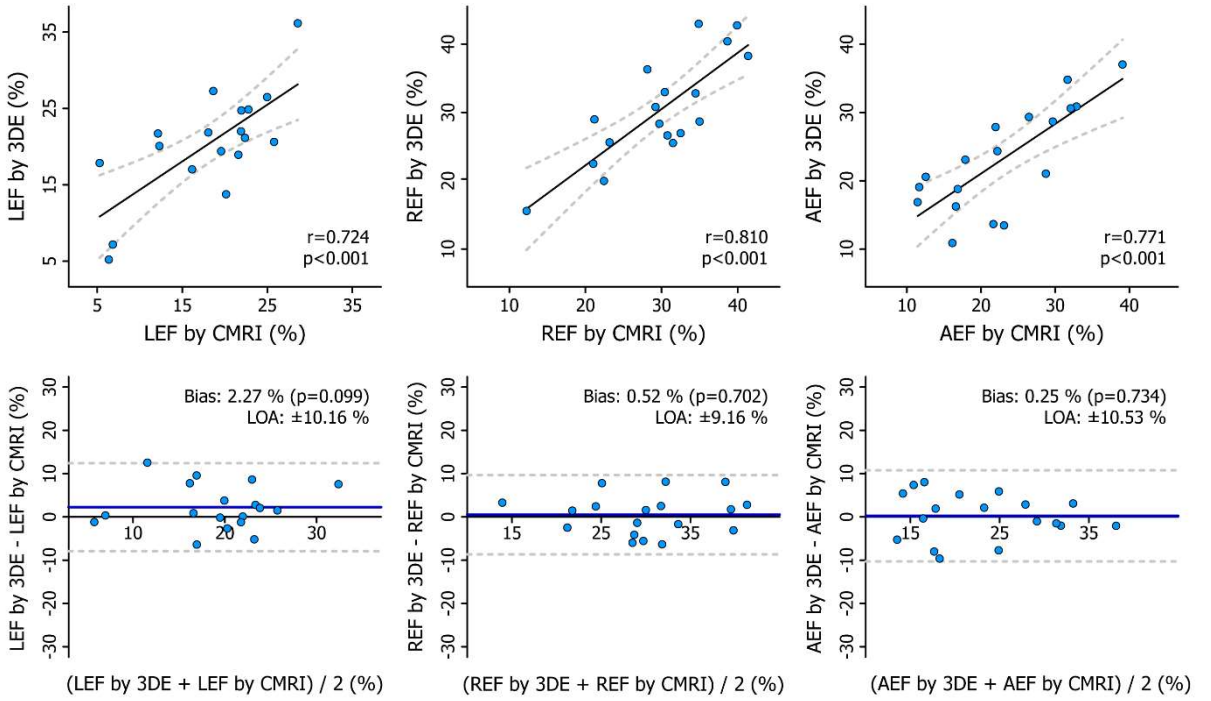

Figure 13. Correlation and agreement between 3DE- and CMRI-derived measurements of RV decomposed ejection fractions depicted by correlation and Bland-Altman plots. AEF: anteroposterior ejection fraction, LEF: longitudinal ejection fraction, REF: radial ejection fraction

Table 4. Summary of the 3DE- and CMRI-derived measurements.

	Healthy controls n=6	Athletes n=6	HFrEF patients n=6
3D echocardiography			
RVEDV, ml	140.7 ± 19.9	185.4 ± 52.6	145.8 ± 37.6
RVESV, ml	60.2 ± 13.8	87.5 ± 27.7	77.8 ± 27.4
RVEF, %	57.4 ± 5.9	52.8 ± 5.2	47.6 ± 5.8
LESV, ml	110.4 ± 13.7	140.8 ± 45	124.0 ± 35.7
RESV, ml	96.4 ± 16.4	135.2 ± 38.3	99.5 ± 34.7
AESV, ml	95.9 ± 15.5	148.0 ± 47.1	120.4 ± 29.3
LEF, %	21.3 ± 3.5	24.7 ± 6.6	15.0 ± 7.4
REF, %	31.4 ± 7.4	26.6 ± 8.2	33.0 ± 7.0
AEF, %	31.9 ± 3.3	20.6 ± 5.9	17.1 ± 3.4
CMRI			
3D RVEDV, ml	154.7 ± 23.9	200.1 ± 56.4	151.9 ± 37.6
3D RVESV, ml	64.1 ± 10.6	92.3 ± 26.0	80.3 ± 26.6
3D RVEF, %	58.2 ± 5.7	53.6 ± 5.2	47.9 ± 5.2
LESV, ml	123.2 ± 14.9	157.4 ± 46.7	133.5 ± 38.0
RESV, ml	110.2 ± 20.3	140.3 ± 30.5	104.0 ± 33.8
AESV, ml	105.5 ± 20.0	156.0 ± 48.2	130.5 ± 33.0
LEF, %	19.9 ± 7.5	21.7 ± 4.2	12.6 ± 5.6
REF, %	28.8 ± 5.8	28.2 ± 9.8	32.5 ± 7.0
AEF, %	32.0 ± 4.2	22.6 ± 3.5	14.2 ± 2.6

AEF: anteroposterior ejection fraction, AESV: anteroposterior end-systolic volume, CMRI: cardiac magnetic resonance imaging, EF: ejection fraction, HFrEF: heart failure with reduced left ventricular ejection fraction, LEF: longitudinal ejection fraction, LESV: longitudinal end-systolic volume, REF: radial ejection fraction, RESV: radial end-systolic volume

Table 5. Correlation and agreement between 3DE- and CMRI-derived measurements.

	Pearson correlation		Bland-Altman analysis	
	r	p value	bias	LOA
RVEDV	0.971	<0.001	-11.60 ml*	± 21.36 ml
RVESV	0.966	<0.001	-3.74 ml*	±12.80 ml
RVEF	0.940	<0.001	-0.62 %	± 4.57 %
LESV	0.958	<0.001	-12.94 ml*	± 20.67 ml
RESV	0.950	<0.001	-7.82 ml*	± 21.25 ml
AESV	0.948	<0.001	-9.23 ml*	± 24.83 ml
LEF	0.724	<0.001	2.27 %	± 10.16 %
REF	0.810	<0.001	0.52 %	± 9.16 %
AEF	0.771	<0.001	0.25 %	± 10.53 %

*p<0.05, paired Wilcoxon signed-rank test vs null values to test the significance of the bias. LOA: limits of agreement, other abbreviations as in Table 4.

7.2. Establishing the normal RV contraction pattern

7.2.1. Normal RV contraction pattern in adults

Basic demographic and morphometric data of the entire study population and the two genders are summarized in Table 6. The mean age of the enrolled patients was 45±15 years. Males were characterized by significantly higher morphometric parameters, higher systolic (SBP), and diastolic blood pressure (DBP) and lower heart rate (HR) (Table 6).

Table 6. Clinical and demographic characteristics of the study groups.

	All (n=300)	**Female (n=150)**	**Male (n=150)**	**p value**
Age, years	44.8±15.6	44.9±15.6	44.7±15.6	0.87
Height, cm	167.2±10.1	160.6±7,6	173.9±7.6	<0.001
Weight, kg	66.7±14.6	59.1±12.1	74.3±12.8	<0.001
BMI, kg/m²	23.7±3.9	22.8±4.0	24.5±3.6	<0.001
BSA, m²	1.75±0.23	1.62±0.19	1.89±0.19	<0.001
SBP, mmHg	131.6±15.4	128.3±15.4	135.2±14.8	<0.001
DBP, mmHg	76.7±11.2	75.3±12.0	78.2±10.1	<0.05
HR, 1/min	68.8±13.5	70.4±14.5	67.0±12.1	<0.05

BMI: body mass index, BSA: body surface area, SBP: systolic blood pressure, DBP: diastolic blood pressure, HR: heart rate

Conventional echocardiographic measures of the RV and 3D LV parameters are shown in Table 7. Male sex was associated with higher RV basal diameter, RV areas, right atrial volume index, and also LV volumes, and LVMi. RV FAC and RV FWLS were higher in women; however, TAPSE did not differ between genders. TDI-derived tricuspid annular velocities and PASP were comparable between males and females (Table 7).

Table 7. Basic echocardiographic characteristics of the study groups.

	All (n=300)	Female (n=150)	Male (n=150)	p value
RV basal diameter (mm)	32.3±5.9	30.2±5.5	34.3±5.0	<0.001
RVEDA (cm^2)	24.6±5.8	21.6±4.6	27.7±5.2	<0.001
RVESA (cm^2)	15.0±3.6	12.9±2.7	17.2±3.1	<0.001
RVFAC (%)	50.2±7.5	51.9±7.6	48.5±7.0	<0.001
TAPSE (mm)	22.2±4.8	21.9±4.6	22.5±5.0	0.31
Tricuspid annulus s' (cm/s)	13.8±2.5	13.7±2.5	13.9±2.4	0.50
Tricuspid annulus e' (cm/s)	15.5±4.2	15.7±4.4	15.2±4.0	0.46
Tricuspid annulus a' (cm/s)	15.2±6.7	14.6±4.6	15.8±8.2	0.32
RV 2D FWLS (%)	29.9±5.4	30.8±5.6	29.1±5.0	<0.01
PASP (mmHg)	25.3±5.7	25.8±5.3	24.8±6.1	0.20
RAVi (ml/m^2)	20.8±9.8	19.2±8.8	22.3±10.5	<0.01
3D LVEDVi (ml/m^2)	63.6±12.8	60.0±10.6	67.2±13.7	<0.001
3D LVESVi (ml/m^2)	27.0±7.5	24.5±5.9	29.6±8.0	<0.001
3D LVEF (%)	57.8±6.1	59.1±6.3	56.4±5.6	<0.001
3D LVGLS (%)	20.0±2.9	21.2±2.6	18.9±2.6	<0.001
3D LVGCS (%)	27.8±4.4	28.4±4.4	27.2±4.2	<0.05
3D LVMi (g/m^2)	62.0±11.0	59.4±10.3	64.6±11.0	<0.001

EDA: end-diastolic area, EDVi: end-diastolic volume index; EF: ejection fraction, ESA: end-systolic volume, ESVi: end-systolic volume index, FAC: fractional area change, GCS: global circumferential strain, GLS: global longitudinal strain, LV: left ventricular, Mi: mass index, PASP: pulmonary artery systolic pressure, RAVi: right atrial end-systolic volume index, TAPSE: tricuspid annular plane systolic excursion, 2D FWLS: two-dimensional free wall longitudinal strain, RV: right ventricular

3D RV volumes and also contraction pattern of the study population and for each gender and age category are summarized in Table 8. Males had significantly higher RVEDVi, RVESVi, while RVEF, RVGLS, RVGCS, and RVGAS were significantly higher in women. Values of LEF/RVEF, REF/RVEF, and AEF/RVEF showed that there were no gender differences in the relative contribution of longitudinal, radial, and anteroposterior motion components. RV volumetric indices, RVEF, RVGLS, RVGAS significantly differed across age categories. No significant interaction between age and gender was found regarding 3D RV parameters. Comparison of the relative contribution of longitudinal, radial, and anteroposterior motion directions in the age categories and the entire study population is illustrated in Figure 14.

	All	20-29 y	30-39 y	40-49 y	50-59 y	60+ y	p value for age	p value for gender	interaction p
RVEDVi (ml/m^2)									
Men	57.0±12.3	62.7±12.4	58.7±14.0	53.1±10.2	54.0±10.2	56.3±12.4			
Women	50.7±11.6	54.6±12.3	50.9±10.6	46.2±10.2	51.3±13.4	50.5±10.2	<0.01	<0.001	0.72
All	53.8±12.3	58.6±12.9	54.8±12.9	49.7±10.7	52.7±11.8	53.4±11.7			
RVESVi (ml/m^2)									
Men	24.1±6.2	26.6±6.4	23.8±6.5	22.1±4.8	23.0±6.5	25.2±5.8			
Women	19.8±5.3	21.4±5.5	19.4±4.6	18.1±5.1	20.2±6.4	20.2±4.2	<0.01	<0.001	0.91
All	22.0±6.1	24.0±6.4	21.6±6.0	20.1±5.3	21.6±6.6	22.7±5.6			
RVEF (%)									
Men	57.3±5.4	57.6±4.8	59.5±4.5	58.4±5.1	56.0±6.0	55.1±5.8			
Women	61.1±5.3	60.7±4.6	61.9±4.5	61.9±4.2	60.9±6.4	59.6±6.4	<0.01	<0.001	0.69
All	59.2±5.7	59.1±4.9	60.7±4.6	60.1±5.0	58.5±6.6	57.3±6.5			
RVGLS (%)									
Men	29.2±5.5	29.7±5.1	31.9±4.7	29.5±5.2	27.3±5.6	27.4±5.8			
Women	33.1±6.6	33.6±4.6	35.6±5.5	33.4±5.7	33.3±7.4	30.4±8.3	<0.001	<0.001	0.91
All	31.1±6.4	31.7±5.2	33.7±5.4	31.5±5.8	29.8±7.0	28.9±7.2			
RVGCS (%)									
Men	27.2±6.3	26.9±6.5	28.9±5.7	28.1±7.1	26.3±5.6	25.5±6.2			
Women	29.9±7.9	29.3±6.6	29.9±8.1	29.4±7.1	31.5±9.4	29.2±8.2	0.57	<0.01	0.48
All	28.5±7.2	28.1±6.6	29.4±7.0	28.8±7.1	28.9±8.1	27.4±7.4			
RVGAS (%)									
Men	38.2±4.9	38.3±4.2	39.6±4.6	39.1±4.7	37.4±5.4	36.7±5.1			
Women	41.8±5.0	41.7±3.8	43.1±3.6	41.7±4.1	41.6±6.3	40.8±6.5	<0.05	<0.001	0.90
All	40.0±5.2	40.0±4.3	41.4±4.5	40.4±4.6	39.5±6.2	38.7±6.1			
LEF/RVEF (%)									
Men	46.2±8.8	46.8±7.3	47.3±10.0	46.9±8.4	44.0±10.8	45.8±7.4			
Women	46.9±8.6	47.0±7.5	49.0±9.5	48.7±8.3	44.9±7.5	45.1±9.7	0.10	0.43	0.92
All	46.6±8.7	46.9±7.3	48.2±9.7	47.8±8.3	44.5±9.3	45.3±8.5			
REF/RVEF (%)									
Men	43.6±9.4	41.7±8.9	42.5±7.0	44.7±10.1	46.4±9.4	42.7±11.0	0.07	0.72	0.99
Women	43.2±11.1	40.7±9.9	42.9±12.0	44.4±9.3	46.0±11.6	41.8±12.4			

All	43.5±10.3	41.2±9.4	42.7±9.7	44.5±9.6	46.2±10.5	41.8±12.4			
AEF/RVEF (%)									
Men	48.5±6.4	47.6±7.3	51.8±6.9	48.7±5.6	47.5±5.3	47.0±6.0			
Women	49.7±7.1	49.2±7.3	50.5±5.7	49.5±7.5	49.7±7.4	49.8±7.9	0.13	0.12	0.50
All	49.1±6.8	48.4±7.3	51.2±6.3	49.1±6.6	48.6±6.5	48.4±7.1			

Table 8. 3D RV mechanics of the study group by age categories and genders. RV: right ventricle, EDVi: end-diastolic volume index, ESVi: end-systolic volume index, EF: ejection fraction, RV 3D GLS: right ventricular three-dimensional global longitudinal strain, RV 3D GCS: right ventricular three-dimensional global circumferential strain, RV 3D GAS: right ventricular three-dimensional global area strain, LEF/RVEF: longitudinal ejection fraction index, REF/RVEF: radial ejection fraction index, AEF/RVEF: anteroposterior ejection fraction index

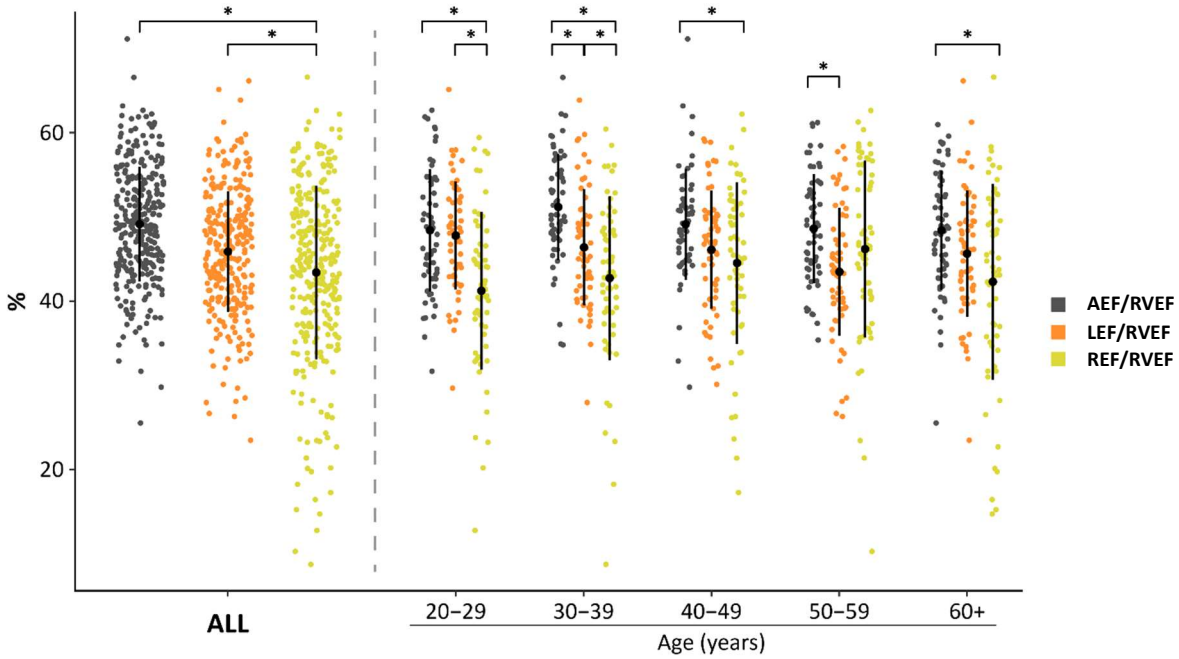

Figure 14. The relative contribution of the 3 RV wall motion components in the five age groups.

Anteroposterior (49.1±6.8%) and longitudinal shortening (46.6±8.7%) were found to be the most prominent motion components of the RV in the pooled population, while radial shortening (43.5±10.3%) was of inferior significance. By analyzing the age categories separately, the relative contribution of longitudinal shortening was significantly higher compared to the radial component in younger age categories (20-29, 30-39). In the older groups, however, LEF/RVEF and REF/RVEF were comparable. Anteroposterior shortening had a higher contribution compared to longitudinal shortening in the 30-39 and 50-59 groups, while it had a higher contribution compared to radial shortening in every age category except 50-59 (Figure 14). We compared subjects in the lowest quartile concerning LEF/RVEF to the rest of the study group (LEF/RVEF: 37.7±4.0 vs 48.9±5.2, $p<0.001$). Lower contribution of longitudinal shortening was not associated with lower RVEF (59.5±6.3 vs 59.0±5.4, $p=0.67$) and AEF/RVEF was also comparable between the two groups (50.4±6.7 vs 48.7±6.8, $p=0.12$); however, the contribution of radial shortening was significantly higher (REF/RVEF: 50.5±7.2 vs 41.0±10.0, $p<0.001$). We also compared subjects in the lowest quartile concerning REF/RVEF to the rest of the population (REF/RVEF: 29.7±7.4 vs 48.0±6.3, $p<0.001$). While patients with the lowest REF/RVEF had significantly lower RVEF (55.4±6.2 vs 60.4±4.9, $p<0.001$), LEF/RVEF (52.1±6.1 vs 43.8±6.2, $p<0.001$) and also AEF/RVEF (51.6±6.1 vs 48.3±6.8, $p<0.001$) were significantly higher suggesting that the other two motion directions may effectively compensate lower radial shortening. Several RV parameters showed weak but statistically significant correlations with age, BSA, and hemodynamic parameters. Age correlated negatively with RVEDVi, RVEF, RVGLS, LEF/RVEF, and RVGAS. BSA showed a negative relationship with RVEF, RVGLS, LEF/RVEF, and AEF/RVEF, while correlated positively with RVEDVi and REF/RVEF. Regarding SBP and DBP, a negative correlation was found between RVGLS and AEF/RVEF, while RVEDVi and REF/RVEF had a positive correlation. SBP also correlated negatively with RVEF. HR showed a positive relationship with

RVEF, RVGCS, RVGAS, and REF/RVEF, while correlated negatively with AEF/RVEF. PASP did not show any correlation with RV parameters in the pooled study group [232]. In the 60+ age group, however, RVEF ($r=-0.45$, $p<0.05$) and REF/RVEF ($r=-0.49$, $p<0.01$) showed a weak negative correlation with PASP. Multivariable models were built with relevant hemodynamic and echocardiographic variables to find independent predictors of REF/RVEF, LEF/RVEF, and AEF/RVEF (Tables 9, 10, 11). Age, BSA, HR, and RVEDVi were independent predictors of LEF/RVEF and REF/RVEF as well; however, all with the opposite effect on the two motion directions. Beyond these variables, LVMi, LVGLS, and PASP were associated with LEF/RVEF in the multivariable analysis. Concerning REF/RVEF, RVEF and LVEF were found to be independent predictors. Race, LVEF, and RVEF were independent predictors of AEF/RVEF.

Table 9. Multivariable linear regression analysis: independent predictors of LEF/RVEF.

Covariate	β	p value	Adjusted R^2	Standard error	Cumulative p value
Age	**-0.23**	**<0.01**	**0.15**	**6.41%**	**<0.0001**
Gender	-0.13	0.29			
Race	-0.03	0.29			
BSA	**-0.29**	**<0.001**			
SBP	0.15	0.07			
DBP	0.05	0.57			
HR	**-0.17**	**<0.05**			
LVEDVi	-0.01	0.88			
LVEF	-0.17	0.60			
LVMi	**0.21**	**<0.05**			
LVGLS	**0.16**	**<0.05**			
LVGCS	0.23	0.42			
PASP	**-0.15**	**<0.05**			
RVEDVi	**-0.20**	**<0.05**			
RVEF	-0.15	0.07			

BSA: body surface area, DBP: diastolic blood pressure, EDVi: end-diastolic volume index, EF: ejection fraction, GLS: global longitudinal strain, GCS: global circumferential strain, HR: heart rate, LEF/RVEF: longitudinal ejection fraction index, LV: left ventricular, Mi: mass index, PASP: pulmonary arterial systolic pressure, RV: right ventricle, SBP: systolic blood pressure

Table 10. Multivariable linear regression analysis: independent predictors of REF/RVEF.

Covariate	β	p value	Adjusted R^2	Standard error	Cumulative p value
Age	**0.24**	**<0.001**	**0.32**	**8.39%**	**<0.0001**
Gender	0.05	0.68			
Race	0.009	0.94			
BSA	**0.29**	**<0.001**			
SBP	-0.13	0.16			
DBP	0.10	0.23			
HR	**0.21**	**<0.01**			
LVEDVi	-0.02	0.86			
LVEF	**-0.22**	**<0.01**			
LVMi	-0.10	0.19			
LVGLS	0.03	0.83			
LVGCS	-0.04	0.86			
PASP	0.001	0.99			
RVEDVi	**0.22**	**<0.01**			
RVEF	**0.56**	**<0.001**			

BSA: body surface area, DBP: diastolic blood pressure, EDVi: end-diastolic volume index, EF: ejection fraction, GLS: global longitudinal strain, GCS: global circumferential strain, HR: heart rate, LV: left ventricular, Mi: mass index, PASP: pulmonary arterial systolic pressure, REF/RVEF: radial ejection fraction index, RV: right ventricle, SBP: systolic blood pressure

Table 11. Multivariable linear regression analysis: independent predictors of AEF/RVEF.

Covariate	β	p value	Adjusted R^2	Standard error	Cumulative p value
Age	-0.005	0.95	**0.20**	**6.41%**	**<0.0001**
Gender	0.005	0.96			
Race	**0.25**	**<0.05**			
BSA	0.01	0.92			
SBP	-0.03	0.79			
DBP	-0.04	0.66			
HR	-0.06	0.47			
LVEDVi	0.15	0.08			
LVEF	**0.44**	**<0.05**			
LVMi	-0.08	0.50			
LVGLS	-0.09	0.48			
LVGCS	-0.25	0.26			
PASP	0.09	0.25			
RVEDVi	-0.17	0.05			
RVEF	**0.26**	**<0.01**			

AEF/RVEF: anteroposterior ejection fraction index, BSA: body surface area, DBP: diastolic blood pressure, EDVi: end-diastolic volume index, EF: ejection fraction, GLS: global longitudinal strain, GCS: global circumferential strain, HR: heart rate, LV: left ventricular, Mi: mass index, PASP: pulmonary arterial systolic pressure, RV: right ventricle, SBP: systolic blood pressure

7.2.2. Normal RV contraction pattern in children

The study population included 166 subjects (Boston = 76; Semmelweis = 90). Demographic and clinical characteristics of the study population are summarized in Table 12. The median age of subjects was 13.8 years (IQR 8.6 to 15.3), with a skewed distribution towards the oldest age group (as a consequence of the recruitment strategy at the Semmelweis site). The majority was male (n=131, 79%), driven by a male-predominant population recruited at the Semmelweis site (n=81, 90%).

Table 12. Pediatric patient characteristics.

	All (n=166)	**Infants (n=13)**	**Toddlers (n=11)**	**School-Aged (n=21)**	**(Pre)Teens (n=121)**
Age, y	13.8 (8.6, 15.3)	0.1 (0.05, 0.1)	3.6 (3.3, 4.1)	6.3 (5.2, 7.9)	14.4 (13.6,15.7)
Female, n (%)	35 (21%)	7 (54%)	5 (45%)	7 (33%)	16 (13%)
Height, m	1.49 ± 0.38	0.53 ± 0.07	1.00 ± 0.08	1.21 ± 0.11	1.69 ± 0.14
Weight, kg	47.7 ± 23.8	4.2 ± 2.0	16.6 ± 3.2	23.3 ± 5.9	59.4 ± 15.3
BMI, kg/m^2	19.1 ± 3.5	14.3 ± 2.0	16.3 ± 1.4	15.5 ± 1.5	20.5 ± 3.0
BSA, m^2	1.39 ± 0.54	0.25 ± 0.07	0.68 ± 0.09	0.88 ± 0.14	1.66 ± 0.29
SBP, mmHg	117 ± 19	92 ± 14	100 ± 10	100 ± 10	125 ± 16
DBP, mmHg	65 ± 12	53 ± 11	53 ± 6	56 ± 8	68 ± 10
HR, 1/min	80 ± 20	130 ± 13	89 ± 12	84 ± 14	73 ± 12

BMI: body mass index, BSA: body surface area, DBP: diastolic blood pressure, HR: heart rate, SBP: systolic blood pressure

Conventional echocardiographic measures of RV and LV function are presented in Table 13. TAPSE increased significantly with age. Most subjects had either no (92, 53%) or trivial (72, 42%) TR. There were no differences between groups in terms of FAC. Age-related variation in 2D FWLS was present, with the largest absolute values seen in the toddler and school-aged groups.

Table 13. Conventional echocardiographic characteristics.

	All (n=166)	Infants (n=13)	Toddlers (n=11)	School-Aged (n=21)	(Pre)Teens (n=121)	p value
TAPSE, mm	21.1 ± 7.2	7.1 ± 3.6	15.2 ± 3.9	16.7 ± 4.3	23.9 ± 5.4	**<0.001**
RV FAC, %	48.8 ± 5.3	47.5 ± 6.5	49.2 ± 5.7	50.9 ± 5.4	48.6 ± 5.1	0.23
RV 2D FWLS, %	-29.9 ± 5.5	-29.0 ± 7.8	-33.6 ± 7.1	-32.0 ± 5.6	-29.3 ± 4.9	**0.019**
2D LVEDV, ml	110 ± 50.5	10 ± 3.7	47 ± 9.9	64 ± 12	135 ± 32.5	**<0.001**
2D LVEDVi, ml/m^2	75.5 ± 15.5	39.5 ± 6.3	68.3 ± 9.7	72.6 ± 8.1	80.7 ± 11.7	**<0.001**
2D LVESV, ml	44 ± 22.6	4 ± 0.8	16 ± 3.6	23 ± 5.0	55 ± 15.9	**<0.001**
2D LVESVi, ml/m^2	29.9 ± 7.8	14.7 ± 2.4	23.3 ± 3.7	25.9 ± 4.0	32.9 ± 6.2	**<0.001**
LV EF, %	60.6 ± 4.5	62.3 ± 5.2	65.8 ± 2.8	64.4 ± 3.2	59.3 ± 3.9	**<0.001**

2D: two-dimensional, EF: ejection fraction, FAC: fractional area change, FWLS: free wall longitudinal strain, LVEDVi: indexed left ventricular end-diastolic volume, LVESVi: indexed left ventricular end-systolic volume, RV: right ventricular, TAPSE: tricuspid annular plane systolic excursion

Table 14 presents 3D RV volumes and contraction patterns. RV volumes, global RVEF, REF and REF/RVEF, longitudinal and circumferential 3D strain parameters significantly differ by age group. Age-related differences were present for global RVEF, REF, and REF/RVEF. Additionally, age-related differences were seen for all components of RV strain.

Table 14. 3DE analysis of right ventricular size and ejection fraction components.

	All (n=166)	Infants (n=13)	Toddlers (n=11)	School-aged (n=21)	(Pre)Teens (n=121)	p value
3D RVEDV, ml	110 ± 53.3	10 ± 3.7	45 ± 10.6	59 ± 12.1	135 ± 36.7	**<0.001**
3D RVEDVi, ml/m^2	74.7 ± 16.9	40.2 ± 6.6	65.2 ± 8.6	67.6 ± 10.8	80.6 ± 13.6	**<0.001**
3D RVESV, ml	47 ± 25	4 ± 1.3	18 ± 6.1	23 ± 4.7	58 ± 19.2	**<0.001**
3D RVESVi, ml/m^2	31.3 ± 8.7	17.0 ± 2.8	26.5 ± 5.9	26.0 ± 4.7	34.2 ± 7.7	**<0.001**
RVEF, %	58.3 ± 4.8	57.2 ± 5.5	59.7 ± 4.8	61.4 ± 4.5	57.7 ± 4.6	**0.007**
LEF, %	25.7 ± 6.0	23.4 ± 6.0	27.2 ± 8.0	26.5 ± 5.7	25.7 ± 5.9	0.39
REF, %	25.1 ± 7.2	27.3 ± 6.0	26.7 ± 6.8	28.5 ± 6.3	24.1 ± 7.3	**0.031**
AEF, %	29.2 ± 6.2	28.3 ± 6.9	32.1 ± 6.5	31.5 ± 6.9	28.6 ± 5.9	0.080
LEF/RVEF, %	44.4 ± 10.0	40.4 ± 9.2	46.9 ± 12.5	44.8 ± 10.2	44.6 ± 9.9	0.42
REF/RVEF, %	43.3 ± 11.6	47.4 ± 10.1	46.8 ± 13.4	48.2 ± 11.0	41.6 ± 11.3	**0.030**
AEF/RVEF, %	49.8 ± 8.7	49.0 ± 8.8	53.6 ± 9.0	51.0 ± 8.5	49.4 ± 8.3	0.39
3D GAS, %	-40.3 ± 4.6	-38.5 ± 5.5	-40.9 ± 5.8	-42.1 ± 5.4	-40.1 ± 4.2	0.13
3D GLS, %	-22.7 ± 4.0	-19.0 ± 6.4	-23.3 ± 5.6	-23.1 ± 4.5	-23.0 ± 3.3	**0.006**
3D GCS, %	-23.2 ± 5.1	-23.5 ± 5.1	-23.0 ± 5.3	-26.2 ± 4.2	-22.7 ± 5.2	**0.039**

3D: three-dimensional, AEF: anteroposterior ejection fraction, EF: ejection fraction, GAS: global area strain, GCS: global circumferential strain, GLS: global longitudinal strain, LEF: longitudinal ejection fraction, REF: radial ejection fraction, RVEDVi: indexed right ventricular end-diastolic volume, RVESVi: indexed right ventricular end-systolic volume

Figure 15 shows the ejection fraction components for the entire cohort as well as broken down by age group. For the entire cohort, the AEF was greater than the other two components; the same pattern was observed for the oldest group. For the school-aged and infant cohort, the AEF was greater than the LEF. No significant differences were observed among any components in toddlers [233].

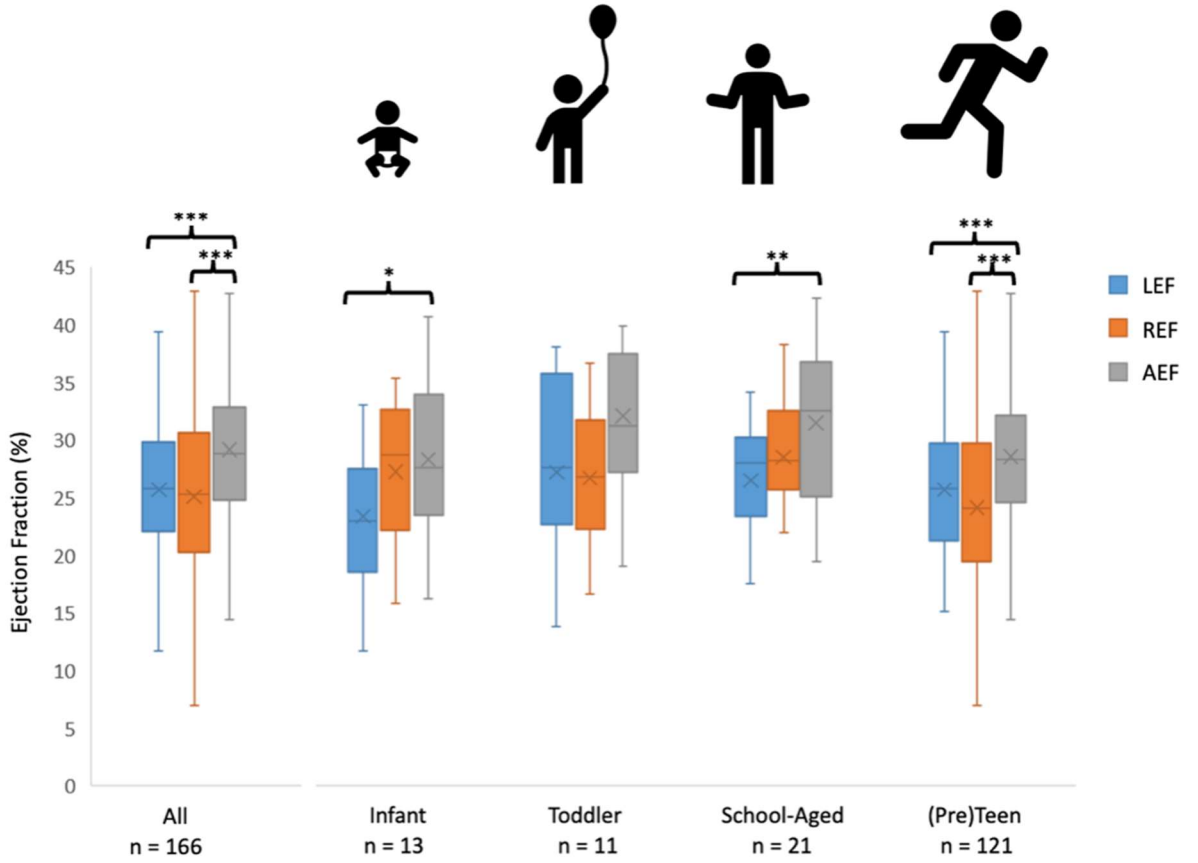

Figure 15. A comparison of longitudinal, radial and anteroposterior ejection fractions. Individual and mean values of LEF, REF, and AEF are shown in the entire population (leftmost column) as well as the different age categories, with statistical comparison among the three motion components. *p<0.05, **p<0.01, *** p<0.001

7.3. Exploring the changes of RV contraction pattern in different clinical scenarios

7.3.1. RV contraction pattern in elite athletes

The mean age of the athletes was 19 years. They were participating in competitive sport for 10±5 years with a training time of 17±6 hours per week. Both control groups were age-matched. Athletes demonstrated higher height, weight, and BSA than the control groups; males also had higher values than females. Athletes had higher systolic but similar diastolic blood pressure compared to the control groups. Males had lower HR compared to females, while athletes also demonstrated lower HR values. Peak oxygen uptake was higher in male athletes compared to female athletes (Table 15).

Table 15. Baseline characteristics of athlete and control groups.

	MA (n=30)	**FA (n=30)**	**MC (n=20)**	**FC (n=20)**	**p value for gender**	**p value for sport**	**p value for interaction**
Age (years)	18.9±4.0	19.0±3.7	19.9±3.8	19.5±2.3	0.81	0.27	0.71
Height, cm	191.3±6.4	174.5±5.8	180.0±8.3	165.7±4.9	<0.001	<0.001	0.40
Weight, kg	90.0±10.6	67.8±6.6	74.8±13.8	56.5±5.9	<0.001	<0.001	0.36
BMI, kg/m²	25.5±2.0	22.3±2.2	23.1±3.9	20.6±2.0	<0.001	<0.01	0.86
BSA, m²	2.2±0.2	1.8±0.1	1.9±0.2	1.6±0.1	<0.001	<0.001	0.37
SBP, mmHg	138.2±19.7	134.1±13.2	118.4±17.8	114.4±13.1	0.33	<0.001	0.98
DBP, mmHg	70.2±11.0	71.6±9.9	71.3±8.2	73.9±12.0	0.45	0.53	0.81
HR, 1/min	67.2±11.5	71.1±12.1	68.4±9.1	84.2±19.2	<0.01	<0.05	0.10
VO_2/kg (ml/kg/min)	51.9±6.7	47.6±4.2			<0.05		

MA: male athlete, FA: female athlete, MC: male control, FC: female control, BMI: body mass index, BSA: body surface area, SBP: systolic blood pressure, DBP: diastolic blood pressure, HR: heart rate, VO_2/kg: peak oxygen uptake

7.3.1.1. Conventional 2D and Doppler echocardiographic data

Linear LV wall thickness and internal diameter measurements showed higher values in athletes with a trivial gender difference as well. Ratio of mitral inflow velocities, deceleration time and E/e' did not differ between groups. Mitral annular systolic velocities were also similar. Left and right atrial volume indices were higher in athletes, while LA volume index was similar between genders. RV linear measurements showed enlargement of the chamber in athletes compared to controls. Athletes had higher TAPSE values than controls, on the other hand, FAC was significantly lower in athletes. Tricuspid annular velocities did not differ between groups. RV FWLS was higher in females (Table 16).

Table 16. Conventional echocardiographic parameters of athlete and control groups.

	MA (n=30)	**FA (n=30)**	**MC (n=20)**	**FC (n=20)**	**p value for gender**	**p value for sport**	**p value for interaction**
LVIDd (mm)	54.0±3.5	48.3±3.9	47.8±4.5	43.4±3.5	<0.001	<0.001	0.47
IVSd (mm)	11.6±1.3	9.3±1.1	9.3±1.4	7.6±0.8	<0.001	<0.001	0.24
PWd (mm)	10.3±1.0	8.6±1.9	8.2±0.6	7.3±1.0	<0.001	<0.001	0.10
RWT (%)	0.41±0.05	0.37±0.05	0.36±0.08	0.34±0.05	0.08	<0.01	0.34
E/A	1.6±0.5	1.81±0.5	1.6±0.4	1.7±0.5	0.14	0.59	0.80
DT (ms)	182.3±59.5	172.9±41.0	155.0±20.9	171.2±29.6	0.62	0.18	0.24
E/e' average	5.7±0.9	5.5±0.9	5.7±1.0	5.3±0.8	0.08	0.99	0.58

Mitral lateral annulus s' (cm/s)	10.1±1.2	11.1±1.6	11.6±1.0	11.1±2.6	0.85	0.35	0.33
Mitral medial annulus s' (cm/s)	8.9±1.1	9.1±1.0	8.6±1.1	8.6±1.1	0.78	0.07	0.65
LAVi (ml/m^2)	29.0±7.9	30.4±9.8	19.1±7.7	16.5±5.0	0.74	<0.001	0.31
RAVi (ml/m^2)	31.2±6.6	25.8±7.6	21.1±9.0	15.2±5.2	<0.01	<0.001	0.88
RV basal diameter (mm)	36.3±4.6	31.4±3.8	32.7±2.3	27.6±2.5	<0.001	<0.001	0.93
RV length (mm)	104.6±6.7	94.7±8.2	90.8±4.9	87.4±8.7	<0.001	<0.001	<0.05
TAPSE (mm)	24.7±3.7	25.6±2.7	23.9±3.5	23.0±4.1	0.95	0.03	0.26
FAC (%)	44.7±4.9	47.0±6.3	50.4±6.1	54.6±5.8	<0.01	<0.001	0.41
Tricuspid annulus s' (cm/s)	12.1±1.7	12.7±2.1	12.7±2.2	12.9±2.3	0.18	0.20	0.68
Tricuspid annulus e' (cm/s)	14.1±2.5	14.2±2.8	14.2±3.1	16.3±3.1	0.08	0.08	0.11
RV septal LS (%)	-24.3±4.4	-25.5±4.5	-24.0±4.7	-26.2±4.4	0.07	0.82	0.59
RV free wall LS (%)	-31.1±4.3	-30.5±3.8	-30.5±4.1	-33.4±3.9	<0.05	0.06	0.15

MA: male athlete, FA: female athlete, MC: male control, FC: female control, LVIDd: left ventricular diastolic internal diameter, IVSd: interventricular septum diastolic thickness, PWd: posterior wall diastolic thickness, RWT: relative wall thickness, DT: deceleration time, LAVi: left atrial volume index, RAVi: right atrial volume index, TAPSE: tricuspid annular plane systolic excursion, FAC: fractional area change, LS: longitudinal strain

7.3.1.2. 3D echocardiographic data

As expected, athletes demonstrated increased LV and RV end-diastolic, end-systolic and stroke volume indices along with significantly higher LVMi. There was significant interaction between gender and athletic activity in the case of various LV and RV morphological parameters (LVEDVi, LVESVi, LVSVi, RVEDVi, RVSVi). Post-hoc analysis showed that gender has a significant impact on the degree of geometrical remodeling: while there was no significant difference in ventricular volume indices between the male and female control groups, male athletes demonstrated significantly higher LV and RV volume indices compared to female athletes (all $p<0.01$). LV and RVEF were significantly lower than controls; however, they remained in the normal range in every athlete. Males had significantly lower LV and RVEF, while SVi did not differ between genders. Similarly, LVGLS and GCS were lower in athletes and also in males (Table 17).

Table 17. Basic 3D echocardiographic data of athlete and control groups.

	MA (n=30)	**FA (n=30)**	**MC (n=20)**	**FC (n=20)**	**p value for gender**	**p value for sport**	**p value for interaction**
LVEDVi (ml/m^2)	93.5±11.1	79.9±6.5	62.9±7.4	64.4±8.9	<0.01	<0.001	<0.001
LVESVi (ml/m^2)	39.5±9.0	33.5±5.1	24.1±3.6	23.1±4.4	<0.001	<0.001	<0.01
LVSVi (ml/m^2)	50.9±10.4	46.4±5.7	38.8±5.1	41.3±5.4	0.55	<0.001	<0.05
LVMi (g/m^2)	103.2±14.9	89.7±8.4	62.1±6.7	64.8±12.9	<0.05	<0.001	<0.01
LVEF (%)	56.3±3.0	58.1±5.5	61.7±3.3	64.0±2.9	<0.05	<0.001	0.77
LVGLS (%)	-18.9±1.7	-19.6±1.9	-21.1±1.6	-22.5±1.5	<0.01	<0.001	0.28
LV GCS (%)	-27.2±2.3	-28.4±3.9	-30.6±2.8	-32.0±2.6	<0.05	<0.001	0.89

RVEDVi (ml/m²)	94.3±9.8	81.1±8.9	65.8±8.3	64.2±10.9	<0.001	<0.001	<0.01
RVESVi (ml/m²)	42.9±6.3	35.2±6.6	26.5±5.2	24.0±6.8	<0.001	<0.001	0.07
RVSVi (ml/m²)	51.4±5.6	46.0±4.6	39.4±4.9	40.2±5.5	0.05	<0.001	<0.01
RVEF (%)	54.6±3.6	56.9±4.9	59.6±4.4	62.5±4.9	<0.01	<0.001	0.75

MA: male athlete, FA: female athlete, MC: male control, FC: female control, LVEDVi: left ventricular end-diastolic index, LVESVi: left ventricular end-systolic volume index, LVSVi: left ventricular stroke volume index, LVMi: left ventricular mass index, LVEF: left ventricular ejection fraction, LVGLS: left ventricular global longitudinal strain, LVGCS: left ventricular global circumferential strain, RVEDVi: right ventricular end-diastolic volume index, RVESVi: right ventricular end-systolic volume index, RVSVi: right ventricular stroke volume index, RVEF: right ventricular ejection fraction

3D echocardiographic parameters of RV mechanics revealed significant differences between the groups (Table 18). RVGLS was comparable between the pooled athlete population and controls (-22±5 vs -23±5 %, p=0.24). On the other hand, RVGCS was significantly lower in athletes (-21±4 vs -26±7 %, p<0.001; Table 18). This functional shift was even more prominent when the relative contribution of longitudinal and radial motion to global function was examined: LEF/RVEF was significantly higher, while REF/RVEF was significantly lower in both athlete groups (Figure 16). REF/RVEF was found to be significantly lower in males compared to females.

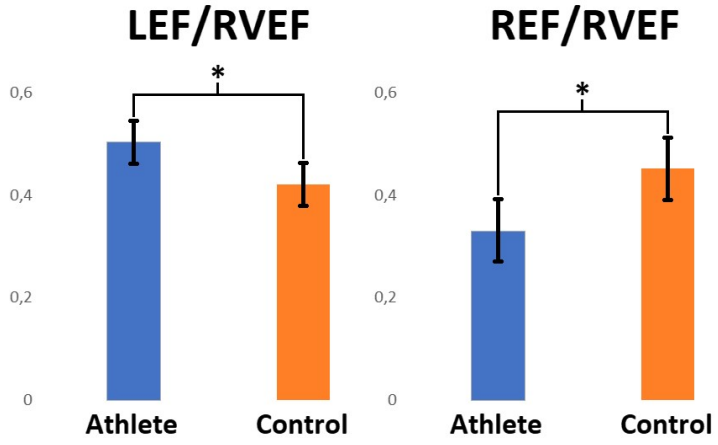

Figure 16. The relative contribution of longitudinal (LEF/RVEF) and radial motion (REF/RVEF) to global right ventricular function in the two study groups. An increased longitudinal contribution can be seen in athletes. On the other hand, the radial contribution significantly decreased compared to the controls. Athletes n=60, controls n=40; *p<0.05

Table 18. 3D global and regional right ventricular deformation data of athlete and control groups.

	MA (n=30)	FA (n=30)	MC (n=20)	FC (n=20)	p value for gender	p value for sport	p value for interaction
RVGLS (%)	-21.7±4.4	-21.8±4.7	-20.9±4.1	-24.8±4.9	<0.05	0.25	0.06
RV free wall LS (%)	-22.2±4.7	-22.4±4.0	-21.4±4.5	-26.2±5.0	<0.01	0.11	<0.05
RV septal LS (%)	-22.2±4.8	-21.4±5.5	-20.2±4.7	-23.5±6.5	0.25	0.98	0.07
RV free wall basal LS (%)	-16.5±6.7	-16.3±5.7	-18.4±4.2	-24.0±8.1	<0.001	<0.05	<0.05
RV free wall mid LS (%)	-30.9±7.6	-31.2±5.4	-29.6±6.8	-36.9±7.8	<0.01	0.16	<0.05
RV free wall apical LS (%)	-19.4±6.9	-19.4±6.3	-16.4±5.5	-17.8±7.3	0.58	0.09	0.62
RVGCS (%)	-20.6±4.4	-21.6±4.2	-24.7±4.0	-27.5±8.4	0.10	<0.001	0.41
RV free wall CS (%)	-22.5±4.7	-25.0±5.6	-29.3±5.2	-33.4±8.0	<0.01	<0.001	0.49
RV septal CS (%)	-20.1±5.9	-21.1±4.6	-21.0±4.8	-23.1±9.6	0.36	0.41	0.49
RV free wall basal CS (%)	-21.7±6.6	-24.0±8.4	-29.7±6.0	-32.6±8.7	0.09	<0.001	0.85
RV free wall mid CS (%)	-23.6±4.4	-26.4±5.4	-30.3±5.2	-35.0±7.5	<0.01	<0.001	0.41
RV free wall apical CS (%)	-22.2±4.6	-24.4±5.3	-27.8±6.0	-32.4±8.7	<0.01	<0.001	0.32
RV early diastolic SR (1/s)	0.29±0.07	0.28±0.06	0.24±0.04	0.30±0.08	0.47	0.10	<0.05
RV LEF (%)	27.5±4.9	27.3±4.9	25.8±5.3	25.9±6.6	0.94	0.17	0.88
RV REF (%)	16.7±3.7	19.2±5.7	25.8±5.2	29.8±7.6	<0.01	<0.001	0.49
RV AEF (%)	24.7±4.4	25.6±4.5	25.0±5.1	27.9±5.1	0.05	0.19	0.31
LEF/RVEF	0.52±0.07	0.49±0.07	0.43±0.07	0.41±0.08	0.16	<0.001	0.98
REF/RVEF	0.31±0.06	0.34±0.09	0.43±0.07	0.47±0.09	<0.05	<0.001	0.72
AEF/RVEF	0.46±0.07	0.46±0.07	0.42±0.08	0.45±0.08	0.28	0.05	0.36

MA: male athlete, FA: female athlete, MC: male control, FC: female control, RVGLS: right ventricular global longitudinal strain, GCS: global circumferential strain, RV early diastolic SR: right ventricular early diastolic global longitudinal strain rate, LEF: longitudinal ejection fraction, REF: radial ejection fraction, AEF: anteroposterior ejection fraction

Moreover, the degree of this functional shift showed a correlation with VO_2/kg (Table 19). Morphological parameters, such as LVEDVi and RVEDVi, also correlated with CPET-derived VO_2/kg, while no other LV or RV parameter showed a relationship with exercise capacity (Table 19).

Table 19. Correlations between VO_2/kg and LV and RV morphological and functional parameters.

	r value	p value
LVEDVi	**0.32**	**0.02**
LVEF	-0.09	0.51
LVGLS	-0.01	0.93
LVGCS	-0.11	0.43
RVEDVi	**0.37**	**<0.01**
RVEF	-0.11	0.43
RVGLS	0.11	0.43
RVGCS	-0.19	0.17
LEF	0.20	0.13
REF	**-0.26**	**0.04**
LEF/RVEF	**0.30**	**0.02**
REF/RVEF	**-0.27**	**0.04**

LVEDVi: left ventricular end-diastolic volume index, LVEF: left ventricular ejection fraction, LVGLS: left ventricular global longitudinal strain, LV GCS: left ventricular global circumferential strain, RVEDVi: right ventricular end-diastolic volume index, RVEF: right ventricular ejection fraction, RV GLS: right ventricular global longitudinal strain, RV GCS: right ventricular global circumferential strain, LEF: longitudinal ejection fraction, REF: radial ejection fraction

3D regional analysis of RV deformation parameters was also applied. In female athletes, free wall LS was significantly lower compared to the corresponding control group ($p<0.01$). RV free wall CS was also lower in athletes and males (Table 18). Septal LS and CS were not significantly different among groups. LS of the free wall basal region showed a significant decrease in athletes, which was attributable to the marked decrease in the case of female athletes ($p<0.001$), while there was no difference in the apical region. Free wall basal, mid, and apical CS were all lower in athletes, without significant interaction between gender and sport. There was a significant interaction between gender and athletic activity in terms of early diastolic SR,

showing significantly better diastolic function in male athletes compared to male controls ($p<0.05$). No regional or diastolic parameter showed a correlation with exercise capacity.

7.3.2. RV contraction pattern in adolescent athletes

Basic demographic, anthropometric, and hemodynamic data of the adolescent athletes and control population are summarized in Table 20. Athletes had significantly higher height and BSA values than the sedentary control group. Athletes also demonstrated significantly higher resting systolic blood pressures and lower HR than controls, whereas diastolic blood pressure was similar in the two groups. Most of the athletes participated in mixed and endurance classes of sports, predominantly soccer (46.0%), water polo (33.4%), and swimming (10.2%); however, other types of sports, such as power and skill, were represented as well in our cohort of athletes (*i.e.,* wrestling, boxing, kenpo, fencing, squash) [234]. The athletes have been participating in competitive sports for 8±3 years with a training duration of 12±6 h/week at the time of the echocardiographic evaluation, and 94 out of the 215 (43.7%) participants were members of the national team in the corresponding age group. The athlete's CPET-derived peak exercise capacity was also quantified with an average value of 54 ml/kg/min (Table 20).

Table 20. Baseline and training-specific characteristics of athlete and control groups.

	Athletes (n=215)	**Controls (n=38)**	**p**
Baseline characteristics			
Age (years)	15.8±1.4	15.3±2.0	0.060
Male, n (%)	169 (78.6)	28 (73.7)	0.503
Height (cm)	175.6±10.3	169.4±11.8	0.022
Weight (kg)	67.0±12.9	61.0±10.4	0.072
BSA (m^2)	1.80±0.2	1.69±0.2	0.045
SBP (mmHg)	129.8±14.5	119.2±13.2	0.005
DBP (mmHg)	71.4±9.0	75.5±6.4	0.076
HR (bpm)	70.5±12.1	78.4±15.0	0.014
Training specific characteristics			
Type of sport			
● **Mixed, n (%)**	180 (83.7)	-	

• **Endurance, n (%)**	26 (12.1)	-
• **Power, n (%)**	3 (1.4)	-
• **Skill, n (%)**	6 (2.8)	-
Since (years)	8.4±3.0	-
Training time (h/week)	12.3±6.1	-
VO_2 (L/min)	3.6±0.8	-
VO_2/kg (ml/kg/min)	54.4±6.9	-

BSA: body surface area, DBP: diastolic blood pressure, HR: heart rate, SBP: systolic blood pressure, VO_2: peak oxygen uptake, VO_2/kg: peak oxygen uptake indexed to body weight

Conventional 2D echocardiographic parameters of athletes and controls are shown in Table 21. Left ventricular end-diastolic internal diameter, wall thicknesses, and calculated LV Mi were significantly higher in athletes compared with controls. Regarding diastolic function, transmitral E-wave velocities were significantly lower in athletes. Systolic, early diastolic, and atrial velocities of the mitral septal and lateral annuli were significantly lower in athletes. Concerning the right heart, RV basal diameter was larger, along with RV systolic pressure, which also showed significantly higher values among the athlete population. RV FAC and FWLS in athletes showed decreased resting values (Table 21).

Table 21. Conventional 2D echocardiographic parameters of athlete and control groups.

	Athletes (n=215)	**Controls (n=38)**	**p**
LVIDd (mm)	49.3±4.1	45.1±4.1	<0.001
IVSd (mm)	9.5±1.4	8.4±1.3	<0.001
PWd (mm)	8.6±1.2	7.4±1.1	<0.001
RWT (%)	0.35±0.05	0.33±0.05	0.072
LV Mi (g/m^2)	86.3±15.5	66.0±12.8	<0.001
E (cm/s)	91.3±17.0	100.4±13.1	0.002
A (cm/s)	58.0±15.5	60.0±13.4	0.445
E/A	1.66±0.47	1.75±0.42	0.299
DT (ms)	168.9±33.3	161.8±34.4	0.230
Mitral lateral s′ (cm/s)	11.8±2.4	12.6±2.5	0.048
Mitral lateral e′ (cm/s)	18.2±3.0	19.5±3.4	0.017
Mitral lateral a′ (cm/s)	6.2±1.9	7.6±2.1	<0.001
Mitral medial s′ (cm/s)	9.1±1.4	9.7±1.5	0.019
Mitral medial e′ (cm/s)	13.6±2.2	15.7±2.7	<0.001
Mitral medial a′ (cm/s)	6.7±1.6	7.4±1.7	0.015
E/e′ average	5.92±1.10	5.89±0.90	0.893
LAVi (ml/m^2)	24.6±7.8	21.4±5.7	0.121

RVd (mm)	33.0±4.2	30.2±2.9	<0.001
RVSP (mmHg)	23.8±4.1	19.7±4.1	<0.001
TAPSE (mm)	23.3±3.7	23.7±3.4	0.618
FAC (%)	47.7±6.1	51.9±5.9	<0.001
RVSLS (%)	-23.4±4.7	-22.4±4.1	0.229
RVFWLS (%)	-29.6±4.2	-31.4±3.7	0.017
RAVi (ml/m^2)	26.1±6.6	25.9±9.1	0.888

A: mitral inflow velocity during atrial contraction, a': peak late (atrial) diastolic annular velocity, DT: deceleration time, E: early diastolic mitral inflow velocity, e': early diastolic annular velocity, FAC: fractional area change, IVSd: interventricular septal thickness at end-diastole, LAVi: left atrial volume index, LV: left ventricle, LVIDd: LV internal diameter at end-diastole, Mi: mass index, PWd: posterior wall thickness at end-diastole, RAVi: right atrial volume index, RV: right ventricle, RVd: RV basal diameter, RVFWLS: RV free wall longitudinal strain, RVSLS: RV septal longitudinal strain, RVSP: right ventricular systolic pressure, RWT: relative wall thickness, s': systolic annular velocity, TAPSE: tricuspid annular plane systolic excursion

3D echocardiographic characteristics of athletes and controls are summarized in Table 22. As expected, there were significant differences between the athlete and the control group concerning LV and RV morphological and functional parameters. Athletes demonstrated significantly higher LV and RV EDVi, ESVi, and SVi values along with a significantly higher LV Mi. In athletes, resting LV and RV EF values were significantly lower than in control adolescents; however, they remained within a normal range. Concerning the contraction pattern of the RV, values of REF and AEF were lower in athletes compared with controls, whereas values of LEF did not show any difference between the two groups. The relative contribution of radial (REF/RVEF) and anteroposterior (AEF/RVEF) motion components to global RV function was significantly lower in athletes. In contrast, the longitudinal (LEF/RVEF) motion component's relative contribution was higher than controls (Table 22).

Table 22. Three-dimensional echocardiographic data of athlete and control groups.

	Athletes (n=215)	**Controls (n=38)**	**p**
LEFT VENTRICLE			
LVEDVi (ml/m^2)	80.0±13.0	64.2±9.5	<0.001
LVESVi (ml/m^2)	34.2±7.2	25.0±5.0	<0.001
LVSVi (ml/m^2)	45.7±7.3	39.2±5.8	0.001
LVMi (g/m^2)	83.8±13.5	67.9±13.0	<0.001

LVEF (%)	57.3±3.9	61.4±3.4	<0.001
RIGHT VENTRICLE			
RVEDVi (ml/m^2)	80.7±14.3	67.6±10.0	0.001
RVESVi (ml/m^2)	36.3±8.5	27.6±4.2	<0.001
RVSVi (ml/m^2)	44.4±7.3	40.0±7.3	0.024
RVEF (%)	55.3±4.5	60.4±4.9	<0.001
RV LEF (%)	25.1±5.3	24.3±4.7	0.364
RV REF (%)	22.4±6.0	29.9±5.2	<0.001
RV AEF (%)	26.0±5.2	30.4±5.4	<0.001
LEF/RVEF	0.45±0.08	0.40±0.07	0.001
REF/RVEF	0.40±0.10	0.49±0.06	<0.001
AEF/RVEF	0.47±0.08	0.50±0.07	0.018

AEF: anteroposterior ejection fraction, EDVi: end-diastolic volume index, EF: ejection fraction, ESVi: end-systolic volume index, LEF: longitudinal ejection fraction, LV: left ventricle, Mi: mass index, REF: radial ejection fraction, RV: right ventricle, SVi: stroke volume index

Sex-differences are summarized in Table 23. We have compared male (n=169) and female (n=46) athletes based on training-specific characteristics and 3D echocardiographic data. Male athletes were younger and had been participating in competitive sports for longer; however, females had a longer average weekly training duration. Male athletes also showed higher CPET-derived peak exercise capacity values than females. Regarding the 3D echocardiographic results, specific morphological and functional differences were observed between male and female athletes. Male sex was associated with higher values of LV and RV EDVi, ESVi, and SVi. Similarly, LVMi values were higher among male athletes than among females. In male athletes, LVEF and RVEF showed significantly decreased resting values compared with females. Concerning the RV mechanics, values of REF and AEF were significantly lower, whereas LEF showed higher values in male athletes. The relative contribution of radial (REF/RVEF) as well as the anteroposterior (AEF/RVEF) component was significantly lower in male athletes [235]. The longitudinal contribution (LEF/RVEF) was higher compared to female athletes (Table 23 and Figure 17).

Table 23. Comparison of training-specific characteristics and 3D echocardiographic data in female and male athletes.

	Male athletes (n=169)	Female athletes (n=46)	p
Age (years)	15.6±1.4	16.4±1.2	<0.001
Since (years)	8.7±3.0	7.3±2.8	0.007
Training time (h/week)	10.7±4.7	17.9±7.1	<0.001
VO_2/kg (ml/kg/min)	56.1±6.1	48.1±5.7	<0.001
LEFT VENTRICLE			
LVEDVi (ml/m²)	82.5±12.5	70.6±10.5	<0.001
LVESVi (ml/m²)	35.7±6.9	28.9±5.5	<0.001
LVSVi (ml/m²)	46.7±7.2	41.6±6.6	<0.001
LVMi (g/m²)	86.2±12.8	75.1±12.4	<0.001
LVEF (%)	56.8±3.7	59.0±4.2	0.001
RIGHT VENTRICLE			
RVEDVi (ml/m²)	83.4±13.4	70.8±13.0	<0.001
RVESVi (ml/m²)	37.8±8.2	30.8±7.3	<0.001
RVSVi (ml/m²)	45.6±6.9	39.9±7.0	<0.001
RVEF (%)	55.0±4.5	56.7±4.3	0.023
RV LEF (%)	25.6±5.5	23.5±4.1	0.017
RV REF (%)	21.7±6.2	24.9±4.6	0.002
RV AEF (%)	25.5±4.9	27.9±5.9	0.005
LEF/RVEF	0.46±0.09	0.41±0.07	<0.001
REF/RVEF	0.39±0.10	0.44±0.07	0.005
AEF/RVEF	0.46±0.08	0.49±0.08	0.047

AEF: anteroposterior ejection fraction, EDVi: end-diastolic volume index, EF: ejection fraction, ESVi: end-systolic volume index, LEF: longitudinal ejection fraction, LV: left ventricle, Mi: mass index, REF: radial ejection fraction, RV: right ventricle, SVi: stroke volume index

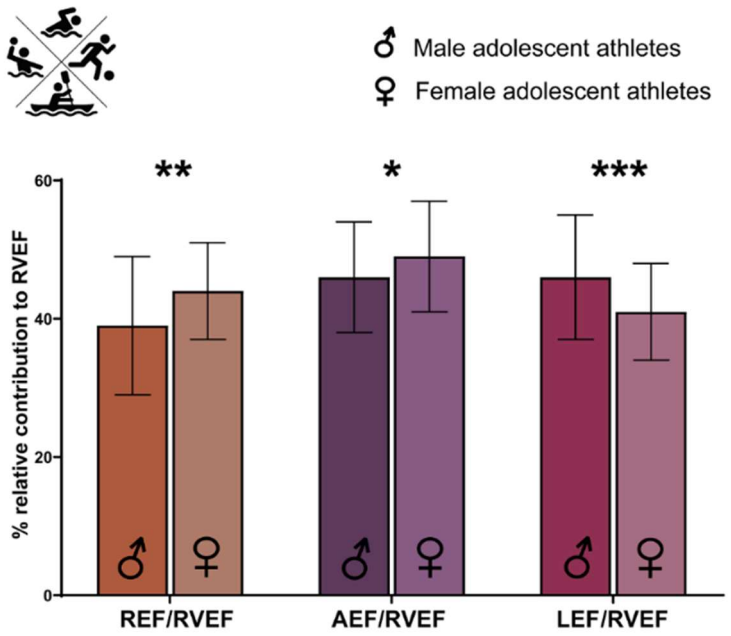

Figure 17. Sex-related differences in RV contraction pattern in adolescent athletes. Male sex was associated with a lower radial contribution to RVEF (REF/RVEF) as well as anteroposterior shortening (AEF/RVEF), while the contribution of longitudinal shortening (LEF/RVEF) was higher.

Univariable correlations between 3DE-derived parameters and VO_2/kg were assessed using the athlete population. LV volumes, such as LVEDVi (r=0.377, p<0.001), LVESVi (r=0.340, p< 0.001), and LVSVi (r=0.344, p<0.001), as well as LVMi (r=0.369, p<0.001), correlated moderately with VO_2/kg. LVEF (r=−0.272, p<0.001) showed a weak inverse correlation with peak exercise capacity. Regarding the right heart, RVEDVi (r=0.377, p<0.001), RVESVi (r=0.340, p<0.001), and RVSVi (r =0.344, p<0.001) showed moderate correlations with VO_2/kg. RVEF had no significant correlation with VO_2/kg. In terms of RV mechanics, LEF/RVEF (r=0.138, p=0.044) showed a weak positive correlation with VO_2/kg, while AEF/RVEF (r=-0.155, p=0.023) showed a weak inverse correlation with it.

7.3.3. Comprehensive mechanical characterization of the athlete's heart

Basic anthropometric, hemodynamic data and training-specific characteristics of the athlete and control groups are summarized in Table 24.

Table 24. Baseline and training-specific characteristics of athlete and control groups.

	Athletes (n=422)	**Controls (n=55)**	**p**
Baseline characteristics			
Age (years)	20.1±5.8	20.1±3.2	0.939
Male, n (%)	295 (69.9)	31 (56.4)	0.061
Height (cm)	177.9±10.6	171.1±9.5	<0.001
Weight (kg)	72.6±14.7	65.2±13.2	<0.001
BSA (m^2)	1.9±0.2	1.8±0.2	<0.001
SBP (mmHg)	131.9±14.8	123.6±12.5	<0.001
DBP (mmHg)	74.5±9.8	78.2±9.8	0.009
HR (bpm)	67.9±12.5	78.9±15.1	<0.001
Training-specific characteristics			
Type of sport			
● **Mixed, n (%)**	293 (69)	-	
● **Endurance, n (%)**	88 (21)	-	
● **Power, n (%)**	33 (8)	-	
● **Skill, n (%)**	8 (2)	-	
Competitive training since (years)	11.9±5.6	-	
Training time (h/week)	15.4±7.3	-	

VO_2 (L/min)	3.8±0.9	2.9±0.8	<0.001
VO_2/kg (ml/kg/min)	52.7±7.7	44.9±7.3	<0.001

BSA: body surface area, DBP: diastolic blood pressure, HR: heart rate, SBP: systolic blood pressure, VO_2: peak oxygen uptake, VO_2/kg: peak oxygen uptake indexed to body weight

Most of the athletes participated in mixed and endurance classes of sports, predominantly water polo (34.8%), soccer (30.6%), and swimming (13.3%); however, other types of sports, such as power and skill, were represented as well in our cohort of athletes. Athletes presented with higher height, weight, and BSA values than the sedentary control group. Athletes also demonstrated significantly higher resting systolic blood pressure and lower diastolic blood pressure and heart rate than controls. Our athletes have been participating in competitive sports for an average of 12 years with an average training duration of 15 hours/week at the time of the echocardiographic evaluation. The athlete group's CPET-derived peak exercise capacity significantly exceeded the control population's (Table 24). Conventional 2DE parameters of athletes and controls showed results as seen in previous studies regarding the athlete's heart. Detailed 3D echocardiographic characteristics of athletes and controls are summarized in Table 25. As expected, there were significant differences between the athlete and the control group concerning LV and RV morphological and functional parameters. Athletes had significantly higher LV and RV end-diastolic (EDVi) and end-systolic volume index (ESVi) values. Similarly, LV mass index (Mi), LV stroke volume index (SVi), and RV SVi values were higher in athletes than controls. In athletes, LVEF, LVGLS, LVGCS, and RVEF, RVGCS showed significantly decreased resting values, in contrast to RVGLS, which did not differ from controls (Table 25). The results above remained the same when comparing male athletes to male controls and female athletes to female controls. Similarly, adolescent athletes (irrespective of sex) presented with the same pattern of exercise-induced cardiac remodeling as seen in the pooled athlete population compared to controls.

Table 25. Three-dimensional echocardiographic data of athlete and control groups.

	Athletes (n=422)	Controls (n=55)	p
LEFT VENTRICLE			
LVEDVi (ml/m²)	81.3±13.2	62.2±11.4	<0.001
LVESVi (ml/m²)	35.3±7.3	24.3±5.5	<0.001
LVSVi (ml/m²)	45.9±7.5	37.9±7.2	<0.001
LVMi (g/m²)	86.7±15.1	66.0±12.0	<0.001
LVEF (%)	56.7±4.2	61.0±4.5	<0.001
LVGLS (%)	-19.2±2.3	-21.2±2.0	<0.001
LVGCS (%)	-27.7±3.0	-31.0±3.5	<0.001
RIGHT VENTRICLE			
RVEDVi (ml/m²)	81.6±14.3	62.7±11.2	<0.001
RVESVi (ml/m²)	36.7±8.7	25.7±5.3	<0.001
RVSVi (ml/m²)	44.9±7.3	37.0±7.4	<0.001
RVEF (%)	55.3±4.8	58.9±4.7	<0.001
RVGLS (%)	-21.8±3.4	-22.2±3.6	0.447
RVGCS (%)	-20.9±4.4	-24.5±4.5	<0.001

EDVi: end-diastolic volume index, EF: ejection fraction, ESVi: end-systolic volume index, GCS: global circumferential strain, GLS: global longitudinal strain, LV: left ventricle, Mi: mass index, RV: right ventricle, SVi: stroke volume index

We have also compared the exercise-induced relative decreases of LVGLS, GCS, and RVGLS and GCS. Left ventricular GLS (average decrease of 10%) and LVGCS (11%) showed a similar, balanced decrease. Meanwhile, the relative decrease of RVGCS (15%) exceeded the decrement in RVGLS (2%, p< 0.001) (Figure 18).

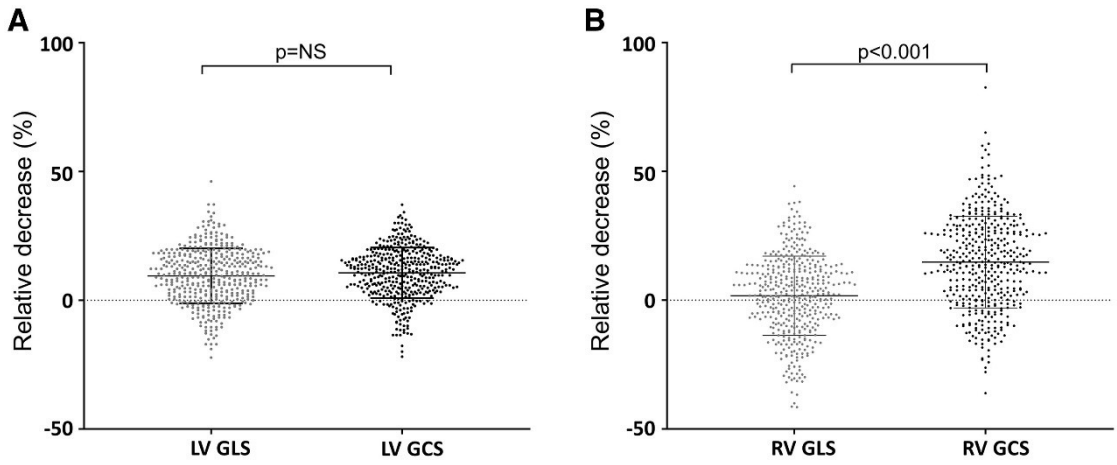

Figure 18. Comparison of the exercise-induced relative decreases of the left ventricular (A) global longitudinal and global circumferential strain and the right ventricular (B) global longitudinal and global circumferential strain in the athlete cohort. Three-dimensional left ventricular global longitudinal strain

and left ventricular global circumferential strain (p=NS) showed a similar exercise-induced relative decrease; however, the decrement in right ventricular global circumferential strain was disproportionately larger compared with right ventricular global longitudinal strain (p<0.001). NS: nonsignificant.

7.3.3.1. Sex-specific differences in athletes

We have compared male (n=295) and female (n=127) athletes based on training-specific characteristics and 3DE data. The results are shown in Table 26. There was no significant age difference between the two groups. Male athletes have been participating in competitive sports for longer periods; however, females have longer average weekly training duration. Male athletes also showed higher values in CPET-derived peak exercise capacity compared with women. Regarding the 3DE results, distinct morphological and functional differences were observed between male and female athletes. Male sex was associated with higher LV and RV EDVi, and ESVi. Similarly, LVMi, LVSVi, and RVSVi values were higher among male athletes compared with females. In male athletes, LVEF, LVGLS, LVGCS, RVEF, and RVGCS showed significantly decreased resting values, in contrast to RVGLS, which did not differ.

Table 26. Comparison of male and female athletes based on training-specific characteristics and 3D echocardiographic data.

	Male athletes (n=295)	**Female athletes (n=127)**	**p**
Age (years)	19.8±6.1	20.7±5.1	0.144
Type of sport			
● **Mixed, n (%)**	217 (74.1)	76 (25.9)	-
● **Endurance, n (%)**	53 (60.2)	35 (39.8)	-
● **Power, n (%)**	21 (63.6)	12 (36.4)	-
● **Skill, n (%)**	4 (50)	4 (50)	-
Competitive training since (years)	12.3±5.9	10.9±4.9	0.026
Training time (h/week)	13.5±6.3	19.9±7.6	<0.001
VO_2/kg (ml/kg/min)	55.2±7.1	46.8±5.7	<0.001
LEFT VENTRICLE			
LVEDVi (ml/m^2)	84.3±13.1	74.3±10.5	<0.001
LVESVi (ml/m^2)	37.0±7.2	31.3±5.9	<0.001
LVSVi (ml/m^2)	47.2±7.6	43.0±6.5	<0.001

LVMi (g/m^2)	89.8±15.2	79.4±11.9	<0.001
LVEF (%)	56.2±4.0	57.9±4.4	<0.001
LVGLS (%)	-18.9±2.3	-19.8±2.1	<0.001
LVGCS (%)	-27.4±2.9	-28.3±3.3	0.006
RIGHT VENTRICLE			
RVEDVi (ml/m^2)	84.7±14.6	73.6±12.1	<0.001
RVESVi (ml/m^2)	38.7±8.8	31.9±7.2	<0.001
RVSVi (ml/m^2)	46.1±7.7	41.7±6.7	<0.001
RVEF (%)	54.6±4.6	56.9±4.8	<0.001
RVGLS (%)	-21.7±3.5	-22.1±3.3	0.243
RVGCS (%)	-20.4±4.1	-22.0±4.7	0.001

EDVi: end-diastolic volume index, EF: ejection fraction, ESVi: end-systolic volume index, GCS: global circumferential strain, GLS: global longitudinal strain, LV: left ventricle, Mi: mass index, RV: right ventricle, SVi: stroke volume index, VO_2/kg: peak oxygen uptake indexed to body weight

We have also compared adult (>18 years of age, n=207) and adolescent (<18 years of age, n=215) athletes based on training-specific characteristics and 3DE data (Table 27). Adolescent athletes had an average training duration of 12 h/week. In comparison, adult athletes had an average training duration of 19 h/week. Despite the differences in the training regimes of the two age groups, adolescent athletes' CPET-derived peak exercise capacity significantly exceeded the adult populations'. Adolescent athletes had significantly lower LVEDVi, LVESVi, and LVMi values than adult athletes; however, LVSVi did not differ between the two age groups. Interestingly, all RV volumes were comparable in the pooled adult vs adolescent athlete groups; however, if the two sexes were compared, only female adolescents showed similar volumes to adult female athletes. In adolescents, LVEF, LVGLS, and GCS showed higher resting values than adults (Table 27). In contrast, RVEF and RVGCS did not differ between adults and adolescents, while RVGLS was significantly higher in adolescents compared with adult athletes (Table 27).

Table 27. Comparison of adolescent and adult athletes based on training-specific characteristics and 3D echocardiographic data.

	Adolescent athletes (n=215)	Adult athletes (n=207)	p
Age (years)	15.8±1.4	24.5±5.2	<0.001
Male, n (%)	169 (78.6)	126 (60.9)	<0.001
Type of sport			
● **Mixed, n (%)**	180 (61.4)	113 (38.6)	-
● **Endurance, n (%)**	26 (29.5)	62 (70.5)	-
● **Power, n (%)**	3 (9.1)	30 (90.9)	-
● **Skill, n (%)**	6 (75)	2 (25)	-
Competitive training since (years)	8.4±3.0	15.5±5.5	<0.001
Training time (h/week)	12.3±6.1	18.6±7.2	<0.001
VO_2/kg (ml/kg/min)	54.4±6.9	50.9±8.2	<0.001
LEFT VENTRICLE			
LVEDVi (ml/m^2)	80.0±13.0	82.6±13.3	0.040
LVESVi (ml/m^2)	34.2±7.2	36.4±7.4	0.003
LVSVi (ml/m^2)	45.7±7.3	46.2±7.7	0.418
LVMi (g/m^2)	83.8±13.5	89.6±16.1	<0.001
LVEF (%)	57.3±3.9	56.1±4.4	0.002
LVGLS (%)	-19.6±2.1	-18.8±2.3	<0.001
LVGCS (%)	-28.0±2.9	-27.4±3.1	0.035
RIGHT VENTRICLE			
RVEDVi (ml/m^2)	80.2±15.2	82.6±14.3	0.104
RVESVi (ml/m^2)	36.1±8.8	37.2±9.0	0.198
RVSVi (ml/m^2)	44.2±7.9	45.4±7.4	0.098
RVEF (%)	55.3±4.5	55.3±5.1	0.965
RVGLS (%)	-22.3±3.4	-21.3±3.4	0.003
RVGCS (%)	-20.6±4.2	-21.1±4.5	0.195

EDVi: end-diastolic volume index, EF: ejection fraction, ESVi: end-systolic volume index, GCS: global circumferential strain, GLS: global longitudinal strain, LV: left ventricle, Mi: mass index, RV: right ventricle, SVi: stroke volume index, VO_2/kg: peak oxygen uptake indexed to body weight

7.3.3.2. Differences among sports classes

We have compared the athlete population categorized by different sports disciplines (Table 28). The subgroups consisted of athletes participating in mixed (n=293), endurance (n=88), power (n=33), and skill (n=8) sports classes, which classification was based on the relative isometric and isotonic components of exercise according to the recommendations of the European Association of Preventive Cardiology (EAPC) and European Association of

Cardiovascular Imaging (EACVI); however, we excluded skill discipline from further analysis due to the very low number of subjects in this subgroup. Power athletes have been competing for the longest time, with an average of 17 years, while endurance athletes have significantly longer training durations, averaging 21 h/week. Endurance athletes also exceeded the other groups in terms of peak exercise capacity. Concerning the 3DE analysis, LVEDVi and LVESVi were comparable between the study groups; however, LVSVi and LVMi were significantly lower in power athletes than in mixed and endurance athletes. Interestingly, RVEDVi and RVESVi were the highest in endurance athletes, while power athletes had lower values of RVEDVi, RVESVi, and RVSVi compared with the other groups. Regarding LV function, power athletes demonstrated lower resting LVGLS and LVGCS values than mixed and endurance athletes. In contrast, resting values of RVEF, RVGLS, and RVGCS were the lowest in endurance athletes, while power athletes demonstrated the highest resting values of RVGCS compared with the other groups (Table 28).

Table 28. Comparison of the athlete population categorized by different sports disciplines.

	Mixed (n=293)	**Endurance (n=88)**	**Power (n=33)**	**Overall p**
Age (years)	18.8±4.9$^{\S\#}$	22.6±6.7$^{*\#}$	25.2±5.9§*	<0.001
Male, n (%)	217 (74.1)§	53 (60.2)*	21 (63.6)	0.031
Competitive training since (years)	10.8±5.1$^{\S\#}$	14.0±5.6$^{*\#}$	16.6±6.2§*	<0.001
Training time (h/week)	13.8±7.1§	21.1±6.3$^{*\#}$	15.3±3.9§	<0.001
VO_2/kg (ml/kg/min)	52.7±7.3$^{\S\#}$	55.4±7.8$^{*\#}$	45.7±7.3§*	<0.001
LEFT VENTRICLE				
LVEDVi (ml/m^2)	81.7±12.6	82.5±15.3	78.1±10.9	0.257
LVESVi (ml/m^2)	35.3±6.9	36.2±8.8	35.3±5.6	0.579
LVSVi (ml/m^2)	46.4±7.4$^{\#}$	46.3±8.2$^{\#}$	42.8±6.§*	0.034
LVMi (g/m^2)	87.4±14.7$^{\#}$	88.7±16.9$^{\#}$	78.5±9.2§*	0.002
LVEF (%)	56.9±4.1$^{\#}$	56.3±5.0	54.9±2.9*	0.024
LVGLS (%)	-19.3±2.0$^{\#}$	-19.2±2.5$^{\#}$	-17.7±2.9§*	0.001
LVGCS (%)	-27.8±2.9$^{\#}$	-27.7±3.5$^{\#}$	-26.4±2.4§*	0.035
RIGHT VENTRICLE				
RVEDVi (ml/m^2)	81.5±13.9$^{\S\#}$	85.1±16.8$^{*\#}$	73.6±13.6§*	0.001
RVESVi (ml/m^2)	36.4±8.2$^{\S\#}$	39.5±10.3$^{*\#}$	32.1±8.3§*	<0.001
RVSVi (ml/m^2)	45.1±7.4$^{\#}$	45.6±8.3$^{\#}$	41.5±6.8§*	0.022
RVEF (%)	55.5±4.7§	53.9±5.0$^{*\#}$	56.7±4.7§	0.004

RVGLS (%)	-22.2±3.4[§]	-20.7±3.1[*]	-21.5±3.5	0.001
RVGCS (%)	-20.7±4.3[#]	-20.3±4.1[#]	-22.5±5.2[§*]	0.042

* p<0.05 vs Mixed, # p<0.05 vs Power, § p<0.05 vs Endurance; EDVi: end-diastolic volume index, EF: ejection fraction, ESVi: end-systolic volume index, GCS: global circumferential strain, GLS: global longitudinal strain, LV: left ventricle, Mi: mass index, RV: right ventricle, SVi: stroke volume index, VO_2/kg: peak oxygen uptake indexed to body weight

7.3.3.3. Associations of resting echocardiographic parameters with exercise capacity

Univariable correlations between 3DE-derived parameters and VO_2/kg were assessed using our entire study population. LV volumes, such as LVEDVi (r 0.457, p<0.001), LVESVi (r=0.427, p<0.001), and LVSVi (r=0.389, p<0.001), as well as LVMi (r=0.397, p<0.001), correlated significantly with VO_2/kg. Left ventricular functional parameters, namely, LVEF (r=-0.184, p<0.001), LVGLS (r=0.198, p<0.001), and LVGCS (r=0.169, p<0.001), showed a weaker inverse correlation with peak exercise capacity. Concerning the right heart, RVEDVi (r=0.477, p<0.001), RVESVi (r=0.449, p<0.001), and RVSVi (r=0.409, p<0.001) showed significant correlations with VO_2/kg. Right ventricular EF (r=-0.223, p<0.001) and RVGCS (r=0.221, p<0.001) had inverse correlations, but RVGLS (r=0.018, p=0.688) did not correlate with VO_2/kg. We have performed multivariable linear regression analysis (using ordinary least squares) to determine the predictors of VO_2/kg among the 3DE LV and RV parameters. Right ventricular EDVi was the strongest independent predictor of VO_2/kg, followed by RVGCS and LVEDVi. The other parameters (LVGLS, LVGCS, LVMi, and RVGLS) were not significant predictors of peak exercise capacity (Figure 19).

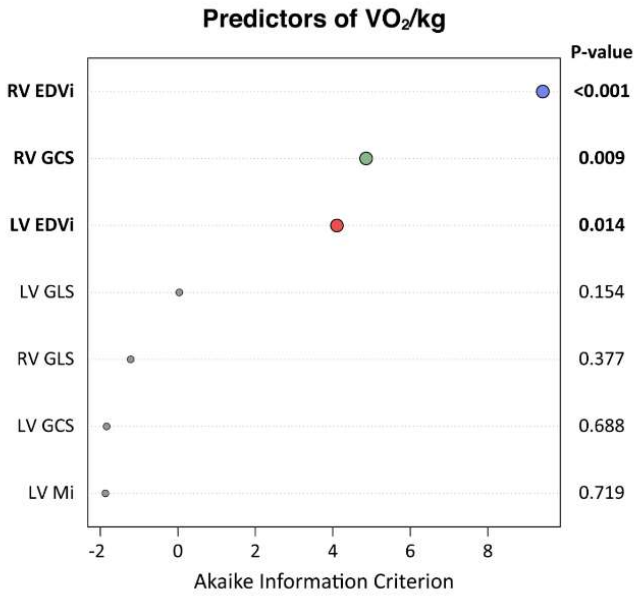

Figure 19. Multivariable linear regression analysis (using ordinary least squares) to determine the predictors of VO_2/kg in the entire study cohort (athletes and controls, n=477).

7.3.4. RV contraction pattern in pulmonary hypertension

7.3.4.1. Characteristics of the study population

Seventy patients were enrolled between November 2020 and December 2021. Eight patients were excluded, as 3D RV beutel construction and export were not possible. Nine further patients with atrial fibrillation were excluded. Of the 53 remaining patients, 11 (21%) were classified as control patients, 36 (68%) had PH, and six (11%) had HFpEF or chronic thromboembolic pulmonary disease without PH (Table 29). The median age of the study population was 68 [57, 76] years, and 36 patients (68%) were female. Further baseline characteristics, including echocardiography, RHC, and conductance catheterization data, are presented in Table 29.

Table 29. Demographic and clinical characteristics of the study population.

Parameter	All participants (n=53)
Age, years	68.0 [57.0, 76.0]
Sex, n (%)	
Male	17 (32)
Female	36 (68)
Body mass index, kg/m²	28.4 [23.6, 33.2]
Tricuspid annular plane systolic excursion, mm	20.9 ± 3.8
S', cm/s	11.0 [9.7, 12.5]
RV fractional area change, %	35.5 [25.3, 43.4]
RV global longitudinal strain, %	−18.6 ± 5.0
RV free wall longitudinal strain, %	−23.3 ± 6.3
RV end-diastolic volume, ml	123 ± 43.1
RV end-diastolic volume indexed to BSA, ml/m²	64.3 ± 23.1
RV end-systolic volume, ml	63.1 [45.6, 89.8]
RV end-systolic volume indexed to BSA, ml/m²	32.6 [23.1, 48.7]
RV stroke volume, ml	51.8 ± 15.3
RV stroke volume indexed to BSA, ml/m²	26.8 ± 6.9
RV ejection fraction, %	46.7 [36.5, 52.2]
LV end-diastolic volume, ml	119 ± 33.9
LV end-diastolic volume indexed to BSA, ml/m²	61.1 ± 13.4
LV end-systolic volume, ml	48.6 ± 16.9
LV end-systolic volume indexed to BSA, ml/m²	24.6 [19.5, 28.3]
LV stroke volume, ml	70.6 ± 19.4
LV stroke volume indexed to BSA, ml/m²	36.3 ± 7.9
LV ejection fraction, %	59.5 ± 5.6
Brain natriuretic peptide, pg/ml	62 [20, 169]
End-diastolic elastance, mm Hg/ml	0.178 [0.140, 0.267]
End-systolic elastance, mm Hg/ml	0.713 ± 0.312
Arterial elastance, mm Hg/ml	0.534 [0.349, 0.864]
Mean pulmonary arterial pressure, mm Hg	27 [19, 40]
Pulmonary arterial wedge pressure, mm Hg	10 [6, 11]
Central venous pressure, mm Hg	6 [5, 9]
Pulmonary vascular resistance, dyn·s/cm⁵	248 [139, 533]
Cardiac index, l/min/m²	2.7 [2.2, 3.1]
Diagnosis, n (%)	
Idiopathic PAH	9 (17)
PAH associated with rheumatologic disease	1 (2)
PAH associated with systemic sclerosis	1 (2)
Portopulmonary hypertension	1 (2)
Pulmonary veno-occlusive disease	1 (2)
HFpEF-PH	6 (11)
HFpEF-non-PH	3 (6)
Chronic thromboembolic PH	17 (32)
Chronic thromboembolic pulmonary disease	3 (6)
Controls	11 (21)
WHO functional class, n (%)	
I	2 (4)
II	13 (25)
III	35 (66)
IV	3 (6)
Mixed venous oxygen saturation, %	67.3 [63.8, 70.4]

Longitudinal ejection fraction, %	18.1 [16.1, 22.1]
Radial ejection fraction, %	17.6 [11.1, 22.0]
Anteroposterior ejection fraction, %	20.1 [14.8, 23.8]

BSA: body surface area, HFpEF: heart failure with preserved ejection fraction, LV: left ventricular, PAH: pulmonary arterial hypertension, PH: pulmonary hypertension, RV: right ventricular, S': peak systolic velocity of the lateral tricuspid annulus, WHO: World Health Organization

Six patients showed RV-PA uncoupling (Ees/Ea < 0.8). The median Ees/Ea value in the remaining patients was 1.3; 23 patients had normal RV-PA coupling (Ees/Ea ≥ 1.3), and 24 patients had intermediate RV-PA coupling (Ees/Ea 0.8–1.29).

7.3.4.2. Hemodynamic alterations relative to RV-PA coupling

Increasing impairment of RV-PA coupling was associated with pulmonary and RV hemodynamic alterations characteristic of PH. Parameters indicating RV afterload (mPAP, PVR, and Ea) were significantly increased in patients with intermediate coupling compared with patients with normal coupling ($p<0.05$) and in patients with uncoupling compared with patients with intermediate coupling ($p<0.05$). RV diastolic stiffness, indicated by Eed, demonstrated a significant increase in patients with uncoupling compared with patients with normal coupling ($p=0.006$). By contrast, RV contractility (Ees) showed no significant increase. The cardiac index was significantly reduced in patients with intermediate coupling compared with those with normal coupling ($p=0.007$) but was similar in patients with uncoupling and those with intermediate coupling [236].

7.3.4.3. Analysis of RV shortening along three spatial axes related to RV-PA coupling and risk stratification

RV shortening was analyzed along three axes, quantifying longitudinal, radial, and anteroposterior shortening. With the early decrease of Ees/Ea from normal to intermediate RV-PA coupling, significant impairment of LEF was noted (from 22 [19–26]% to 17 [14–19]%; p<0.001), whereas REF (p=0.18) and AEF (p=0.97) demonstrated no significant alterations (Figure 20A). In patients with RV-PA uncoupling compared with patients with intermediate RV-PA coupling, AEF was significantly decreased (12 [7–15]% compared with 21 [13–25]%; p=0.033), whereas REF (p=0.27) and LEF (p=0.49) remained unchanged.

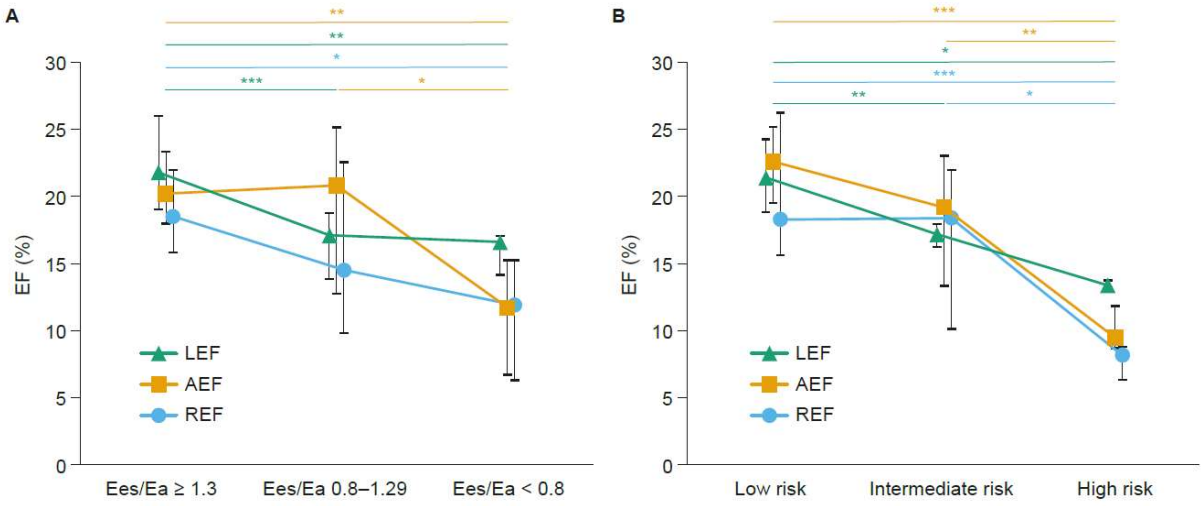

Figure 20. LEF for longitudinal, REF for radial, and AEF for anteroposterior shortening of the right ventricle (A) in relation to RV-PA coupling as indicated by Ees/Ea and (B) in relation to risk stratification according to European Society of Cardiology/European Respiratory Society guidelines [237]. *p<0.05; **p<0.01; ***p<0.001.

2D echocardiographic parameters reflecting longitudinal RV function (TAPSE, S', RVGLS, and RVFWLS) declined with decreasing Ees/Ea. TAPSE, RVGLS, and RVFWLS demonstrated a significant longitudinal RV functional impairment between normal and intermediate RV-PA coupling (p=0.041 for TAPSE, p=0.022 for RVGLS, and p=0.009 for

RVFWLS) but not between intermediate coupling and uncoupling; the decline in S' was not statistically significant in either comparison. FAC altered significantly between normal and intermediate coupling (p=0.020), as well as between intermediate coupling and uncoupling (p=0.003) [236].

The study population was additionally subdivided by risk stratification according to ESC/ERS guidelines (Figure 20B) [237]. Comparing intermediate risk (n=20) with low risk (n=27), a significant loss of LEF was noted (17 [16–18]% vs 21 [19–24]%; p=0.003), whereas REF (p=0.21) and AEF (p=0.10) remained unaltered. Comparing high risk (n=6) with intermediate risk, significant reductions in AEF (10 [9–12]% vs 19 [13–23]%; p=0.004) and REF (8 [6–9]% vs 18 [10–22]%; p=0.028) were observed, whereas LEF showed no significant change (p=0.12). Of note, LEF was not able to discriminate between patients at high risk and low/intermediate risk (Figure 21; area under the receiver operating characteristic curve [AUROC]: 0.780 [95% confidence interval (CI): 0.529, 1.000]) whereas AEF had a high discriminatory power (AUROC: 0.933 [95% CI: 0.856, 1.000]). The optimal AEF threshold to detect high-risk patients was 15%, with high sensitivity, specificity, negative predictive values, and accuracy (100%, 83%, 100%, and 85%, respectively). REF showed intermediate discriminatory power (AUROC: 0.883 [95% CI: 0.786, 0.980]) with acceptable accuracy (77%).

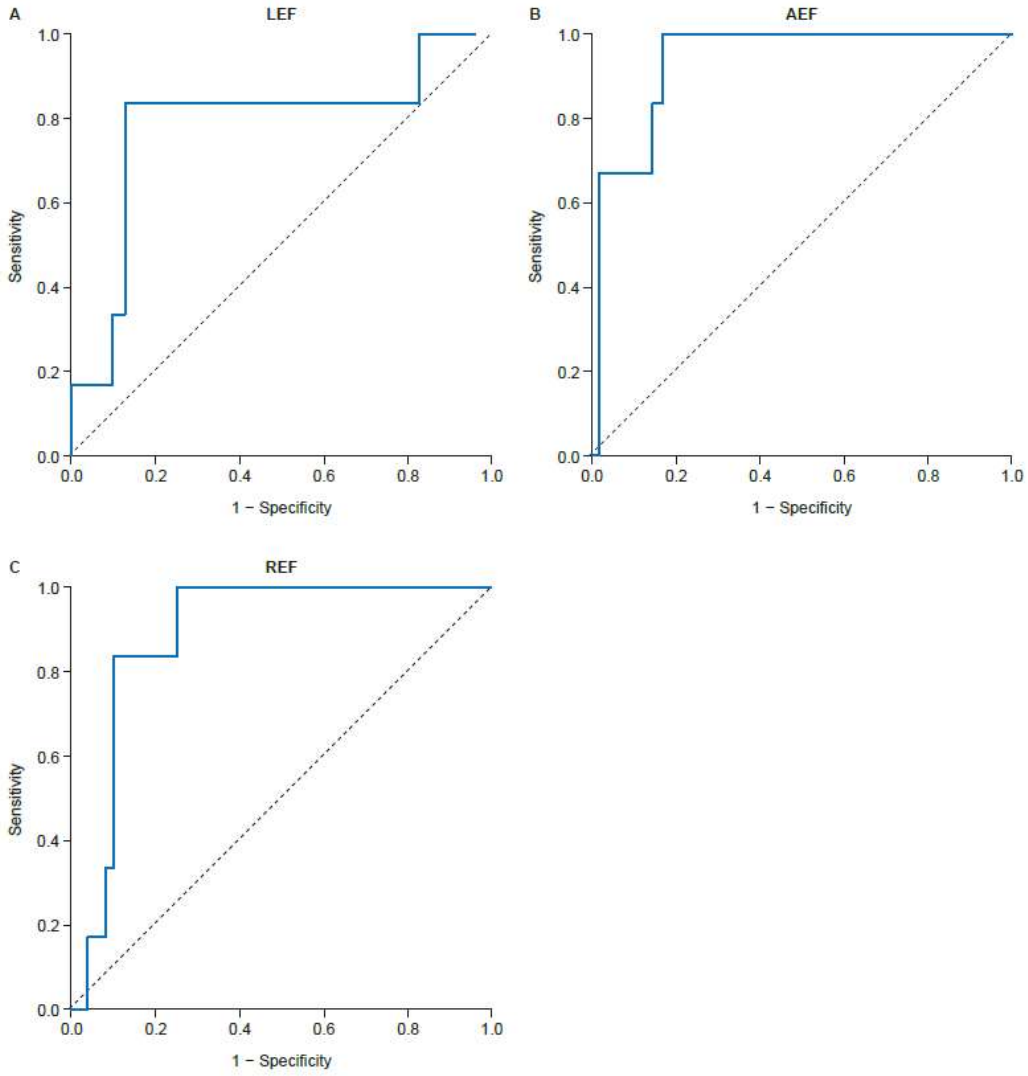

Figure 21. The ability of right ventricular contraction parameters to discriminate risk. Receiver operating characteristic curves show the ability of (A) LEF, (B) AEF, and (C) REF to discriminate between patients at high risk and those at low/intermediate risk based on the European Society of Cardiology/European Respiratory Society risk stratification scheme [237].

7.3.4.4. Ventricular interdependence and RV and LV volumetry

To demonstrate the evolution of the spatial interventricular relationship in the course of PH-related remodeling, RV and LV volumetry were compared between distinct levels of RV-PA coupling (Figure 22). RVEF (Figure 22A) demonstrated a significant decrease from normal to intermediate RV-PA coupling (p=0.021), as well as from intermediate RV-PA coupling to uncoupling (p=0.044), with no change in RVSV indexed to BSA (RVSVi; p=0.93 and p=0.71,

respectively; Figure 22B). RVEDV indexed to BSA (RVEDVi; Figure 22C) and RVESV indexed to BSA (RVESVi; Figure 22D) both increased significantly from normal RV-PA coupling to uncoupling (p=0.041 and p=0.003, respectively). RVESVi also showed a significant increase from normal to intermediate RV-PA coupling (p=0.039) and a borderline significant increase (p=0.050) from intermediate RV-PA coupling to uncoupling (Figure 22D), whereas the corresponding increases in RVEDVi were not significant (p=0.15 and p=0.13, respectively; Figure 22C). In contrast to RV findings, LV ejection fraction (LVEF) was not significantly altered with impairment of RV-PA coupling (p=0.96 between normal and intermediate RV-PA coupling, and p=0.13 between intermediate RV-PA coupling and uncoupling; Figure 22E). LV stroke volume indexed to BSA (LVSVi) showed significant impairment with RV-PA uncoupling (p=0.019) but remained stable between normal and intermediate coupling (p=0.88; Figure 22F). Consistent with this finding, LV end-diastolic volume indexed to BSA (LVEDVi) showed a significant decrease with RV-PA uncoupling (p=0.015; Figure 22G), whereas LV end-systolic volume indexed to BSA (LVESVi) demonstrated no significant change (p=0.71 between normal and intermediate RV-PA coupling, and p=0.37 between intermediate RV-PA coupling and uncoupling; Figure 22H).

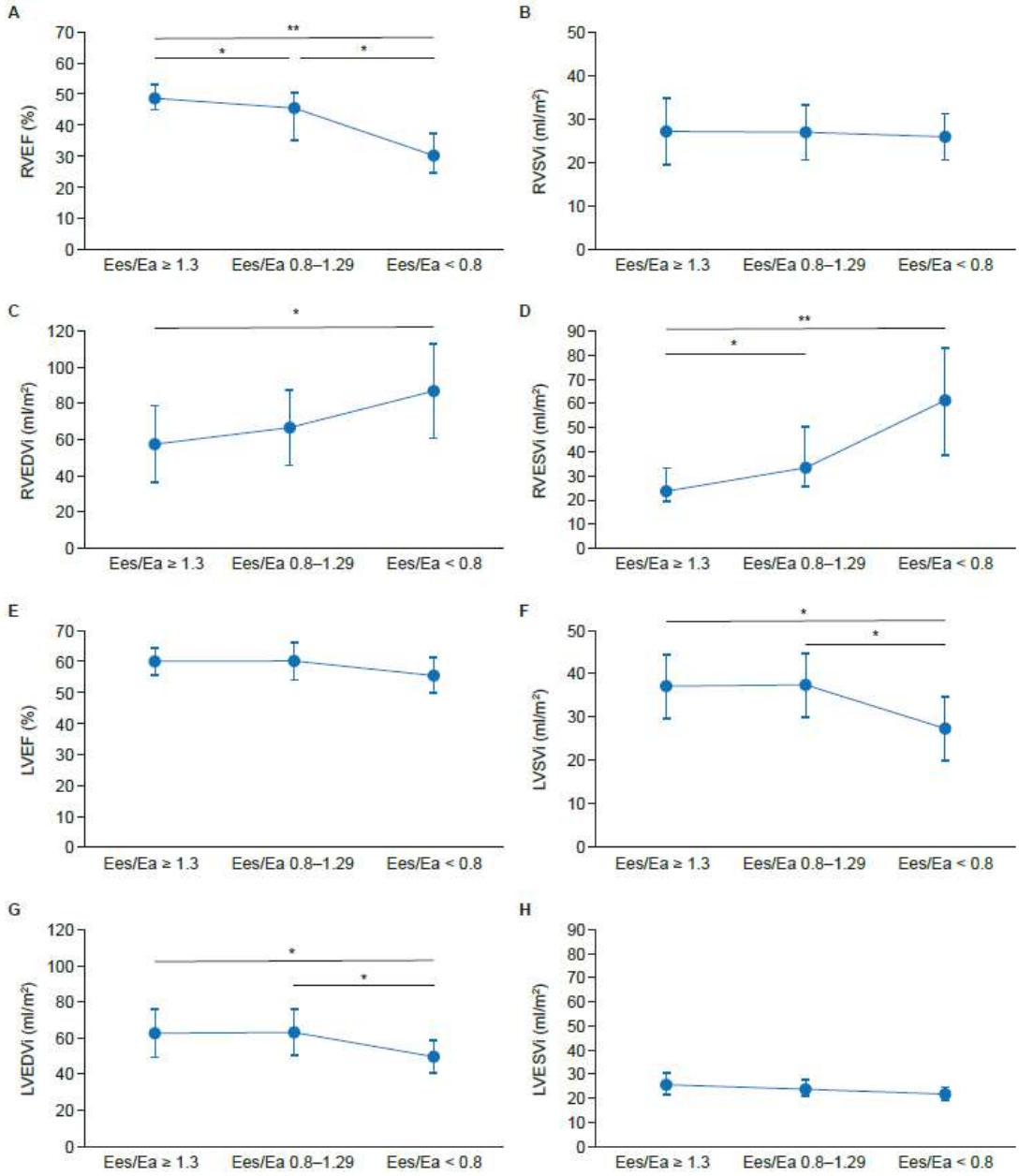

Figure 22. Ventricular volumetry and systolic function in relation to RV-PA coupling (A) RVEF, (B) RVSVi, (C) RVEDVi, (D) RVESVi, (E) LVEF, (F) LVSVi, (G) LVEDVi, and (H) LVESVi stratified by RV-PA coupling. Medians and interquartile ranges are shown for RVEF, RVESVi, and LVESVi; means and standard deviations are shown for the remaining parameters. *p<0.05; **p<0.01

7.3.5. RV contraction pattern after heart transplantation

Demographic characteristics of the study groups are shown in Table 30. The mean age of the predominantly male HTX patients was 52 years. The age- and gender-matched control group did not show any statistically significant difference in height, weight, BMI, BSA, systolic, and diastolic blood pressure compared to the HTX group (Table 30). HTX patients had significantly higher heart rates attributable to the denervation of the heart. The bicaval surgical technique was used in every patient.

LV end-diastolic-, end-systolic volumes, and stroke volume, along with their BSA-indexed values, showed no difference between the study groups (Table 30). LVEF and GLS were also similar, excluding the presence of LV systolic dysfunction. There was a trend toward significance in terms of higher LVM in HTX patients (Table 30).

Table 30. Baseline characteristics and left ventricular echocardiographic data of HTX and controls.

	HTX (n=51)	**Control (n=30)**	**p value**
Age, years	52.3±10.8	50.1±13.0	0.60
Female, n (%)	11 (22)	11(36)	0.14
Height, cm	173.3±9.4	170.1±11.7	0.19
Weight, kg	74.0± 2.9	70.0±11.0	0.16
BMI, kg/m²	24.6 ± 4.0	24.1±2.8	0.56
BSA, m²	1.9±0.2	1.8±0.2	0.11
SBP, mm Hg	122.4±14.0	124.2±13.1	0.53
DBP, mm Hg	79.4±8.1	74.7±8.4	0.41
HR, 1/min	86.5±13.1	65.8±10.4	<0.001
LVEDV, ml	100.5±24.8	95.4±24.2	0.46
LVEDVi, ml/m²	53.6±12.0	52.4±10.4	0.66
LVESV, ml	38.5±13.3	35.1±9.7	0.31
LVESVi, ml/m²	20.5±6.7	19.2±4.4	0.71
LVSV, ml	62.1±13.5	58.3±19.0	0.53
LVSVi, ml/m²	33.1±6.6	33.1±6.7	0.99

LVEF, %	62.4±5.8	63.2±3.4	0.44
LVGLS, %	−19.3±1.8	−19.1±2.0	0.57
LVM, g	131.6±22.2	122.5±20.0	0.14
LVMi, g/m²	71.0±14.0	67.8±9.2	0.85

BMI: body mass index, BSA: body surface area, DBP: diastolic blood pressure, EDV: end-diastolic volume, EF: ejection fraction, ESV: end-systolic volume, GLS: global longitudinal strain, HR: heart rate, i: indexed to BSA, LV: left ventricle, LVM: left ventricular mass, SBP: systolic blood pressure, SV: stroke volume

The basic clinical characteristics of HTX patients are presented in Table 31. About 51% of patients were transplanted due to end-stage HF with nonischemic etiology, and the operation was performed at a mean age of 51 years. Several hemodynamic and procedural parameters were collected to investigate the potential effects of perioperative circumstances. The median time elapsed after HTX was 226 days, ranging from 8 days to 18 years.

Table 31. Indications for HTX, peri- and postoperative parameters.

	HTX (n=51)
Etiology	
Nonischemic dilated cardiomyopathy, n (%)	26 (51)
Ischemic dilated cardiomyopathy, n (%)	21 (41)
Arrhythmogenic cardiomyopathy, n (%)	1 (2)
Other, nonspecified, n (%)	3 (6)
Age at HTX, years	50.5±11.1
Peri- andpostoperative parameters	
Preoperative pulmonary vascular resistance, Wood	2.73±1.1
Cold ischemic time, min	216.3±44.3
Aortic cross-clamping time, min	106.0±23.1
Cardiopulmonary bypass time, min	197.3±35.5
Age of donors, years	41.3±11.6
Gender of donors, female, n (%)	8 (16)

Length of intensive care unit stay, days	16.7±17.0
Postoperative sildenafil use, n (%)	44 (86)
Sildenafil use at time-point of echocardiography, n (%)	5 (10)
Elapsed time after HTX at the time-point of echocardiography, days	226 (95-827)

Conventional and 3DE parameters of the RV are summarized in Table 32. In terms of conventional linear measurements, RV mid diameter and length were similar; the basal diameter showed enlargement of the RV in HTX patients. Measurements referring to longitudinal shortening showed lower values than the control group (TAPSE, s′ by TDI, free wall, and septal longitudinal strain). Nevertheless, FAC, which partly incorporates radial function as assessed on a 2D apical four-chamber view, was normal and similar to healthy volunteers in HTX patients (44%, Table 32). There was no statistically significant difference in terms of end-diastolic and end-systolic RV volumes. RV EF was lower in HTX patients but remained within the normal range's lower limits. Correspondingly, stroke volume and stroke volume index were lower in HTX patients. Only four patients with moderate TR were in our HTX group (severe regurgitation was an exclusion criterion). PASP was higher in the transplanted cohort than in controls (Table 32).

Table 32. Conventional parameters of the right heart in HTX vs controls.

	HTX (n=51)	**Control (n=30)**	**p value**
RV basal diameter, mm	34.7 ± 7.6	27.6 ± 5.1	<0.001
RV mid diameter, mm	32.1 ± 7.6	29.1 ± 5.2	0.07
RV length, mm	73.4 ± 8.1	74.2 ± 6.6	0.65
TAPSE, mm	10.8 ± 5.2	21.1 ± 3.7	<0.001
FAC, %	44.2 ± 8.8	44.1 ± 4.8	0.99
PW TDI s′, cm/s	10.3 ± 2.3	13.9 ± 2.0	<0.001
RV Free wall LS, %	20.1 ± 5.3	29.5 ± 3.7	<0.001

RV Septal LS, %	11.9 ± 4.9	19.5 ± 4.0	<0.001
RVEDV, ml	96.3 ± 27.2	97.3 ± 23.6	0.87
RVEDVi, ml/m²	50.8 ± 12.3	53.9 ± 11.8	0.28
RVESV, ml	51.2 ± 15.1	44.9 ± 12.5	0.06
RVESVi, ml/m²	27.2 ± 7.0	24.8 ± 6.2	0.13
RVSV, ml	45.1 ± 15.3	52.4 ± 12.5	0.03
RVSVi, ml/m²	23.6 ± 7.1	29.1 ± 4.0	<0.001
RVEF, %	46.7 ± 7.2	54.1 ± 4.0	<0.001
Moderate TR, n (%)	4 (8)	0 (0)	<0.001
PASP, mmHg	34.2 ± 7.2	16.1 ± 5.4	<0.001
IVC at expiration, mm	16.2 ± 4.4	14.2 ± 5.6	0.16

EDV: end-diastolic volume, ESV: end-systolic volume, FAC: fractional area change, i: indexed to body surface area, IVC: inferior vena cava, LS: longitudinal strain, PASP: pulmonary arterial systolic pressure, PW TDI s′: pulsed-wave tissue Doppler imaging systolic velocity, RV: right ventricular, SV: stroke volume, TAPSE: tricuspid annular plane systolic excursion, RVEF: RV ejection fraction, TR: tricuspid regurgitation.

Figure 23 depicts our results regarding the relative contribution of longitudinal, radial, and anteroposterior wall motions to global RV function. In line with conventional echocardiographic parameters, longitudinal EF and its ratio to RVEF were significantly lower in HTX patients compared to healthy controls. However, the REF/RVEF ratio was significantly higher in HTX patients than in controls. AEF value alone was lower in HTX patients, and its ratio to RVEF was not significantly different from that of healthy volunteers (Figure 23). In HTX patients, REF/RVEF was significantly higher compared to both LEF/RVEF and AEF/RVEF (LEF/RVEF vs REF/RVEF vs AEF/RVEF: 0.27±0.08 vs 0.50±0.10 vs 0.38±0.07, ANOVA, $p<0.001$), which confirmed the radial wall motion to be dominant determining global RV function after HTX (Figure 23). On the contrary, in healthy volunteers, only AEF/RVEF ratio was smaller than LEF/RVEF, while REF/RVEF and LEF/RVEF were similar (LEF/RVEF vs REF/RVEF vs AEF/RVEF: 0.47±0.07 vs 0.45±0.07 vs 0.41±0.06, ANOVA $p=0.003$).

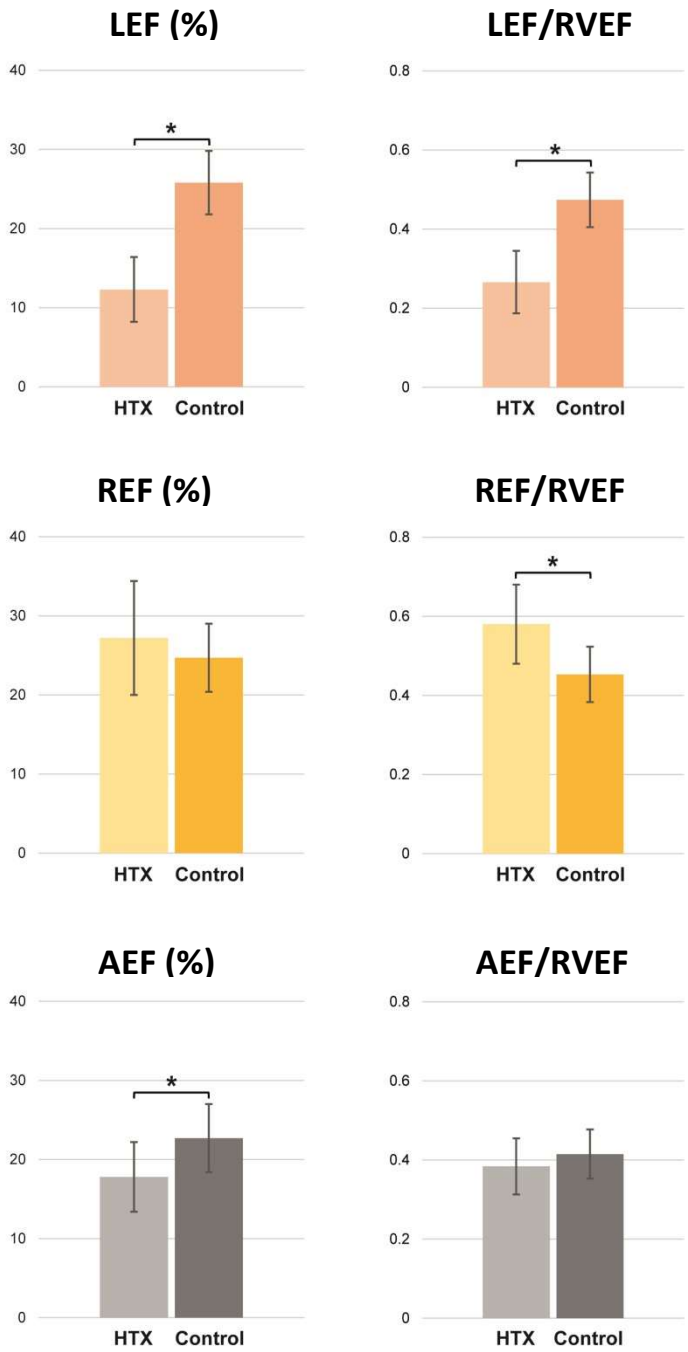

Figure 23. The relative contribution of the different wall motion components to RVEF in heart transplant recipients vs controls.

In HTX patients, RVEF assessed by 3DE correlated with FAC (r=0.762, p<0.001), free wall LS (r=0.394, p=0.018), and septal LS (r=0.430, p=0.032); however, TAPSE did not. LEF correlated moderately (r=0.421, p=0.002), while REF strongly with RVEF (r=0.767, p<0.001) in HTX recipients. We found no association between the perioperative hemodynamic or procedural parameters and the RV functional measurements at follow-up. Similarly, no

correlation was established between postoperative sildenafil usage and RV morphology and function. The time elapsed after HTX showed a correlation with RV longitudinal function (time vs TAPSE: r=0.577, p<0.001; vs free wall LS: r=0.483, p<0.001; vs septal LS: r=0.492, p<0.001; vs LEF/RVEF, r=0.289, p=0.004), on the other hand, it had a negative correlation with the dominance of radial contribution (REF/RVEF: r=−0.285, p=0.042). There was no association between anteroposterior shortening of the RV and time after HTX. We have also compared our HTX patients within 1 year and over 1 year after transplantation (29 vs 22 patients, respectively). There was no difference between the two groups in terms of 3D volumetric RV parameters (HTX within vs over 1 year; RVEDVi: 51.7±13.5 vs 49.7±11.0 ml/m^2, p=0.57; RVESVi: 27.4±7.8 vs 26.9±6.1 ml/m^2, p=0.80; RVSVi: 24.2±7.2 vs 22.7±7.1 ml/m^2, p=0.45; RVEF: 47.1±6.5 vs 46.3±8.3%, p=0.72). While FAC remained unchanged (42.3±7.8 vs 46.9±9.7%, p=0.075), parameters referring to longitudinal shortening showed a significant increase in time (TAPSE: 9.0±3.8 vs 13.3±6.1 mm; p=0.04, free wall LS: −18.2±3.9 vs −22.4±6.2%, p=0.005; septal LS: −10.6±3.8 vs 13.5±5.9%, p=0.037). The relative contribution of longitudinal and radial wall motions to global RV function was different: the LEF/RVEF ratio was significantly higher (0.23 ± 0.08 vs 0.31±0.06, p<0.001), the REF/RVEF ratio was significantly lower (0.60±0.09 vs 0.54±0.10, p=0.004) in patients transplanted over 1 year. On the other hand, there was no significant difference in terms of AEF/RVEF between the groups (0.37±0.07 vs 0.40±0.07, p=0.12). We found no correlations between perioperative parameters and RV functional measurements in either subgroup.

7.4. Establishing the added prognostic value of 3D RV assessment

7.4.1. Added prognostic value of 3D echocardiography over conventional RV functional measures

The final study population consisted of 174 patients with an average age of 62 years and a male predominance (72%). Seventy-eight subjects (45%) were HFrEF patients, of whom 69 patients were referred to our electrophysiology department to assess a potential *de novo* device implantation or upgrade. Later, 14 patients received an implantable cardioverter defibrillator (ICD), while 49 patients underwent cardiac resynchronization therapy (CRT-D) device implantation during the follow-up period. Nine patients were investigated for candidacy for a long-term LV assist device (LVAD) implantation, and after that, all received such a device. Twenty-eight subjects (16%) were heart transplant recipients (HTX) with a median of 96 days after the operation (ranging from 9 to 515 days). Sixty-eight subjects (39%) were patients with severe primary mitral valve regurgitation (MVR; 29 patients with Barlow's disease, 39 with fibroelastic deficiency) and underwent mitral valve repair or replacement after the echocardiography [238]. In this cohort of 174 patients, coronary artery disease status was previously established (and, if required, treated accordingly). There were also no subjects having moderate or severe stenosis on any valve.

Twenty-four patients met the primary endpoint of all-cause mortality at two years: 16 HFrEF patients (2 with ICD, 10 with CRT-D, 4 with LVAD implanted), 1 HTX patient, and 7 MVR patients. Two patients from the LVAD and two from the MVR cohort died in the early postoperative period.

Patients who met the endpoint were compared to those who did not in Table 33. Patients who died were older (68±10 years), but there was no difference in anthropometric measures, blood pressures, and serum creatinine levels (at the time of echocardiographic examination).

We did not find a difference in medical history either: prevalence of coronary artery disease, arterial hypertension, diabetes mellitus, and atrial fibrillation was similar in the two groups. The presence of significant (defined as moderate or severe) valvular regurgitations was also comparable (Table 33). Concerning conventional and 3DE characteristics, patients who died had higher LVESVi, along with a lower LVEF and LVGLS. However, LVEDVi, LVSVi, and LVMi were similar. LV diastolic function measures, including E/A and E/e' ratios, did not differ either. The group with adverse outcomes had significantly higher RVEDVi, RVESVi, but RVSVi was similar. Among RV functional parameters, RVEF and FAC and 2D free wall longitudinal strain significantly deteriorated in patients who experienced adverse outcomes. Importantly, however, TAPSE and RVSP did not differ.

Table 33. Baseline clinical and echocardiographic characteristics of the study population.

	All (n=174)	**Alive (n=150)**	**Dead (n=24)**	**p value**
Demographics, anthropometrics, medical history				
Age, years	62.3 ± 13.5	61.4 ± 13.7	68.1 ± 10.4	0.026
Male, n (%)	126 (72.4)	108 (72)	18 (75)	0.953
Height, cm	173.4 ± 12.2	173.6 ± 12.4	171.9 ± 11.1	0.867
Weight, kg	79.2 ± 15.7	78.8 ± 14.8	82.5 ± 20.7	0.796
Body surface area, m^2	1.9 ± 0.2	1.9 ± 0.2	2 ± 0.3	0.700
Systolic blood pressure, mmHg	126.2 ± 19.7	127.5 ± 18.6	118.9 ± 24.9	0.460
Diastolic blood pressure, mmHg	74.7 ± 16.5	75.3 ± 17.3	71.1 ± 11.5	0.353
Serum creatinine level, µmol/l	97.8 ± 39.3	96.7 ± 39.6	104.5 ± 37.7	0.380
Coronary artery disease, n (%)	38 (22)	33 (22)	5 (21.7)	1.000
Hypertension, n (%)	113 (65.3)	98 (65.3)	15 (65.2)	1.000
Diabetes mellitus, n (%)	39 (22.5)	33 (22)	6 (26.1)	0.866
History or present atrial fibrillation, n (%)	60 (34.7)	52 (34.7)	8 (34.8)	1.000
Moderate or severe mitral regurgitation, n (%)	82 (47.1)	70 (46.7)	12 (50)	0.933

Moderate or severe tricuspid regurgitation, n (%)	21 (12.1)	16 (10.7)	5 (20.8)	0.279
Echocardiographic parameters				
LVEDVi, ml/m²	94.8 ± 32.6	93.7 ± 32.7	102.6 ± 30.9	0.139
LVESVi, ml/m²	52.3 ± 30.5	50.6 ± 30.3	64 ± 30	0.026
LVSVi, ml/m²	42.6 ± 19.2	43.1 ± 19.6	38.6 ± 16.3	0.348
LVEF, %	47.5 ± 17.5	48.6 ± 17.4	39.6 ± 16.3	0.009
LVMi, g/m²	113.8 ± 37	112.9 ± 36.2	119.8 ± 42.3	0.385
LVGLS, %	-15.5 ± 7.4	-16 ± 7.3	-12.1 ± 7.3	0.017
E/A	1.6 ± 0.7	1.6 ± 0.7	1.7 ± 0.8	0.639
Deceleration time, ms	183.1 ± 67.1	182.5 ± 66.4	186.6 ± 72.9	0.998
Mitral lateral annular e', cm/s	10.3 ± 3.5	10.3 ± 3.6	9.9 ± 3.2	0.763
Mitral medial annular e', cm/s	7.2 ± 2.8	7.3 ± 2.8	6.1 ± 2.4	0.091
E/e'	12 ± 5.5	11.8 ± 5.6	13.1 ± 4.8	0.122
RV basal diameter, mm	30.5 ± 8.3	30.1 ± 8.1	32.8 ± 9.5	0.160
RVEDVi, ml/m²	75.5 ± 25	73.8 ± 24	85.8 ± 28.7	0.037
RVESVi, ml/m²	41.1 ± 18.7	39.5 ± 17.3	51.5 ± 24.2	0.009
RVSVi, ml/m²	34.3 ± 10.8	34.3 ± 11.1	34.4 ± 8.9	0.730
RVEF, %	46.9 ± 9	47.6 ± 8.8	42.2 ± 9.2	0.005
TAPSE, mm	20.2 ± 6.6	20.6 ± 6.8	18 ± 4.2	0.118
FAC, %	41.1 ± 8.7	41.7 ± 8.5	37.6 ± 9.5	0.037
RV free-wall longitudinal strain, %	-23.6 ± 7	-24.1 ± 6.9	-20.5 ± 7.1	0.024
RVSP, mmHg	36.5 ± 14.9	36.1 ± 15	38.7 ± 14.7	0.313

EDVi: end-diastolic volume index, EF: ejection fraction, ESVi: end-systolic volume index, FAC: fractional area change, GLS: global longitudinal strain, LV: left ventricular, Mi: mass index, RV: right ventricular, SP: systolic pressure, SVi: stroke volume index, TAPSE: tricuspid annular systolic excursion

By univariable Cox analysis, among the left-heart echocardiographic parameters, only LVEF (HR [95% CI]: 0.973 [0.950 – 0.997], $p<0.05$), and LV GLS (1.075 [1.009 – 1.146], $p<0.05$) were significantly associated with the primary endpoint, whereas LV volumes, LVMi, and diastolic function parameters were not. Concerning the metrics of the right heart, beyond RVEDVi, RVESVi, FAC, and 2D FWLS, RVEF (HR [95% CI]: 0.945 [0.908 – 0.984], $p<0.01$)

was found to be associated with adverse outcomes, while TAPSE and RVSP were not (Table 34).

Table 34. Univariable Cox proportional hazards models concerning the primary endpoint of 2-year all-cause mortality.

	HR [95% CI for HR]	p value
LVEDVi	1.007 [0.996 – 1.019]	0.226
LVESVi	1.012 [1 – 1.023]	0.052
LVSVi	0.987 [0.961 – 1.013]	0.312
LVEF	**0.973 [0.95 – 0.997]**	**0.026**
LVMi	1.005 [0.994 – 1.015]	0.402
LVGLS	**1.075 [1.009 – 1.146]**	**0.025**
E/A	1.136 [0.61 – 2.113]	0.688
Mitral lateral annular e'	0.968 [0.849 – 1.104]	0.626
Mitral medial annular e'	0.842 [0.687 – 1.031]	0.096
E/e'	1.03 [0.966 – 1.097]	0.367
RVEDVi	**1.017 [1.003 – 1.031]**	**0.020**
RVESVi	**1.027 [1.01 – 1.045]**	**0.002**
RVSVi	1.002 [0.966 – 1.039]	0.931
RVEF	**0.945 [0.908 – 0.984]**	**0.006**
TAPSE	0.943 [0.884 – 1.007]	0.078
FAC	**0.951 [0.907 – 0.996]**	**0.032**
RV free-wall longitudinal strain	**1.071 [1.01 – 1.135]**	**0.021**
RVSP	1.01 [0.986 – 1.035]	0.418

CI: confidence interval, EDVi: end-diastolic volume index, EF: ejection fraction, ESVi: end-systolic volume index, FAC: fractional area change, GLS: global longitudinal strain, HR: hazard ratio, LV: left ventricular, Mi: mass index, RV: right ventricular, SP: systolic pressure, SVi: stroke volume index, TAPSE: tricuspid annular systolic excursion

Using ROC analysis, we have investigated the relative discriminatory power of RV systolic function parameters (TAPSE, FAC, FWLS, RVEF) in predicting the primary endpoint. Among these metrics, RVEF exhibited the highest AUC value (0.679; 95% CI: 0.566 – 0.791)

compared with the other RV functional measures (Table 35). TAPSE and RVEF were directly compared by their ROC curves, and the outcome of the patient subgroups was dichotomized at the calculated optimal cut-offs of each parameter in Figure 24.

Table 35. Comparison of the discriminatory power by receiver-operator characteristic analysis of right ventricular systolic function parameters concerning the primary endpoint of 2-year all-cause mortality.

	AUC [95% CI]	Optimal cut-off	Sensitivity	Specificity
RVEF	0.679 [0.566 – 0.791]	48.2 %	0.57	0.79
TAPSE	0.600 [0.501 – 0.698]	24.0 mm	0.35	0.96
FAC	0.630 [0.495 – 0.766]	34.1 %	0.80	0.52
RV free-wall longitudinal strain	0.643 [0.515 – 0.771]	-19.4 %	0.57	0.75

AUC: area under the curve, CI: confidence interval, FAC: fractional area change, RV: right ventricular, RVEF: right ventricular ejection fraction, TAPSE: tricuspid annular systolic excursion

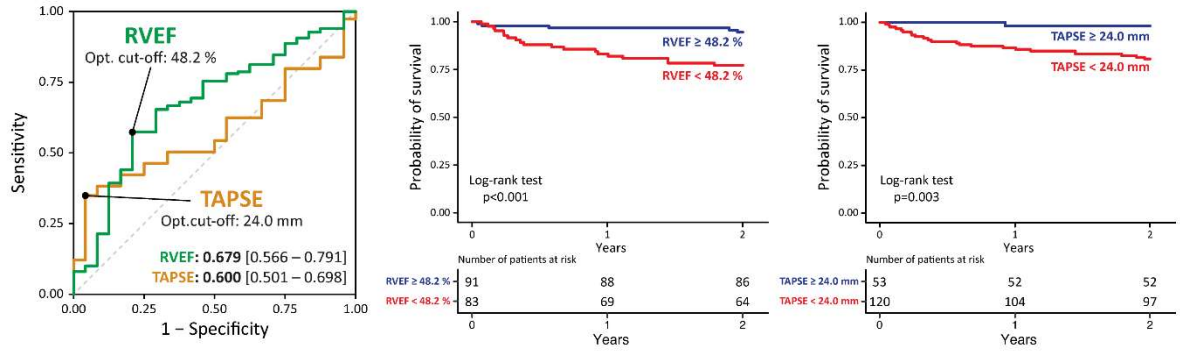

Figure 24. Comparison of the discriminatory power of tricuspid annular plane systolic excursion (TAPSE) versus right ventricular ejection fraction (RVEF) by receiver-operator characteristic analysis concerning the primary endpoint of 2-year all-cause mortality. Outcomes of the patient subgroups dichotomized at the calculated optimal cut-offs of each parameter are visualized on Kaplan-Meier curves.

7.4.2. Added prognostic value of 3D echocardiography over conventional RV functional measures – meta-analysis

7.4.2.1. Study selection and characteristics

A total of 189 articles were subject to full-text review. According to the predefined inclusion and exclusion criteria, 13 studies were found suitable. In three instances (including 3-3 studies), there was an apparent overlap between the patient cohorts [4, 48, 228, 239-241]; therefore, studies with a higher number of participants were included [48, 239, 241]. Overall, ten [48, 239, 241-248] independent studies were included in the final quantitative analysis (Figure 25), which reported the impact of unit change of RVEF and TAPSE (n=8) [239, 240, 242, 244-248], or FAC (n=7) [239, 243-248], or FWLS (n=7) [241, 243-248], on clinical outcomes (all-cause mortality and/or cardiopulmonary adverse events) as HRs. Four studies were prospective, while six were retrospective. Only three studies reported associations with all-cause mortality [239, 246, 248], the others reported composite cardiopulmonary endpoints (Table 36). We assessed the risk of bias within the studies using the QUIPS tool [1].

Table 36. Study designs and clinical endpoints.

Study	Sample size (n)	Design	Population	FU duration (months)	Endpoint	Events, n (%)
Murata ***(2016)***	86	Retrospective	PAH	14.1	cardiac events (death, hosp, intervention including PEA or BPA)	19 (22.1)
Moceri ***(2017)***	104	Prospective	PH	6.7	cardio-pulmonary death	16 (15.4)
Surkova ***(2019)***	394	Retrospective	various cardiac diseases	44.4	all-cause mortality	56 (14.2)
Zhang ***(2021)***	128	Prospective	COVID-19	3	all-cause mortality	18 (14.1)
Vîjîiac ***(2021)***	50	Prospective	DCM	16	cardiac death, nonfatal cardiac arrest, acute HF hosp	29 (53.7)
Li ***(2021)***	203	Retrospective	PH	20.9	PH-related hosp; intervention or surgery including PEA or BPA; death	87 (42.9)
Meng ***(2021)***	81	Prospective	HFpEF	17	HF death or HF rehosp	39 (48.1)
Tolvaj ***(2021)***	174	Retrospective	various cardiac diseases	24	all-cause mortality	24 (13.8)
Nabeshima ***(2021)***	367	Retrospective	AS	26.7	cardiac death, HF hosp, VT/VF, or non-fatal MI	57 (15.5)
Kitano ***(2022)***	341	Retrospective	various cardiac diseases	19.8	cardiac death, VT, or HF hosp	49 (14.4)

AS: aortic stenosis, BPA: balloon pulmonary angioplasty, DCM: dilated cardiomyopathy, HF: heart failure, HFpEF: heart failure with preserved left ventricular ejection fraction, hosp: hospitalization, MI: myocardial infarction, PAH: pulmonary arterial hypertension, PEA: pulmonary endarterectomy, PH: pulmonary hypertension, VF: ventricular fibrillation, VT: ventricular tachycardia

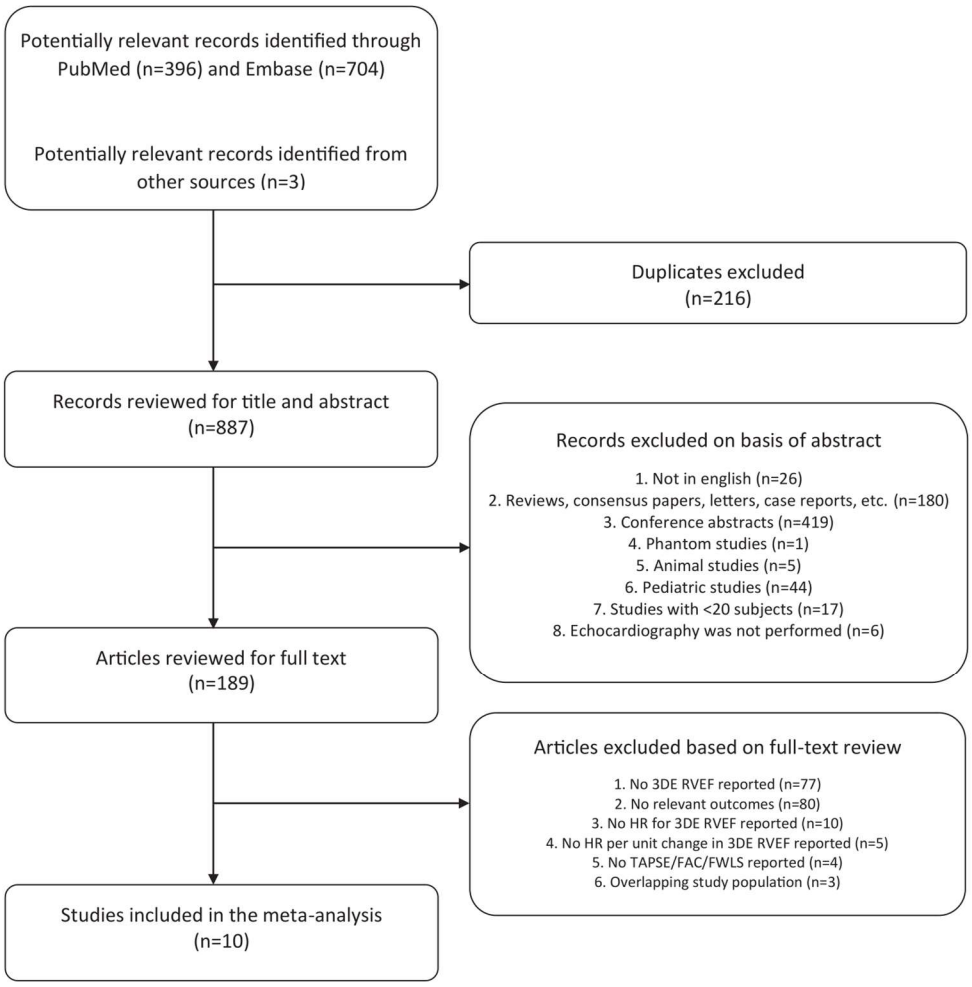

Figure 25. Study selection flowchart. 3DE: three-dimensional echocardiography, FAC: fractional area change, FWLS: free-wall longitudinal strain, HR: hazard ratio, RVEF: right ventricular ejection fraction, TAPSE: tricuspid annular plane systolic excursion

7.4.2.2. Echocardiographic measurements

All study subjects in the selected ten studies underwent standard echocardiographic examination by experienced sonographers using commercially available ultrasound scanners. All of the measurements were performed and reported in the published articles by the corresponding study investigators. RVEF was measured by a single commercially available software in all the cases (TomTec 4D RV-Function, TomTec Imaging GmbH, Unterschleissheim, Germany; reported version 2.0 or newer, standalone or embedded into

another vendor's platform). In most cases, an RV-focused apical window was used to acquire the full-volume 3DE dataset using multi-beat reconstruction, which was finally utilized to measure RVEF. The investigators further corrected the initial semi-automated 3D contouring manually. Feasibility of RVEF measurement ranged from 81% to 98% across the ten studies, which also reported good interobserver agreement. TAPSE was measured using an M-mode recording, while FAC was assessed by contouring the end-diastolic and end-systolic RV endocardial surfaces in accordance with current guidelines [221]. Two-dimensional FWLS was measured using commercially available software packages from two vendors [1].

7.4.2.3. Patient characteristics

The ten studies comprised data on 1928 patients. Clinical characteristics and definitions of composite endpoints are shown in Tables 36 and 37. The patient population's mean (±SD) age was 63±15 years, 46% were females, and the follow-up duration ranged from 3 to 44 months. Three studies included patients with PH exclusively [48, 241, 245], one included patients with COVID-19 only [248], one included patients with dilated cardiomyopathy only [247], one included patients with aortic stenosis only [243], one included HFpEF only [244], and the remaining three studies included populations with a mixture of cardiovascular diseases [239, 242, 246].

Table 37. Demographic and clinical characteristics of the study populations.

Study	Age, years	Female, n (%)	BMI, kg/m^2	BSA, m^2	HR, bpm	SBP, mmHg	DBP, mmHg	DM, n (%)	HTN, n (%)	DLP, n (%)	CAD, n (%)	CKD, n (%)
Murata (*2016)*	50±17	63 (72)	NA	1.6±0.2	72±14	111±17	64±13	NA	NA	NA	NA	NA
Moceri *(2017)*	66 (62-69)	58 (56)	NA	1.72±0.2	NA	NA	NA	NA	NA	NA	NA	NA
Surkova *(2019)*	57 (42-69)	136 (35)	24.5 (22.1-26.8)	1.81 (1.67-1.95)	68 (59-77)	120 (110-130)	70 (70-80)	51 (12.9)	190 (48.2)	143 (36.3)	119 (30.2)	NA
Zhang *(2021)*	61±13	80 (50)	NA	1.67±0.15	86 (80-99)	130 (120-140)	80 (73-88)	18 (14.1)	52 (40.6)	NA	NA	1 (0.8)
Vîjîiac *(2021)*	61±14	16 (32)	NA	NA	79±16	124±13	75±11	9 (18)	34 (68)	NA	0 (0)	NA
Li *(2021)*	49±15	146 (72)	NA	1.7±0.2	NA	NA	NA	NA	NA	NA	NA	NA
Meng *(2021)*	62±12	18 (35)	25.5±3.6	NA	72.4±11.5	136.3±22.6	83.0±14.9	36 (44.4)	46 (56.8)	NA	NA	NA
Tolvaj *(2021)*	62±14	48 (28)	NA	1.9±0.2	NA	126.2±19.7	74.7±16.5	39 (22.5)	113 (65.3)	NA	38 (22)	NA
Nabeshima *(2021)*	77±10	199 (54)	22.7±3.9	1.52±0.21	69.5±12.6	147.5±23.5	75.0±13.5	115 (31)	295 (80)	NA	79 (22)	174 (47)
Kitano *(2022)*	68 (58-76)	115 (34)	NA	1.62 (1.50-1.75)	67 (59-76)	127 (112-145)	71 (63-79)	101 (30)	191 (56)	149 (44)	143 (42)	149 (44)

BMI: body mass index, BSA: body surface area, CAD: coronary artery disease, CKD: chronic kidney disease, DBP: diastolic blood pressure, DLP: dyslipidemia, DM: diabetes mellitus, HR: heart rate, HTN: systemic arterial hypertension, SBP: systolic blood pressure

7.4.2.4. Outcomes

Table 36 contains the definitions of endpoints assessed in each included study. Among the 1928 patients, 394 (20.4%) reached the endpoint of all-cause mortality and/or adverse cardiopulmonary events.

In the ten studies, 1 SD reduction in RVEF was associated with a 2.64-fold (95% CI: 2.18 to 3.20, p<0.001) increase in the risk of all-cause mortality and/or adverse cardiopulmonary events (Figure 26). The moderate heterogeneity (I^2=65%, p=0.002) found across studies was not explained by differences between follow-up duration (pseudo-R^2=2%, p=0.062), endpoint definitions (pseudo-R^2=0%, p=0.806), or primary diagnosis of PH (pseudo-R^2=0%, p=0.524). Regarding endpoint definitions, three studies comprising 696 patients reported all-cause mortality. Accordingly, 1 SD reduction in RVEF was associated with 2.63-times (95% CI: 1.60-4.30, p<0.001) higher risk of death from any cause. Furthermore, we conducted a subgroup analysis of studies reporting outcomes on patients with a primary diagnosis of pulmonary hypertension (n=3 studies, overall: 393 patients) versus those studies including patients with other cardiopulmonary conditions (n=7 studies, overall: 1535 patients). We found that RVEF showed a robust correlation with adverse outcomes in patients with (HR: 2.97 [95% CI: 2.12-4.14]) and without (HR: 2.57 [95% CI: 2.04-3.24]) PH. Given the vast overlap of confidence intervals, the interaction between these two subgroups was non-significant (p=0.49), suggesting that RVEF correlates with clinical outcomes regardless of whether pulmonary hypertension is the primary cause of RV dysfunction.

The funnel plot and Begg's test for small-study effects (z=-1.43, p=0.15) showed that the risk of publication bias was low. Accordingly, the trim-and-fill analysis showed that even if significant one-tailed publication bias occurred that favored the publication of highly positive studies (suggesting that reduction in RVEF is strongly associated with adverse clinical

outcomes), our pooled study estimate would not have been significantly altered (adjusted HR: 2.32 [95% CI: 1.86 to 2.90]) [1].

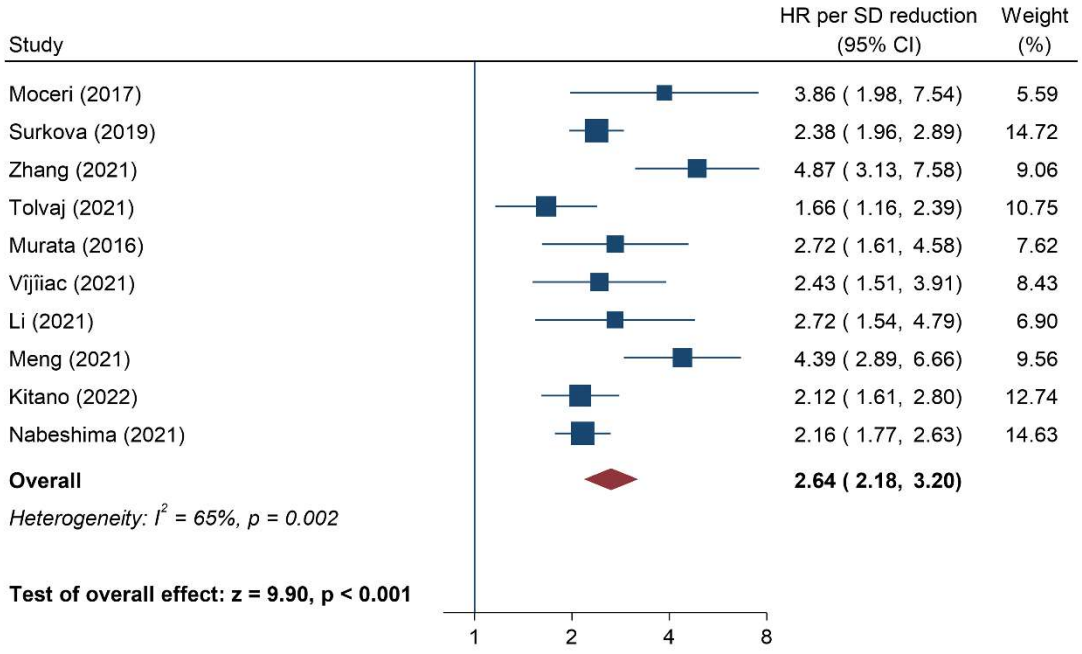

Figure 26. Three-dimensional echocardiography-derived right ventricular ejection fraction (RVEF) and its association with all-cause mortality and/or composite adverse cardiopulmonary endpoints. The hazard ratios (HR) are per 1 standard deviation (SD) reduction in RVEF according to each study. Accordingly, a HR of >1.00 means that 1 SD reduction in RVEF is associated with increased risk of adverse events. CI: confidence interval

In studies reporting HRs for RVEF and TAPSE simultaneously in the same cohort (n=8, 1358 patients), the SD reduction in RVEF (HR: 2.76 [95% CI: 2.16 to 3.54]) and TAPSE (HR: 1.81 [95% CI: 1.43 to 2.28]) were both significantly associated with adverse clinical outcomes. However, the HR per SD change for RVEF as a correlate of outcomes was 1.54 (95% CI: 1.04 to 2.28, p=0.031) times greater than that of TAPSE, with moderate heterogeneity (I^2=74%, p<0.001) (Figure 27). The latter was not related to study differences in follow-up duration (pseudo-R^2=17%, p=0.15), endpoint definitions (pseudo-R^2=0%, p=0.95), or primary diagnosis of PH (pseudo-R^2=0%, p=0.68). Begg's test for small-study effects (z=0.62, p=0.54) indicated no evidence of substantial one-sided publication bias.

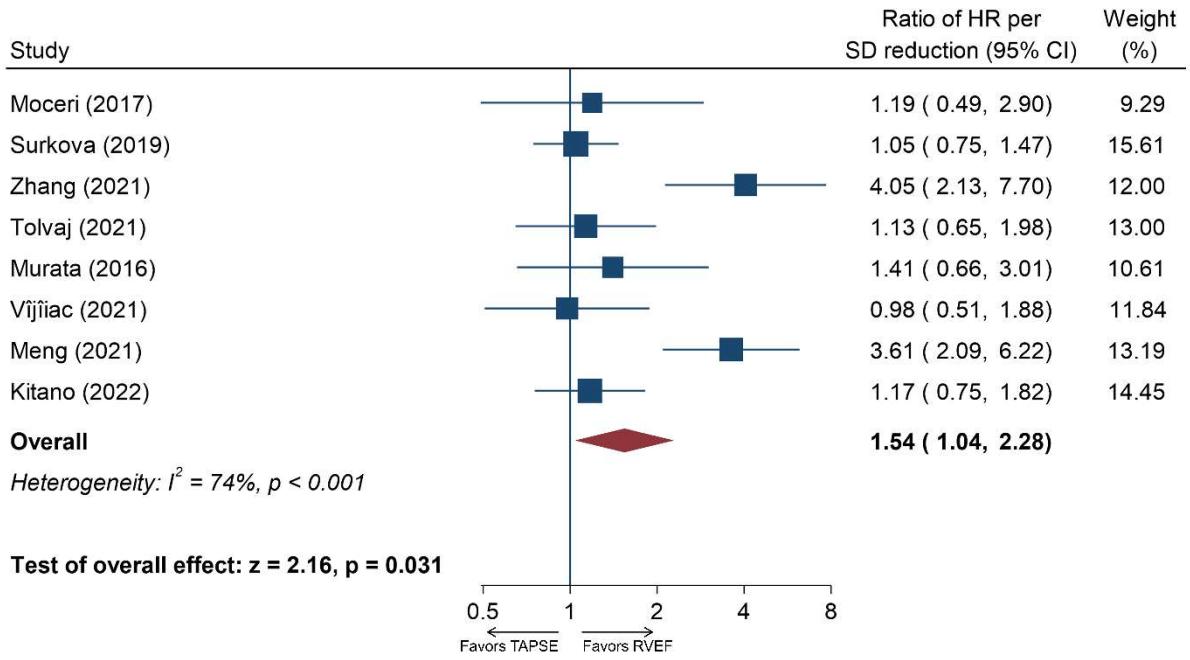

Figure 27. Three-dimensional echocardiography-derived right ventricular ejection fraction (RVEF) versus tricuspid annular plane systolic excursion (TAPSE) by their association with all-cause mortality and/or composite adverse cardiopulmonary endpoints. The ratios of hazard ratios (HR) per 1 standard deviation (SD) reduction in RVEF/TAPSE are depicted. Accordingly, a ratio of HR >1.00 means that 1 SD reduction in RVEF is associated with a higher risk of adverse events compared to 1 SD reduction in TAPSE. CI: confidence interval

In studies reporting HRs for RVEF and FAC in the same cohort (n=7, 1280 patients), we found that 1 SD reduction in RVEF (HR: 2.68 [95% CI: 2.09 to 3.42]) and FAC (HR: 1.71 [95% CI: 1.44 to 2.02]), respectively, were associated with adverse outcomes in patients with various diseases. The above HR per SD reduction in RVEF translates into 1.45 (95% CI: 1.15 to 1.81, p=0.001) times greater risk of adverse outcomes as compared to that of FAC (Figure 28). In this analysis, heterogeneity was low (I^2=39%, p=0.13), to which differences in follow-up duration (pseudo-R^2=0%, p=0.39), endpoint definitions (pseudo-R^2=0%, p=0.22), and primary diagnosis of PH (pseudo-R^2=0%, p=0.89) had no significant contribution. The presence of publication bias in this analysis was not supported by the visual inspection of the funnel plot and Begg's test (z=0.30, p=0.76).

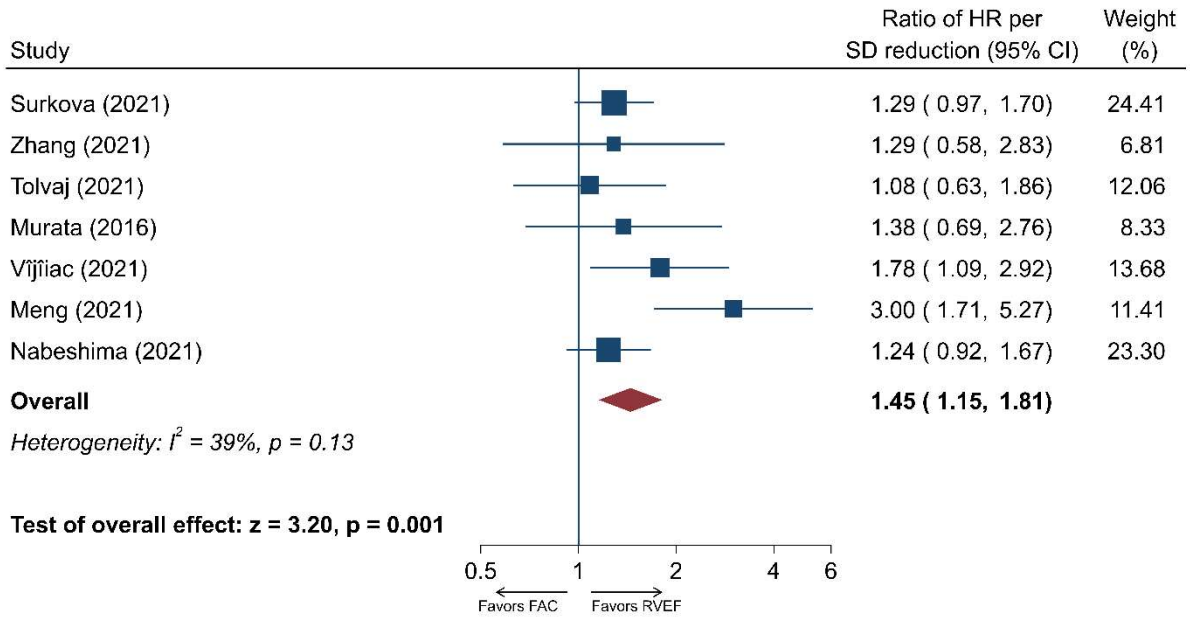

Figure 28. Three-dimensional echocardiography-derived right ventricular ejection fraction (3D RVEF) versus fractional area change (FAC) by their association with all-cause mortality and/or composite adverse cardiopulmonary endpoints. The ratios of hazard ratios (HR) per 1 standard deviation (SD) reduction in RVEF/FAC are shown. Accordingly, a ratio of HR >1.00 means that 1 SD reduction in RVEF is associated with a higher risk of adverse events compared to 1 SD reduction in FAC.
CI: confidence interval

Finally, in studies reporting the association of unit change in RVEF and FWLS on clinical outcomes in the same cohort (n=7, 1089 patients), we found that 1 SD decrease in these parameters was significantly associated with adverse events (RVEF, HR: 2.76 [95% CI: 2.06 to 3.70]; FWLS, HR: 1.77 [95% CI: 1.42 to 2.21]). However, the strength of effect for the HR per SD reduction for RVEF was 1.44 (95% CI: 1.07 to 1.95, p=0.018) times higher than that of FWLS, suggesting a more robust association (Figure 29). None of the investigated factors (follow-up duration: pseudo-R^2=0%, p=0.96; endpoint differences: pseudo-R^2=0%, p=0.18; primary diagnosis of PH: pseudo-R^2=0%, p=0.60) contributed significantly to the low level of heterogeneity (I^2=47%, p=0.08). No substantial small study effect was present based on the funnel plot and Begg's test (z=0.30, p=0.76) [1].

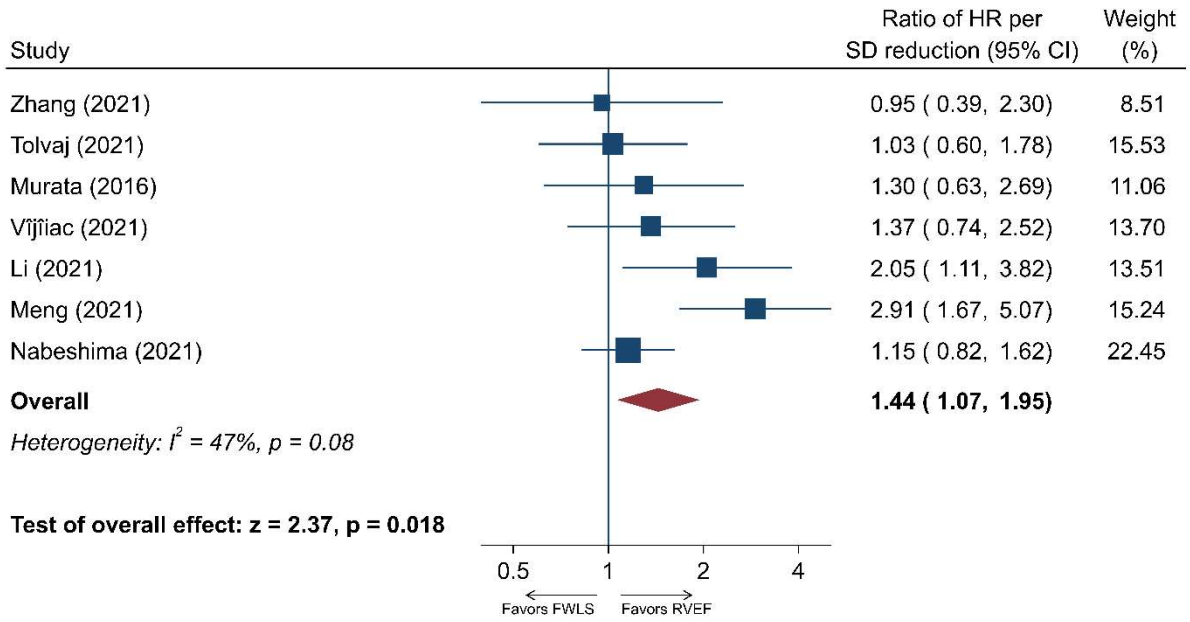

Figure 29. Three-dimensional echocardiography-derived right ventricular ejection fraction (3D RVEF) versus free-wall longitudinal strain (FWLS) by their association with all-cause mortality and/or composite adverse cardiopulmonary endpoints. The ratios of hazard ratios (HR) per 1 standard deviation (SD) reduction in RVEF/FWLS are depicted. Accordingly, a ratio of HR >1.00 means that 1 SD reduction in RVEF is associated with a higher risk of adverse events compared to 1 SD reduction in FWLS. CI: confidence interval

7.4.3. Perioperative changes and prognostic value of RV contraction pattern in patients with severe mitral regurgitation

7.4.3.1. Population characteristics

The mean age of the MVR patient population was 63±11 years, and predominantly males were included (69%). The healthy control population was age- and gender-matched (60±7 years, 19 [63%] males). The underlying etiology of primary MR was fibroelastic deficiency (n=22 [52%]), Barlow's disease (n=17 [41%]), and rheumatic mitral valve disease (n=3 [7%]). Mitral valve leaflet prolapse involved the anterior (n=2 [5%]), posterior (n=23 [55%]), or both leaflets (n=14 [33%]). Ruptured chordae tendineae were observed in 26 (62%) patients. The median of the European System for Cardiac Operative Risk Evaluation

(EUROSCORE) II was 1.53 [0.91-2.12]. Severe MR was confirmed with the PISA method during the preoperative echocardiographic examination in each case (EROA: 73 [55-87] mm^2, regurgitation volume: 102 [89-115] ml).

7.4.3.2. Surgery and ICU stay

Twenty-six patients (62%) underwent mitral valve replacement (mechanical or bioprosthetic valve), and 16 patients (38%) had mitral valve repair. Tricuspid valve repair (DeVega annuloplasty) was performed in 9 (21%) patients. The CPB and aortic cross-clamp time median was 100 [89-109] minutes and 76 [67-88] minutes, respectively. The length of stay at ICU was 47 [26-94] hours, and the length of hospital stay was 7 [6-8] days in our study cohort. During ICU stay, 16 patients (38%) required dual inotropic agent therapy (dobutamine and milrinone) and/or received inotropic support longer than 24 hours. The incidence of new-onset atrial fibrillation was 17% (7 patients), and 3 cases (7%) had stage 1 acute kidney injury (based on the criteria of Kidney Disease Improving Global Outcomes [249]) in the postoperative period. None of the patients undergoing mitral valve repair had moderate or severe residual MR, whereas trace or mild MR was observed in 2 (13%) patients postoperatively. No in-hospital or 6-month death was observed.

7.4.3.3. Adaptation to chronic primary MR

Patients' echocardiographic characteristics are presented in Table 38. Patients had larger LVEDVi and LVMi at the preoperative examination ($p<0.001$ vs controls). Higher values of EROA and regurgitant volume were associated with a more pronounced LV remodeling (LVEDVi vs EROA: $\beta=0.60$, $R^2=0.33$, $p<0.001$; LVEDVi vs regurgitant volume: $\beta=0.75$, $R^2=0.54$, $p<0.001$; LVMi vs EROA: $\beta=0.57$, $R^2=0.28$, $p=0.002$; LVMi vs regurgitant volume:

β=0.61, R^2=0.33, p<0.001). The LVEF was higher in our patient population than in controls (p=0.011), confirming the hyperdynamic state. Higher RV volumes were also observed compared to controls (all p<0.001). Global RV systolic function as assessed by FAC and RVEF was slightly reduced (both p<0.001), whereas indicators of longitudinal function demonstrated preserved (tricuspid TDI S', LEF) or even elevated values (TAPSE, 2D RV FWLS and 3D RVGLS, all p<0.05) compared to controls. Decreased radial function as quantified by REF and REF/RVEF was also noted (both p<0.001), suggesting that the decline in radial contractions might explain the slight decrease in global RV function. At baseline, the longitudinal shortening was the main contributor to global systolic function (LEF/RVEF vs REF/RVEF; 0.53 [0.47-0.58] vs 0.33 [0.22-0.42]; p<0.001), whereas in controls the longitudinal and radial shortenings contributed equally to RVEF (0.48 [0.42-0.51] vs 0.43 [0.37-0.48]; p=0.251) (Figure 30). The magnitude of EROA and regurgitant volume also were also associated with RV geometrical remodeling (RVEDVi vs EROA: β=0.41, R^2=0.15, p=0.034; RVEDVi vs regurgitant volume: β=0.57, R^2=0.31, p<0.001). Preoperatively measured CVP, mPAP, PAWP, PVR, and DPG were 13 [10-16] mmHg, 28 [21-36] mmHg, 17 [14-23] mmHg, 2.5 [1.8-3.5] Wood Unit and 3 [1-9] mmHg, respectively. These findings confirm the presence of isolated post-capillary pulmonary hypertension as defined by the current guidelines [250]. Preoperative RVEF was inversely related to mPAP (β=-0.48, R^2=0.29, p=0.002) and PAWP (β=-0.48, R^2=0.31, p=0.001).

Table 38. Echocardiographic characteristics of healthy controls and patients undergoing MVR.

	Controls	Preoperative	Postoperative	6-month FU	p
	n=30	n=42	n=35	n=35	
			Left Ventricle		
LVMi (g/m²)	62 [56-67]	95 [78-112]*	88 [73-105]*	67 [60-75]*†‡	<0.001
LVEDVi (ml/m²)	59 [52-64]	91 [74-109]*	74 [65-90]*§	61 [53-70]†‡	<0.001
LVESVi (ml/m²)	23 [21-26]	34 [27-40]*	38 [29-45]*	25 [23-29]*†‡	<0.001
LVEF (%)	61 [59-62]	63 [61-65]*	51 [46-57]*§	58 [56-61]*†‡	<0.001
LVGLS (%)	-22 [(-23)-(-19)]	-22 [(-24)-(-20)]	-16 [(-18)-(-13)]*§	-18 [(-20)-(-16)]*†‡	<0.001
LVGCS (%)	-31 [(-33)-(-27)]	-32 [(-34)-(-29)]	-24 [(-28)-(-20)]*§	-29 [(-31)-(-27)]†‡	<0.001
			Right Ventricle		
RV diam (mm)	32 [29-33]	35 [30-37]*	36 [32-38]*	34 [31-36]*	0.139
RV length (mm)	81 [74-86]	86 [81-93]*	82 [76-92]	77 [73-83]†‡	<0.001
TAPSE (mm)	24 [21-26]	26 [23-30]*	13 [11-15]*§	17 [13-18]*†‡	<0.001
RV S' (cm/s)	15 [14-17]	14 [13-16]	9 [7-11]*§	10 [8-12]*†	<0.001
RV FWLS (%)	-22 [(-25)-(-19)]	-27 [(-32)-(-22)]*	-19 [(-23)-(-17)]*§	-28 [(-32)-(-23)]*‡	<0.001
FAC (%)	54 [50-58]	39 [34-47]*	41 [35-46]*	47 [42-52]*†‡	<0.001
RVEDVi (ml/m²)	57 [51-60]	66 [58-82]*	66 [55-82]*	60 [53-70]†‡	<0.001
RVESVi (ml/m²)	21 [20-24]	31 [28-42]*	32 [28-44]*	27 [24-37]*†‡	<0.001
RVEF (%)	61 [58-65]	52 [50-55]*	51 [46-54]*§	53 [49-57]*‡	0.005
LEF (%)	29 [26-31]	28 [23-32]	17 [12-20]*§	23 [20-27]*†‡	<0.001
REF (%)	26 [21-31]	16 [12-23]*	23 [17-27]*	21 [19-27]*	0.032
LEF/RVEF	0.48 [0.42-0.51]	0.53 [0.47-0.58]*	0.33 [0.28-0.43]*§	0.44 [0.38-0.50]†‡	<0.001
REF/RVEF	0.43 [0.37-0.48]	0.33 [0.22-0.42]*	0.46 [0.37-0.51]§	0.41 [0.36-0.49]†	0.008
RVGLS (%)	-24 [(-26)-(-21)]	-28 [(-33)-(-22)]*	-19 [(-22)-(-15)]*§	-24 [(-28)-(-21)]†‡	<0.001
RVGCS (%)	-24 [(-28)-(-22)]	-24 [(-27)-(-19)]	-26 [(-28)-(-21)]	-25 [(-28)-(-19)]	0.956

*p<0.05 vs healthy controls, §p<0.05 preoperative vs postoperative, †p<0.05 preoperative vs 6-month follow-up, ‡p<0.05 postoperative vs 6-month follow-up

7.4.3.4. Morphological and functional changes in LV following MVR

LVEDVi decreased after MVR, while 6 months after the surgery, it became comparable to controls' (Table 38). LVMi did not change significantly right after surgery, but it showed a pronounced reduction at the 6-month follow-up. LVEF and LV myocardial deformation exhibited lower values after surgery and recovered only partially at 6 months (Table 38). Sixteen (46%) patients exhibited LVEF<50% at the postoperative echocardiographic assessment, and LVEF reduction greater than 10% in comparison with the preoperative values was observed in 18 (51%) patients. Higher preoperative 3D LVGLS was found to be associated with a greater reduction in LVEF (β=-0.73, R^2=0.50, p<0.001).

7.4.3.5. Postoperative shift in RV contraction pattern

RV geometry, as assessed by RVEDVi, did not change right after surgery; however, it showed some reduction at the 6-month follow-up (Table 38). While RVEF decreased only slightly after MVR (52 [50-55] vs 51 [46-54] %, p=0.001), there were marked changes in RV mechanical pattern: the radial motion became the dominant component after surgery (LEF/RVEF vs REF/RVEF; 0.33 [0.28-0.43] vs 0.46 [0.37-0.51]; p=0.004). However, this temporary shift recovered 6 months later, and the contraction pattern was found to be similar to controls showing equal contribution of the two components (0.44 [0.38-0.50] vs 0.41 [0.36-0.49]; p=0.775). The postoperative decline and the tendency towards normalization could also be observed in other indices of longitudinal RV function (TAPSE, RV S' and 2D FWLS).

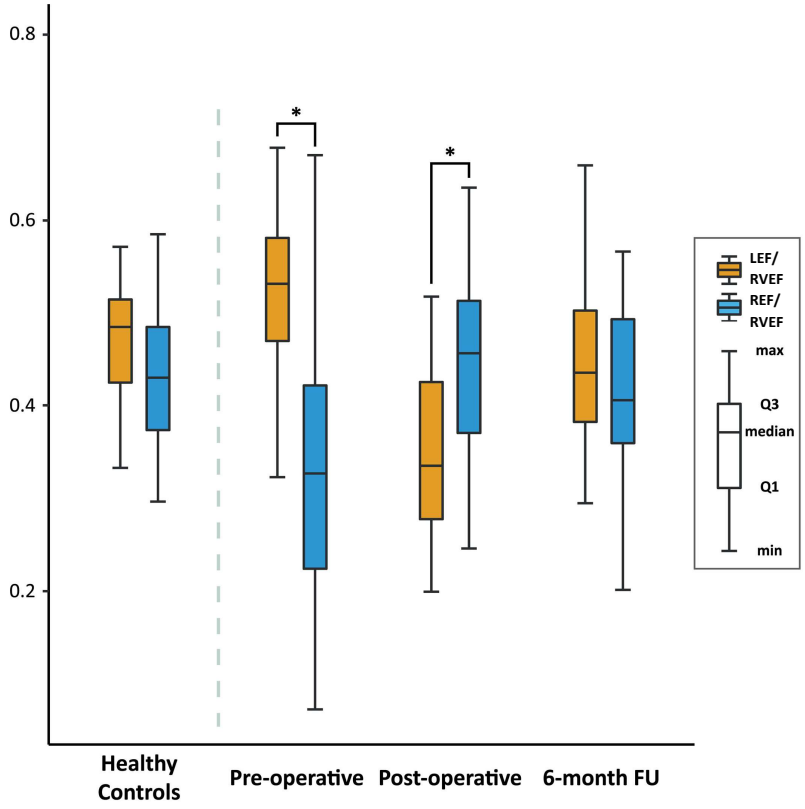

Figure 30. Contribution of longitudinal and radial contractions to global systolic RV function in healthy controls and patients undergoing MVR. Before surgery, the longitudinal shortening was the major contributor to global RV function, whereas, after MVR, the radial contraction became the dominant component. However, this shift was temporary as 6 months later, the contribution of the two components equalized, and the contraction pattern became similar to healthy controls'. $^{*}p<0.05$

7.4.3.6. Predictive value of preoperative parameters on postoperative RVD

In our patient cohort, postoperative RVSWi was 336 [279-488] mmHg*ml/m^2. Among preoperative parameters, LEF (β=-0.55, R^2=0.28, p<0.001) and 3D RVGLS (β=0.55, R^2=0.30, p<0.001) were associated with postoperative RVSWi. Nonetheless, postoperative RVSWi demonstrated no correlation with preoperative LVEDVi, LVEF, LVGLS, MR regurgitant volume, LAESVi, RVEF, RVEDVi, and PASP (estimated by echocardiography). Postoperative RVD (defined as RVSWi below 300 mmHg*ml/m^2) was detected in 14 [32%] patients. In these patients, lower preoperative values of LVMi (p=0.020), RV basal diameter (p=0.012), and RVESVi (p=0.023) were measured than in patients without RVD (Table 39). However, RV 2D free wall longitudinal strain (p=0.031), LEF (p=0.006), LEF/RVEF (p=0.011), and 3D RVGLS

(p=0.007) were found to be increased compared to patients without postoperative RVD (Table 39). Except for the higher prevalence of chronic anemia among RVD patients, there were no other differences regarding baseline clinical and intraoperative characteristics between the two groups (Table 39). Importantly, the advanced 3D parameters of longitudinal RV function were predictors of postoperative RVD (preoperative LEF: OR=1.33 [95% CI: 1.08-1.77], p<0.05; preoperative 3D RVGLS: OR=0.82 [95% CI: 0.68-0.94], p<0.05). Despite their established prognostic value [251, 252], neither preoperative 3D LAESVi nor PASP (by echo) predicted RVD in our study cohort.

Table 39. Comparison of patients with and without postoperative right ventricular dysfunction (RVD).

	No postoperative RVD n=28	**Postoperative RVD n=14**	**p value**
	Demographics		
Age (years)	67 [54-70]	64 [61-69]	0.666
Male	20 (71)	9 (64)	0.729
BMI (kg/m^2)	27 [24-30]	25 [24-27]	0.270
Hypertension	21 (75)	10 (71)	1.000
Hyperlipidemia	15 (54)	5 (36)	0.338
Diabetes mellitus	5 (18)	0 (0)	0.151
CKD (GFR<60 ml/min/1.73 m^2)	1 (4)	1 (7)	1.000
Chronic anemia*	1 (4)	4 (29)	0.035
Tobacco abuse	7 (25)	2 (14)	0.692
History of atrial fibrillation	7 (25)	3 (21)	1.000
NYHA			
I	8 (29)	1 (7)	
II	5 (18)	4 (29)	
III	15 (54)	9 (64)	
IV	0 (0)	0 (0)	0.340
EUROSCORE II (%)	1.60 [1.08-2.26]	1.21 [0.88-1.76]	0.379
	Preoperative echocardiogram		
LAESVi (ml/m^2)	66 [53-81]	54 [44-78]	0.470
LVMi (g/m^2)	108 [84-114]	80 [76-91]	0.020
LVEDVi (ml/m^2)	97 [81–111]	74 [67-95]	0.075
LVESVi (ml/m^2)	37 [29-41]	31 [25-33]	0.063
LVEF (%)	63 [62-65]	63 [60-65]	0.576
LVGLS (%)	-23 [(-24)-(-21)]	-21 [(-22)-(-19)]	0.357
LVGCS (%)	-32 [(-33)-(-29)]	-32 [(-35)-(-30)]	0.988
RV basal diameter (mm)	35 [33-38]	30 [28-35]	0.012
RV length (mm)	86 [82-94]	84 [77-91]	0.485
TAPSE (mm)	26 [23-30]	26 [23-28]	0.965

RV S' (cm/s)	14 [13-17]	13 [12-15]	0.143
RV 2D free wall LS (%)	-26 [(-29)-(-20)]	-31 [(-35)-(-25)]	0.031
Fractional Area Change (%)	38 [34-43]	44 [38-49]	0.143
RVEDVi (ml/m^2)	73 [62-88]	60 [54-70]	0.071
RVESVi (ml/m^2)	35 [29-47]	29 [24-33]	0.023
RVEF (%)	52 [49-55]	53 [52-55]	0.189
LEF (%)	26 [21-30]	31 [27-34]	0.006
REF (%)	18 [12-24]	15 [12-20]	0.416
LEF/RVEF	0.49 [0.46-0.55]	0.57 [0.53-0.63]	0.011
REF/RVEF	0.35 [0.22-0.43]	0.29 [0.24-0.37]	0.141
RVGLS (%)	-27 [(-32)-(-21)]	-35 [(-39)-(-29)]	0.007
RVGCS (%)	-25 [(-29)-(-21)]	-21 [(-25)-(-19)]	0.531
Intraoperative parameters			
Type of surgery			
Annuloplasty or Valvuloplasty	9 (32)	7 (50)	
Biological valve implantation	7 (25)	2 (14)	
Mechanical valve implantation	12 (43)	5 (36)	0.536
DeVega annuloplasty	8 (29)	1 (7)	0.230
Cross-clamp time (min)	79 [69-87]	71 [61-88]	0.584
Cardiopulmonary bypass time (min)	100 [93-112]	98 [82-104]	0.461

*Chronic anemia was defined as hemoglobin concentration <120 g/L in females or <130 g/L in males.

7.4.4. Added prognostic value of circumferential RV mechanics in left-sided cardiac diseases

7.4.4.1. Baseline clinical characteristics

Three hundred fifty-seven patients (age: 64±15 years, 70% males) with established left-sided cardiac disease and 3DE recordings suitable for LV and RV analysis were identified from the RVENet dataset (444 patients were initially identified of whom we excluded 80 due to inadequate 3D image quality for RV analysis, and further 7 due to inadequate image quality for LV analysis). During the median follow-up time of 41 months (ranging from 1 to 87 months), 55 (15%) patients died. Demographics and clinical characteristics of the study cohort and a comparison of patients alive versus those who died are presented in Table 40.

Table 40. Demographic and clinical characteristics.

	Overall (n=357)	Alive (n=302)	Dead (n=55)	p
Baseline demographic characteristics				
Age (years)	64.2±14.5	63.4±14.6	68.6±13.1	**0.014**
Male, n (%)	249 (69.7)	211 (69.9)	38 (69.1)	0.908
BSA (m^2)	1.93±0.22	1.93±0.22	1.91±0.22	0.494
BMI (kg/m^2)	26.8±4.2	27.0±4.3	26.0±3.6	0.288
Systolic blood pressure (mmHg)	126.5±18.4	126.1±17.2	128.0±23.2	0.585
Diastolic blood pressure (mmHg)	74.6±15.3	74.0±15.9	77.4±12.3	0.230
Heart rate (bpm)	77.6±14.6	77.7±15.0	77.4±12.5	0.935
Risk factors and medical history				
Hypertension, n (%)	260 (72.8)	218 (72.2)	42 (76.4)	0.522
History of smoking, n (%)	82 (23.0)	66 (21.9)	16 (29.1)	0.241
COPD, n (%)	40 (11.2)	33 (10.9)	7 (12.7)	0.735
Diabetes, n (%)	99 (27.7)	78 (25.8)	21 (38.2)	0.060
History of atrial fibrillation, n (%)	116 (32.5)	89 (29.5)	27 (49.1)	**0.005**
PM, n (%)	49 (13.7)	38 (12.6)	11 (20.0)	0.159
ICD, n (%)	33 (9.2)	23 (7.6)	10 (18.2)	**0.015**
CRT, n (%)	15 (4.2)	12 (4.0)	3 (5.5)	0.637
CAD, n (%)	77 (21.6)	55 (18.2)	22 (40.0)	**<0.001**
● **Previous CABG, n (%)**	19 (5.3)	13 (4.3)	6 (10.9)	**0.045**
● **Previous PCI, n (%)**	67 (18.8)	49 (16.2)	18 (32.7)	**0.004**
● **Previous AMI, n (%)**	48 (13.4)	34 (11.3)	14 (25.5)	**0.005**
Laboratory parameters				
GFR ($ml/min/1.73m^2$)	61.0±19.4	62.1±19.1	56.3±20.2	0.056
Creatinine (µmol/L)	101.1±41.7	99.1±38.6	112.1±54.5	**0.035**
Hgb (g/dL)	12.9±2.1	12.9±2.1	12.6±2.2	0.385
CRP (mg/L)	6.7±11.9	6.3±12.1	9.0±10.5	0.134

AMI: acute myocardial infarction, BMI: body mass index, BSA: body surface area, CABG: coronary artery bypass grafting, CAD: coronary artery disease, COPD: chronic obstructive pulmonary disease, CRP: C-reactive protein, CRT: cardiac resynchronization therapy, GFR: glomerular filtration rate, Hgb: hemoglobin, ICD: implantable cardioverter defibrillator, PCI: percutaneous coronary intervention, PM: pacemaker

Ninety-five subjects (27%) were HFrEF patients, of whom 81 patients were referred to our electrophysiology department for assessment prior to device implantation (pacemaker/ICD/CRT). Fourteen patients were investigated for candidacy for a long-term LVAD implantation. Ninety-one subjects (26%) were HTX with a median of 157 days after the operation (ranging from 8 to 6571 days). Sixty-seven subjects (19%) were patients with severe primary mitral valve regurgitation (MVR). Seventy-nine patients (22%) were investigated to evaluate aortic stenosis severity (moderate or severe). Twenty-five patients (7%) with a history of atrial fibrillation were referred for evaluation before a potential catheter ablation. The most frequently observed comorbidities were hypertension (73%), diabetes (28%), coronary artery disease (22%), and atrial fibrillation (33%).

Patients who died were older, had a higher prevalence of coronary artery disease and atrial fibrillation, and more frequently underwent ICD implantation in their medical history. Importantly, these patients had higher serum creatinine values than those who survived (Table 40).

7.4.4.2. Echocardiographic characteristics

Interestingly, conventional morphological parameters of the LV, the LA, and the RV did not differentiate between patients who died versus those who survived. Mitral annular velocities by TDI, both in systole and diastole, were more impaired in those patients who died. However, E/e' was similar. The right atrial size was larger in those patients who died, along with a more impaired RV longitudinal function (TAPSE, FWLS); however, RV systolic pressure and FAC were similar [253].

3DE parameters are summarized in Table 41. Patients who died had larger LV and RV volumes, along with a more impaired systolic function. Notably, LVSVi and RVSVi were

similar. In terms of longitudinal and circumferential biventricular strains, both LV and RV GLS and GCS were more impaired in patients who died.

Table 41. 3D echocardiographic parameters.

	Overall (n=357)	Alive (n=302)	Dead (n=55)	p
Left ventricle				
LVEDVi (ml/m²)	82.2±32.2	80.3±32.3	91.9±30.3	**0.019**
LVESVi (ml/m²)	44.5±30.4	42.2±30.0	56.3±30.0	**0.003**
LVSVi (ml/m²)	37.7±14.6	38.1±15.1	35.6±11.2	0.269
LVMi (g/m²)	102.5±36.8	100.4±35.1	113.4±43.0	**0.023**
LVEF (%)	49.0±15.7	50.2±15.3	42.3±16.1	**0.001**
LVGLS (%)	-15.2±6.0	-15.7±5.9	-12.5±6.2	**<0.001**
LVGCS (%)	-23.9±9.1	-24.6±9.0	-20.2±9.3	**0.001**
Right ventricle				
RVEDVi (ml/m²)	70.2±23.5	68.9±23.1	76.6±24.6	**0.033**
RVESVi (ml/m²)	37.4±18.7	36.0±17.8	44.4±21.3	**0.003**
RVSVi (ml/m²)	32.7±9.0	32.8±9.3	32.2±7.5	0.648
RVEF (%)	48.3±9.4	49.1±9.2	44.1±9.5	**<0.001**
RVGLS (%)	-16.4±5.1	-16.9±5.0	-13.8±4.6	**<0.001**
RVGCS (%)	-17.7±6.1	-18.3±5.9	-14.3±6.2	**<0.001**

EDVi: end-diastolic volume index, EF: ejection fraction, ESVi: end-systolic volume index, GCS: global circumferential strain, GLS: global longitudinal strain, LV: left ventricle, Mi: mass index, RV: right ventricle, SVi: stroke volume index

Using univariable Cox regression, we identified variables associated with all-cause mortality. Then, we created several multivariable Cox models with a maximum of 5 predictors by adding covariates to a baseline model sequentially (Figure 31). This analysis comprised three consecutive steps. In the first step, we created a baseline model (Model 0) that included age, sex, and serum creatinine level, as the latter was found to be a significant predictor during univariable analysis. In the second step, we added LVEF, LVGLS, or LVGCS to the baseline

model one by one (Model 1, Model 2, and Model 3, respectively), and we found that the model with LVGLS (Model 2) had the lowest AIC among the constructed models (Figure 31A). In step 3, we built Models 4, 5, and 6 by adding RVEF, RVGLS, or RVGCS to Model 2, respectively. Among these models, the one with RVGCS (Model 6) exhibited the lowest AIC (Figure 31B). In this model, age and RVGCS were independent predictors of all-cause mortality, whereas sex, creatinine level, and LVGLS were not (Table 42). We have confirmed that our approach identified the best combination of covariates by constructing multivariable models with all possible LV and RV parameter combinations. In multivariable models, including the medical history of coronary artery disease or atrial fibrillation instead of sex, RVGCS remained an independent predictor of all-cause mortality. On ROC analysis, LVGLS had the highest discriminative power among LV functional parameters (AUROC: 0.644 [95% CI: 0.561 - 0.726, p<0.001]); nevertheless, RVGCS had the highest discriminative power among all the investigated 2D and 3D echocardiographic parameters (0.690 [95% CI: 0.614 - 0.765, p<0.001] [253].

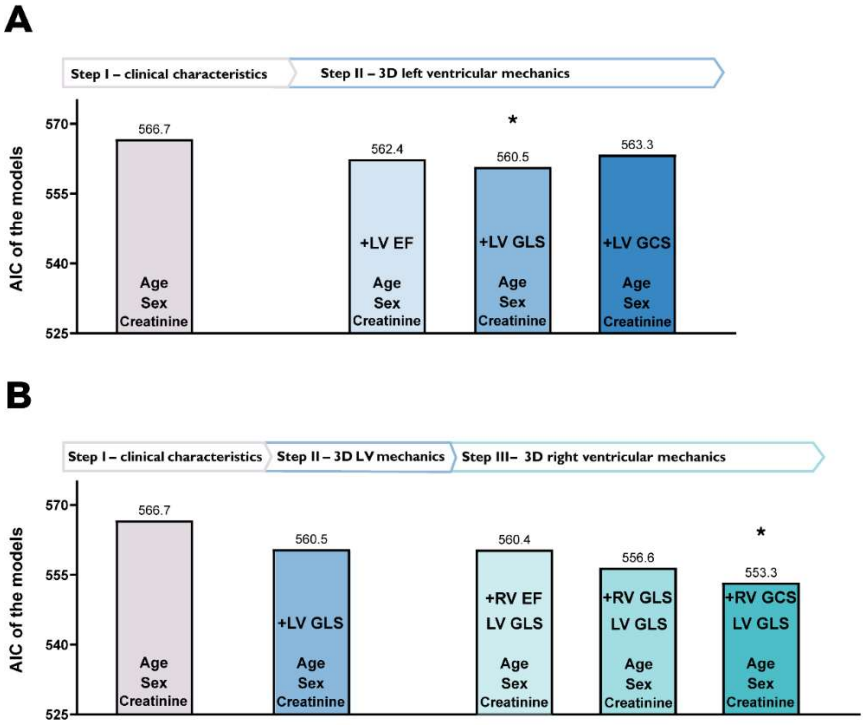

Figure 31. Identification of the best-fit models, including left (LV) and right ventricular (RV) functional parameters by multivariable Cox regression analysis based on Akaike Information Criterion (AIC).

Table 42. Independent predictors of all-cause mortality identified using multivariable Cox regression.

	Multivariable Cox regression	
	HR [95% CI]	**p**
Age	1.036 [1.011-1.061]	**0.004**
Sex	0.690 [0.376-1.266]	0.231
Creatinine[#]	1.005 [0.999-1.012]	0.087
LVGLS	1.017 [0.963-1.075]	0.543
RVGCS	1.091 [1.032-1.152]	**0.002**

[#]creatinine levels were available in 341 patients
CI: confidence interval, HR: hazard ratio, LVGLS: left ventricular global longitudinal strain, RVGCS: right ventricular global circumferential strain

7.4.4.3. Subgroup analysis

As the model, which included LVGLS and RVGCS, was identified as the best among the evaluated models, we created four subgroups based on the median values of LVGLS and RVGCS (-15.9% and -17.9%, respectively). In Group 1, patients had both LVGLS and RVGCS above the median, while in Group 4, both LVGLS and RVGCS were below the median. Group 2 patients had LVGLS values below the median while RVGCS above the median. Group 3 had patients with LVGLS above the median and RVGCS below the median.

Out of the 125 patients in Group 1, thirty-seven (30%) were HTX recipients, nineteen (15%) were evaluated before atrial fibrillation ablation, eighteen (14%) had aortic stenosis, and fifty-one (41%) had mitral valve disease. Group 2 consisted of 53 patients, of whom sixteen (30%) had HFrEF, eleven (21%) were HTX recipients, six (11%) were evaluated before atrial fibrillation ablation, and twenty (38%) had aortic stenosis. Group 3 had 54 patients in total, one (2%) with HFrEF, thirty (56%) HTX recipients, eight (15%) with aortic stenosis, and fifteen (28%) with mitral valve disease. Group 4 was composed of 125 patients and had seventy-eight (62%) HFrEF patients, thirteen (10%) HTX recipients, thirty-three (26%) patients with aortic stenosis, and one (1%) with mitral valve disease.

In Group 1, 7.2% of the patients died during the follow-up, while 7.5% died in Group 2. Group 3 and Group 4 patients experienced adverse outcomes more frequently, with 20.3% mortality in the former and 24.8% in the latter. These differences in the outcomes between patient subgroups were visualized via Kaplan-Meier curves (Figure 32). Patients with both LVGLS and RVGCS below the median (Group 4) had a more than 5-fold increased risk of death compared with those in Group 1 and more than 3.5-fold compared with those in Group 2. Interestingly, there was no significant difference in mortality between Group 3 (with LVGLS above the median) and Group 4, but being categorized into Group 3 versus Group 1 still held a more than 3-fold risk [253].

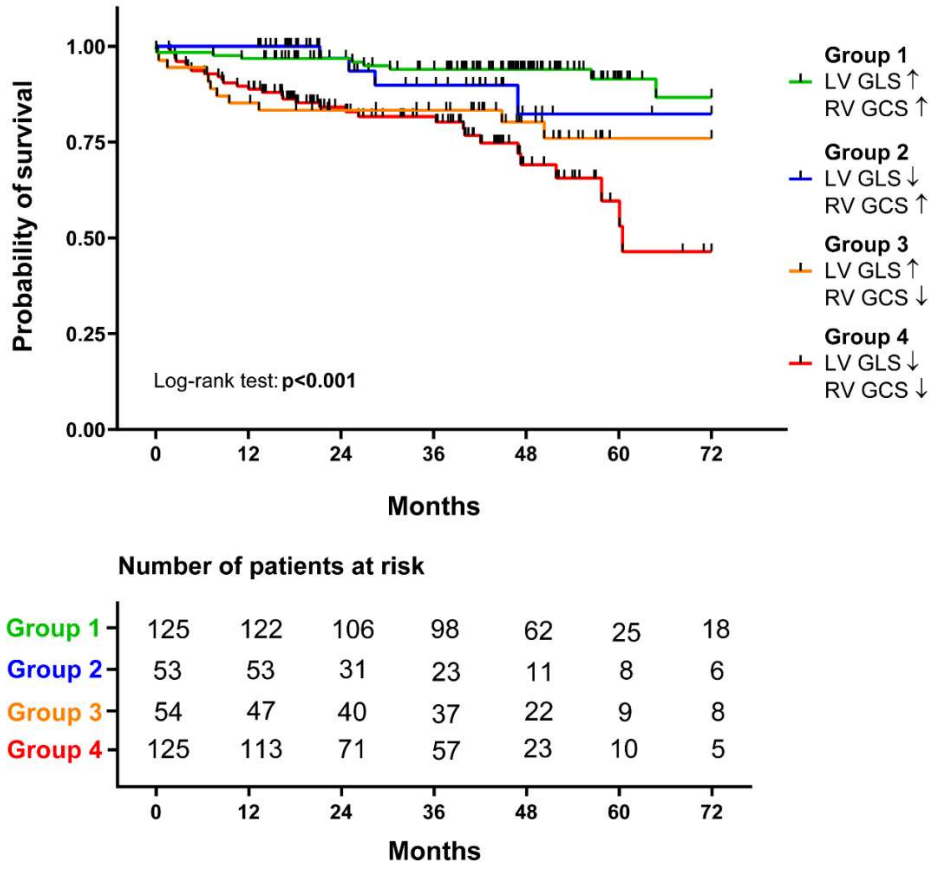

Figure 32. Survival analysis of the different groups. Based on the respective median values of left ventricular global longitudinal strain (LVGLS, -15.9%) and right ventricular global circumferential strain (RVGCS, -17.9%), patients were divided into four groups. The survival of the four groups is visualized on Kaplan-Meier curves, and the log-rank test was performed for comparison.

Regarding the baseline characteristics of these groups, Group 4 patients were older, presented with lower systolic blood pressure, more frequently had diabetes and coronary artery disease, and had ICD implantation in their medical history. Their creatinine levels were also the highest among the groups. On the contrary, in Group 3, there were relatively younger patients, less frequently with diabetes, coronary artery disease, or atrial fibrillation in their medical history. Group 4 patients were presented with the highest LV, RV, and RA dimensions and E/e', while LAVi or RV systolic pressure did not differ between the four subgroups. Beyond the aforementioned significant chamber dilation and biventricular functional impairment seen in Group 4 patients, Group 3 patients had the lowest LVMi with a preserved average LV and RVEF (60±5 and 49±6%, respectively) [253].

7.4.5. Changes and prognostic value of RV contraction pattern in different degrees of left ventricular systolic dysfunction

Of a total of 462 patients screened, 71 patients (15%) had echocardiographic images unsuitable for 3DE analysis: 42 patients due to unavailability of either the RV or the LV 3DE data sets; 21 patients because of poor acoustic window; and 8 patients because of irregular rhythm and stitching artifacts. From the remaining 391, 292 patients had primary left-sided heart disease, and they formed the study cohort. The mean follow-up time was 6.7±2.2 years.

Baseline demographic, clinical, and echocardiographic characteristics were summarized in Tables 43 and 44. The main etiologies of left-sided heart disease in our study cohort were arterial hypertension (diagnosed in 170 patients, 58.2%), coronary artery disease (132, 45.2%), mitral or aortic valve disease (≥moderate stenosis or regurgitation; 78, 26.7%), and cardiomyopathies (54, 18.4%).

Table 43. Demographic and clinical characteristics of study samples.

Variable	Overall (n=292)	Patients with preserved LVEF (n=163)	Patients with reduced LVEF (n=129)	p value
Age, years	59±17	59±17	61±17	0.148
Gender, male (%)	203 (69.5)	98 (60.1)	105 (81.4)	<0.001
Body surface area, m^2	1.82±0.2	1.78±0.2	1.88±0.2	<0.001
BMI, kg/m^2	24.9±3.5	24.5±3.5	25.6±3.5	0.008
Heart rate, bpm	69±16	67±14	71±19	0.027
Systolic blood pressure, mmHg	124±18	128±18	120±18	<0.001
Diastolic blood pressure, mmHg	74±10	76±10	73±11	0.017
Risk factors:				
• **Smoking (%)**	105 (36.0)	52 (31.9)	53 (41.1)	0.104
• **Diabetes (%)**	46 (15.7)	18 (11.0)	28 (21.7)	0.013
• **Dyslipidemia (%)**	125 (42.8)	61 (36.7)	64 (49.6)	0.027
• **Obesity (BMI ≥30 kg/m^2) (%)**	23 (7.9)	11 (6.7)	12 (9.3)	0.558
• **Family history of CAD (%)**	72 (24.7)	38 (23.3)	34 (26.4)	0.542
• **History of atrial fibrillation (%)**	48 (16.4)	21 (12.9)	27 (20.9)	0.092
Etiologies of left-sided heart disease				
Hypertension (%)	170 (58.2)	94 (57.7)	76 (58.9)	0.837
CAD in total (%)	132 (45.2)	61 (37.4)	71 (55.0)	0.004
• **Previous CABG (%)**	9 (3.1)	3 (1.8)	6 (4.7)	0.155
• **Previous PCI (%)**	40 (13.7)	19 (11.7)	21 (16.3)	0.258
Significant mitral/aortic valve disease (%)	78 (26.7)	60 (36.8)	18 (14.0)	<0.001
• **Mitral valve disease (%)**	29 (9.9)	26 (16.0)	3 (2.3)	<0.001
• **Aortic valve disease (%)**	25 (8.6)	19 (11.7)	6 (4.7)	0.035
• **Both mitral and aortic valve disease (%)**	3 (1.0)	1 (0.6)	2 (1.6)	0.404
• **Previous MVR and/or AVR (%)**	21 (7.2)	14 (8.6)	7 (5.4)	0.294
Cardiomyopathies in total (%)	54 (18.4)	15 (9.2)	39 (30.2)	<0.001
• **Dilated cardiomyopathy (%)**	41 (14.0)	3 (1.8)	38 (29.5)	<0.001
• **Hypertrophic cardiomyopathy (%)**	7 (2.4)	7 (4.3)	0	0.017
• **Restrictive cardiomyopathy (%)**	3 (1.0)	3 (1.8)	0	0.126
• **Takotsubo (%)**	3 (1.0)	2 (1.2)	1 (0.8)	0.736

AVR: aortic valve replacement or repair, BMI: body mass index, CABG: coronary artery bypass grafting, CAD: coronary artery disease, MVR: mitral valve replacement or repair, PCI: percutaneous coronary intervention

Table 44. Echocardiographic characteristics of study samples.

Variable	Overall (n=292)	Patients with preserved LVEF (n=163)	Patients with reduced LVEF (n=129)	p value
LV end-diastolic volume index, ml/m²	87.0±34.2	72.3±21.0	106.1±38.4	<0.001
LV end-systolic volume index, ml/m²	47.1±32.3	29.1±10.1	70.4±36.4	<0.001
LV ejection fraction, %	49.5±14.3	59.9±5.6	36.4±10.9	<0.001
LV sphericity index	0.44±0.12	0.42±0.1	0.47±0.1	<0.001
LV mass index, g/m²	102.9±23.7	93.7±20.3	113.9±22.9	<0.001
2DE LVGLS, %	-14.7±5.1	-17.8±3.5	-10.6±3.7	<0.001
2DE left atrial volume index, ml/m²	49.8±42.6	49.5±48.3	50.0±35.2	0.935
RV end-diastolic volume index, ml/m²	81.3±22.7	78.4±21.2	85.1±24.1	0.011
RV end-systolic volume index, ml/m²	44.2±18.8	39.5±14.7	50.3±21.5	<0.001
RVEF, %	46.5±9.2	49.8±6.9	42.3±10.0	<0.001
RV longitudinal ejection fraction, %	18.1±6.4	20.6±5.8	14.9±5.6	<0.001
RV radial ejection fraction, %	24.7±7.0	25.7±6.7	23.4±7.2	0.006
RV anteroposterior ejection fraction, %	17.5±5.8	19.4±5.3	15.0±5.5	<0.001
LEF/RVEF	0.38±0.09	0.41±0.09	0.35±0.09	<0.001
REF/RVEF	0.53±0.10	0.51±0.10	0.55±0.09	0.001
AEF/RVEF	0.37±0.08	0.39±0.08	0.35±0.08	<0.001
TAPSE, mm	20.5±5.5	21.9±5.2	18.8±5.3	<0.001
FAC, %	39.4±10.2	41.7±9.1	36.4±10.8	<0.001
2DE free-wall longitudinal strain, %	-25.2±6.7	-27.4±5.9	-22.4±6.7	<0.001
PASP, mmHg*	30.8±12.7	29.7±12.0	32.4±13.5	0.085

* PASP estimation was feasible in 262 patients (89.7%).
2DE: two-dimensional echocardiography, AEF/RVEF: anteroposterior ejection fraction/ RVEF, FAC: fractional area change, GLS: global longitudinal strain, LEF/RVEF: longitudinal ejection fraction/RVEF, LV: left ventricular, PASP: pulmonary artery systolic pressure, REF/RVEF: radial ejection fraction/RVEF, RV: right ventricular, TAPSE: tricuspid annular plane systolic excursion.

One hundred sixty-three patients (55.8%) had preserved LVEF (59.9±5.6%, range 50-72%), and 129 patients (44.2%) had reduced LVEF (36.4±10.9%, range 5-49%). Patients from the latter subgroup were more likely to be diagnosed with coronary artery disease, dilated cardiomyopathy, diabetes, or dyslipidemia. Significant mitral or aortic valve diseases were more frequent in patients with preserved LVEF (Table 43).

Patients with reduced LVEF also had poorer RV systolic function compared to the patients with preserved LVEF (RVEF 42.3±10.0% vs 49.8±6.9%, p<0.001; FAC 36.4±10.8% vs 41.7±9.1%, p<0.001; and TAPSE 18.8±5.3 mm vs 21.9±5.2 mm, p<0.001, respectively) (Table 44). Accordingly, the prevalence of reduced RVEF was significantly higher in patients with reduced LVEF compared to those with preserved LVEF (45% vs 19%, p<0.001).

LV end-diastolic and end-systolic volumes increased significantly, starting from the early stages of LV systolic dysfunction, while stroke volume dropped (Table 45). However, RV volumes started increasing significantly only in patients with moderate LV dysfunction, and the RV stroke volume dropped significantly in those with severely reduced LVEF (Table 45).

Table 45. Echocardiographic characteristics of patients stratified according to left ventricular ejection fraction.

Parameter	LV EF ≥50% (n=163)	LV EF 40-49.9% (n=59)	LV EF 30-39.9% (n=36)	LV EF <30% (n=34)	Overall p value
LV end-diastolic volume index, ml/m²	71.8 ± 21.9	83.5 ± 19.9*	109.0 ± 29.2*†	140.1 ± 43.9*†‡	<0.001
LV end-systolic volume index, ml/m²	29.0 ± 10.4	45.6 ± 11.8*	70.2 ± 19.6*†	112.0 ± 39.5*†‡	<0.001
LV stroke volume index, ml/m²	42.9 ± 13.1	36.1 ± 11.9*	37.7 ± 11.1*	28.3 ± 8.9*†‡	<0.001
LVEF, %	59.9 ± 5.6	45.7 ± 2.6*	35.8 ± 2.9*†	21.0 ± 6.0*†‡	<0.001
RV end-diastolic volume index, ml/m²	78.3 ±21.2	74.4 ± 17.5	85.5 ± 21.6*†	103.0 ± 26.6*†‡	<0.001
RV end-systolic volume index, ml/m²	39.4 ± 14.7	39.2 ± 10.6	48.3 ± 16.7*†	71.6 ± 24.7*†‡	<0.001
RV stroke volume index, ml/m²	38.5 ± 10.2	35.3 ± 9.0*	37.3 ± 10.6	31.5 ± 8.7*†‡	0.001
RVEF, %	50.0 ± 6.9	47.4 ± 5.3*	44.2 ± 8.6*	31.9 ± 9.7*†‡	<0.001
RVEF ≤45 (%)	31 (19.0)	17 (28.8)	12 (33.3)	29 (85.3)*†‡	<0.001
RV LEF, %	20.6 ± 5.8	17.2 ± 4.3*	15.8 ± 5.6*	10.1 ± 4.6*†‡	<0.001
RV REF, %	25.7 ± 6.7	26.2 ± 5.6	24.3 ± 6.9	17.6 ± 6.8*†‡	<0.001
RV AEF, %	19.4 ± 5.3	17.6 ± 4.5*	15.4 ± 4.3*†	10.0 ± 5.0*†‡	<0.001
LEF/RVEF	0.41 ± 0.09	0.36 ± 0.08*	0.35 ± 0.09*	0.32 ± 0.09*	<0.001
REF/RVEF	0.51 ± 0.10	0.55 ± 0.09*	0.55 ± 0.10	0.55 ± 0.10	0.013
AEF/RVEF	0.39 ± 0.08	0.37 ± 0.07	0.35 ± 0.06*	0.30 ± 0.08*†‡	<0.001
TAPSE, mm	21.9 ± 5.3	20.5 ± 5.1*	19.2 ± 4.6*	15.3 ± 4.7*†‡	<0.001
FAC, %	41.7 ± 9.1	42.1 ± 6.5	37.9 ± 9.7*†	25.1 ± 9.2*†‡	<0.001
2DE free-wall longitudinal strain, %	-27.4 ± 5.9	-24.6 ± 5.7*	-23.5 ± 5.6*	-17.3 ± 6.8*†‡	<0.001
PASP, mmHg	29.7 ± 12.0	28.5 ± 9.2	31.1 ± 14.0	40.3 ± 15.9*†‡	0.005

*p<0.05 vs LV EF ≥50%. † p<0.05 vs LV EF 40-49.9%. ‡ p<0.05 vs LV EF 30-39.9%.
2DE: two-dimensional echocardiography, AEF: anteroposterior ejection fraction, AEF/RVEF: anteroposterior ejection fraction/RVEF, EF: ejection fraction, FAC: fractional area change, LEF: longitudinal ejection fraction, LEF/RVEF: longitudinal ejection fraction/RVEF, LV: left ventricular, PASP: pulmonary artery systolic pressure, REF: radial ejection fraction, REF/RVEF: radial ejection fraction/RVEF, RV: right ventricular, TAPSE: tricuspid annular plane systolic excursion.

7.4.5.1. Different components of the RVEF in patients with left-sided heart disease

The relative contribution of the radial component to the total RVEF was significantly higher than that of longitudinal and anteroposterior components both in patients with preserved LVEF (REF/RVEF: 0.51±0.10 vs LEF/RVEF: 0.41±0.09 vs AEF/RVEF: 0.39±0.08; p<0.001) and reduced LVEF (REF/RVEF: 0.55±0.09 vs LEF/RVEF: 0.35±0.09 vs AEF/RVEF: 0.35±0.08; p<0.001). The relative contribution of the longitudinal and anteroposterior components decreased, while radial component contribution further increased in patients with reduced LVEF compared to those with preserved LVEF (Table 44).

RV LEF and AEF showed moderate correlations with LVEF (Spearman's Rho 0.51 and 0.48, respectively, p<0.001) and with LV global longitudinal strain (-0.60 and -0.51, respectively, p<0.001), while the correlations between RV REF and the same parameters were weak (0.23, p<0.001 and -0.14, p=0.032, respectively). RV REF weakly correlated with the 3DE-derived LV sphericity index (Spearman's Rho -0.24, p<0.001), while other components did not. All three components demonstrated weak correlations with PASP (Spearman's Rho: LEF -0.27, p<0.001, REF -0.18, p=0.003, and AEF -0.33, p<0.001).

7.4.5.2. Changes in RV contraction pattern at different degrees of LV systolic dysfunction

When patients were further stratified according to the degree of LVEF impairment (Table 45), there was a significant drop in both RV LEF and AEF, and in their relative contribution to the total RVEF, starting from the earlier stages of LV dysfunction (Figure 33, A-B). However, in patients with mildly and moderately reduced LVEF, there was a significant increase in the radial RV component: REF/RVEF increased from 0.51 [0.44; 0.58] in patients with normal LVEF to 0.55 [0.48; 0.61] (p=0.012) in those with mild LV dysfunction, and to 0.56 [0.48; 0.63] (p=0.031) in those with moderate LV dysfunction (Figure 33A, B). As a result,

total RVEF remained normal in patients with normal, mildly, and moderately reduced LVEF (RVEF 50 [46; 54]%, 47 [44; 52]%, and 46 [42; 49]%, respectively) (Figure 33C). Conversely, in patients with severely reduced LVEF, a significant reduction in all RVEF components was observed, which ultimately led to a decrease in the total RVEF (30 [25; 39]%; p<0.001) (Figure 33C; Table 45).

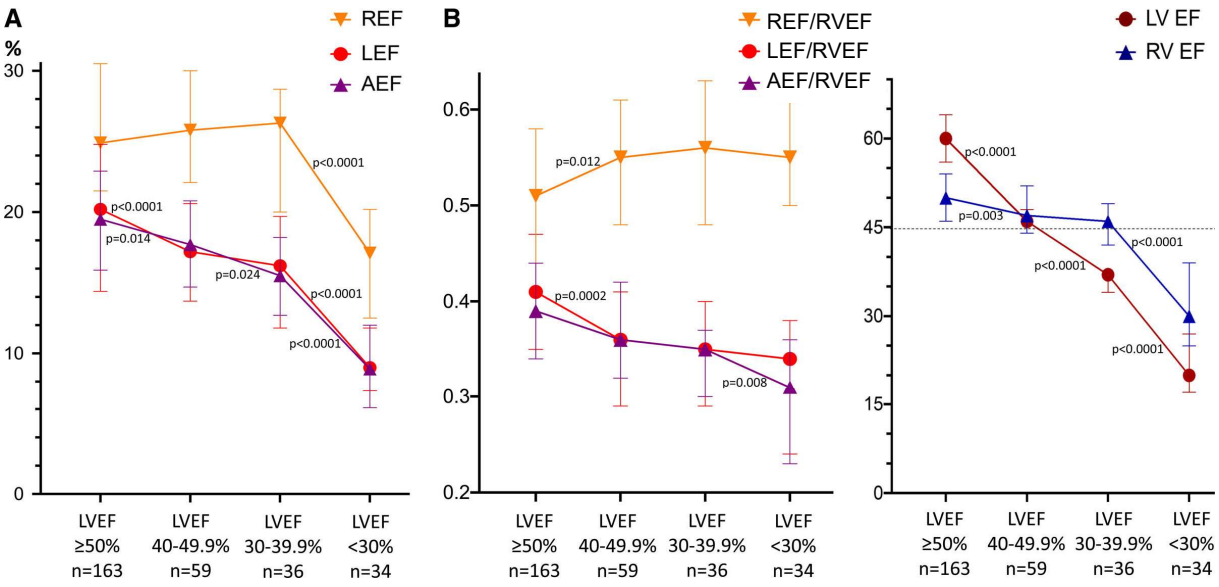

Figure 33. Comparison of right ventricular (RV) longitudinal, radial, and anteroposterior ejection fractions (LEF, REF, and AEF, respectively) and their relative contributions at different stages of left ventricular (LV) dysfunction. **A**, Longitudinal (red line) and anteroposterior (purple line) ejection fraction (EF) values are decreasing continuously and parallel with the decrease of LVEF. However, REF (orange line) is even increasing in mild and moderately decreased stages of LV dysfunction but drops significantly below LVEF of 30%. **B**, The relative contributions show similar phenomena, with REF being the dominant contributor to RVEF even in severe LV dysfunction. **C**, In our cohort, total RVEF remained preserved (>45%) in patients with mild and moderate LV dysfunction but decreased significantly below LVEF of 30%, which is clearly attributable to the drop in REF values at this stage. The dotted line demonstrates a cutoff value of RVEF 45%.

7.4.5.3. Prognostic value of the different components of RV mechanics

In our cohort, 107 patients (37%) met the composite endpoint: 76 patients were hospitalized due to HF, and 31 patients died due to cardiac cause (these patients were not hospitalized for HF during the follow-up period). Out of the 76 patients who were hospitalized

for HF, 29 died due to cardiac cause during the follow-up period. Patients with adverse outcomes were older and more likely diagnosed with diabetes or atrial fibrillation compared to patients who remained free of events. RV functional parameters were all significantly decreased except for the relative contribution of radial shortening (REF/RVEF). Multivariable Cox regression models were built, including significant demographic and medical history parameters, LVEF, and RV measures (RV parameters were added one-by-one to the models to avoid collinearity). In multivariable models including LVEF, age, diabetic status, history of atrial fibrillation, cardiomyopathies and valvular heart diseases as etiological factors, several RV morphological and functional measurements (including RVEF, LEF, AEF, and AEF/RVEF) were found to be independently associated with adverse outcomes (Table 46). In the ROC analysis, RV AEF exhibited the highest AUC value compared with the other RV functional measures (Figure 34) [4].

Table 46. Factors associated with cardiac death and heart failure hospitalization in the entire study cohort.

	Univariable		Multivariable*		Multivariable*		Multivariable*		Multivariable*	
	HR [95% CI]	p value	HR [95% CI]	p value	HR [95% CI]	p value	HR [95% CI]	p value	HR [95% CI]	p value
Age	1.019 [1.006 – 1.032]	0.003								
Diabetes	2.456 [1.602 – 3.766]	<0.001	2.076 [1.313 – 3.282]	0.002	2.018 [1.277 – 3.190]	0.003	2.074 [1.313 – 3.275]	0.002	2.080 [1.315 – 3.288]	0.002
Atrial fibrillation	2.514 [1.653 – 3.824]	<0.001								
Cardiomyopathy	1.660 [1.067 – 2.583]	0.025								
Valvular heart disease	1.485 [0.994 – 2.217]	0.054	2.046 [1.276 – 3.279]	0.003	2.280 [1.426 – 3.646]	<0.001	2.081 [1.301 – 3.329]	0.002	2.156 [1.347 – 3.451]	0.001
LV ejection fraction	0.967 [0.944 – 0.990]	<0.001	0.978 [0.962 – 0.995]	0.012	0.973 [0.957 – 0.989]	0.001	0.979 [0.963 – 0.995]	0.011	0.969 [0.954 – 0.984]	<0.001
RV ejection fraction	0.940 [0.925 – 0.956]	<0.001	0.960 [0.936 – 0.984]	0.001						
RV LEF	0.903 [0.873 – 0.933]	<0.001			0.948 [0.910 – 0.989]	0.013				
RV AEF	0.893 [0.865 – 0.923]	<0.001					0.926 [0.887 – 0.967]	<0.001		
RV AEF/RVEF	0.946 [0.924 – 0.967]	<0.001							0.971 [0.945 – 0.997]	0.028

*RV functional parameters were added one-by-one to the multivariable models due to their collinearity.

We further investigated patients with normal RV function (RVEF>45%, n=202). Fifty-three patients met the composite endpoint: 37 patients were hospitalized due to HF, and 16 patients died due to cardiac cause (these patients were not hospitalized for HF during the follow-up period). Out of the 37 patients who were hospitalized for heart failure, 7 died due to cardiac causes during the follow-up period. Patients who experienced adverse outcomes were older, more likely to have diabetes or a history of atrial fibrillation, had larger LV and left atrial volumes, and had lower LVEF than patients who did not. RV end-diastolic volume, RVEF, FAC, and RV FWLS did not differ between the two groups. Conversely, AEF and AEF/RVEF were significantly lower, whereas REF/RVEF was significantly higher among patients who met the endpoint. The latter three RV mechanical component measures were also significantly associated with adverse outcomes by univariable Cox analysis, while the RVEF was not. In a multivariable Cox regression model including age, diabetic status, atrial fibrillation, LVEF, and AEF/RVEF, AEF/RVEF (HR: 0.960 [CI:0.925-997], p=0.032) was found to be independently associated with adverse outcomes in patients with preserved RVEF besides diabetes and atrial fibrillation (Table 47). No other RV morphological or functional parameter was found to be independently associated with the outcome in this model. In the ROC analysis, AEF/RVEF exhibited the highest AUC value (Figure 34) [4].

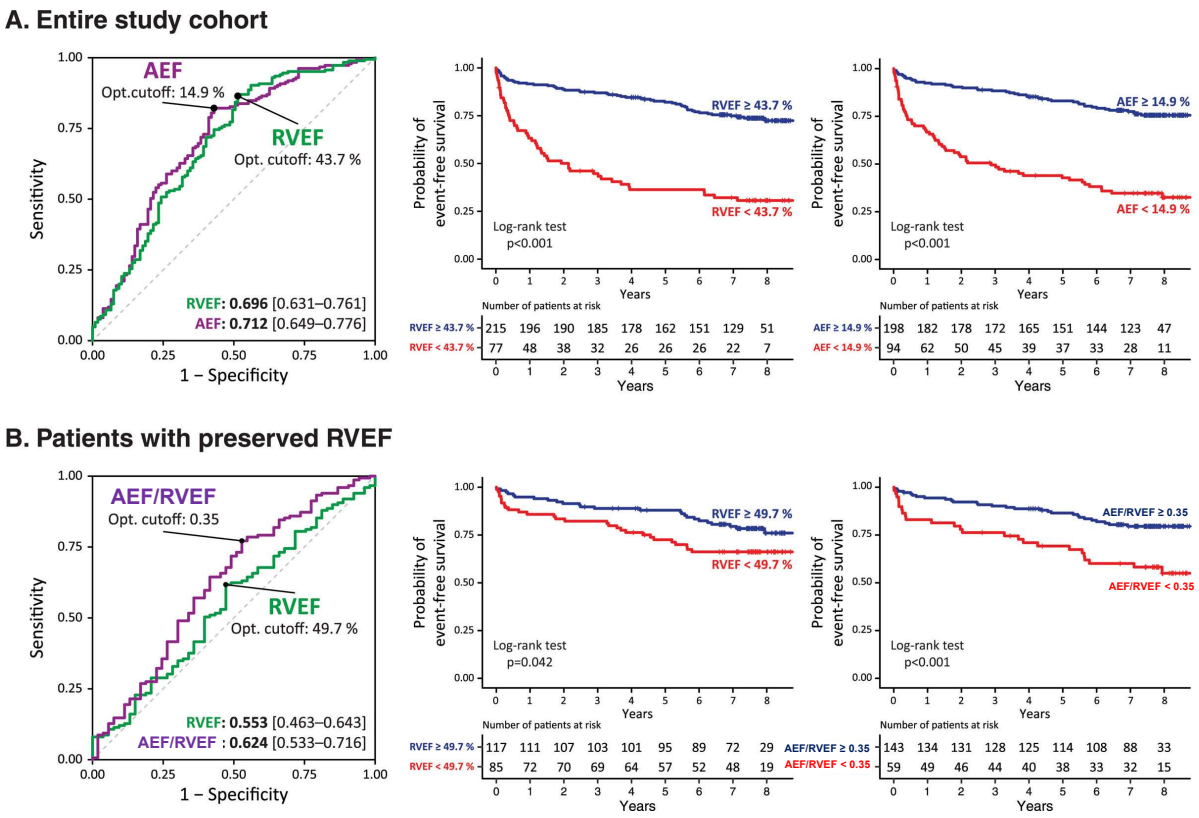

Figure 34. Comparison of the discriminatory power of right ventricular ejection fraction (RVEF) vs parameters of anteroposterior shortening with regards to the composite endpoint. **A**, RVEF vs anteroposterior ejection fraction (AEF) in the entire population; (**B**) RVEF vs AEF/RVEF in patients with preserved (>45%) RVEF. Patient cohorts were dichotomized, and their outcomes were visualized using Kaplan-Meier curves based on the optimal cutoff values of each parameter assessed with the receiver operating characteristic (ROC) analysis. The area under the ROC curve values (with 95% CIs) is displayed in the ROC plots' bottom right corner.

Table 47. Factors associated with cardiac death and heart failure hospitalization in patients with preserved right ventricular ejection fraction.

	Univariable		Multivariable	
	HR [95% CI]	**p value**	**HR [95% CI]**	**p value**
Age	1.028 [1.009 – 1.048]	0.004		
Diabetes	2.829 [1.512 – 5.294]	0.001	2.291 [1.197 – 4.387]	0.012
Atrial fibrillation	2.720 [1.452 – 5.094]	0.002	2.260 [1.167 – 4.376]	0.016
LV ejection fraction	0.967 [0.944 – 0.990]	<0.001		
AEF/RVEF	0.949 [0.915 – 0.984]	0.004	0.960 [0.925 – 0.997]	0.032

8. Discussion

8.1. Development and validation of a software tool to quantify RV contraction patterns

The accurate evaluation of RV function is essential for managing many cardiovascular diseases. Measuring RV volumes and EF by 3DE offers a relatively simple and fast but more complete way to quantify the "forgotten chamber". However, EF alone is not enough. We need more comprehensive metrics that can capture the RV's complex mechanical pattern and spot subtle, often segmental dysfunction. With the ReVISION software, we aimed to provide a tool for the detailed assessment of the different motion components and to enable segmental analysis using 3DE-derived RV models.

As part of the ReVISION development process, we have proposed a new, rule-based way to standardize the orientation of RV 3D models, which could lead to a general approach for the analysis of 3D models from other vendors or imaging methods. This is an improvement from our previous way: each input mesh series was aligned to a reference mesh (pre-oriented manually by expert agreement). Furthermore, we have created and tested the volumetric division of the 3D model into 15 segments to evaluate and visualize regional differences and identify possible changes in the segmental contraction pattern. The reproducibility of global and segmental volumes was acceptable and in line with previous reports. In addition, using a custom CMRI-based 3D reconstruction algorithm, we have found a strong agreement between 3DE- and CMRI-derived decomposed volumes and EF, confirming the validity and reliability of our method to express the relative contribution of longitudinal, radial, and anteroposterior motions to global RV function.

8.1.1. Volumetric segmentation of the RV

Unlike the left side, no widely accepted and consistent method for dividing the RV into segments exists. This is because of its more complicated 3D shape and the relatively lower importance of segmental RV analysis in coronary artery disease compared to LV. However, local changes in RV myocardial mechanics may be crucial for finding hidden changes that global measures cannot detect.

The RV has been segmented using different methods. Moceri et al. divided the 3D endocardial surface into four regions on the septum (membranous, infundibular, trabecular, inlet) and four regions on the free wall (inferior, lateral, anterior, and outflow tract) using the TomTec solution output [48]. They observed that the inferior free wall region had the highest values of area and circumferential strains in healthy subjects, while longitudinal deformation was dominant in the inferior free wall segment. They also found that PH patients had significantly lower longitudinal, circumferential, and area strains than healthy controls in all regions. Additionally, GAS was a strong independent predictor of survival. Satriano et al. reported that principle strain (measured with contraction angle analysis) could reliably differentiate patients with pulmonary arterial hypertension [254]. They separated six surface segments (septal body, septal apex, free wall body, free wall apex, inflow, and outflow) for their analysis. The most significant difference (compared to healthy controls) was seen in the principal strain values of the free wall segments, indicating that these segments had the most severe contractile dysfunction in PH patients.

Using the triangular mesh model created with the TomTec software solution, Addetia and colleagues divided the RV into four subvolumes: apex, body, inflow tract, and outflow tract [36]. They also separated the body's septal and free wall surfaces and the apex to examine regional curvature indices on six endocardial surfaces in total. They have shown that the normal "bellows effect" disappears in PH patients as the RV free wall regions keep the same convex

shape from end-diastole to end-systole. This result matches literature data and our own observations with the ReVISION software, as the pressure overload affects the radial movement of the RV free wall early, and therefore, it may be a more sensitive marker of even mild RV dysfunction than global measures and especially, than parameters based on longitudinal shortening only. To determine the reference ranges for regional indices, they measured volumes and EFs for the four subvolumes mentioned above and curvature for the six endocardial surfaces in 245 healthy subjects, and they reported differences in the values of these metrics based on sex and age [25].

Bernardino et al. recently suggested a mesh-independent, automated way to divide the RV cavity and calculate regional volumes and EFs in three regions (apex, inlet, and outflow) [255]. Their method uses clear anatomical landmarks (the apex, the tricuspid, and the pulmonary annuli) to avoid errors from inconsistent anatomical vertex positions between different 3D meshes, and each vertex belongs to the region with the closest landmark based on geodesic distance. Their method might be able to analyze 3D RV models made using other post-processing software solutions, even though they used meshes from the TomTec solution in their analysis.

Another commercially available RV-specific 3D speckle tracking tool from Canon Medical Systems (Otawara, Japan) can calculate global and regional longitudinal, circumferential, and area strains, besides the methods that use the triangular meshes created with the TomTec software [256]. This software solution uses manually placed anatomical landmarks (attachment sites of the moderator band to the septum and anterior papillary muscle to the free wall) to divide the inlet, the outflow, and the apical segments during 3D reconstruction. Then, it identifies seven surface segments: inlet lateral, inlet inferior, inlet septum, outflow septum, outflow free wall, apical free wall, and apical septum [257]. Ishizu et al. evaluated the reliability and feasibility of this algorithm in a group of patients with different

heart diseases and proposed that measuring RV dyssynchrony could be one of the main clinical applications of regional RV myocardial deformation by 3D speckle tracking echocardiography [257].

In summary, clinical data show the value of the 3D-derived segmental RV analysis. Most studies concentrated on PH, but we can speculate that it has a similar diagnostic and prognostic role in RV volume overload, ischemia, or arrhythmogenic cardiomyopathy. Our software provides a distinctive solution for RV segmentation as it divides the RV into 15 segments, and it can calculate segmental EFs and longitudinal, circumferential, and area strain values.

8.1.2. The relative contribution of longitudinal, radial, and anteroposterior motion components

Our validation studies confirmed a strong agreement between 3DE- and CMRI-derived decomposed ESVs and EFs measurements. These results also support examining longitudinal, radial, and anteroposterior motions separately. During relevant clinical investigations, we determined normal values in both adult and pediatric populations, showed how RV contraction pattern varies in response to different physiological and pathophysiological stimuli, and that these metrics also provide prognostic value on top of conventional RV functional metrics, such as RVEF. In addition, we improved the software's online interface, enabling users to upload and examine 3D RV meshes, view the segments in 3D, create time-volume or time-strain curves, and store the results of clinical cases.

8.2. Establishing the normal RV contraction pattern

Our dual-center adult study aimed to determine the physiological contribution of RV longitudinal, radial, and anteroposterior motion to global RV function and their relation to relevant morphometric and demographic parameters. According to our results, the anteroposterior and longitudinal shortening are the most prominent motion directions of RV performance. However, there is an age-dependent increase in the relative contribution of radial motion with a concomitant decrease in the relative contribution of longitudinal shortening to global RV function. Over 40 years of age, the longitudinal and radial motion equally contribute to global RV function. Individuals over 60 represent a distinct group regarding RV contraction pattern, which may be attributable to the age-related increase in PASP.

In daily clinical practice, RV geometry and function are usually assessed by simple linear measurements that have some limitations. Traditional measures of RV function, such as TAPSE and FAC, have shown their link with RVEF and also their diagnostic and prognostic value in different cardiovascular conditions [258]. However, TAPSE only captures the longitudinal movement of the chamber, and several potential sources of measurement error need to be considered. FAC also reflects the radial movement of the RV free wall, but it only represents the RV's function in one two-dimensional plane [26]. 3DE gives more information about RV shape and function by accurately measuring volumes without making any assumptions about the geometry, allowing the definition of reference values of RVEF. Importantly, preserved RVEF does not exclude significant changes compared to the normal RV contraction pattern.

As previously discussed, three main mechanisms generate RV ejection: shortening along the longitudinal axis with the traction of the tricuspid annulus towards the apex (longitudinal motion), inward movement of the RV free wall (radial motion), and traction of

the RV free wall insertion lines by the circumferential deformation of LV myocardium (anteroposterior motion). These motion components correspond to the myocardial architecture of the RV. Previous data suggested that the longitudinal shortening accounts for 80% of RV ejection, while the inward motion of the free wall has only a minor role [27]. However, several publications contradict these observations, highlighting the potential importance of the "bellows" action (radial shortening) and anteroposterior shortening in healthy individuals and cardiovascular diseases as well [46, 258, 259]. While the longitudinal motion of the tricuspid annulus appears quite prominent, it is important to emphasize that due to its large surface, even subtle inward motion of the RV free wall can result in considerable volume change. Nevertheless, current clinical practice lacks any RV functional parameter, which selectively represents the nonlongitudinal motions of the chamber. According to previous results, RV circumferential deformation (summation of radial and anteroposterior motions) appears to be higher than longitudinal deformation, which also supports our findings [48, 257].

We found a functional shift with age (increasing radial and decreasing longitudinal contribution), which appears to be independent of the age-related changes in RV morphology. Previous studies using TDI-derived velocities and speckle-tracking echocardiography found an age-dependent decrease in RV longitudinal contraction, which is concurrent with our data [260]. Similarly to our results concerning LEF/RVEF, Muraru et al. identified age, LVGLS, and PASP as independent predictors of RV longitudinal performance [260]. Compared to the longitudinal function, the radial motion of the RV has been scarcely investigated in clinical studies. In a pediatric study, a functional shift was observed from neonatal to early adulthood: the authors found a radial predominance of RV systolic function at younger age with a shift to dominantly longitudinal shortening at older age; however, they were using simple linear parameters to quantify these motion directions [261]. Our results suggest that a less prominent, but still considerable shift in adulthood can be seen with decreasing longitudinal and increasing

radial motion, which can be attributable to the age-related changes in RV myofiber architecture [262].

The anteroposterior shortening of the RV is even more often neglected; therefore, clinical data regarding this motion direction are minimal. We hypothesize that RV anteroposterior shortening may reflect the effect of LV contraction on RV function and, thus, can refer to LV-RV interaction.

Interestingly, a different RV deformation pattern characterized the oldest age category (60+). Moreover, REF/RVEF showed a negative correlation with RV afterload in this group. Previous clinical and also experimental data suggest that decreased RV radial shortening may be an early marker of elevated PASP [46, 263]. Therefore, our finding may refer to early RV functional change in response to mildly elevated RV afterload in older adults.

We observed no gender differences in the relative contribution of the three major components; however, RVGLS and RVGCS were higher in women, which could be associated with lower RV volumes and higher RVEF. We have also evaluated racial differences by comparing the two enrolling centers' study cohorts. Japanese subjects were characterized by significantly lower RV volume indices and RVEF. Interestingly, RV contraction pattern also differed with significantly higher longitudinal and anteroposterior, and significantly lower radial contributions to global function in the Japanese population. The final results from the large-scale international WASE (World Alliance of Societies of Echocardiography) study have more comprehensively addressed the racial differences in RV morphology and function [264].

When we compared patients in the lowest quartile concerning LEF/RVEF with the rest of the population, no difference in RVEF was found; however, REF/RVEF was markedly higher, further supporting that lower longitudinal function of the RV may not be an unequivocal sign of dysfunction in every case. Several demographic and hemodynamic parameters

correlated with RV morphology and deformation pattern. Similar associations of RVEDVi and RVEF with age, BSA, HR, and SBP were previously reported in the literature [265, 266]. The inverse relationship of REF/RVEF and LEF/RVEF with BSA suggests that body size also affects RV function, which may be attributable to the distinct hemodynamic load. We found a positive correlation of REF/RVEF and a negative correlation of AEF/RVEF with systemic blood pressure, which may also refer to the importance of ventricular interaction. Experimental data suggest that changes in LV systolic function in response to altered LV loading conditions result in opposite radial and anteroposterior shortening changes, which aligns with our results [267]. Moreover, in accordance with previous data, RVGLS and LEF/RVEF did not correlate with HR, while RVGCS and REF/RVEF had a positive, and AEF/RVEF had a negative correlation with it. According to these findings, the RV longitudinal and circumferential fibers may have a different inotropic response to HR changes (force-frequency relationship) [268].

The primary aim of our other two-center study was to define the specific contributions of longitudinal, radial, and anteroposterior contraction to global RV function in a cohort of healthy children. We also sought to describe the maturational changes that occur in each of the components of the RV function, in addition to the global value. Our primary finding was that whereas the contributions of the longitudinal and radial components were similar, a predominance of anteroposterior contraction was present in the overall cohort. Moreover, age-related differences were present for global RVEF, REF, REF/RVEF, and all components of RV strain.

Prior groups have used 2D echocardiography to show that the contraction pattern of the RV in children changes over the first year of life as children transition from fetal circulation, in which the RV faces a high afterload to post-natal circulation in which the PVR gradually declines over the first few months of life. One group used measurements of TAPSE and a

surrogate marker of radial contraction to demonstrate a clear transition from predominantly radial contraction to more longitudinal contraction around four months of age [269]. While likely underpowered to detect significant differences between the contribution of radial contraction in neonates (*i.e.*, under one month of age) and older children, we did find differences in the contribution of radial shortening with increasing age. Others have used 2D speckle-tracking strain analysis to demonstrate that longitudinal contraction increases in premature infants' first year of life [269]. In contrast, our study suggests that the pattern of longitudinal shortening may be complex, with an early increase in magnitude followed by a later return to baseline values. Moreover, we are the first to describe anteroposterior contraction patterns in children. The anteroposterior contraction is primarily determined by the circumferential shortening of the LV mid-layer myofibers, which draw the RV free-wall insertion lines towards each other. It has been shown previously that AEF is strongly associated with LVEF in both healthy volunteers and those with congenital heart disease with a systemic RV [270].

The maturational differences in the directional contraction of the RV identified in this work emphasize the importance of using advanced techniques to assess RV contraction patterns in children with simple and complex congenital heart disease. Understanding and quantifying the relative contribution of each component of RV contraction could have potential applications across multiple subsets of RV pathology by providing insights into the long-term effects of (1) pressure overload on the RV in children with chronic RV outflow tract obstruction (*i.e.*, children with Tetralogy of Fallot, congenital pulmonic stenosis, idiopathic pulmonary hypertension), (2) volume overload in children with a long-standing left-right shunt (*i.e.*, partial anomalous pulmonary venous connections, ASDs), (3) primary RV myopathy (*i.e.*, arrhythmogenic cardiomyopathy) and finally (4) complex anatomy leading to the use of the right ventricle as the systemic ventricle in either a single ventricle circulation (*i.e.*, hypoplastic left heart syndrome) or a biventricular circulation (*i.e.*, “congenitally corrected” transposition of the great

arteries). A more refined understanding of the evolution and progression of changes in RV contraction could help providers identify the effects of medical therapy and better define the optimal timing for procedural interventions.

8.3. Exploring the changes of RV contraction pattern in different clinical scenarios

In our first athlete's heart study, we aimed to characterize RV morphological and functional changes in response to long-term, intense exercise training in a group of elite water polo athletes. According to our results, typical features of RV mechanics include a functional shift compared to healthy, non-trained controls: the relative contribution of longitudinal motion to global function is increased, while the radial shortening is significantly decreased in athletes (Figure 35). Moreover, this functional pattern is correlated with aerobic exercise performance, as measured by CPET.

Our water polo athletes showed significant RV morphological remodeling, as expected. Compared to the conventional RV linear dimensions, 3D volumetric assessment demonstrated more pronounced RV dilation in athletes. Still, from a purely clinical view, quantification of RV volumes holds low diagnostic value: along with the morphological changes of the athlete's heart, slightly reduced RV function measured by FAC or RVEF are often present as well; therefore, a considerable group of athletes fulfill the Task Force criteria of AC [271]. These similarities hamper a confident distinction between an athlete's heart and pathological conditions but also show the need for detailed functional characterization, which may offer more specific and sensitive markers to differentiate these entities. Our results comprise a functional shift in RV function with increased longitudinal function contribution and decreased importance of free wall radial motion. Several underlying factors may explain the presence of this functional shift.

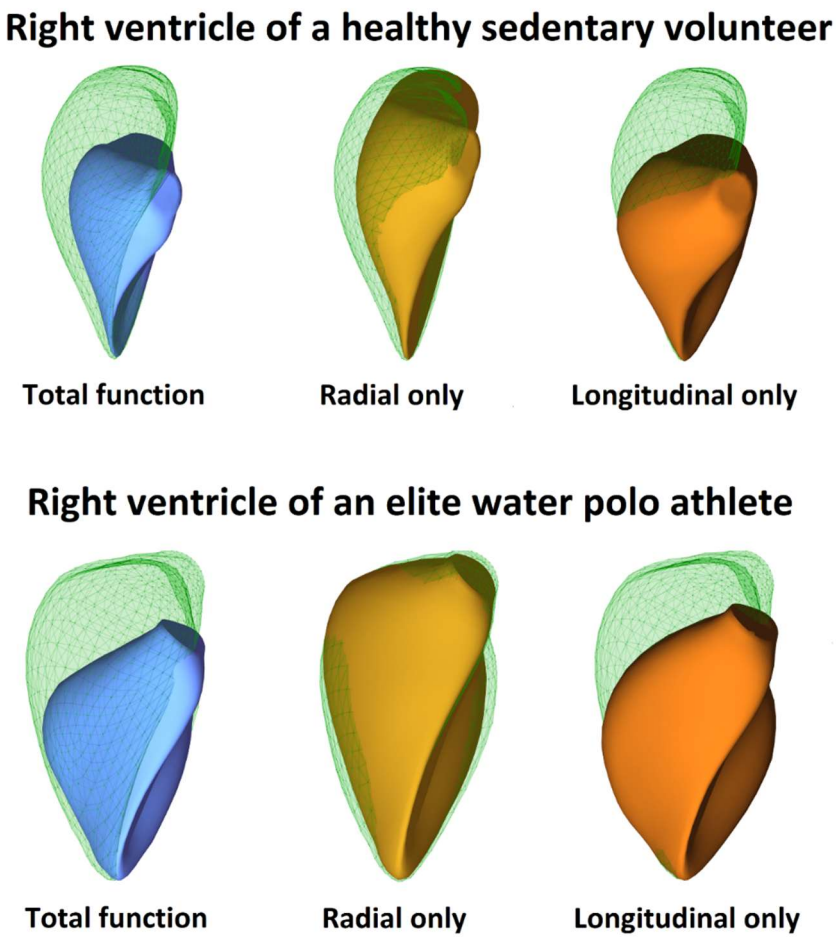

Figure 35. Representative cases of a healthy sedentary volunteer and a water polo athlete. Green mesh represents EDV, and the blue surface is the ESV with all motion directions enabled. By decomposing the motion of the 3D RV model, the different anatomically relevant wall motion directions can be separately quantified. Yellow surface represents the volume loss at end-systole generated by only the radial motion. Orange surface represents the volume loss at end-systole generated by only the longitudinal motion. In the healthy subject, the longitudinal and radial motion roughly equally contributes to global RV function (LEF/RVEF: 0.46; REF/RVEF: 0.48; RVEF: 63%). In the athlete, the relative contribution of right ventricular longitudinal motion is higher; however, a decreased radial motion is also present (LEF/RVEF: 0.54; REF/RVEF: 0.25; RVEF: 57%).

As previously mentioned, repetitive, vigorous exercise bouts are associated with marked hemodynamic demands, which results in a disproportionate hemodynamic load compared to the LV [207]. Beyond the volume overload associated with significantly increased CO, during intense exercise, elevated RV pressures also develop, which may act as important promoting factors of RV functional remodeling. In pathological states, RV volume and pressure overload display distinct mechanical responses. In patients with isolated RV volume overload, such as

by the consequence of ASD, it has been shown that increased preload results in higher TAPSE and RVGLS along with similar FAC (partly incorporating the radial motion), which may point to a higher contribution of longitudinal shortening to global function [87, 89, 272]. In patients with RV pressure overload, such as primary pulmonary hypertension or chronic thromboembolic pulmonary hypertension, the loss of radial function may be a more sensitive and earlier marker of RV dysfunction [44].

According to our results, in athletes of mixed exercise nature, the RV mechanics share the features of both volume overload (with the increased relative contribution of longitudinal shortening) and pressure overload (decreased radial shortening). In our population of healthy young athletes, this functional shift has to be perceived as a physiological adaptation to regular, intense exercise. Evidence suggests that exercise-induced RV dysfunction develops due to the varying contribution of individual susceptibility and the hemodynamic overload of intense training [197, 273]. Sensitive imaging markers are still lacking in screening for at-risk athletes and in monitoring exercise-induced changes.

The revealed gender differences may result from females' significantly higher resting HR. Higher HR was shown to be independently associated with higher LV longitudinal deformation in a pooled population of athletes and controls [274]. Considering that the frequency-dependent inotropy (Bowditch phenomenon) also applies to the RV, it may result in higher deformation values in females. Concomitant remodeling of the LV may also play a role in the functional shift: LV contraction significantly contributes to RV function, which the marked morphological and functional adaptation of the ventricles can also alter. Interestingly, despite the supernormal relative contribution of longitudinal motion to global RV function, females demonstrate a marked decrease in longitudinal deformation, especially at the basal level of the free wall. This result corresponds to several previous papers where the importance of the basal free wall segment was highlighted [275, 276] but also shows worrisome similarity

with the RV longitudinal contraction pattern reported in subclinical AC mutation carriers [123]. Interestingly, this unique RV functional pattern of the athlete's heart correlated with exercise capacity measured by CPET. EF or other functional parameters of each ventricle did not correlate with peak oxygen uptake. On the other hand, there was a significant correlation between REF/RVEF, LEF/RVEF, and VO_2/kg, indicating that the degree of this mechanical shift may be related to peak exercise capacity pointing at a continuum of training level and functional alterations seen even during resting conditions. Therefore, the increased relative contribution of RV longitudinal function along with a decreased radial motion, may be an important marker of athlete's heart.

Our second athlete's heart study specifically investigated adolescent athletes' hearts. Our main findings are the following: (i) adolescent athletes have already presented with characteristic athletic features on echocardiography to adults, (ii) the RV contraction pattern changes to a dominant longitudinal direction (similarly to adults), and (iii) biventricular morphological and functional remodeling - including the altered RV contraction pattern - is correlated with peak exercise capacity measured by CPET.

Historically, there has been a debate about whether classical athletes' heart features could be present during childhood; however, recent evidence clearly shows that pediatric subjects are also on the phenotypic spectrum. A recent systematic review and meta-analysis confirmed a 27% increase in LV mass accompanied by less prominent but significant increases in LV and LA dimensions [277]. Our results are in line with these observations, irrespective of the method used for the evaluation (conventional or 3D). Moreover, the development of exercise-induced changes in LV morphology is fast in adolescents: a study established LV remodeling within 10 weeks of supervised endurance training for 8-10 hours per week [278].

Another study showed that similarly to other exercise-naïve age groups, pre-adolescent athletes initially present with a concentric-type hypertrophy, which later transitions into an excentric-type [279]. Adolescence may be perceived as a physiological but strong anabolic state that also affects the cardiovascular system, and it may act synergistically with physical exercise [280, 281]. The development and regression dynamics of exercise-induced changes are burning questions of sports cardiology that can have important differential diagnostic and also prognostic consequences [282]. However, these questions are even more complex when considering pediatric subjects; therefore, further, large-scale, longitudinal studies are warranted in this age category. Nevertheless, a growing body of data indicates that robust cardiac structure and function changes can be expected in both male and female adolescent athletes [277, 278, 283-285].

Mainly attributable to its more problematic evaluation using conventional methods, we also know relatively less about the RV in this age category. It has been shown that five months of training results in a greater degree of RV dilation than in non-athletic children during natural growth [283]. Also, there is an association between weekly training hours and RV size [279]. A previous study also showed that endurance-trained adolescents have increased RV longitudinal function (assessed by TAPSE and TDI-derived s' velocity) [285]. Our results reinforce these findings using more advanced methods, including 3DE-derived volumetric models. Additionally, this relative increase in longitudinal shortening is accompanied by a decrease in radial and anteroposterior shortening. This phenomenon was already established in our previous study - and RV mechanical shift also correlated with better exercise capacity [224]. We also hypothesize that the exercise-induced RV adaptation incorporates changes in the myofiber arrangement, resulting in a more oblique, more longitudinal direction [286]. Thus, longitudinal shortening will predominate while the other two components (radial shortening representing the RV free wall inward motion and anteroposterior shortening representing the

traction of the free wall by LV contraction) will be relatively decreased. Here, we have shown that this characteristic feature is already present in adolescent athletes, maintaining its relationship with a better exercise capacity. Our study is unique in that we have quantified LV and RV volumes and mechanics using 3D echocardiography. Most recently, using 3D echocardiography, Jone et al. provided sex-specific reference values for pediatric RV volumes, EF, and *z*-score equations from children across five centers in North America [287]. The RV volumes measured in our athletic population are remarkably higher, also pointing at significant remodeling of the left heart and its right counterpart [288]. Importantly, female adolescent athletes are also presented with the phenomena mentioned above – but with less of a degree. As such, we should also consider young female athletes as part of the spectrum. Furthermore, evidence suggests that the classical hypothesis of Morganroth (more concentric hypertrophy in strength-trained athletes versus more dilation in endurance-trained athletes) is applicable to the female athlete's heart [289]. All these results imply that during a clinical evaluation, irrespective of age and sex, "outliers" (*i.e.*, high ventricular volumes, high LV mass, etc., in a moderately trained athlete or amateur) should be downstream evaluated with more advanced modalities (*i.e.*, stress testing, CMRI, genetic testing) to exclude the presence of an underlying disease. Of note, the phenotypic features of these diseases often overlap with the ones of a normal athletic heart [290]. However, examining the pediatric athlete's heart is even more challenging due to several confounders, like sex differences, maturation, and growth [291]. Therefore, a deeper understanding of the physiology of the healthy pediatric athlete's heart is a prerequisite for further research and clinical evaluation. Physical examination, family history, and even ECG do not provide granular information, and therefore, echocardiography is gaining momentum to be included as an essential screening tool in clinical protocols. Still, emerging echocardiographic techniques (speckle tracking or 3DE) that have already started to permeate cardiology practice are underutilized in sports medicine despite their additional value in the

geometrical and functional characterization of the heart [292]. 3DE provides characteristic morphological and functional features of the athlete's heart, even during resting conditions that are correlated with exercise capacity. Thus, our current results promote further research using advanced echocardiographic techniques in the clinical context of adolescent athletes to test their capability to distinguish between a healthy athlete's heart and different pathologies.

In our third athlete's heart study, we aimed at a comprehensive biventricular mechanical characterization by LV and RV GLS and GCS using a large database of elite athletes to allow comparison between sexes, age categories, and different types of sports.

Although adaptation is generally similar in male and female athletes, sex may impact cardiac remodeling as previous studies have shown that male athletes have greater absolute cardiac dimensions [293-295]. Similarly, in our findings, male athletes had significantly higher LV and RV volumes and LV mass; however, it is important to emphasize that in female athletes, all the features of exercise-induced remodeling are present compared to sedentary female controls. As expected, adult athletes participated in competitive sports for longer; thus, larger LV volumes and mass were observed. Still, despite the higher absolute training load of adults, the RV volumes were comparable between adolescent and adult athletes. These findings suggest that the right heart remodeling precedes its left counterpart with significant dilation even at a younger age, especially in females. Furthermore, endurance athletes are often described as having the most extensive but balanced dilation of all four cardiac chambers; however, a recent publication suggested that the RV undergoes a disproportionate remodeling compared with the LV, which resonated with our findings [207]. The direct association between increased biventricular volumes and enhanced athletic performance was previously investigated [296-298], and our findings also confirmed it as LV and RV volumes significantly correlate

with peak exercise capacity; however, RVEDVi was found to be the strongest independent predictor among other volumetric or functional parameters. According to our findings, LVEF and RVEF resting values were mildly but significantly reduced compared with sedentary controls. Regarding the associations between resting systolic functions and exercise capacity, similarly to La Gerche et al. [297], our data showed significant inverse correlations between 3DE-derived LVEF and RVEF and VO_2/kg.

The deterioration of LV longitudinal vs circumferential shortening is often dissociated in different pathological conditions; thus, the balanced decrease seen in athletes may rather point to a physiologic process. Power athletes showed the lowest resting values compared with the other sports classes. This may be explained by the different training profiles of these athletes: a mainly static exercise regime imposes a significant pressure load on the LV, which manifests in reduced LV deformation. Correlations of decreased LV deformation with higher SBP and increased LV mass were previously reported in power athletes [289, 299].

We faced a knowledge gap regarding the RV mechanical pattern since RV circumferential shortening has scarcely been investigated in athletes. Our study demonstrated that the athlete's heart is characterized by a disproportionate decrease in RVGCS compared with RVGLS. 3D-based RVGLS was similar between athletes and controls in this study, which is particularly interesting since the decrease in LV longitudinal shortening implies a parallel decrease in RV longitudinal shortening. In pathological conditions (such as left-heart diseases), due to the change in the function of the interventricular septum and myofiber arrangement, such a decrease in LV and subsequent RV longitudinal shortening is compensated with an increase in RV radial (circumferential) shortening [4]. However, in the context of the athlete's heart, circumferential shortening is decreased along with maintained or even supernormal longitudinal shortening, which was also confirmed by a recent meta-analysis [300]. As previously mentioned, this may be explained by the myofiber meshwork transitioning into a

more advantageous (more oblique) orientation that will result in the aforementioned mechanical pattern despite the significant chamber dilation. A supernormal RV longitudinal shortening may also support right atrial filling by enhancing venous return in systole, which can be an advantageous component of cardiac function, especially during exercise.

In our PH study, we showed that RV contraction patterns change as a function of progressive RV-PA uncoupling and increased hemodynamics-based mortality risk, from decreased longitudinal shortening in patients with low hemodynamic risk and no or mild RV-PA uncoupling to decreased anteroposterior shortening in patients with severe RV-PA uncoupling, increased RV volumes, decreased LV preload, and advanced hemodynamic mortality risk. The present study is original in relating different directions of RV shortening to invasive measurements of Ees/Ea and risk as assessed by invasive hemodynamics (Figure 36). The results confirm the predominant loss of longitudinal shortening in less severe PH and the predominant loss of anteroposterior shortening in more advanced PH, and provide additional information on the functional and clinical relevance of RV contraction patterns.

Previous studies suggest a sequence of changes in RV-PA coupling as PH progresses, with initial preservation of Ees/Ea (by an adapted increase in Ees) and unchanged RV volumes followed by a late decrease in Ees/Ea (when Ees/Ea falls below the reserve threshold), RV dilatation, septal shift, and terminal decrease in LV preloading. While admittedly, this sequence of events was not determined in prospectively followed patients, physiological rationale and clinical experience allow for the definition of stages of RV-PA uncoupling from normal to right HF values as were defined in the present study. The apparent interest in 3DE is that this bedside technology allows for repetitive measurements of RVEF, which can be considered a relevant surrogate for the Ees/Ea ratio, is a potent predictor of outcome in severe PH, and is now listed

in the updated ESC/ERS guidelines [225]. The further added value of 3DE, as previously underscored and shown in the present study, is that it allows analysis of the contribution of regional changes in RV function to ejection. The present data show the high relevance of this approach.

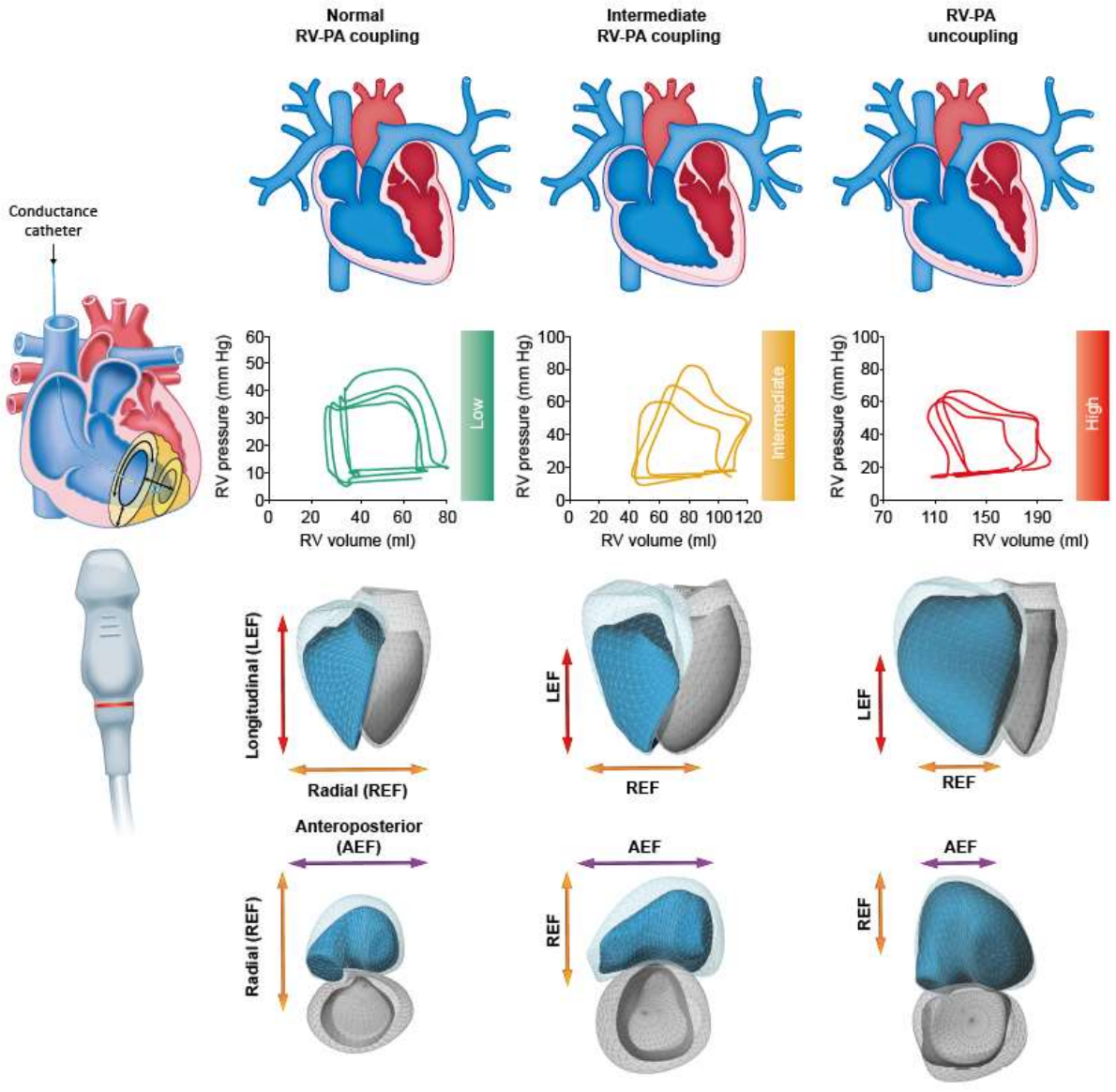

Figure 36. RV contraction patterns at different levels of RV-PA coupling and mortality risk. In a cohort comprising 53 patients with suspected or confirmed pulmonary hypertension, RV contraction patterns showed characteristic alterations at different levels of RV-PA uncoupling and hemodynamic risk. Early RV-PA uncoupling was characterized by reduced RV longitudinal function, whereas advanced RV-PA uncoupling was accompanied by reduced RV anteroposterior shortening. RV-PA coupling was measured from multi-beat pressure-volume loops obtained by conductance catheterization with Valsalva-induced reduction of RV preload.

2D echocardiographic parameters reflecting longitudinal function (TAPSE, RVGLS, and RVFWLS) showed a significant decrease from no or mild RV-PA uncoupling to intermediate uncoupling but not from intermediate to severe uncoupling, similar to LEF. Interestingly, however, s', which is also commonly applied in RV longitudinal function assessment, showed no significant difference between the distinct levels of RV-PA uncoupling. Interestingly, LVEF was maintained in the presence of severe RV-PA uncoupling, whereas LVSVi was decreased. This is compatible with the notion that RV-PA uncoupling leads to impaired LVSVi through impaired LV preload. There is, however, evidence that at later stages of PH than in the present study, negative diastolic ventricular interaction and LV underfilling ultimately lead to depressed LV systolic function.

The main results of our HTX study are that (i) the longitudinal shortening of the RV is significantly decreased in HTX patients without relevant differences in RV geometry and global function; (ii) this phenomenon is attributable to the supernormal radial motion of the RV free wall, which maintains RV ejection fraction; (iii) in time, there is a tendency toward the recovery of RV longitudinal shortening in HTX recipients.

About 50% of cardiac complications and 20% of mortality are related to RV failure in the early postoperative period after HTX. RV systolic dysfunction, as assessed by conventional echocardiography, is a common finding in HTX patients. However, the decrease in RV function defined by routine measurements is poorly associated with clinically manifested right HF. The possible cause is that conventional measurements, which refer mainly to the longitudinal shortening of the chamber (TAPSE, s′ by TDI), are not accurate in evaluating global RV function in HTX recipients. Echocardiographic data of our cohort of patients showed the same characteristics: parameters of longitudinal function were decreased not only in the early

postoperative period but also during long-term follow-up. Nevertheless, global function, as assessed by 3DE, was maintained. TAPSE, the most widely used parameter of RV function, failed to show a correlation with 3DE-derived EF. There are also several technical issues; however, the altered motion pattern of the structurally complex RV may play a pivotal role in this underestimation. Therefore, the other motion directions must also be considered in order to characterize the RV function comprehensively. According to our and others' experience with visual estimation, we hypothesized that radial motion is dominant in determining global RV function in HTX patients. In our study, FAC was similar in HTX patients and healthy subjects while correlating well with EF. However, FAC suffers from the inherent 2D nature of its calculation, referring to a single plane of the large RV free wall surface. Using ReVISION, our results confirmed the dominance of radial wall motion in HTX patients. REF/RVEF ratio was supernormal, while LEF/RVEF was decreased similarly to other parameters of longitudinal function. Furthermore, our results show that RV longitudinal shortening decreases throughout long-term follow-up. Patients transplanted over one year still presented with decreased longitudinal function. However, a slow recovery is suggested to be present while global function and geometry remain unchanged. We found direct correlations between TAPSE, longitudinal strain, LEF/RVEF, and the time elapsed after HTX. Therefore, the instantaneous dominance of the radial wall motion after transplantation may be shifted back toward longitudinal shortening in time. The relative contribution of anteroposterior shortening to global function was unaffected by time, which may be related to the maintained LV function throughout follow-up.

As discussed previously, several underlying mechanisms may cause this functional change. First and foremost, the elevated pulmonary pressure of the recipient may be a factor. However, PVR decreases after the procedure, and only slightly elevated pressures are expected later, even in cases of severe preoperative PH [183-185]. Therefore, we should be cautious in

highlighting only pulmonary pressures regarding RV functional shift on a long-term follow-up. Besides hemodynamics, (patho)physiological changes associated with the donor's brain death and organ preservation may contribute to the functional shift [177, 178]. It has been shown that the loss of pericardial constraint due to the incomplete closure of the pericardial sac and mismatch in the donor-recipient heart size significantly impact cardiac mechanics. We should also mention the potential detrimental effects of immunosuppressive regimens [191]. Beyond the aforementioned potential causes, loss of the substantial innervation of the RV myocardium may be another important factor resulting in complex functional changes of the RV. However, it has been suggested that the transplanted heart can be reinnervated by both sympathetic and parasympathetic fibers [187-189]. Hypothetically, the slow recovery of longitudinal function can also result from reinnervation.

8.4. Establishing the added prognostic value of 3D RV assessment

In our first „outcome" study, we investigated a diverse patient population with left-sided heart diseases who underwent specific cardiac interventional or surgical procedures. We found that the conventional echocardiographic measurements may be inadequate to support a granular risk stratification; however, RVEF may be a robust clinical parameter significantly associated with adverse outcomes.

TAPSE, s' wave by TDI and even longitudinal strain by speckle tracking refers only to the longitudinal shortening of the RV in a single apical four-chamber cut and neglects two other "axes" of geometry and function: the radial and the anteroposterior. Conventionally, the RV longitudinal shortening was considered the essential determinant of RV global function; therefore, there is a strong clinical belief that TAPSE is the one-stop shop for RV function. However, as we explored above, the radial and anteroposterior motion directions in healthy

volunteers are at least equally important [232]. Routine 2D echocardiographic measurements entirely neglect anteroposterior motion [219, 301]. Relatively small amounts of inward movement in these directions can produce significant stroke volume due to the massive surface of the RV free wall. These results support the use of 3DE, but the mechanical patterns that evolve in different cardiac diseases reinforce it. As the mechanical pattern and, thus, the relative usefulness of the surrogate 2D measures vary, only RVEF by 3DE represents an integrative, robust, informative measure independent of the clinical scenario. This feature makes RVEF a good candidate for predicting prognosis even in unselected, diverse patient populations.

Nagata and colleagues published one of the first publications that described the predictive value of RVEF by 3DE [136]. They investigated 446 patients with various cardiovascular diseases and followed them up to record cardiac death and major adverse cardiovascular events (MACE). RVEF was significantly associated with future cardiac death and MACE (similar to E/e′ and LVEF) and was significantly related to future cardiac events after adjusting for relevant clinical and echocardiographic parameters. Later, Surkova and coworkers confirmed in 394 patients (again with various cardiovascular diseases) that RVEF was associated with all-cause mortality and cardiac death, and the impairment of RVEF carried a significantly higher risk of mortality independent of LVEF [239]. The latter two groups also determined those cut-offs of RVEF values that separate the cohorts according to the risk and, therefore, suggested to be applied in routine clinical practice (45%, 40%, and 30%) [302].

Our results add to this current knowledge by investigating a higher-risk population (dominantly HFrEF patients or patients with severe valvular heart disease) – higher risk, not just in terms of current functional status but also because of the previous or upcoming invasive procedures and related potential adverse events [238, 303]. Moreover, we compared head-to-head the conventionally used parameters and RVEF and showed the superior discriminatory power of the latter in predicting 2-year all-cause mortality. The optimal cut-off points identified

during ROC analysis were close to the ones defined by current recommendations regarding RVEF, FAC, and 2D FWLS. However, regarding TAPSE, it was 24 mm, which is a clear normal value as RV dysfunction is generally suggested below 17 mm [31]. This result also highlights that TAPSE cannot be used in general, and the exact clinical scenario must be considered. We may hypothesize that mainly the MVR population can bias that value: a dominant ("supernormal") longitudinal shortening is suggested to be a sign of adverse functional remodeling in patients with severe MR that is also associated with short-term, perioperative outcomes [238].

We aimed to confirm the superiority of 3DE-derived RVEF by a meta-analysis of available studies (including our own above). We found that RV dysfunction is robustly associated with all-cause mortality and adverse cardiopulmonary outcomes in patients with various cardiopulmonary diseases. All four investigated echocardiographic parameters of RV systolic function were associated with these endpoints; however, 1 SD reduction in 3DE-derived RVEF showed a significantly stronger correlation with adverse events compared with a comparable change in TAPSE, FAC, or FWLS (Figure 37).

Studies over the last decade have identified RV dysfunction as a correlate of symptom burden and a powerful predictor of adverse outcomes not only in right-sided heart diseases but also in conditions affecting the left ventricle primarily [304]. In fact, the prevalence of RV dysfunction in patients with HFrEF is 50%, being independently associated with excess mortality and HF admissions [305]. Furthermore, one-third of patients with HFpEF present with a significant RV dysfunction [306]. The presence of RV systolic dysfunction alongside the diagnosis of HFpEF harbors a ~6-times higher risk of two-year mortality compared with the absence of it [306]. Therefore, timely identification of RV dysfunction using sensitive and

reliable functional parameters might enable a more sophisticated risk stratification in the clinical setting.

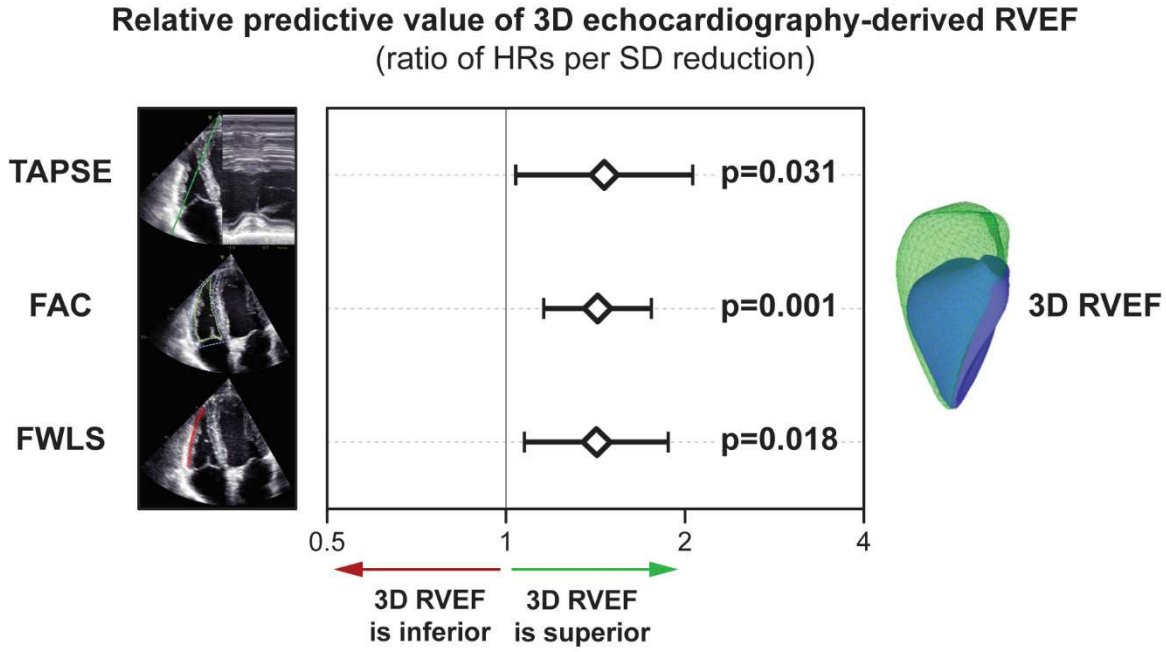

Figure 37. Better association of three-dimensional (3D) echocardiography-derived right ventricular ejection fraction (RVEF) versus conventional metrics of RV systolic function with adverse clinical outcomes: a meta-analysis of 10 studies.

According to two recent surveys, the most commonly used echocardiographic parameters to assess RV systolic function in the clinical routine is the M-mode TAPSE, followed by tissue Doppler imaging-derived s' and FAC [307, 308]. Evidence shows that RV dysfunction is diagnosed in 37% of HFpEF patients by TAPSE, whereas FAC identifies a considerably lower fraction of cases [26%] [309]. A meta-analysis also reported vast differences in identifying RV dysfunction across parameters, with TAPSE suggesting RV dysfunction in 31% of HFpEF subjects, compared with 26% and 13% by S' and FAC, respectively [18]. These considerable diagnostic dissimilarities between conventional echocardiography-derived indices of RV function might stem from the RV's complex 3D anatomy and distinct contraction patterns [4, 48]. Therefore, a unifying RV functional

parameter that can circumvent such limitations would be ideal for quantifying RV dysfunction and associated clinical risk in various pathological conditions. 3DE maps the entire endocardial surface of the RV independent of any assumption about its shape and function, providing an integrative parameter of RV systolic function – RVEF [304].

The present meta-analysis demonstrated that 3DE-derived RVEF showed a robust association with adverse outcomes. We estimated that 1 SD reduction in RVEF conferred a ~2.6 times higher risk of all-cause mortality and/or adverse cardiopulmonary events in a broad spectrum of patients with various cardiopulmonary conditions. This association was unaffected by whether the population consisted of patients with a primary diagnosis of PH. In fact, reduction in RVEF correlates with adverse clinical outcomes to a similar extent in patients with and without PH. Therefore, our meta-analysis extends previous studies by showing that RV dysfunction forecasts adverse clinical events not only in patients with PH [310] but also in those with HF, COVID-19, and aortic stenosis. Furthermore, our estimate was not affected by differences in follow-up durations and whether the studied endpoint included all-cause mortality only or other composite cardiopulmonary endpoints. Specifically, we found that 1 SD reduction in RVEF is associated with ~2.6-times higher risk of death from any cause. Finally, we estimated that even if substantial publication bias occurred, our estimate would not significantly change.

As for the other parameters, we calculated that reduction in TAPSE, FAC, and FWLS also correlated with adverse clinical outcomes, respectively. In fact, 1 SD reduction in each of these parameters was associated with a 1.71-1.81 times higher risk of unfavorable events. Therefore, RV dysfunction is associated with clinical outcomes irrespective of the echocardiographic parameter used. However, in a head-to-head comparison, we found that 1 SD reduction in RVEF conferred a 1.44-1.54 times higher risk of adverse outcomes as compared with a comparable reduction in TAPSE, FAC, and FWLS, respectively, in the very

same patient populations. Consequently, 3DE-derived RVEF might identify a broader spectrum of high-risk patients with RV dysfunction, in contrast with the other parameters, rendering it a more valuable tool to risk-stratify patients with various cardiopulmonary conditions. This might translate into a timely identification of high-risk patients, also paving the way for future studies to develop effective countermeasures.

In a similar attempt to assess the pooled prognostic significance of different parameters of LV systolic function, a previous meta-analysis showed that LVGLS had a superior predictive value compared to LVEF [33]. Notably, in our present meta-analysis focusing on RV function, RVEF was better associated with adverse outcomes than FWLS. This important finding may be attributable to the fact that FWLS reflects only one mechanical component (longitudinal shortening) in a single 2D tomographic plane (unlike three planes for LVGLS assessment) and, therefore, may not be an adequate representation of the contraction pattern of the complex 3D structure of the RV, especially under different pathophysiological conditions.

Overall, the results of our current meta-analysis support the broader implementation of 3DE for assessing RV systolic function in patients with cardiopulmonary disorders – irrespective of the primary site of the disease. Of note is that 3D image acquisition and postprocessing require advanced hardware and software environments and have a learning curve. According to a worldwide survey, 50% of current ultrasound systems already have transthoracic 3D probes available, yet only 17% of the participants use them frequently to measure RVEF [311]. There is a common belief that the quantification of RVEF is a lengthy process with low success rates. However, it has been recently demonstrated that contemporary automated 3D software solutions may even result in shorter analysis times than routine 2D evaluations [312]. Recently published articles (including those incorporated in the current analysis) reported a feasibility of over 90% and good reproducibility, which aligns with our experience. As the seemingly most powerful index of RV function, the inclusion of RVEF in

everyday clinical decision-making and risk stratification models seems justified by the current knowledge base. Moreover, the assessment of RVEF as a trigger for specific therapies may also lead to clinical benefits for patients in the future. However, these need to be tested in rigorous clinical trials.

Our prospective outcome study investigated patients with severe primary MR undergoing MVR. Advanced diagnostic and therapeutic options have become increasingly available concerning LV, while RVD remains a frequent clinical challenge in perioperative care. It is common that RVD remains unrecognized, which can lead to adverse outcomes. In the PREPARE-MVR study, we intended to provide further insights into RV mechanics in patients undergoing MVR and to identify its association with the development of early postoperative RVD. We have found that severe MR resulted in decreased radial and increased longitudinal contribution to global RV function, which pattern underwent an instantaneous shift due to open-heart surgery. The observed increase in preoperative longitudinal contractions was associated with decreased postoperative RV contractility as assessed by PAC. However, at 6-month follow-up, normal RV contraction pattern was restored.

RVEF is a conventional and useful measure of RV systolic performance. However, just as it has been described concerning the LV, the elemental components of myocardial mechanics could be more sensitive and predictive because the native RV contraction pattern could be disrupted even before RVEF starts to decline. In our current study, patients with severe primary MR but with preserved biventricular function were recruited. Despite this fact, a reduction in radial and an increase in longitudinal wall motion could be observed, pointing to a functional shift induced by the severe valvular disease and the subsequent post-capillary PH.

Chronic primary MR triggers eccentric hypertrophy with geometric changes of the LV cavity as an adaptive mechanism to volume overload. Its shape becomes more spherical, and the consequent rise of LV and pericardial constraint likely contributes to the alterations of RV function [313]. Chronic MR results in a progressive deterioration of LV contractile function, although the LVEF is maintained over a relatively long period. Due to the aforementioned mechanisms, the normal function of the interventricular septum may be hampered early during the course of the disease. Furthermore, longstanding MR induces elevation in LA, pulmonary wedge, and pulmonary arterial pressures that result in pressure overload of the RV [314]. Still, the overall RV performance was influenced by pulmonary pressures in our patients, as confirmed by the inverse relation of RVEF to the levels of mPAP and PAWP. Moreover, the functional consequences of pressure overload could be observed in the RV contraction pattern: the radial motion (the so-called bellows effect) was impaired despite the preserved RVEF. The preoperative alterations attributable to MR make the RV susceptible to developing overt RVD during and immediately after the open heart surgery. MVR diminishes LV volume overload, resulting in the reduction of LV and pericardial constraint. The apparent deficit in RV function after surgery, when evaluated exclusively by the longitudinal contraction, has been described previously [140, 315]. As discussed above, different causes have been proposed to explain this loss in longitudinal RV performance, such as geometric changes in the RV, intraoperative ischemia, pericardial disruption, and suboptimal cardioprotection. The decline in longitudinal function occurs immediately after the opening of the pericardium, which supports the hypothesis on the fundamental role of the pericardium in maintaining physiological RV geometry and function [157]. However, the reductions in longitudinal measures after surgery might reflect a single aspect of a modified and complex contraction pattern. Thus, conventional M-mode and 2D indices may be inadequate for the postoperative assessment of RV function. Our results clearly demonstrated that the radial motion could effectively compensate for the

postoperative decline of longitudinal motion to maintain RVEF. Interestingly, we have found that six months after the successful operation, the native contraction pattern is restored in MVR patients as RV longitudinal and radial contributions (LEF/RVEF, REF/RVEF) are comparable to healthy controls'. However, the M-mode and 2D longitudinal RV function indices indicate incomplete recovery. To our knowledge, this is the first observational study that comprehensively characterized the dynamic perioperative changes of RV mechanics in MR patients (Figure 38).

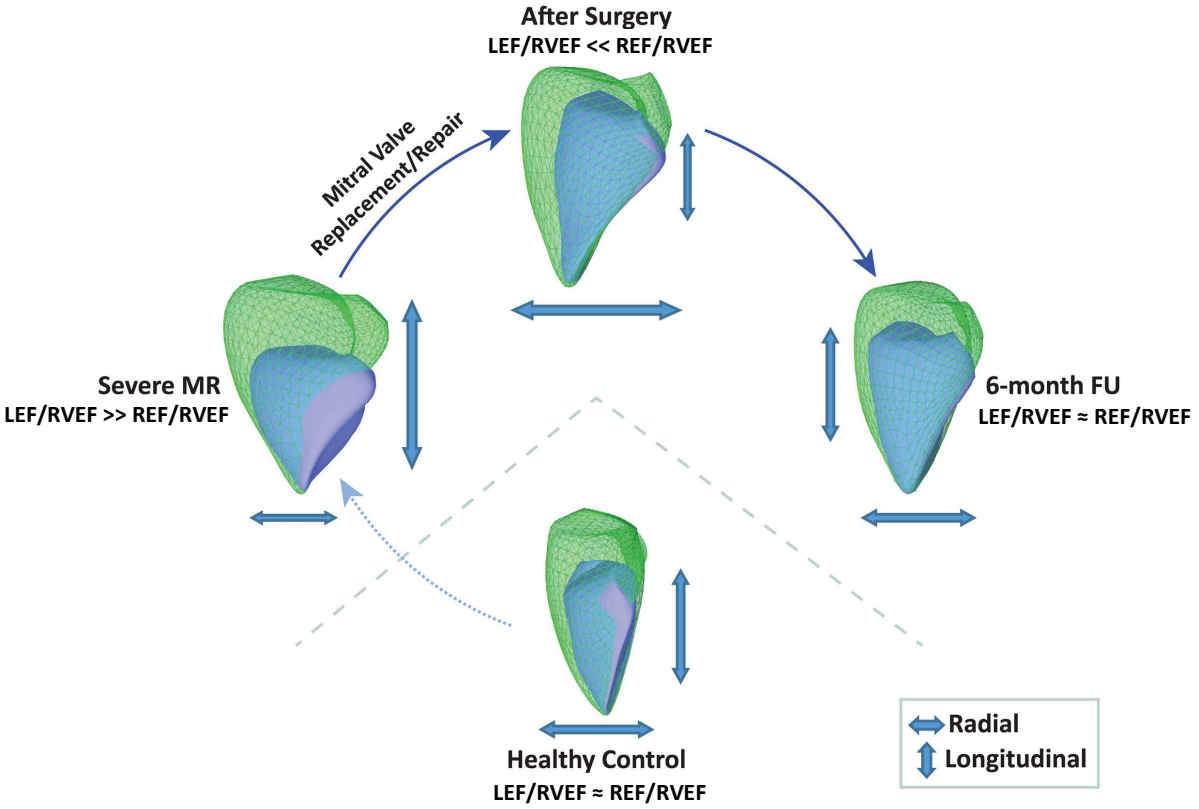

Figure 38. RV mechanics in healthy controls and patients undergoing surgical treatment of severe primary MR: representative cases. By decomposing the motion of the 3D RV model, the different wall motion components can be quantified separately. The green mesh represents the end-diastolic volume, and the blue surface is the end-systolic volume of the RV. In the healthy subject, the longitudinal and radial motion contributed equally to global RV function (LEF/RVEF vs REF/RVEF: 0.48 vs 0.44). The preoperatively observed longitudinal dominance in the patient with severe MR (LEF/RVEF vs REF/RVEF: 0.54 vs 0.29) shifted to radial dominance (LEF/RVEF vs REF/RVEF: 0.39 vs 0.51). However, this shift was temporary as six months later, the contribution of the two components equalized, and the contraction pattern became similar to healthy control's (LEF/RVEF vs REF/RVEF: 0.46 vs 0.43).

RVD is a challenging perioperative clinical scenario without a clean-cut method for an accurate diagnosis. The leading causes include myocardial ischemia and acute RV pressure overload, besides the effect of the pericardial sac opening [316, 317]. While intraoperative RV failure can be evident as it hinders the weaning from CPB, early postoperative RVD often remains subclinical and requires an integrated diagnostic approach involving physical examination, blood tests for end-organ damage, hemodynamic, and imaging-based monitoring [318]. We have chosen a robust parameter of RV contractility (*i.e.*, RVSWi) to define RVD; however, performing PAC is not part of routine care in MVR patients. Increased preoperative 3D parameters of RV longitudinal function predicted decreased contractility after the operation. According to our results, 3DE may facilitate a more profound preoperative risk stratification of MVR patients. Improving perioperative care might enable timely diagnosis and, potentially, the prevention of severe RVD. A more in-depth understanding of perioperative changes in RV hemodynamics and mechanics may also contribute to establishing the real-life prevalence of RVD and evaluating its detrimental consequences.

In our retrospective outcome study involving patients with different left-heart diseases, we specifically aimed to assess the prognostic value of both LV and RV circumferential shortening using 3DE. Our main findings can be summarized as follows: (1) Impaired values of both LV and RV GCS were associated with all-cause mortality in univariable Cox models. (2) Among the evaluated multivariable models, the one with LVGLS and RVGCS fitted our data the best. Interestingly, however, only RVGCS was found to be an independent predictor of mortality, whereas LVGLS and creatinine levels were not. (3) Based on the median values of LVGLS and RVGCS, we created four groups that differed significantly regarding all-cause mortality. Importantly, reduced RVGCS was associated with worse outcomes even if LVGLS was maintained.

Besides longitudinal shortening, circumferential shortening also contributes significantly to the global systolic function of both ventricles. A mathematical model showed that LVGCS contributes more than twice as much to LVEF than LVGLS and a small increase in LVGCS could compensate for a significant reduction of LVGLS [319]. LVEF was shown to be quadratically dependent on circumferential shortening and only linearly dependent on longitudinal shortening. Previously, numerous publications reported GCS by 2D echocardiography; however, due to its complicated calculation (3 levels of parasternal short-axis view are needed to be acquired and analyzed) and poor reproducibility, the majority of software vendors discontinued the possibility of its measurement [320, 321]. Using 3DE, a single acquisition (and the same cardiac cycle) can be used to calculate both GCS and GLS; thus, it may overcome the limitations of 2D-based calculations.

Importantly, circumferential shortening contributes substantially to global RV pump function, which can be measured only using 3DE. Notably, the circumferential motion may also hold particular importance in the global RV function: as discussed previously, even subtle deterioration in the circumferential shortening of the large RV free wall may result in significant global functional damage [322]. Circumferential shortening is composed of the inward motion of the RV free wall (radial shortening) and the traction of the free wall insertion lines towards each other by the LV contraction (anteroposterior shortening) [26]. Beyond the latter functional connection of the two ventricles, evidence suggests that LV-RV interactions exist on many layers: alterations of geometry, loading conditions, and contractility of a ventricle will significantly influence its counterpart [323]. This complex interplay underpins that practically every disease process may have consequences on both sides of the interventricular septum, with potential importance in terms of diagnosis and outcomes.

Similarly to the left ventricle, the assessment of the RV deformation may exceed the added diagnostic and prognostic value of even RVEF. Small cohort studies with various RV

pathologies, such as PH, ASD, or patients following cardiac surgery, unveiled distinct changes in RV mechanics; still, they were using simple 2D-derived measures of RV function [44, 141, 324]. Our results add another layer to the evidence about the importance of RV non-longitudinal shortening from a diagnostic and a prognostic point of view. As a previously neglected marker of ventricular systolic performance, circumferential deformation may be able to describe a novel aspect of RV systolic function with established prognostic value. RVGCS may represent a robust, universal biomarker of the status of the entire cardiopulmonary system as it overpowers conventional echocardiographic metrics and is associated with adverse clinical outcomes not just in "classical" right-heart diseases but also in primary left-heart diseases. The exact pathophysiological processes (ventricular interdependence, RV pressure overload, etc.) that result in the deterioration of circumferential shortening and the potential usefulness of RVGCS for screening purposes remain to be investigated.

Our last outcome study investigated the changes in RVEF and RV contraction patterns at the different grades of LV systolic dysfunction in patients with left-sided heart disease. Our main findings can be summarized as follows (Figure 39): (1) in patients with left-sided heart disease, the longitudinal and anteroposterior components of the RV pump function were directly related to the LV systolic function and decreased significantly even in patients with mild LV dysfunction; (2) the relative increase in the radial component of the RV pump function compensated the decrease of the RV longitudinal and anteroposterior components to maintain the total RVEF in patients with mild and moderate LV dysfunction; (3) in patients with severe LV dysfunction all the three components of the RV pump function were impaired resulting in a significant reduction of the total RVEF; (4) 3DE-derived RVEF was significantly, and independently of LV systolic function, associated with a composite outcome of cardiac death

or heart failure hospitalization; and (5) anteroposterior RV motion component held additional prognostic value in patients with normal RVEF.

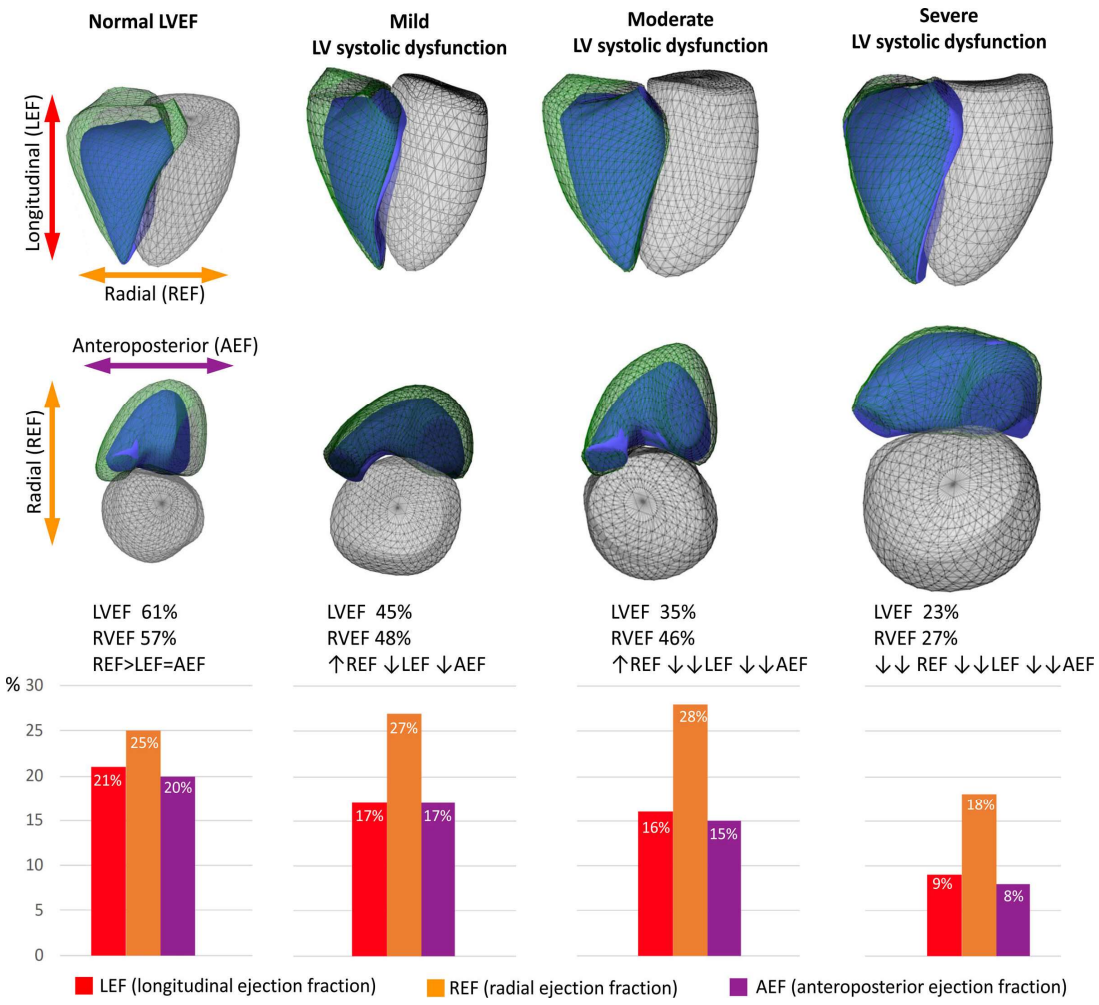

Figure 39. Functional adaptation of the RV to the different degrees of left ventricular (LV) systolic dysfunction in patients with left-sided heart disease: representative cases. Three-dimensional schematic representation of the three major components contributing to total RV pump function: (i) longitudinal shortening along the long-axis (red) contributing to RV longitudinal ejection fraction component (LEF), (ii) inward (radial) motion of the RV free wall (orange) contributing to radial ejection fraction component (REF), and (iii) short-axis shortening in the anteroposterior direction (purple) contributing to anteroposterior ejection fraction component (AEF). Green mesh represents RV end-diastolic and the blue surface the RV end-systolic volume. In the case of preserved LV ejection fraction (LVEF), the three components show a balanced relative contribution. RV shortening along the longitudinal and anteroposterior directions continuously decreases with LVEF. However, shortening in the radial direction shows a compensatory increase in mild and moderate LV dysfunction, maintaining RVEF. In severe LV dysfunction, all motion components drop significantly, resulting in severe RV dysfunction.

As discussed extensively before, three main mechanisms contribute to the total RV pump function: shortening of the longitudinal axis with the traction of the tricuspid valve towards the apex; inward motion of the RV free wall; and contraction of the interventricular septum and its bulging into the RV. The RV fiber orientation determines these mechanisms: free wall has predominantly circumferential fibers, which narrow the cavity during systole, while the septal helical fibers twist and shorten the longitudinal axis of the RV [27].

Reduction of LV contractility and stretching of the septum in patients with left-sided heart disease alter the helical fiber orientation to >60 degrees, making the helix fibers more transverse, thus impairing the efficiency of the longitudinal contraction [27]. At the compensatory stage, the RV increases its transverse function in relation to the decrease of the longitudinal shortening [24]. If the injury persists, the RV transitions from a compensated to a decompensated phenotype characterized by myocyte loss and replacement fibrosis, limiting the free-wall inward motion alongside the longitudinal function. As the LV becomes progressively more spherical, the septal fibers become less oblique, dramatically reducing their mechanical advantage and further impairing RV contractile function. These mechanisms ultimately lead to clinical RV failure [325].

We found significant correlations between LEF and AEF and LV systolic function parameters *(i.e.*, LVEF and GLS), confirming that these motion components are the most related to LV systolic function. RV radial component, on the contrary, may be partially explained by the alterations in LV shape, as demonstrated by the correlation between REF and LV sphericity index. Because all RV components correlated rather weakly with PASP, one can speculate that the mechanisms behind the RV functional adaptation and remodeling are more complex than just postcapillary PH but may be a combination of LV contractility, LV shape, and RV afterload. Future research is needed to identify the pathophysiological determinants of the various RVEF components.

No data specifically addresses the changes in RV contraction patterns at different grades of LV systolic dysfunction. Our results suggest that the LV remodeling occurring in left-sided heart disease is associated with an early and steady reduction in both the RV longitudinal and anteroposterior components of RV pump function, compensated by an increase in the RV radial component, which leads to the maintenance of the total RVEF in patients with mild and moderate LV systolic dysfunction. Consequently, in these patients, the RV systolic function may be underestimated if assessed by parameters that reflect the longitudinal shortening only (*i.e.*, TAPSE, s'). In patients with severe LV systolic dysfunction, this compensatory mechanism is lost due to a decrease of the radial RV shortening, resulting in both the reduction of the total RVEF and the development of severe RV systolic dysfunction.

Our study confirmed the findings from similar cohorts that RVEF is significantly associated with adverse outcomes, independently from LVEF [239]. Importantly, in patients with normal RVEF, only the anteroposterior component's relative contribution to RV function was significantly and independently associated with the composite endpoint of cardiac death and hospitalization for HF, whereas neither RVEF nor LVEF was.

As mentioned above, the systolic anteroposterior shortening of the RV is mainly the result of LV circumferential contraction by stretching the RV free-wall insertion lines. Accordingly, the parameters referring to the anteroposterior component of total RVEF may be perceived as surrogates of the function of the interventricular septum and also of the LV contribution to RV performance. We hypothesize that, in patients with normal RVEF, this additional prognostic value of AEF is still related to LV dysfunction and deteriorated ventricular interdependence that could not be sensitively captured by LVEF either. The relative predictive power of the different RV components may vary according to the underlying pathophysiology. Therefore, further research is warranted either in cardiac diseases affecting the function of the interventricular septum (left bundle branch block, septal myocardial

ischemia/infarction, etc.) or in conditions with different RV pressure- and volume-overload profiles. Of note, no conventional 2D echocardiographic parameter represents anteroposterior RV motion. Therefore, our results strongly emphasize the usefulness of 3D imaging in the thorough characterization of RV function in the cases of LV dysfunction.

8.5. Limitations

The ReVISION software and the presented analyses have some limitations that should be acknowledged. The current version of our software relies on the 3D RV meshes generated using another commercially available software. However, we are working on the next version that will enable an AI-based auto-contouring of the 3D RV surface using raw DICOM files as inputs. The TomTec software package used in our study is clinically well-validated and has shown good concordance with the RVEF obtained by CMRI [5, 326]. Additional large-scale studies are required to evaluate the reliability, reproducibility, and repeatability of ReVISION parameters in a multi-centric, prospective manner using datasets acquired with ultrasound systems of various manufacturers. Volumetric segmentation and strain analysis were not applicable to the CMRI-derived 3D meshes; therefore, we could not assess their agreement between the two modalities. We may also argue whether RVEF represents the gold standard for RV systolic function assessment. However, it is debatable whether there is a true gold standard parameter of RV function except for those obtained from invasively derived PV loops that cannot be used in population studies [327]. Theoretically, contractility (the intrinsic ability of the myocardium to shorten, independent of loading conditions) should be the target measure of all functional evaluations. Yet, conventional parameters, including RVEF, reflect ventriculo-arterial coupling rather than contractility [328].

Regarding our normative studies, further multiethnic expansion was necessary to confirm our findings. We have accomplished that by analyzing and publishing data from the WASE study [264]. Concerning our pediatric normative study, our analyses were limited by a smaller number of subjects in the younger age groups, which is particularly important in considering the significant hemodynamic changes to which the RV is subjected in the first weeks to months of life. Moreover, the differing recruitment methods contributed to a predominance of males in the oldest age group. Consequently, our exploratory analysis intended to identify sex-specific differences in EF parameters among various age groups was likely underpowered.

Regarding our athlete's heart studies, this was a single-center, retrospective, cross-sectional database with a limited number of athletes and only resting echocardiographic evaluations performed. Nevertheless, advanced echocardiographic techniques along with a same-day CPET, elevate their value. In some of the youngest male athletes, it is possible that they did not start their adolescent growth spurt. The temporal changes in RV mechanics, such as throughout a training season or dynamics of deconditioning, remain unknown.

Concerning the PH study, the number of patients included was small; however, sophisticated methodology with combined standard and conductance catheterization, 3DE, and strain analysis limits the recruitment of severely ill patients. Also, patients with atrial fibrillation were excluded. Therefore, larger, prospective studies are warranted. A simplified version of the ESC/ERS risk stratification scheme without a 6-minute walking distance and functional class was used, but this scheme has not been validated for patients with HFpEF or individuals without PH.

Regarding HTX patients, the population was broad in terms of time elapsed after transplantation. This way, however, the correlations of functional parameters vs time could be

demonstrated. On the other hand, we could not show the potential significance of the perioperative hemodynamic and procedural parameters. Complete exclusion of higher-grade rejection episodes and chronic allograft vasculopathy (which can deteriorate biventricular myocardial mechanics) is difficult, especially in patients transplanted for a longer time. Regular biopsies are discontinued after one year according to our institutional protocol, while chronic allograft vasculopathy is assessed on a yearly basis using invasive or CT coronary angiography.

Concerning our first outcome study, we did not assess long-term outcomes. We also did not have the power to separately assess the importance of the different etiologies on our results. However, the specific cardiac procedures give a framework to our results that still makes them unique, and the predictive value of RVEF could be established even in the short term. We could not construct multivariable models due to the relatively low event number. Inclusion criteria consist of the availability of 3DE acquisitions suitable for RVEF measurement that may represent a selection bias: patients with poor echo windows or higher body mass may be underrepresented.

The validity of the meta-analysis is subject to the quality of the reporting of the included studies, rendering our findings hypothesis-generating only. The studies included in this meta-analysis were non-uniform in design and varied in the inclusion criteria, patients' populations, echocardiographic equipment, technical aspects of 3D RV data acquisition, duration of follow-up, and definition of endpoints. Therefore, we opted to use a random-effects meta-analysis and performed a mixed-effects meta-regression to estimate the contribution of select factors (differences in patient populations, follow-up, and endpoint definitions) to the observed results. Also, not all ten studies included in the current meta-analysis provided quantification of 3DE-derived RVEF and all three other RV parameters of interest at the same time, which led to a smaller number of studies included in each comparison (8 for RVEF vs TAPSE, 7 for RVEF vs FAC, and 7 for RVEF vs FWLS).

Concerning our prospective study in MVR patients, the small sample size represents a limitation; however, the main aim was to correlate 3DE data to invasively measured RV contractility, and PAC is not part of routine perioperative care in the case of MVR surgery. Patients were selected for perioperative PAC based on the cardiac anesthesiologist's individual decision to adhere to the institutional protocol. We chose a PAC-based contractility index to indicate RVD; however, we could not pair these low-risk patients with decreased postoperative RVSWi to other hard endpoints, such as mortality. Further studies are warranted in higher-risk populations and with preoperatively decreased RV function. The repair rate in this specific cohort of patients was rather low, which might lead to a biased interpretation of our results. Thus, we have thoroughly compared the early and late clinical and echocardiographic outcomes of patients who underwent repair versus replacement, and no significant differences were found. Moreover, linear and logistic regression models were also adjusted for the type of surgery.

In our second retrospective outcome study, the mixed cohort of patients with some etiologies of left-sided cardiac diseases might not represent the actual patient population treated at a tertiary clinic. However, patients with HFrEF and valvular heart diseases were dominantly included, who are of crucial clinical importance. Due to the lack of cause-specific mortality data, we could not investigate the association between the 3DE-derived parameters and cardiac death. The event number has limited the number of covariates in the multivariable models. The validity of our results regarding the predictive value of RVGCS should be tested in prospective outcome studies in different clinical scenarios.

Concerning our last retrospective outcome study, the results need to be confirmed in longitudinal studies designed to assess the adaptations of the RV function to the changes of LV function over time and also in specific subgroups (*i.e.*, patients with coronary artery disease, cardiomyopathies, etc.) with a larger number of cases. Also, since the study protocol included the acquisition of 3DE data sets of the cardiac chambers, only patients with sinus rhythm,

relatively good image quality, and the ability to tolerate breath-holding for at least 4 to 6 cardiac cycles have been selected. This may have caused a selection bias. The extent to which the results can be extrapolated to other patient groups (*e.g.*, patients with atrial fibrillation) is unknown.

9. Conclusions

3DE imaging has revolutionized echocardiography, but its impact is rarely as apparent as its implementation for assessing the right heart. 3DE-derived RVEF identifies a broader spectrum of patients at risk than other RV systolic functional parameters. RVEF is a universal marker of RV function, which might further refine the risk stratification of patients with cardiopulmonary diseases and inform clinical decision-making, potentially facilitating timely interventions. However, similarly to what happened to LVEF, we must look beyond RVEF and recognize that several hemodynamic states pseudonormalize the value of RVEF, and therefore, a more comprehensive global and segmental characterization is needed to capture subclinical RV dysfunction in epidemiologically relevant diseases, like PH or HF. We created the ReVISION software to address this timely clinical issue.

ReVISION started as a custom method developed by clinicians to address some scientific questions. Over the years, several publications justified its added value in specific clinical scenarios; however, the lessons learned from these studies are also influential to everyday clinical practice: they contribute towards a better understanding of (patho)physiological concepts that may or may not be reflected using conventional parameters. For example, while the assessment of RV radial (transverse) free-wall shortening has been targeted previously, no focused, comprehensive solution was available for the evaluation. However, anteroposterior RV shortening as a reflection of ventricular interdependence is a rather new idea. We are enthusiastic about seeing the adoption of these concepts in everyday practice, scientific meetings, society scientific statements, and hopefully, in the future, in guideline recommendations.

Currently, ReVISION is a validated, FDA-cleared, commercially available software medical device for a comprehensive assessment of global and segmental RV function.

ReVISION is now known and used worldwide thanks to those investigators who recognized its potential and made huge efforts to validate it clinically. Hopefully, the above will open the doors to ultrasound machine and analysis platform vendors about integration and/or distribution to democratize access and share related knowledge about the amazing and momentous RV function.

10. Summary of novel scientific findings

1. We developed and validated the ReVISION software that quantifies the relative contribution of the global RV pump function's three anatomically relevant motion components by postprocessing 3DE-derived RV models. These newly defined metrics show a close correlation between 3DE and CMRI-derived models.

2. We further developed and validated ReVISION to enable the quantification of RV global longitudinal, circumferential, and area strains and, by the segmentation of the 3D model, to assess regional and segmental changes in RV shape and function.

3. By dual-center, large-scale normative studies, we showed that longitudinal, radial, and anteroposterior motion components are of similar importance in determining global RV pump function in both adults and children. Their relative importance is affected by age, sex, heart rate, body surface area, and RV volumes.

4. By investigating the athlete’s heart, we showed that a supernormal longitudinal shortening and a decreased radial/circumferential shortening are characteristic of an elite athlete’s RV. That functional pattern is associated with CPET-derived peak oxygen uptake.

5. We showed in pulmonary hypertension patients that at moderately impaired RV-PA coupling, the RV longitudinal shortening is decreased, while radial and anteroposterior shortenings are unchanged. The longitudinal shortening is unchanged at severe uncoupling, but anteroposterior shortening is decreased. This functional pattern is also associated with clinical risk categories.

6. After heart transplantation, we determined that the global RV function is maintained in the face of decreased conventional 2D echocardiographic measurements referring to longitudinal shortening, as radial shortening compensates and dominates. In time, longitudinal shortening can recover.

7. Using a retrospective clinical database with follow-up data and meta-analysis of available international studies, we showed that 3DE-derived RVEF is better associated with adverse cardiopulmonary outcomes than conventional 2D echocardiographic parameters. Thus, RVEF supports better clinical risk stratification and may be a trigger for therapeutic decisions in the future. Its clinical implementation is, therefore, justified.

8. In a prospective follow-up study of patients undergoing mitral valve replacement/repair due to severe primary mitral regurgitation, we showed that these patients' RV is characterized by a preoperative hyperdynamic longitudinal shortening, which pattern is associated with postoperative RV dysfunction. The dominant postoperative radial contribution normalizes to the control level 6 months after the procedure.

9. Using a large-scale retrospective clinical database with long-term follow-up data, we showed that ReVISION-derived RVGCS is the best predictor of all-cause mortality among all echocardiographic variables in patients with left-sided cardiac diseases. It has established added value even compared to RVEF.

10. In a large-scale study enrolling consecutive patients with different left-sided cardiac diseases, we characterized RV mechanical adaptation to the different degrees of LV systolic dysfunction. Radial shortening effectively compensates parallel decreases in longitudinal and anteroposterior shortenings with LVEF impairment up until severe LV dysfunction. Anteroposterior shortening has added prognostic value compared with conventional echocardiographic parameters, including RVEF.

11. References

1. Sayour, A.A., et al., *Association of Right Ventricular Functional Parameters With Adverse Cardiopulmonary Outcomes: A Meta-analysis.* J Am Soc Echocardiogr, 2023. **36**(6): p. 624-633 e8.
2. Ansari Ramandi, M.M., et al., *Right ventricular dysfunction in patients with new-onset heart failure: longitudinal follow-up during guideline-directed medical therapy.* Eur J Heart Fail, 2022. **24**(12): p. 2226-2234.
3. Konstam, M.A., et al., *Evaluation and Management of Right-Sided Heart Failure: A Scientific Statement From the American Heart Association.* Circulation, 2018. **137**(20): p. e578-e622.
4. Surkova, E., et al., *Contraction Patterns of the Right Ventricle Associated with Different Degrees of Left Ventricular Systolic Dysfunction.* Circ Cardiovasc Imaging, 2021. **14**(10): p. e012774.
5. Muraru, D., et al., *New speckle-tracking algorithm for right ventricular volume analysis from three-dimensional echocardiographic data sets: validation with cardiac magnetic resonance and comparison with the previous analysis tool.* Eur Heart J Cardiovasc Imaging, 2016. **17**(11): p. 1279-1289.
6. Hahn, R.T., et al., *Multimodality Imaging of Right Heart Function: JACC Scientific Statement.* J Am Coll Cardiol, 2023. **81**(19): p. 1954-1973.
7. Loukas, M., et al., *History of cardiac anatomy: a comprehensive review from the Egyptians to today.* Clin Anat, 2016. **29**(3): p. 270-84.
8. D., B., *De l'asystolie veineuse dans l'hypertrophie du cœur gauche par sténose concomitante du ventricule droit.* Rev Med, 1910(39): p. 785–801.
9. Henderson Y., P.A., *The relative systolic discharges of the right and left ventricles and their bearing on pulmmonary congestion and depletion.* . Heart, 1914(5): p. 217–226.
10. Starr, I., W.A. Jeffers, and R.H. Meade Jr., *The absence of conspicuous increments of venous pressure after severe damage to the right ventricle of the dog, with a discussion of the relation between clinical congestive failure and heart disease.* Am Heart J, 1943. **26**(3): p. 291-301.
11. Donald, D.E. and H.E. Essex, *Pressure studies after inactivation of the major portion of the canine right ventricle.* Am J Physiol, 1954. **176**(1): p. 155-61.
12. Rose, J.C., et al., *The effects of exclusion of the right ventricle from the circulation in dogs.* J Clin Invest, 1955. **34**(11): p. 1625-31.
13. Fontan, F. and E. Baudet, *Surgical repair of tricuspid atresia.* Thorax, 1971. **26**(3): p. 240-8.
14. Zehender, M., et al., *Right ventricular infarction as an independent predictor of prognosis after acute inferior myocardial infarction.* N Engl J Med, 1993. **328**(14): p. 981-8.
15. Mehta, S.R., et al., *Impact of right ventricular involvement on mortality and morbidity in patients with inferior myocardial infarction.* J Am Coll Cardiol, 2001. **37**(1): p. 37-43.
16. Assali, A.R., et al., *Prognostic importance of right ventricular infarction in an acute myocardial infarction cohort referred for contemporary percutaneous reperfusion therapy.* Am Heart J, 2007. **153**(2): p. 231-7.

17. Lewis, J.F., et al., *Discordance in degree of right and left ventricular dilation in patients with dilated cardiomyopathy: recognition and clinical implications.* J Am Coll Cardiol, 1993. **21**(3): p. 649-54.
18. Gorter, T.M., et al., *Right ventricular dysfunction in heart failure with preserved ejection fraction: a systematic review and meta-analysis.* Eur J Heart Fail, 2016. **18**(12): p. 1472-1487.
19. van de Veerdonk, M.C., et al., *Progressive right ventricular dysfunction in patients with pulmonary arterial hypertension responding to therapy.* J Am Coll Cardiol, 2011. **58**(24): p. 2511-9.
20. Lampert, B.C. and J.J. Teuteberg, *Right ventricular failure after left ventricular assist devices.* J Heart Lung Transplant, 2015. **34**(9): p. 1123-30.
21. Baumgartner, H., et al., *ESC Guidelines for the management of grown-up congenital heart disease (new version 2010).* Eur Heart J, 2010. **31**(23): p. 2915-57.
22. Ho, S.Y. and P. Nihoyannopoulos, *Anatomy, echocardiography, and normal right ventricular dimensions.* Heart, 2006. **92 Suppl 1**: p. i2-13.
23. Ghonim, S., et al., *Myocardial Architecture, Mechanics, and Fibrosis in Congenital Heart Disease.* Front Cardiovasc Med, 2017. **4**: p. 30.
24. Gorter, T.M., et al., *Right heart dysfunction and failure in heart failure with preserved ejection fraction: mechanisms and management. Position statement on behalf of the Heart Failure Association of the European Society of Cardiology.* Eur J Heart Fail, 2018. **20**(1): p. 16-37.
25. Addetia, K., et al., *Morphologic Analysis of the Normal Right Ventricle Using Three-Dimensional Echocardiography-Derived Curvature Indices.* J Am Soc Echocardiogr, 2018. **31**(5): p. 614-623.
26. Lakatos, B., et al., *Quantification of the relative contribution of the different right ventricular wall motion components to right ventricular ejection fraction: the ReVISION method.* Cardiovasc Ultrasound, 2017. **15**(1): p. 8.
27. Buckberg, G. and J.I. Hoffman, *Right ventricular architecture responsible for mechanical performance: unifying role of ventricular septum.* J Thorac Cardiovasc Surg, 2014. **148**(6): p. 3166-71 e1-4.
28. Dell'Italia, L.J., *The right ventricle: anatomy, physiology, and clinical importance.* Curr Probl Cardiol, 1991. **16**(10): p. 653-720.
29. Geva, T., et al., *Evaluation of regional differences in right ventricular systolic function by acoustic quantification echocardiography and cine magnetic resonance imaging.* Circulation, 1998. **98**(4): p. 339-45.
30. Kukulski, T., et al., *Normal regional right ventricular function and its change with age: a Doppler myocardial imaging study.* J Am Soc Echocardiogr, 2000. **13**(3): p. 194-204.
31. Rudski, L.G., et al., *Guidelines for the echocardiographic assessment of the right heart in adults: a report from the American Society of Echocardiography endorsed by the European Association of Echocardiography, a registered branch of the European Society of Cardiology, and the Canadian Society of Echocardiography.* J Am Soc Echocardiogr, 2010. **23**(7): p. 685-713; quiz 786-8.
32. Matyas, C., et al., *Comparison of speckle-tracking echocardiography with invasive hemodynamics for the detection of characteristic cardiac dysfunction in type-1 and type-2 diabetic rat models.* Cardiovascular Diabetology, 2018. **17**.
33. Kalam, K., P. Otahal, and T.H. Marwick, *Prognostic implications of global LV dysfunction: a systematic review and meta-analysis of global longitudinal strain and ejection fraction.* Heart, 2014. **100**(21): p. 1673-80.
34. Kovacs, A., et al., *Genetically determined pattern of left ventricular function in normal and hypertensive hearts.* J Clin Hypertens (Greenwich), 2018. **20**(5): p. 949-958.

35. Patrizio, L., et al., *The EACVI Textbook of Echocardiography*. 2017, New York: Oxford University Press.
36. Addetia, K., et al., *Three-dimensional echocardiography-based analysis of right ventricular shape in pulmonary arterial hypertension.* Eur Heart J Cardiovasc Imaging, 2016. **17**(5): p. 564-75.
37. Shang, Q., et al., *Myocardial deformation assessed by longitudinal strain: Chamber specific normative data for CMR-feature tracking from the German competence network for congenital heart defects.* Eur Radiol, 2018. **28**(3): p. 1257-1266.
38. Gertz, R.J., et al., *Inter-vendor reproducibility of left and right ventricular cardiovascular magnetic resonance myocardial feature-tracking.* PLoS One, 2018. **13**(3): p. e0193746.
39. Arvidsson, P.M., et al., *Left and right ventricular hemodynamic forces in healthy volunteers and elite athletes assessed with 4D flow magnetic resonance imaging.* Am J Physiol Heart Circ Physiol, 2017. **312**(2): p. H314-H328.
40. Vonk Noordegraaf, A., B.E. Westerhof, and N. Westerhof, *The Relationship Between the Right Ventricle and its Load in Pulmonary Hypertension.* Journal of the American College of Cardiology, 2017. **69**(2): p. 236-243.
41. SUGA, H., K. SAGAWA, and A.A. SHOUKAS, *Load Independence of the Instantaneous Pressure-Volume Ratio of the Canine Left Ventricle and Effects of Epinephrine and Heart Rate on the Ratio.* Circulation Research, 1973. **32**(3): p. 314-322.
42. Sunagawa, K., W.L. Maughan, and K. Sagawa, *Optimal arterial resistance for the maximal stroke work studied in isolated canine left ventricle.* Circulation Research, 1985. **56**(4): p. 586-595.
43. Tezuka, F., et al., *Muscle fiber orientation in the development and regression of right ventricular hypertrophy in pigs.* Acta Pathol Jpn, 1990. **40**(6): p. 402-7.
44. Swift, A.J., et al., *Longitudinal and transverse right ventricular function in pulmonary hypertension: cardiovascular magnetic resonance imaging study from the ASPIRE registry.* Pulm Circ, 2015. **5**(3): p. 557-64.
45. Brown, S.B., et al., *Longitudinal Shortening Accounts for the Majority of Right Ventricular Contraction and Improves After Pulmonary Vasodilator Therapy in Normal Subjects and Patients With Pulmonary Arterial Hypertension.* CHEST, 2011. **140**(1): p. 27-33.
46. Kind, T., et al., *Right ventricular ejection fraction is better reflected by transverse rather than longitudinal wall motion in pulmonary hypertension.* J Cardiovasc Magn Reson, 2010. **12**: p. 35.
47. Smith, B.C.F., et al., *Three-Dimensional Speckle Tracking of the Right Ventricle: Toward Optimal Quantification of Right Ventricular Dysfunction in Pulmonary Hypertension.* Journal of the American College of Cardiology, 2014. **64**(1): p. 41-51.
48. Moceri, P., et al., *Three-dimensional right-ventricular regional deformation and survival in pulmonary hypertension.* Eur Heart J Cardiovasc Imaging, 2018. **19**(4): p. 450-458.
49. Jaijee, S.K., et al., *Exercise cardiac MRI unmasks right ventricular dysfunction in acute hypoxia and chronic pulmonary arterial hypertension.* Am J Physiol Heart Circ Physiol, 2018.
50. Aguero, J., et al., *Characterization of right ventricular remodeling and failure in a chronic pulmonary hypertension model.* Am J Physiol Heart Circ Physiol, 2014. **307**(8): p. H1204-15.
51. Cheng, T.C., et al., *Multi-scale Structure-Function Relationships in Right Ventricular Failure Due to Pressure Overload.* Am J Physiol Heart Circ Physiol, 2018.

52. Sano, M., et al., *p53-induced inhibition of Hif-1 causes cardiac dysfunction during pressure overload.* Nature, 2007. **446**(7134): p. 444-8.
53. Sarnoff, S.J., et al., *Hemodynamic determinants of oxygen consumption of the heart with special reference to the tension-time index.* Am J Physiol, 1958. **192**(1): p. 148-56.
54. Wong, Y.Y., et al., *Right ventricular failure in idiopathic pulmonary arterial hypertension is associated with inefficient myocardial oxygen utilization.* Circ Heart Fail, 2011. **4**(6): p. 700-6.
55. van Wolferen, S.A., et al., *Right coronary artery flow impairment in patients with pulmonary hypertension.* Eur Heart J, 2008. **29**(1): p. 120-7.
56. Vogel-Claussen, J., et al., *Right and left ventricular myocardial perfusion reserves correlate with right ventricular function and pulmonary hemodynamics in patients with pulmonary arterial hypertension.* Radiology, 2011. **258**(1): p. 119-27.
57. Rain, S., et al., *Right ventricular diastolic impairment in patients with pulmonary arterial hypertension.* Circulation, 2013. **128**(18): p. 2016-25, 1-10.
58. Alaa, M., et al., *Right ventricular end-diastolic stiffness heralds right ventricular failure in monocrotaline-induced pulmonary hypertension.* Am J Physiol Heart Circ Physiol, 2016. **311**(4): p. H1004-h1013.
59. Trip, P., et al., *Clinical relevance of right ventricular diastolic stiffness in pulmonary hypertension.* Eur Respir J, 2015. **45**(6): p. 1603-12.
60. Gan, C., et al., *Impaired left ventricular filling due to right-to-left ventricular interaction in patients with pulmonary arterial hypertension.* Am J Physiol Heart Circ Physiol, 2006. **290**(4): p. H1528-33.
61. Marcus, J.T., et al., *Interventricular mechanical asynchrony in pulmonary arterial hypertension: left-to-right delay in peak shortening is related to right ventricular overload and left ventricular underfilling.* J Am Coll Cardiol, 2008. **51**(7): p. 750-7.
62. Palau-Caballero, G., et al., *Why septal motion is a marker of right ventricular failure in pulmonary arterial hypertension: mechanistic analysis using a computer model.* Am J Physiol Heart Circ Physiol, 2017. **312**(4): p. H691-h700.
63. Zimbarra Cabrita, I., et al., *Validation of the isovolumetric relaxation time for the estimation of pulmonary systolic arterial blood pressure in chronic pulmonary hypertension.* European Heart Journal - Cardiovascular Imaging, 2013. **14**(1): p. 51-55.
64. Ernande, L., et al., *Right Isovolumic Contraction Velocity Predicts Survival in Pulmonary Hypertension.* Journal of the American Society of Echocardiography, 2013. **26**(3): p. 297-306.
65. Apitz, C., et al., *Biventricular structural and functional responses to aortic constriction in a rabbit model of chronic right ventricular pressure overload.* J Thorac Cardiovasc Surg, 2012. **144**(6): p. 1494-501.
66. Schranz, D., et al., *Pulmonary artery banding in infants and young children with left ventricular dilated cardiomyopathy: a novel therapeutic strategy before heart transplantation.* J Heart Lung Transplant, 2013. **32**(5): p. 475-81.
67. Gorter, T.M., et al., *Right ventricular recovery after bilateral lung transplantation for pulmonary arterial hypertension†.* Interactive CardioVascular and Thoracic Surgery, 2017. **24**(6): p. 890-897.
68. Kasimir, M.T., et al., *Reverse cardiac remodelling in patients with primary pulmonary hypertension after isolated lung transplantation.* Eur J Cardiothorac Surg, 2004. **26**(4): p. 776-81.
69. Kramer, M.R., et al., *Recovery of the right ventricle after single-lung transplantation in pulmonary hypertension.* Am J Cardiol, 1994. **73**(7): p. 494-500.

70. Moulton, M.J., et al., *Magnetic resonance imaging provides evidence for remodeling of the right ventricle after single-lung transplantation for pulmonary hypertension.* Circulation, 1996. **94**(9 Suppl): p. II312-9.
71. Ritchie, M., et al., *Echocardiographic characterization of the improvement in right ventricular function in patients with severe pulmonary hypertension after single-lung transplantation.* Journal of the American College of Cardiology, 1993. **22**(4): p. 1170-1174.
72. Schulman, L.L., et al., *Variability of right ventricular functional recovery after lung transplantation.* Transplantation, 1996. **62**(5): p. 622-5.
73. Katz, W.E., et al., *Immediate effects of lung transplantation on right ventricular morphology and function in patients with variable degrees of pulmonary hypertension.* J Am Coll Cardiol, 1996. **27**(2): p. 384-91.
74. Humbert, M., et al., *Survival in patients with idiopathic, familial, and anorexigen-associated pulmonary arterial hypertension in the modern management era.* Circulation, 2010. **122**(2): p. 156-63.
75. Kuehne, T., et al., *Effects of pulmonary insufficiency on biventricular function in the developing heart of growing swine.* Circulation, 2003. **108**(16): p. 2007-13.
76. Shah, A.S., et al., *Early effects of right ventricular volume overload on ventricular performance and beta-adrenergic signaling.* J Thorac Cardiovasc Surg, 2000. **120**(2): p. 342-9.
77. Rodes-Cabau, J., M. Taramasso, and P.T. O'Gara, *Diagnosis and treatment of tricuspid valve disease: current and future perspectives.* Lancet, 2016. **388**(10058): p. 2431-2442.
78. Wald, R.M., A.M. Valente, and A. Marelli, *Heart failure in adult congenital heart disease: Emerging concepts with a focus on tetralogy of Fallot.* Trends Cardiovasc Med, 2015. **25**(5): p. 422-32.
79. Sanchez-Quintana, D., V. Garcia-Martinez, and J.M. Hurle, *Myocardial fiber architecture in the human heart. Anatomical demonstration of modifications in the normal pattern of ventricular fiber architecture in a malformed adult specimen.* Acta Anat (Basel), 1990. **138**(4): p. 352-8.
80. Sanchez-Quintana, D., et al., *Myoarchitecture and connective tissue in hearts with tricuspid atresia.* Heart, 1999. **81**(2): p. 182-91.
81. Sanchez-Quintana, D., R.H. Anderson, and S.Y. Ho, *Ventricular myoarchitecture in tetralogy of Fallot.* Heart, 1996. **76**(3): p. 280-6.
82. Agger, P., et al., *Changes in overall ventricular myocardial architecture in the setting of a porcine animal model of right ventricular dilation.* J Cardiovasc Magn Reson, 2017. **19**(1): p. 93.
83. Salih, C., K.P. McCarthy, and S.Y. Ho, *The fibrous matrix of ventricular myocardium in hypoplastic left heart syndrome: a quantitative and qualitative analysis.* Ann Thorac Surg, 2004. **77**(1): p. 36-40.
84. Broberg, C.S., et al., *Quantification of diffuse myocardial fibrosis and its association with myocardial dysfunction in congenital heart disease.* Circ Cardiovasc Imaging, 2010. **3**(6): p. 727-34.
85. Linardi, D., et al., *Ventricular and pulmonary vascular remodeling induced by pulmonary overflow in a chronic model of pretricuspid shunt.* J Thorac Cardiovasc Surg, 2014. **148**(6): p. 2609-17.
86. Borgdorff, M.A., et al., *Distinct loading conditions reveal various patterns of right ventricular adaptation.* Am J Physiol Heart Circ Physiol, 2013. **305**(3): p. H354-64.
87. Dragulescu, A., et al., *Differential effect of right ventricular dilatation on myocardial deformation in patients with atrial septal defects and patients after tetralogy of Fallot repair.* Int J Cardiol, 2013. **168**(2): p. 803-10.

88. Van De Bruaene, A., et al., *Regional right ventricular deformation in patients with open and closed atrial septal defect.* Eur J Echocardiogr, 2011. **12**(3): p. 206-13.
89. Eroglu, E., et al., *Time course of right ventricular remodeling after percutaneous atrial septal defect closure: assessment of regional deformation properties with two-dimensional strain and strain rate imaging.* Echocardiography, 2013. **30**(3): p. 324-30.
90. Akula, V.S., et al., *Right Ventricle before and after Atrial Septal Defect Device Closure.* Echocardiography, 2016. **33**(9): p. 1381-8.
91. Brida, M. and M.A. Gatzoulis, *Pulmonary arterial hypertension in adult congenital heart disease.* Heart, 2018.
92. Giusca, S., et al., *Is Right Ventricular Remodeling in Pulmonary Hypertension Dependent on Etiology? An Echocardiographic Study.* Echocardiography, 2016. **33**(4): p. 546-54.
93. Kopec, G., et al., *Left ventricular mass is preserved in patients with idiopathic pulmonary arterial hypertension and Eisenmenger's syndrome.* Heart Lung Circ, 2014. **23**(5): p. 454-61.
94. Moceri, P., et al., *Cardiac remodelling amongst adults with various aetiologies of pulmonary arterial hypertension including Eisenmenger syndrome-implications on survival and the role of right ventricular transverse strain.* Eur Heart J Cardiovasc Imaging, 2017. **18**(11): p. 1262-1270.
95. Kwok, S.Y., et al., *Ventricular mechanics after repair of subarterial and perimembranous VSDs.* Eur J Clin Invest, 2017. **47**(12).
96. Klitsie, L.M., et al., *Disparity in right vs left ventricular recovery during follow-up after ventricular septal defect correction in children.* Eur J Cardiothorac Surg, 2013. **44**(2): p. 269-74.
97. Buckberg, G.D. and R. Group, *The ventricular septum: the lion of right ventricular function, and its impact on right ventricular restoration.* Eur J Cardiothorac Surg, 2006. **29 Suppl 1**: p. S272-8.
98. Geva, T., *Repaired tetralogy of Fallot: the roles of cardiovascular magnetic resonance in evaluating pathophysiology and for pulmonary valve replacement decision support.* J Cardiovasc Magn Reson, 2011. **13**: p. 9.
99. Toro, K.D., B.D. Soriano, and S. Buddhe, *Right ventricular global longitudinal strain in repaired tetralogy of Fallot.* Echocardiography, 2016. **33**(10): p. 1557-1562.
100. Stephensen, S., et al., *The relationship between longitudinal, lateral, and septal contribution to stroke volume in patients with pulmonary regurgitation and healthy volunteers.* Am J Physiol Heart Circ Physiol, 2014. **306**(6): p. H895-903.
101. Kopic, S., et al., *Isolated pulmonary regurgitation causes decreased right ventricular longitudinal function and compensatory increased septal pumping in a porcine model.* Acta Physiol (Oxf), 2017. **221**(3): p. 163-173.
102. Kjaergaard, J., et al., *Impacts of acute severe pulmonary regurgitation on right ventricular geometry and contractility assessed by tissue-Doppler echocardiography.* Eur J Echocardiogr, 2010. **11**(1): p. 19-26.
103. Chowdhury, S.M., et al., *Speckle-Tracking Echocardiographic Measures of Right Ventricular Function Correlate With Improvement in Exercise Function After Percutaneous Pulmonary Valve Implantation.* J Am Soc Echocardiogr, 2015. **28**(9): p. 1036-44.
104. Latus, H., et al., *Impact of residual right ventricular outflow tract obstruction on biventricular strain and synchrony in patients after repair of tetralogy of Fallot: a cardiac magnetic resonance feature tracking study.* Eur J Cardiothorac Surg, 2015. **48**(1): p. 83-90.

105. Bove, T., et al., *Role of myocardial hypertrophy on acute and chronic right ventricular performance in relation to chronic volume overload in a porcine model: relevance for the surgical management of tetralogy of Fallot.* J Thorac Cardiovasc Surg, 2014. **147**(6): p. 1956-65.
106. Brida, M., G.P. Diller, and M.A. Gatzoulis, *Systemic Right Ventricle in Adults With Congenital Heart Disease: Anatomic and Phenotypic Spectrum and Current Approach to Management.* Circulation, 2018. **137**(5): p. 508-518.
107. Suntratonpipat, S., et al., *Impaired Single Right Ventricular Function Compared to Single Left Ventricles during the Early Stages of Palliation: A Longitudinal Study.* J Am Soc Echocardiogr, 2017. **30**(5): p. 468-477.
108. Eindhoven, J.A., et al., *Quantitative assessment of systolic right ventricular function using myocardial deformation in patients with a systemic right ventricle.* Eur Heart J Cardiovasc Imaging, 2015. **16**(4): p. 380-8.
109. Lin, L.Q., et al., *Reduced Right Ventricular Fractional Area Change, Strain, and Strain Rate before Bidirectional Cavopulmonary Anastomosis is Associated with Medium-Term Mortality for Children with Hypoplastic Left Heart Syndrome.* J Am Soc Echocardiogr, 2018.
110. Diller, G.P., et al., *Systemic right ventricular longitudinal strain is reduced in adults with transposition of the great arteries, relates to subpulmonary ventricular function, and predicts adverse clinical outcome.* Am Heart J, 2012. **163**(5): p. 859-66.
111. Avitabile, C.M., et al., *Tricuspid annular plane systolic excursion does not correlate with right ventricular ejection fraction in patients with hypoplastic left heart syndrome after Fontan palliation.* Pediatr Cardiol, 2014. **35**(7): p. 1253-8.
112. Pettersen, E., et al., *Contraction pattern of the systemic right ventricle shift from longitudinal to circumferential shortening and absent global ventricular torsion.* J Am Coll Cardiol, 2007. **49**(25): p. 2450-6.
113. Di Salvo, G., et al., *Transverse strain predicts exercise capacity in systemic right ventricle patients.* Int J Cardiol, 2010. **145**(2): p. 193-196.
114. Calkins, H., D. Corrado, and F. Marcus, *Risk Stratification in Arrhythmogenic Right Ventricular Cardiomyopathy.* Circulation, 2017. **136**(21): p. 2068-2082.
115. Kirchhof, P., et al., *Age- and training-dependent development of arrhythmogenic right ventricular cardiomyopathy in heterozygous plakoglobin-deficient mice.* Circulation, 2006. **114**(17): p. 1799-806.
116. Fabritz, L., et al., *Load-reducing therapy prevents development of arrhythmogenic right ventricular cardiomyopathy in plakoglobin-deficient mice.* J Am Coll Cardiol, 2011. **57**(6): p. 740-50.
117. James, C.A., et al., *Exercise increases age-related penetrance and arrhythmic risk in arrhythmogenic right ventricular dysplasia/cardiomyopathy-associated desmosomal mutation carriers.* J Am Coll Cardiol, 2013. **62**(14): p. 1290-1297.
118. Saberniak, J., et al., *Vigorous physical activity impairs myocardial function in patients with arrhythmogenic right ventricular cardiomyopathy and in mutation positive family members.* Eur J Heart Fail, 2014. **16**(12): p. 1337-44.
119. Haugaa, K.H., et al., *Comprehensive multi-modality imaging approach in arrhythmogenic cardiomyopathy-an expert consensus document of the European Association of Cardiovascular Imaging.* Eur Heart J Cardiovasc Imaging, 2017. **18**(3): p. 237-253.
120. Bourfiss, M., et al., *Feature tracking CMR reveals abnormal strain in preclinical arrhythmogenic right ventricular dysplasia/ cardiomyopathy: a multisoftware feasibility and clinical implementation study.* J Cardiovasc Magn Reson, 2017. **19**(1): p. 66.

121. Prati, G., et al., *Right Ventricular Strain and Dyssynchrony Assessment in Arrhythmogenic Right Ventricular Cardiomyopathy: Cardiac Magnetic Resonance Feature-Tracking Study.* Circ Cardiovasc Imaging, 2015. **8**(11): p. e003647; discussion e003647.
122. Saberniak, J., et al., *Comparison of patients with early-phase arrhythmogenic right ventricular cardiomyopathy and right ventricular outflow tract ventricular tachycardia.* Eur Heart J Cardiovasc Imaging, 2017. **18**(1): p. 62-69.
123. Teske, A.J., et al., *Early detection of regional functional abnormalities in asymptomatic ARVD/C gene carriers.* J Am Soc Echocardiogr, 2012. **25**(9): p. 997-1006.
124. Heermann, P., et al., *Biventricular myocardial strain analysis in patients with arrhythmogenic right ventricular cardiomyopathy (ARVC) using cardiovascular magnetic resonance feature tracking.* J Cardiovasc Magn Reson, 2014. **16**: p. 75.
125. Shehata, M.L., et al., *Regional and global biventricular function in pulmonary arterial hypertension: a cardiac MR imaging study.* Radiology, 2013. **266**(1): p. 114-22.
126. Marra, M.P., et al., *Imaging study of ventricular scar in arrhythmogenic right ventricular cardiomyopathy: comparison of 3D standard electroanatomical voltage mapping and contrast-enhanced cardiac magnetic resonance.* Circ Arrhythm Electrophysiol, 2012. **5**(1): p. 91-100.
127. Molnar, A.A., et al., *Sinus of Valsalva aneurysm protruding intramurally into right ventricle: does size really matter?* Eur Heart J Cardiovasc Imaging, 2018. **19**(2): p. 234.
128. Nagy, V.K., et al., *Role of Right Ventricular Global Longitudinal Strain in Predicting Early and Long-Term Mortality in Cardiac Resynchronization Therapy Patients.* PLoS One, 2015. **10**(12): p. e0143907.
129. Aschauer, S., et al., *Modes of death in patients with heart failure and preserved ejection fraction.* Int J Cardiol, 2017. **228**: p. 422-426.
130. Tanaka, H., et al., *Comparative mechanical activation mapping of RV pacing to LBBB by 2D and 3D speckle tracking and association with response to resynchronization therapy.* JACC Cardiovasc Imaging, 2010. **3**(5): p. 461-71.
131. Kosztin, A., et al., *De novo implantation vs. upgrade cardiac resynchronization therapy: a systematic review and meta-analysis.* Heart Fail Rev, 2018. **23**(1): p. 15-26.
132. Merkely, B., et al., *Rationale and design of the BUDAPEST-CRT Upgrade Study: a prospective, randomized, multicentre clinical trial.* Europace, 2017. **19**(9): p. 1549-1555.
133. Stankovic, I., et al., *Long-Term Outcome After CRT in the Presence of Mechanical Dyssynchrony Seen With Chronic RV Pacing or Intrinsic LBBB.* JACC Cardiovasc Imaging, 2017. **10**(10 Pt A): p. 1091-1099.
134. Polos, M., et al., *Acute thrombosis of the ascending aorta causing right ventricular failure: first manifestation of antiphospholipid syndrome.* Eur J Cardiothorac Surg, 2018.
135. Carluccio, E., et al., *Prognostic Value of Right Ventricular Dysfunction in Heart Failure With Reduced Ejection Fraction: Superiority of Longitudinal Strain Over Tricuspid Annular Plane Systolic Excursion.* Circ Cardiovasc Imaging, 2018. **11**(1): p. e006894.
136. Nagata, Y., et al., *Prognostic Value of Right Ventricular Ejection Fraction Assessed by Transthoracic 3D Echocardiography.* Circ Cardiovasc Imaging, 2017. **10**(2).
137. Hedman, A., et al., *Decreased right ventricular function after coronary artery bypass grafting and its relation to exercise capacity: a tricuspid annular motion-based study.* J Am Soc Echocardiogr, 2004. **17**(2): p. 126-31.
138. Hyllen, S., et al., *Right ventricular performance after valve repair for chronic degenerative mitral regurgitation.* Ann Thorac Surg, 2014. **98**(6): p. 2023-30.

139. Lakatos, B.K., et al., *Dominance of free wall radial motion in global right ventricular function of heart transplant recipients.* Clin Transplant, 2018. **32**(3): p. e13192.
140. Maffessanti, F., et al., *Evaluation of right ventricular systolic function after mitral valve repair: a two-dimensional Doppler, speckle-tracking, and three-dimensional echocardiographic study.* J Am Soc Echocardiogr, 2012. **25**(7): p. 701-8.
141. Raina, A., et al., *Marked changes in right ventricular contractile pattern after cardiothoracic surgery: implications for post-surgical assessment of right ventricular function.* J Heart Lung Transplant, 2013. **32**(8): p. 777-83.
142. Yadav, H., et al., *Selective right ventricular impairment following coronary artery bypass graft surgery.* European Journal of Cardio-Thoracic Surgery, 2010. **37**(2): p. 393-398.
143. Keyl, C., et al., *Right ventricular function after aortic valve replacement: a pilot study comparing surgical and transcatheter procedures using 3D echocardiography.* Eur J Cardiothorac Surg, 2016. **49**(3): p. 966-71.
144. Tamborini, G., et al., *Is right ventricular systolic function reduced after cardiac surgery? A two- and three-dimensional echocardiographic study.* Eur J Echocardiogr, 2009. **10**(5): p. 630-4.
145. Unsworth, B., et al., *Contrasting effect of different cardiothoracic operations on echocardiographic right ventricular long axis velocities, and implications for interpretation of post-operative values.* International Journal of Cardiology, 2013. **165**(1): p. 151-160.
146. Schuuring, M.J., et al., *Right ventricular function declines after cardiac surgery in adult patients with congenital heart disease.* The International Journal of Cardiovascular Imaging, 2012. **28**(4): p. 755-762.
147. Paparella, D., T.M. Yau, and E. Young, *Cardiopulmonary bypass induced inflammation: pathophysiology and treatment. An update.* Eur J Cardiothorac Surg, 2002. **21**(2): p. 232-44.
148. Day, J.R.S. and K.M. Taylor, *The systemic inflammatory response syndrome and cardiopulmonary bypass.* International Journal of Surgery, 2005. **3**(2): p. 129-140.
149. Bond, B.R., et al., *Endothelin-1 during and after cardiopulmonary bypass: association to graft sensitivity and postoperative recovery.* J Thorac Cardiovasc Surg, 2001. **122**(2): p. 358-64.
150. Ford, R.L., et al., *Endothelin-A receptor inhibition after cardiopulmonary bypass: cytokines and receptor activation.* Ann Thorac Surg, 2008. **86**(5): p. 1576-83.
151. Diller, G.-P., et al., *Effect of coronary artery bypass surgery on myocardial function as assessed by tissue Doppler echocardiography.* European Journal of Cardio-Thoracic Surgery, 2008. **34**(5): p. 995-999.
152. Pegg, T.J., et al., *Effects of Off-Pump Versus On-Pump Coronary Artery Bypass Grafting on Early and Late Right Ventricular Function.* Circulation, 2008. **117**(17): p. 2202-2210.
153. Velissaris, T., et al., *A prospective randomized study to evaluate stress response during beating-heart and conventional coronary revascularization.* Ann Thorac Surg, 2004. **78**(2): p. 506-12; discussion 506-12.
154. Fritz, T., et al., *Simulation of the contraction of the ventricles in a human heart model including atria and pericardium.* Biomech Model Mechanobiol, 2014. **13**(3): p. 627-41.
155. Schosser, R., et al., *Open chest and open pericardium affect the distribution of myocardial blood flow in the right ventricle.* Basic Res Cardiol, 1990. **85**(5): p. 508-18.
156. Assanelli, D., et al., *Influence of the pericardium on right and left ventricular filling in the dog.* J Appl Physiol (1985), 1987. **63**(3): p. 1025-32.

157. Unsworth, B., et al., *The right ventricular annular velocity reduction caused by coronary artery bypass graft surgery occurs at the moment of pericardial incision.* Am Heart J, 2010. **159**(2): p. 314-22.
158. Forsberg, L.M., et al., *Left and right ventricular function in aortic stenosis patients 8 weeks post-transcatheter aortic valve implantation or surgical aortic valve replacement.* Eur J Echocardiogr, 2011. **12**(8): p. 603-11.
159. Kempny, A., et al., *Impact of transcatheter aortic valve implantation or surgical aortic valve replacement on right ventricular function.* Heart, 2012. **98**(17): p. 1299-304.
160. Okada, D.R., et al., *Assessment of right ventricular function by transthoracic echocardiography following aortic valve replacement.* Echocardiography, 2014. **31**(5): p. 552-7.
161. Dalén, M., et al., *Comparison of right ventricular function after ministernotomy and full sternotomy aortic valve replacement: a randomized study.* Interactive CardioVascular and Thoracic Surgery, 2018. **26**(5): p. 790-797.
162. Zanobini, M., et al., *Postoperative Echocardiographic Reduction of Right Ventricular Function: Is Pericardial Opening Modality the Main Culprit?* BioMed Research International, 2017. **2017**: p. 4808757.
163. Lindqvist, P., et al., *Effect of pericardial repair after aortic valve replacement on septal and right ventricular function.* Int J Cardiol, 2012. **155**(3): p. 388-93.
164. Boldt, J., et al., *Myocardial temperature during cardiac operations: influence on right ventricular function.* J Thorac Cardiovasc Surg, 1990. **100**(4): p. 562-8.
165. Christakis, G.T., et al., *Randomized study of right ventricular function with intermittent warm or cold cardioplegia.* Ann Thorac Surg, 1996. **61**(1): p. 128-34.
166. Jasinski, M., et al., *Comparison of retrograde versus antegrade cold blood cardioplegia: randomized trial in elective coronary artery bypass patients.* Eur J Cardiothorac Surg, 1997. **12**(4): p. 620-6.
167. Appleyard, R.F. and L.H. Cohn, *Myocardial stunning and reperfusion injury in cardiac surgery.* J Card Surg, 1993. **8**(2 Suppl): p. 316-24.
168. Joshi, S.B., et al., *Mechanism of paradoxical ventricular septal motion after coronary artery bypass grafting.* Am J Cardiol, 2009. **103**(2): p. 212-5.
169. Roshanali, F., et al., *Decreased right ventricular function after coronary artery bypass grafting.* Tex Heart Inst J, 2008. **35**(3): p. 250-5.
170. Zhao, Y., et al., *Trans-catheter aortic valve implantation--early recovery of left and preservation of right ventricular function.* Interact Cardiovasc Thorac Surg, 2011. **12**(1): p. 35-9.
171. Stobierska-Dzierzek, B., H. Awad, and R.E. Michler, *The evolving management of acute right-sided heart failure in cardiac transplant recipients.* J Am Coll Cardiol, 2001. **38**(4): p. 923-31.
172. Yusen, R.D., et al., *The Registry of the International Society for Heart and Lung Transplantation: Thirty-third Adult Lung and Heart-Lung Transplant Report-2016; Focus Theme: Primary Diagnostic Indications for Transplant.* J Heart Lung Transplant, 2016. **35**(10): p. 1170-1184.
173. Bacal, F., et al., *Normalization of right ventricular performance and remodeling evaluated by magnetic resonance imaging at late follow-up of heart transplantation: relationship between function, exercise capacity and pulmonary vascular resistance.* J Heart Lung Transplant, 2005. **24**(12): p. 2031-6.
174. D'Andrea, A., et al., *Right heart morphology and function in heart transplantation recipients.* J Cardiovasc Med (Hagerstown), 2013. **14**(9): p. 648-58.
175. Hyden, M., et al., *A Comparison of Two-Dimensional Echocardiography Parameters with Cardiac Magnetic Resonance Imaging in the Assessment of Right Ventricular*

Function Post Orthotopic Heart Transplantation. The Journal of Heart and Lung Transplantation, 2017. **36**(4): p. S156-S157.
176. Kovacs, A., et al., *Response to Ivey-Miranda and Farrero-Torres "Is there dominance of free wall radial motion in global right ventricular function in heart transplant recipients or in all heart surgery patients?".* Clin Transplant, 2018: p. e13286.
177. Bittner, H.B., et al., *Myocardial beta-adrenergic receptor function and high-energy phosphates in brain death--related cardiac dysfunction.* Circulation, 1995. **92**(9 Suppl): p. Ii472-8.
178. Stoica, S.C., et al., *Brain death leads to abnormal contractile properties of the human donor right ventricle.* The Journal of Thoracic and Cardiovascular Surgery, 2006. **132**(1): p. 116-123.
179. Ferrera, R., et al., *Brain death provokes very acute alteration in myocardial morphology detected by echocardiography: preventive effect of beta-blockers.* Transpl Int, 2011. **24**(3): p. 300-6.
180. Ojeda-Rivero, R., et al., *Experimental treatment with beta blockers of hemodynamic and myocardial changes in organ donors.* Transplant Proc, 2002. **34**(1): p. 185-6.
181. Pandalai, P.K., et al., *Acute beta-blockade prevents myocardial beta-adrenergic receptor desensitization and preserves early ventricular function after brain death.* J Thorac Cardiovasc Surg, 2008. **135**(4): p. 792-8.
182. Nyhan, D.P., et al., *Prolonged pulmonary vascular hyperreactivity in conscious dogs after cardiopulmonary bypass.* J Appl Physiol (1985), 1994. **77**(4): p. 1584-90.
183. Bhatia, S.J., et al., *Time course of resolution of pulmonary hypertension and right ventricular remodeling after orthotopic cardiac transplantation.* Circulation, 1987. **76**(4): p. 819-26.
184. Bourge, R.C., et al., *Analysis and predictors of pulmonary vascular resistance after cardiac transplantation.* J Thorac Cardiovasc Surg, 1991. **101**(3): p. 432-44; discussion 444-5.
185. Tedford, R.J., et al., *Prognostic value of the pre-transplant diastolic pulmonary artery pressure-to-pulmonary capillary wedge pressure gradient in cardiac transplant recipients with pulmonary hypertension.* J Heart Lung Transplant, 2014. **33**(3): p. 289-97.
186. Wink, J., et al., *Thoracic Epidural Anesthesia Reduces Right Ventricular Systolic Function With Maintained Ventricular-Pulmonary Coupling.* Circulation, 2016. **134**(16): p. 1163-1175.
187. Bernardi, L., et al., *Demonstrable Cardiac Reinnervation After Human Heart Transplantation by Carotid Baroreflex Modulation of RR Interval.* Circulation, 1995. **92**(10): p. 2895-2903.
188. Buendia-Fuentes, F., et al., *Sympathetic reinnervation 1 year after heart transplantation, assessed using iodine-123 metaiodobenzylguanidine imaging.* Transplant Proc, 2011. **43**(6): p. 2247-8.
189. Lovric, S.S., et al., *Sympathetic reinnervation after heart transplantation, assessed by iodine-123 metaiodobenzylguanidine imaging, and heart rate variability.* Eur J Cardiothorac Surg, 2004. **26**(4): p. 736-41.
190. Beniaminovitz, A., et al., *Improved atrial function in bicaval versus standard orthotopic techniques in cardiac transplantation.* Am J Cardiol, 1997. **80**(12): p. 1631-5.
191. Peura, J.L., et al., *Effects of conversion from cyclosporine to tacrolimus on left ventricular structure in cardiac allograft recipients.* J Heart Lung Transplant, 2005. **24**(11): p. 1969-72.

192. Hu, R., C.D. Mazer, and C. Tousignant, *Relationship between tricuspid annular excursion and velocity in cardiac surgical patients.* J Cardiothorac Vasc Anesth, 2014. **28**(5): p. 1198-202.
193. Tousignant, C., et al., *Evaluation of TAPSE as a measure of right ventricular output.* Can J Anaesth, 2012. **59**(4): p. 376-83.
194. Badano, L.P., et al., *European Association of Cardiovascular Imaging/Cardiovascular Imaging Department of the Brazilian Society of Cardiology recommendations for the use of cardiac imaging to assess and follow patients after heart transplantation.* Eur Heart J Cardiovasc Imaging, 2015. **16**(9): p. 919-48.
195. D'Andrea, A., et al., *Range of right heart measurements in top-level athletes: the training impact.* Int J Cardiol, 2013. **164**(1): p. 48-57.
196. Naeije, R., et al., *Exercise-induced pulmonary hypertension: physiological basis and methodological concerns.* Am J Respir Crit Care Med, 2013. **187**(6): p. 576-83.
197. La Gerche, A., D.J. Rakhit, and G. Claessen, *Exercise and the right ventricle: a potential Achilles' heel.* Cardiovasc Res, 2017. **113**(12): p. 1499-1508.
198. La Gerche, A., et al., *Cardiac MRI: a new gold standard for ventricular volume quantification during high-intensity exercise.* Circ Cardiovasc Imaging, 2013. **6**(2): p. 329-38.
199. Gjerdalen, G.F., et al., *The Scandinavian athlete's heart; echocardiographic characteristics of male professional football players.* Scand J Med Sci Sports, 2014. **24**(5): p. e372-80.
200. La Gerche, A., et al., *Cardiac imaging and stress testing asymptomatic athletes to identify those at risk of sudden cardiac death.* JACC Cardiovasc Imaging, 2013. **6**(9): p. 993-1007.
201. Aaron, C.P., et al., *Physical activity and right ventricular structure and function. The MESA-Right Ventricle Study.* Am J Respir Crit Care Med, 2011. **183**(3): p. 396-404.
202. Bohm, P., et al., *Right and Left Ventricular Function and Mass in Male Elite Master Athletes: A Controlled Contrast-Enhanced Cardiovascular Magnetic Resonance Study.* Circulation, 2016. **133**(20): p. 1927-35.
203. Arbab-Zadeh, A., et al., *Cardiac remodeling in response to 1 year of intensive endurance training.* Circulation, 2014. **130**(24): p. 2152-61.
204. Wilson, M., et al., *Diverse patterns of myocardial fibrosis in lifelong, veteran endurance athletes.* J Appl Physiol (1985), 2011. **110**(6): p. 1622-6.
205. La Gerche, A., et al., *Biochemical and functional abnormalities of left and right ventricular function after ultra-endurance exercise.* Heart, 2008. **94**(7): p. 860-6.
206. Ector, J., et al., *Reduced right ventricular ejection fraction in endurance athletes presenting with ventricular arrhythmias: a quantitative angiographic assessment.* Eur Heart J, 2007. **28**(3): p. 345-53.
207. La Gerche, A., et al., *Disproportionate exercise load and remodeling of the athlete's right ventricle.* Med Sci Sports Exerc, 2011. **43**(6): p. 974-81.
208. La Gerche, A., et al., *Exercise-induced right ventricular dysfunction and structural remodelling in endurance athletes.* Eur Heart J, 2012. **33**(8): p. 998-1006.
209. D'Ascenzi, F., et al., *Right ventricular remodelling induced by exercise training in competitive athletes.* Eur Heart J Cardiovasc Imaging, 2016. **17**(3): p. 301-7.
210. Heidbuchel, H. and A. La Gerche, *The right heart in athletes. Evidence for exercise-induced arrhythmogenic right ventricular cardiomyopathy.* Herzschrittmacherther Elektrophysiol, 2012. **23**(2): p. 82-6.
211. Sen-Chowdhry, S., et al., *Clinical and genetic characterization of families with arrhythmogenic right ventricular dysplasia/cardiomyopathy provides novel insights into patterns of disease expression.* Circulation, 2007. **115**(13): p. 1710-20.

212. Heidbuchel, H., et al., *High prevalence of right ventricular involvement in endurance athletes with ventricular arrhythmias. Role of an electrophysiologic study in risk stratification.* Eur Heart J, 2003. **24**(16): p. 1473-80.
213. La Gerche, A., et al., *Lower than expected desmosomal gene mutation prevalence in endurance athletes with complex ventricular arrhythmias of right ventricular origin.* Heart, 2010. **96**(16): p. 1268-74.
214. Boggs, P.T. and J.E. Roger, *Orthogonal distance regression.* Contemporary Mathematics, 1990. **112**: p. 183-194.
215. Cha, Z. and C. Tsuhan. *Efficient feature extraction for 2D/3D objects in mesh representation*. in *Proceedings 2001 International Conference on Image Processing (Cat. No.01CH37205)*. 2001.
216. *World Medical Association Declaration of Helsinki: ethical principles for medical research involving human subjects.* Jama, 2013. **310**(20): p. 2191-4.
217. Bingol, O.R. and A. Krishnamurthy, *NURBS-Python: An open-source object-oriented NURBS modeling framework in Python.* SoftwareX, 2019. **9**: p. 85-94.
218. Paul Chew, L., *Constrained delaunay triangulations.* Algorithmica, 1989. **4**(1): p. 97-108.
219. Tokodi, M., et al., *Partitioning the Right Ventricle Into 15 Segments and Decomposing Its Motion Using 3D Echocardiography-Based Models: The Updated ReVISION Method.* Front Cardiovasc Med, 2021. **8**: p. 622118.
220. Mosteller, R.D., *Simplified calculation of body-surface area.* N Engl J Med, 1987. **317**(17): p. 1098.
221. Lang, R.M., et al., *Recommendations for cardiac chamber quantification by echocardiography in adults: an update from the American Society of Echocardiography and the European Association of Cardiovascular Imaging.* J Am Soc Echocardiogr, 2015. **28**(1): p. 1-39 e14.
222. Lai, W.W., et al., *Guidelines and standards for performance of a pediatric echocardiogram: a report from the Task Force of the Pediatric Council of the American Society of Echocardiography.* J Am Soc Echocardiogr, 2006. **19**(12): p. 1413-30.
223. Babity, M., et al., *Cardiopulmonary examinations of athletes returning to high-intensity sport activity following SARS-CoV-2 infection.* Sci Rep, 2022. **12**(1): p. 21686.
224. Lakatos, B.K., et al., *Exercise-induced shift in right ventricular contraction pattern: novel marker of athlete's heart?* Am J Physiol Heart Circ Physiol, 2018. **315**(6): p. H1640-H1648.
225. Humbert, M., et al., *2022 ESC/ERS Guidelines for the diagnosis and treatment of pulmonary hypertension.* Eur Heart J, 2022. **43**(38): p. 3618-3731.
226. Stroup, D.F., et al., *Meta-analysis of observational studies in epidemiology: a proposal for reporting. Meta-analysis Of Observational Studies in Epidemiology (MOOSE) group.* JAMA, 2000. **283**(15): p. 2008-12.
227. Hayden, J.A., et al., *Assessing bias in studies of prognostic factors.* Ann Intern Med, 2013. **158**(4): p. 280-6.
228. Li, Y., et al., *Right Ventricular Function Predicts Adverse Clinical Outcomes in Patients With Chronic Thromboembolic Pulmonary Hypertension: A Three-Dimensional Echocardiographic Study.* Front Med (Lausanne), 2021. **8**: p. 697396.
229. Higgins, J.P., et al., *Measuring inconsistency in meta-analyses.* BMJ, 2003. **327**(7414): p. 557-60.
230. Duval, S. and R. Tweedie, *A Nonparametric "Trim and Fill" Method of Accounting for Publication Bias in Meta-Analysis.* Journal of the American Statistical Association, 2000. **95**(449): p. 89-98.

231. Lancellotti, P., et al., *Recommendations for the echocardiographic assessment of native valvular regurgitation: an executive summary from the European Association of Cardiovascular Imaging.* Eur Heart J Cardiovasc Imaging, 2013. **14**(7): p. 611-44.
232. Lakatos, B.K., et al., *Importance of Nonlongitudinal Motion Components in Right Ventricular Function: Three-Dimensional Echocardiographic Study in Healthy Volunteers.* J Am Soc Echocardiogr, 2020. **33**(8): p. 995-1005 e1.
233. Valle, C., et al., *Right ventricular contraction patterns in healthy children using three-dimensional echocardiography.* Front Cardiovasc Med, 2023. **10**: p. 1141027.
234. Pelliccia, A., et al., *European Association of Preventive Cardiology (EAPC) and European Association of Cardiovascular Imaging (EACVI) joint position statement: recommendations for the indication and interpretation of cardiovascular imaging in the evaluation of the athlete's heart.* European Heart Journal, 2017. **39**(21): p. 1949-1969.
235. Ujvari, A., et al., *Right Ventricular Structure and Function in Adolescent Athletes: A 3D Echocardiographic Study.* Int J Sports Med, 2024.
236. Rako, Z.A., et al., *Clinical and functional relevance of right ventricular contraction patterns in pulmonary hypertension.* J Heart Lung Transplant, 2023. **42**(11): p. 1518-1528.
237. Galie, N., et al., *2015 ESC/ERS Guidelines for the diagnosis and treatment of pulmonary hypertension: The Joint Task Force for the Diagnosis and Treatment of Pulmonary Hypertension of the European Society of Cardiology (ESC) and the European Respiratory Society (ERS): Endorsed by: Association for European Paediatric and Congenital Cardiology (AEPC), International Society for Heart and Lung Transplantation (ISHLT).* Eur Heart J, 2016. **37**(1): p. 67-119.
238. Tokodi, M., et al., *Right ventricular mechanical pattern in patients undergoing mitral valve surgery: a predictor of post-operative dysfunction?* ESC Heart Fail, 2020. **7**(3): p. 1246-1256.
239. Surkova, E., et al., *Relative Prognostic Importance of Left and Right Ventricular Ejection Fraction in Patients With Cardiac Diseases.* J Am Soc Echocardiogr, 2019. **32**(11): p. 1407-1415 e3.
240. Moceri, P., et al., *Additional prognostic value of echocardiographic follow-up in pulmonary hypertension—role of 3D right ventricular area strain.* European Heart Journal - Cardiovascular Imaging, 2021.
241. Li, Y., et al., *Right Ventricular Function and Its Coupling With Pulmonary Circulation in Precapillary Pulmonary Hypertension: A Three-Dimensional Echocardiographic Study.* Front Cardiovasc Med, 2021. **8**: p. 690606.
242. Kitano, T., et al., *Prognostic Value of Right Ventricular Strains Using Novel Three-Dimensional Analytical Software in Patients With Cardiac Disease.* Front Cardiovasc Med, 2022. **9**: p. 837584.
243. Nabeshima, Y., T. Kitano, and M. Takeuchi, *Prognostic Value of the Three-Dimensional Right Ventricular Ejection Fraction in Patients With Asymptomatic Aortic Stenosis.* Front Cardiovasc Med, 2021. **8**: p. 795016.
244. Meng, Y., et al., *Prognostic Value of Right Ventricular 3D Speckle-Tracking Strain and Ejection Fraction in Patients With HFpEF.* Front Cardiovasc Med, 2021. **8**: p. 694365.
245. Murata, M., et al., *Prognostic value of three-dimensional echocardiographic right ventricular ejection fraction in patients with pulmonary arterial hypertension.* Oncotarget, 2016. **7**(52): p. 86781-86790.
246. Tolvaj, M., et al., *Added predictive value of right ventricular ejection fraction compared with conventional echocardiographic measurements in patients who underwent diverse cardiovascular procedures.* Imaging, 2021. **13**(2): p. 130-137.

247. Vijiiac, A., et al., *The prognostic value of right ventricular longitudinal strain and 3D ejection fraction in patients with dilated cardiomyopathy.* Int J Cardiovasc Imaging, 2021. **37**(11): p. 3233-3244.
248. Zhang, Y., et al., *Prognostic Value of Right Ventricular Ejection Fraction Assessed by 3D Echocardiography in COVID-19 Patients.* Front Cardiovasc Med, 2021. **8**: p. 641088.
249. Kellum, J.A., et al., *Kidney disease: Improving global outcomes (KDIGO) acute kidney injury work group. KDIGO clinical practice guideline for acute kidney injury.* Kidney International Supplements, 2012. **2**(1): p. 1-138.
250. Galie, N., et al., *2015 ESC/ERS Guidelines for the diagnosis and treatment of pulmonary hypertension: The Joint Task Force for the Diagnosis and Treatment of Pulmonary Hypertension of the European Society of Cardiology (ESC) and the European Respiratory Society (ERS): Endorsed by: Association for European Paediatric and Congenital Cardiology (AEPC), International Society for Heart and Lung Transplantation (ISHLT).* Eur Heart J, 2016. **37**(1): p. 67-119.
251. Le Tourneau, T., et al., *Impact of left atrial volume on clinical outcome in organic mitral regurgitation.* J Am Coll Cardiol, 2010. **56**(7): p. 570-8.
252. Hyllén, S., et al., *Right Ventricular Performance After Valve Repair for Chronic Degenerative Mitral Regurgitation.* The Annals of Thoracic Surgery, 2014. **98**(6): p. 2023-2030.
253. Tolvaj, M., et al., *There is more than just longitudinal strain: Prognostic significance of biventricular circumferential mechanics.* Front Cardiovasc Med, 2023. **10**: p. 1082725.
254. Satriano, A., et al., *Characterization of Right Ventricular Deformation in Pulmonary Arterial Hypertension Using Three-Dimensional Principal Strain Analysis.* J Am Soc Echocardiogr, 2019. **32**(3): p. 385-393.
255. Bernardino, G., et al., *Volumetric parcellation of the right ventricle for regional geometric and functional assessment.* ArXiv, 2020. **abs/2003.08423**.
256. Seo, Y., et al., *Right ventricular three-dimensional echocardiography: the current status and future perspectives.* J Echocardiogr, 2020.
257. Ishizu, T., et al., *Global and Regional Right Ventricular Function Assessed by Novel Three-Dimensional Speckle-Tracking Echocardiography.* J Am Soc Echocardiogr, 2017. **30**(12): p. 1203-1213.
258. Kovacs, A., et al., *Right ventricular mechanical pattern in health and disease: beyond longitudinal shortening.* Heart Fail Rev, 2019. **24**(4): p. 511-520.
259. Sakuma, M., et al., *Right ventricular ejection function assessed by cineangiography--Importance of bellows action.* Circ J, 2002. **66**(6): p. 605-9.
260. Muraru, D., et al., *Sex- and Method-Specific Reference Values for Right Ventricular Strain by 2-Dimensional Speckle-Tracking Echocardiography.* Circ Cardiovasc Imaging, 2016. **9**(2): p. e003866.
261. Hashimoto, I. and K. Watanabe, *Alternation of right ventricular contraction pattern in healthy children-shift from radial to longitudinal direction at approximately 15 mm of tricuspid annular plane systolic excursion.* Circ J, 2014. **78**(8): p. 1967-73.
262. Sanchez-Quintana, D., et al., *Morphological changes in the normal pattern of ventricular myoarchitecture in the developing human heart.* Anat Rec, 1995. **243**(4): p. 483-95.
263. Cho, E.J., et al., *Right ventricular free wall circumferential strain reflects graded elevation in acute right ventricular afterload.* Am J Physiol Heart Circ Physiol, 2009. **296**(2): p. H413-20.

264. Cotella, J.I., et al., *Three-dimensional echocardiographic evaluation of longitudinal and non-longitudinal components of right ventricular contraction: results from the World Alliance of Societies of Echocardiography study.* Eur Heart J Cardiovasc Imaging, 2024. **25**(2): p. 152-160.
265. Maffessanti, F., et al., *Age-, body size-, and sex-specific reference values for right ventricular volumes and ejection fraction by three-dimensional echocardiography: a multicenter echocardiographic study in 507 healthy volunteers.* Circ Cardiovasc Imaging, 2013. **6**(5): p. 700-10.
266. Addetia, K., et al., *Worldwide normal values for left and right ventricular size and function using 3D echocardiography: first report from the World Alliance of Societies of Echocardiography (WASE) Normal Values Study*, in *Paper presented at: The Annular Meeting of the American Society of Echocardiography*. 2019.
267. Woodard, J.C., E. Chow, and D.J. Farrar, *Isolated ventricular systolic interaction during transient reductions in left ventricular pressure.* Circ Res, 1992. **70**(5): p. 944-51.
268. Mulieri, L.A., et al., *Regional differences in the force-frequency relation of human left ventricular myocardium in mitral regurgitation: implications for ventricular shape.* Am J Physiol Heart Circ Physiol, 2005. **288**(5): p. H2185-91.
269. Levy, P.T., et al., *Maturational Patterns of Systolic Ventricular Deformation Mechanics by Two-Dimensional Speckle-Tracking Echocardiography in Preterm Infants over the First Year of Age.* J Am Soc Echocardiogr, 2017. **30**(7): p. 685-698 e1.
270. Surkova, E., et al., *Contraction patterns of the systemic right ventricle: a three-dimensional echocardiography study.* Eur Heart J Cardiovasc Imaging, 2022. **23**(12): p. 1654-1662.
271. D'Ascenzi, F., et al., *RV Remodeling in Olympic Athletes.* JACC Cardiovasc Imaging, 2017. **10**(4): p. 385-393.
272. Vitarelli, A., et al., *Assessment of right ventricular function by three-dimensional echocardiography and myocardial strain imaging in adult atrial septal defect before and after percutaneous closure.* Int J Cardiovasc Imaging, 2012. **28**(8): p. 1905-16.
273. Sanz-de la Garza, M., et al., *Severity of structural and functional right ventricular remodeling depends on training load in an experimental model of endurance exercise.* Am J Physiol Heart Circ Physiol, 2017. **313**(3): p. H459-H468.
274. Lo Iudice, F., et al., *Determinants of myocardial mechanics in top-level endurance athletes: three-dimensional speckle tracking evaluation.* Eur Heart J Cardiovasc Imaging, 2017. **18**(5): p. 549-555.
275. Sanz-de la Garza, M., et al., *Influence of gender on right ventricle adaptation to endurance exercise: an ultrasound two-dimensional speckle-tracking stress study.* Eur J Appl Physiol, 2017. **117**(3): p. 389-396.
276. Sanz de la Garza, M., et al., *Inter-individual variability in right ventricle adaptation after an endurance race.* Eur J Prev Cardiol, 2016. **23**(10): p. 1114-24.
277. McClean, G., et al., *Electrical and structural adaptations of the paediatric athlete's heart: a systematic review with meta-analysis.* Br J Sports Med, 2018. **52**(4): p. 230.
278. Churchill, T.W., et al., *Exercise-induced cardiac remodeling during adolescence.* Eur J Prev Cardiol, 2020. **27**(19): p. 2148-2150.
279. Bjerring, A.W., et al., *The developing athlete's heart: a cohort study in young athletes transitioning through adolescence.* Eur J Prev Cardiol, 2019. **26**(18): p. 2001-2008.
280. Styne, D.M., *The regulation of pubertal growth.* Horm Res, 2003. **60**(Suppl 1): p. 22-6.
281. Hietalampi, H., et al., *Left ventricular mass and geometry in adolescence: early childhood determinants.* Hypertension, 2012. **60**(5): p. 1266-72.

282. Olah, A., et al., *Characterization of the dynamic changes in left ventricular morphology and function induced by exercise training and detraining.* Int J Cardiol, 2019. **277**: p. 178-185.
283. D'Ascenzi, F., et al., *Training-induced right ventricular remodelling in pre-adolescent endurance athletes: The athlete's heart in children.* Int J Cardiol, 2017. **236**: p. 270-275.
284. Ragazzoni, G.L., et al., *How to evaluate resting ECG and imaging in children practising sport: a critical review and proposal of an algorithm for ECG interpretation.* Eur J Prev Cardiol, 2023. **30**(5): p. 375-383.
285. Rundqvist, L., et al., *Regular endurance training in adolescents impacts atrial and ventricular size and function.* Eur Heart J Cardiovasc Imaging, 2017. **18**(6): p. 681-687.
286. Gomez, A.D., et al., *Right Ventricular Fiber Structure as a Compensatory Mechanism in Pressure Overload: A Computational Study.* J Biomech Eng, 2017. **139**(8): p. 0810041-08100410.
287. Jone, P.N., et al., *Three-Dimensional Echocardiography Right Ventricular Volumes and Ejection Fraction Reference Values in Children: A North American Multicentre Study.* Can J Cardiol, 2022. **38**(9): p. 1426-1433.
288. Fabian, A., et al., *Geometrical remodeling of the mitral and tricuspid annuli in response to exercise training: a 3-D echocardiographic study in elite athletes.* Am J Physiol Heart Circ Physiol, 2021. **320**(5): p. H1774-H1785.
289. Doronina, A., et al., *The Female Athlete's Heart: Comparison of Cardiac Changes Induced by Different Types of Exercise Training Using 3D Echocardiography.* Biomed Res Int, 2018. **2018**: p. 3561962.
290. Kovacs, A., et al., *Left ventricular untwisting in athlete's heart: key role in early diastolic filling?* Int J Sports Med, 2014. **35**(3): p. 259-64.
291. Ragazzoni, G.L., et al., *How to evaluate resting ECG and imaging in children practising sport: critical review and proposal of an algorithm for ECG interpretation.* Eur J Prev Cardiol, 2022.
292. Fabian, A., et al., *Biventricular mechanical pattern of the athlete's heart: comprehensive characterization using three-dimensional echocardiography.* Eur J Prev Cardiol, 2022. **29**(12): p. 1594-1604.
293. Sun, B., et al., *The upper limit of physiological cardiac hypertrophy in elite male and female athletes in China.* Eur J Appl Physiol, 2007. **101**(4): p. 457-63.
294. Csecs, I., et al., *The impact of sex, age and training on biventricular cardiac adaptation in healthy adult and adolescent athletes: Cardiac magnetic resonance imaging study.* Eur J Prev Cardiol, 2020. **27**(5): p. 540-549.
295. Lakatos, B.K., et al., *Relationship between Cardiac Remodeling and Exercise Capacity in Elite Athletes: Incremental Value of Left Atrial Morphology and Function Assessed by Three-Dimensional Echocardiography.* J Am Soc Echocardiogr, 2020. **33**(1): p. 101-109 e1.
296. Bernardino, G., et al., *Three-dimensional regional bi-ventricular shape remodeling is associated with exercise capacity in endurance athletes.* Eur J Appl Physiol, 2020. **120**(6): p. 1227-1235.
297. La Gerche, A., et al., *Maximal oxygen consumption is best predicted by measures of cardiac size rather than function in healthy adults.* Eur J Appl Physiol, 2012. **112**(6): p. 2139-47.
298. Steding, K., et al., *Relation between cardiac dimensions and peak oxygen uptake.* J Cardiovasc Magn Reson, 2010. **12**: p. 8.
299. Szauder, I., A. Kovacs, and G. Pavlik, *Comparison of left ventricular mechanics in runners versus bodybuilders using speckle tracking echocardiography.* Cardiovasc Ultrasound, 2015. **13**: p. 7.

300. Dawkins, T.G., et al., *Right Ventricular Function and Region-Specific Adaptation in Athletes Engaged in High-Dynamic Sports: A Meta-Analysis.* Circ Cardiovasc Imaging, 2021. **14**(5): p. e012315.
301. Surkova, E., et al., *Anteroposterior Contraction of the Systemic Right Ventricle: Underrecognized Component of the Global Systolic Function.* JACC: Case Reports, 2021. **3**(5).
302. Muraru, D., et al., *Development and prognostic validation of partition values to grade right ventricular dysfunction severity using 3D echocardiography.* Eur Heart J Cardiovasc Imaging, 2020. **21**(1): p. 10-21.
303. Tokodi, M., et al., *Sex-Specific Patterns of Mortality Predictors Among Patients Undergoing Cardiac Resynchronization Therapy: A Machine Learning Approach.* Front Cardiovasc Med, 2021. **8**: p. 611055.
304. Surkova, E., et al., *The dysfunctional right ventricle: the importance of multi-modality imaging.* Eur Heart J Cardiovasc Imaging, 2022.
305. Iglesias-Garriz, I., et al., *Contribution of right ventricular dysfunction to heart failure mortality: a meta-analysis.* Rev Cardiovasc Med, 2012. **13**(2-3): p. e62-9.
306. Melenovsky, V., et al., *Right heart dysfunction in heart failure with preserved ejection fraction.* Eur Heart J, 2014. **35**(48): p. 3452-62.
307. Schneider, M., et al., *Echocardiographic assessment of right ventricular function: current clinical practice.* Int J Cardiovasc Imaging, 2019. **35**(1): p. 49-56.
308. Ajmone Marsan, N., et al., *EACVI survey on standardization of cardiac chambers quantification by transthoracic echocardiography.* Eur Heart J Cardiovasc Imaging, 2020. **21**(2): p. 119-123.
309. Lejeune, S., et al., *Right Ventricular Global Longitudinal Strain and Outcomes in Heart Failure with Preserved Ejection Fraction.* J Am Soc Echocardiogr, 2020. **33**(8): p. 973-984 e2.
310. Dong, Y., et al., *Prognostic Value of Cardiac Magnetic Resonance-Derived Right Ventricular Remodeling Parameters in Pulmonary Hypertension: A Systematic Review and Meta-Analysis.* Circ Cardiovasc Imaging, 2020. **13**(7): p. e010568.
311. Soliman-Aboumarie, H., et al., *EACVI survey on the multi-modality imaging assessment of the right heart.* Eur Heart J Cardiovasc Imaging, 2022. **23**(11): p. 1417-1422.
312. Volpato, V., et al., *Feasibility and Time Analysis of Three-Dimensional and Myocardial Deformation versus Conventional Two-Dimensional Echocardiography to Assess Cardiac Chambers.* J Am Soc Echocardiogr, 2022.
313. Le Tourneau, T., et al., *Right ventricular systolic function in organic mitral regurgitation: impact of biventricular impairment.* Circulation, 2013. **127**(15): p. 1597-608.
314. Barbieri, A., et al., *Prognostic and therapeutic implications of pulmonary hypertension complicating degenerative mitral regurgitation due to flail leaflet: a multicenter long-term international study.* Eur Heart J, 2011. **32**(6): p. 751-9.
315. Zanobini, M., et al., *Postoperative Echocardiographic Reduction of Right Ventricular Function: Is Pericardial Opening Modality the Main Culprit?* BioMed research international, 2017. **2017**: p. 4808757-4808757.
316. Haddad, F., et al., *The right ventricle in cardiac surgery, a perioperative perspective: II. Pathophysiology, clinical importance, and management.* Anesth Analg, 2009. **108**(2): p. 422-33.
317. Zochios, V., A.D. Protopapas, and K. Parhar, *Markers of Right Ventricular Dysfunction in Adult Cardiac Surgical Patients.* Journal of Cardiothoracic and Vascular Anesthesia, 2017. **31**(5): p. 1570-1574.

318. Konstam, M.A., et al., *Evaluation and Management of Right-Sided Heart Failure: A Scientific Statement From the American Heart Association.* Circulation, 2018. **137**(20): p. e578-e622.
319. Stokke, T.M., et al., *Geometry as a Confounder When Assessing Ventricular Systolic Function: Comparison Between Ejection Fraction and Strain.* J Am Coll Cardiol, 2017. **70**(8): p. 942-954.
320. Kovacs, A., et al., *Impact of hemodialysis, left ventricular mass and FGF-23 on myocardial mechanics in end-stage renal disease: a three-dimensional speckle tracking study.* Int J Cardiovasc Imaging, 2014. **30**(7): p. 1331-7.
321. Lee, H.F., et al., *Prognostic value of global left ventricular strain for conservatively treated patients with symptomatic aortic stenosis.* J Cardiol, 2013. **62**(5): p. 301-6.
322. Buckberg, G. and J.I. Hoffman, *Right ventricular architecture responsible for mechanical performance: unifying role of ventricular septum.* J Thorac Cardiovasc Surg, 2014. **148**(6): p. 3166-71.e1-4.
323. Friedberg, M.K., *Imaging Right-Left Ventricular Interactions.* JACC Cardiovasc Imaging, 2018. **11**(5): p. 755-771.
324. Jategaonkar, S.R., et al., *Two-dimensional strain and strain rate imaging of the right ventricle in adult patients before and after percutaneous closure of atrial septal defects.* Eur J Echocardiogr, 2009. **10**(4): p. 499-502.
325. Schwarz, K., et al., *Right ventricular function in left ventricular disease: pathophysiology and implications.* Heart Lung Circ, 2013. **22**(7): p. 507-11.
326. Nagata, Y., et al., *Prognostic Value of Right Ventricular Ejection Fraction Assessed by Transthoracic 3D Echocardiography.* Circulation: Cardiovascular Imaging, 2017. **10**(2): p. e005384.
327. Brener, M.I., et al., *Invasive Right Ventricular Pressure-Volume Analysis: Basic Principles, Clinical Applications, and Practical Recommendations.* Circulation: Heart Failure, 2022. **15**(1): p. e009101.
328. Lakatos, B.K., et al., *Right ventricular pressure-strain relationship-derived myocardial work reflects contractility: Validation with invasive pressure-volume analysis.* J Heart Lung Transplant, 2024.

12. List of publications related to the present thesis

1. Lakatos B, Tősér Z, Tokodi M, Doronina A, Kosztin A, Muraru D, Badano LP, **Kovács A***, Merkely B*
   Quantification of the relative contribution of the different right ventricular wall motion components to right ventricular ejection fraction: the ReVISION method
   CARDIOVASCULAR ULTRASOUND 2017, 15:8
   *Equal contribution
   IF: 1.652

2. Tokodi M, Staub L, Budai Á, Lakatos B, Csákvári M, Suhai FI, Szabó L, Fábián A, Vágó H, Tősér Z, Merkely B, **Kovács A**
   Partitioning the Right Ventricle into 15 Segments and Decomposing its Motion using 3D Echocardiography-based Models: The Updated ReVISION Method
   FRONTIERS IN CARDIOVASCULAR MEDICINE 2021, 8:622118
   IF: 6.050

3. Lakatos B, Nabeshima Y, Tokodi M, Nagata Y, Tősér Z, Otani K, Kitano T, Fábián A, Ujvári A, Boros AM, Merkely B, **Kovács A***, Takeuchi M*
   Importance of Nonlongitudinal Motion Components in Right Ventricular Function: Three-Dimensional Echocardiographic Study in Healthy Volunteers
   JOURNAL OF THE AMERICAN SOCIETY OF ECHOCARDIOGRAPHY 2020, 33:995-1005
   *Equal contribution
   IF: 5.251

4. Valle C, Ujvári A, Elia E, Lu M, Gauthier N, Hoganson D, Marx G, Powell AJ, Ferraro A, Lakatos B, Tősér Z, Merkely B, **Kovács A***, Harrild DM*
   Right ventricular contraction patterns in healthy children using three-dimensional echocardiography
   FRONTIERS IN CARDIOVASCULAR MEDICINE 2023, 10:1141027
   *Equal contribution
   IF: 3.6

5. Lakatos B, Kiss O, Tokodi M, Tősér Z, Sydó N, Merkely G, Babity M, Szilágyi M, Komócsin Z, Bognár C, **Kovács A***, Merkely B*
   Exercise-induced shift in right ventricular contraction pattern: novel marker of athlete's heart?
   AMERICAN JOURNAL OF PHYSIOLOGY: HEART AND CIRCULATORY PHYSIOLOGY 2018, 315:H1640-H1648
   *Equal contribution
   IF: 4.048

6. Ujvári A, Fábián A, Lakatos B, Tokodi M, Ladányi Z, Sydó N, Csulak E, Vágó H, Juhász V, Grebur K, Szűcs A, Zámodics M, Babity M, Kiss O, Merkely B, **Kovács A**
   Right Ventricular Structure and Function in Adolescent Athletes: A 3D Echocardiographic Study
   INTERNATIONAL JOURNAL OF SPORTS MEDICINE 2024, doi: 10.1055/a-2259-2203. Epub ahead of print.
   IF: 2.5

7. Fábián A, Ujvári A, Tokodi M, Lakatos BK, Kiss O, Babity M, Zámodics M, Sydó N, Csulak E, Vágó H, Szabó L, Kiss AR, Szűcs A, Hizoh I, Merkely B, **Kovács A**
   Biventricular mechanical pattern of the athlete's heart: comprehensive characterization using three-dimensional echocardiography
   EUROPEAN JOURNAL OF PREVENTIVE CARDIOLOGY 2022, 29(12):1594-1604
   IF: 8.3

8. Rako ZA, Yogeswaran A, Lakatos BK, Fábián A, Yildiz S, da Rocha BB, Vadász I, Ghofrani HA, Seeger W, Gall H, Kremer NC, Richter MJ, Bauer P, Tedford RJ, Naeije R, **Kovács A***, Tello K*
   Clinical and functional relevance of right ventricular contraction patterns in pulmonary hypertension
   JOURNAL OF HEART AND LUNG TRANSPLANTATION 2023, 42(11):1518-1528
   *Equal contribution
   IF: 8.9

9. Lakatos B, Tokodi M, Assabiny A, Tősér Z, Kosztin A, Doronina A, Rácz K, Koritsánszky K, Berzsenyi V, Németh E, Sax B, **Kovács A***, Merkely B*
Dominance of free wall radial motion in global right ventricular function of heart transplant recipients
CLINICAL TRANSPLANTATION 2018, 32:e13192
*Equal contribution
IF: 1.667

10. Tolvaj M, Tokodi M, Lakatos BK, Fábián A, Ujvári A, Bakija FZ, Ladányi Z, Tarcza Z, Merkely B, **Kovács A**
Added predictive value of right ventricular ejection fraction compared with conventional echocardiographic measurements in patients who underwent diverse cardiovascular procedures.
IMAGING 2021, 13(2), 130-137.

11. Sayour AA, Tokodi M, Celeng C, Takx RAP, Fábián A, Lakatos BK, Friebel R, Surkova E, Merkely B, **Kovács A**
Association of Right Ventricular Functional Parameters With Adverse Cardiopulmonary Outcomes: A Meta-analysis
JOURNAL OF THE AMERICAN SOCIETY OF ECHOCARDIOGRAPHY 2023, 36(6):624-633.e8
IF: 6.5

12. Tokodi M, Németh E, Lakatos B, Kispál E, Tősér Z, Staub L, Rácz K, Soltész Á, Szigeti S, Varga T, Gál J, Merkely B, **Kovács A**
Right ventricular mechanical pattern in patients undergoing mitral valve surgery: a predictor of post-operative dysfunction?
ESC HEART FAILURE 2020, 7:1246-1256
IF: 4.411

13. Tolvaj M, Fábián A, Tokodi M, Lakatos B, Assabiny A, Ladányi Z, Shiida K, Ferencz A, Schwertner W, Veres B, Kosztin A, Szijártó Á, Sax B, Merkely B, **Kovács A**
There is more than just longitudinal strain: Prognostic significance of biventricular circumferential mechanics

FRONTIERS IN CARDIOVASCULAR MEDICINE 2023, 10:1082725
IF: 3.6

14. Surkova E*, **Kovács A***, Tokodi M, Lakatos B, Merkely B, Muraru D, Ruocco A, Parati G, Badano LP.
Contraction Patterns of the Right Ventricle Associated with Different Degrees of Left Ventricular Systolic Dysfunction
CIRCULATION-CARDIOVASCULAR IMAGING 2021, 14:e012774
*Equal contribution
IF: 7.792

15. **Kovács A**, Lakatos B, Tokodi M, Merkely B
Right ventricular mechanical pattern in health and disease: beyond longitudinal shortening (review)
HEART FAILURE REVIEWS 24:511-520
IF: 3.538

13. Acknowledgements

It was a difficult challenge to return to the research and development field after finishing my PhD. It was a remarkable journey for me, and I owe it to the great help and advice that many people gave me.

My main expression of gratitude goes to my supervisor, Prof. Béla Merkely, for his priceless support and constant guidance. I appreciate your recognition of my abilities as both a clinician and a researcher.

The one person who helped me the most to get back on track to a successful research career is my former PhD fellow and great friend, Bálint Lakatos. We discovered this whole RV area together, worked side by side and collected thousands of 3D echos, endured irrelevant reviews from irrelevant journals and doubts about the idea of ReVISION and also rejoiced together in its success as a globally recognized approach. I have learnt a lot from you and your contribution to the present thesis cannot be overestimated.

I want to express my sincere gratitude to Zoltán Tősér and the whole Argus Cognitive team for turning my wild ideas into reality about a software medical device. I discovered not only very skilled tech guys at Argus but also a second family. I am eager to see how far we can take this thing ahead.

I'm very grateful to (former) PhD fellows and great friends Márton Tokodi, Alexandra Fábián and Máté Tolvaj. You boosted my research efforts and publication success to a whole new level I never imagined. I hope that we can continue to working together for the next decades.

I'm very grateful to my wonderful collaborators and friends from different countries and disciplines. Annamária Kosztin, Orsolya Kiss, Andrea Szűcs, Csilla Celeng, Elena Surkova, Luigi Badano, Roberto Lang, Masaaki Takeuchi, Khodr Tello, Attila Oláh, Ali Sayour, Pál

Maurovich-Horvat, Tamás Radovits and many more. Your extensive knowledge and valuable experience have motivated me in my academic research and daily life.

Many thanks to all PhD students and student researchers. Without their help, none of my achievements would have been possible. I'm grateful to all the colleagues at the Heart and Vascular Center for helping me with everyday life and showing me how to be a good medical doctor, a good cardiologist.

My deepest gratitude goes to my wife, Kinga, for always giving me love and support, for all the long nights and early mornings, and being the one I love, and my other half. Thanks for my baby boys in helping me stay grounded and inspired to be a good person. Last but not least, I want to thank my parents for being my backbone in life. Words can never express how much I am grateful to them.